STUDIES ON MACROSCOPIC MORPHOLOGY FORMATION AND ELECTRICAL PROPERTY OF SOL-GEL DERIVED TITANIA FILMS

KOICHI KAJIHARA

2000

STUDIES ON MACROSCOPIC MORPHOLOGY FORMATION AND ELECTRICAL PROPERTY OF SOL-GEL DERIVED TITANIA FILMS

KOICHI KAJIHARA

2000

Contents

General introduction

Electrical conductors and semiconductors are important and indispensable materials in many current industries. Various kinds of materials, in particular inorganic materials such as metals, non-metals, and their composites, have been utilized to meet widely different uses such as electrical power transfer, switching and operation of electrical signals, energy sensing and conversion, and so on. The discovery of efficient materials often stimulates the innovation of devices because the performance of devices is largely limited by the properties of comprising materials. In order to find superior materials, much attention should be payed not only to the chemical structure but also to the structures from microscopic to macroscopic scales.

Oxides as electroconductive materials

Oxides are interesting as electroconductive materials because numerous compounds are known under an atmospheric condition and their electrical conductivity differs from insulating level to almost metallic regime [1]. In addition, oxides are gifted with a lot of functional properties such as magnetism, ferroelectricity, piezoelectricity, pyroelectricity, considerable nonlinear properties, high-T_c superconductivity, and so on [2,3].

Electrical conductivity (σ) of condensed materials is typically defined by the following equation [4]:

$$\sigma = en\mu_d = \frac{e^2 n\tau}{m}, \tag{1}$$

where e denotes the elementary charge, n the carrier density, μ_d the drift mobility, τ the relaxation time of carrier, and m the effective mass of carrier, respectively. From the viewpoint of electronic structure, metals and alloys are usually described as the largely-overlapped valence orbitals of adjacent atoms and the partly-filled conduction band. Since the former and the latter respectively result in larger μ_d and n, metallic compounds can be good electrical conductors.

In contrast, electrical conductivity of oxides is relatively low for the following reasons [1,5]. First, n is essentially small because the constituent ions prefer closed-shell structure. Second, the smaller overlap of adjacent atomic orbitals results in smaller μ_d because valence electrons tend to be localized on atomic orbitals. Third, thermal excitation of electrons is not easy at room temperature because of the larger bandgap energy (E_g). In general, E_g increases by increasing the difference of electron affinity between metal and oxygen atoms. Fourth, considerable increase in m, named as polaron, is often observed because the electrostatic interaction between the free carrier and the ionic lattice is not negligible in oxides. The above situations mainly result from the stronger ionic nature of oxide ion and the larger difference and anisotropy of the valence electronic structures among the relevant ions. Oxides consisting of typical light metals tend to be good insulators such as MgO, Al_2O_3, and SiO_2.

However, oxides displaying significant electrical conduction are not rare [1]. The SnO_2 has been known as a typical n-type conductive oxide. Since SnO_2 has relatively wide conduction band which mainly consists of isotropic Sn5s orbital, Hole mobility (μ_H) of SnO_2 ($240\,cm^2{\cdot}V^{-1}s^{-1}$) is about one tenth as large as that of Si ($1{,}900\,cm^2{\cdot}V^{-1}s^{-1}$). Several transition metal oxides such as Fe_3O_4 and CoO are semiconductive because the valence state of metal cations is variable. The conductive carriers are supposed to move between the metal ions by thermal hopping and tunneling mechanisms due to the smaller overlap of the adjacent metal orbitals. It is well known that n of conductive oxides is dominated by nonstoichiometry, and is susceptible to the ambient conditions and the preparation procedures. Doping aliovalent ion is often effective to increase n as seen from Sn-doped In_2O_3 (ITO), Al-doped ZnO, and Li-doped NiO for example. Several oxides such as ReO_3 and $Na_{x>0.25}WO_3$ exhibit even metallic conduction because of the wide and partly-filled conduction bands. A group of perovskite compounds typically $La_{1-x}Sr_xMO_3$ (M = Cr, Mn, Fe, Co, and Ni) is quite unique from the standpoint of the composition-dependent metal-insulator transition (MIT) as well as the considerable oxide ion conduction. Most of high-T_c superconductors are copper-based oxides doped with conductive holes such as $La_{2-x}Ba_xCuO_{4+\delta}$ [6] and $YBa_2Cu_3O_{6+\delta}$ [7]. The period of stacking can be an additional parameter to modulate the electrical properties of homologous compounds like

$Bi_2Sr_2Ca_{n-1}Cu_nO_{4+2n+\delta}$ [8] and $(ZnO)_nIn_2O_3$ [9]. Recently, the importances of *p*-block cations and monovalent 1B group cations have been respectively pointed out for designing n-type and p-type transparent conductive oxides equipped with isotropic and delocalized conduction and valence bands. Based on the strategy, several n-type transparent conductive oxides such as $MgIn_2O_4$ [10], a-2CdO·GeO_2 [11], and $AgInO_2$ [12] have been discovered, and $CuAlO_2$ [13] and $SrCu_2O_2$ [14] have also been developed as first practical p-type transparent conductive oxides of which σ can be $1\,S{\cdot}cm^{-1}$ at room temperature.

Titania as semiconductive material

Titania (TiO_2) is a transparent n-type semiconductor of which E_g is about 3 eV. The valence and conduction bands of TiO_2 mainly consist of O2*p* and Ti3*d* orbitals, respectively. The origin of conductive electrons is considered to be trivalent and tetravalent interstitial titanium ions [15, 16], and divalent oxide ion vacancies. Three crystalline phases named rutile, anatase, and brookite have been well known as the polymorphic forms of TiO_2 but the electrical properties of the latter two compounds are not known sufficiently because the preparation of single crystal is difficult. Although μ_H of rutile is as small as 0.1–0.4 $cm^2{\cdot}V^{-1}s^{-1}$ at room temperature probably due to the larger *m* [17, 18] and the narrower and anisotropic *d*-like conduction band, relatively large μ_H as 4–20 $cm^2{\cdot}V^{-1}s^{-1}$ has recently been reported for anatase thin films [19, 20]. The standard enthalpy of formation of rutile ($-944.0\,kJ{\cdot}mol^{-1}$) is comparable to SiO_2 ($-910.7\,kJ{\cdot}mol^{-1}$) and is much larger than other oxides such as SnO_2 ($-577.6\,kJ{\cdot}mol^{-1}$) and ZnO ($-350.5\,kJ{\cdot}mol^{-1}$) [21]. Hence TiO_2 is quite stable against the chemical corrosion by acids and bases at room temperature. Since both the valence band edge and the decomposition potential of TiO_2 are more anodic than the potential of oxygen evolution in aqueous solutions (0.82 V vs NHE at pH 7), oxygen is generated steadily from TiO_2 surface by illuminating ultraviolet light without the degradation of TiO_2 electrode [22].

The TiO_2 has been applied to many types of devices. The spectral response of TiO_2-based photoelectrode is extended to visible region by sensitizing the TiO_2 surface with typically organometallic dyes [23]. The overall light to electricity conversion efficiency of the dye-sensitized photoelectrode can be increased more than several percent by choosing

appropriate dye and increasing the surface area of electrode [24–26]. On the other hand, TiO_2 has recently attracted as photocatalysts to decompose organic substances [27–29] because of the efficient stability and the larger oxidation power of holes photogenerated in the valence band of TiO_2. The surface of oxides is normally adsorbed by various gas molecules depending on their partial pressures. Since the adsorption of gas molecules is accompanied by the injection of charged carriers and the formation of space charge layers, TiO_2 can be applicable for gas sensors by utilizing the change in electrical conductivity. At elevated temperatures, the bulk nonstoichiometry also affects the conductivity in relation to the oxygen partial pressure. The TiO_2-based sensors are reported to be effective in detecting oxygen (air to fuel ratio) [30–33], CO and H_2 [34], NO_x [35], and humidity [34, 36]. The colorless Ti^{4+} state can be reduced to Ti^{3+} state accompanied by the coloration in deep blue. The color change of TiO_2 films caused by the electrochemical insertion and extraction of typically monovalent cations such as H^+ and Li^+ can be applicable for electrochromic displays [37]. Partially crystallized TiO_2 is also expected to be used as electrode materials of lithium ion batteries by utilizing the potential plateau during the Li^+ insertion and extraction [38,39]. Especially for spinel-type lithium titanate $Li[Li_{1/3}Ti_{5/3}]O_4$, the unchanged lattice constant during the Li^+ insertion up to $Li_2[Li_{1/3}Ti_{5/3}]O_4$ is noteworthy [40].

Sol-gel method and its application for film deposition

Sol-gel method is a fundamental process to fabricate glasses and ceramics particularly advantageous in the operation at lower temperature under an atmospheric pressure, the homogeneous mixing of starting materials, and the purity and stoichiometry control [41–43]. Several functional inorganic-organic composites have also been prepared by utilizing the advantage of low-temperature fabrication [44–48]. It is also believed that the sol-gel method is suitable to prepare oxides because the polycondensation of metal alkoxides commonly forms the metalloxane bond network. The resultant gels are not so dense, because the polycondensation occurs at random and the evaporation and decomposition of residual organic substances during heat treatment leave vacant spaces. Since the structure of the alkoxide-based cluster is quite sensitive to the reactivity and the coordination

number of precursors, the pore structure depends much on preparation conditions such as solution composition, catalytic condition, additives, and gelation and aging conditions [43, 49]. In addition, mesoporous structure of gels and resultant ceramics has been tailored actively by controlling the aging condition or by incorporating template materials such as organic polymers [50, 51], surfactants [52], or fatty acids [53]. The domain formation via phase separation is interesting because the pore structure of macroscopic scale can be controlled [54, 55]. Three-dimensionally interconnected macroporous silica gels have been prepared by incorporating polar solvent in a water-poor conditions [56,57] or water-soluble organic polymers [58–60] so as to induce the spinodal decomposition parallel to the gelation.

The deposition of oxide films by sol-gel method has been explored intensively because large and uniform films can be prepared via relatively simple process. So-called vapor-phase method including sputtering, chemical vapor deposition (CVD), and laser ablation is another conventional method to prepare oxide thin films. In the vapor-phase method, the films are generally deposited through the reaction limited aggregation of atomized higher energy particles, then dense and flat films tend to be formed. In contrast, substantial porosity is characteristic feature of the films prepared by sol-gel method. Compared to the case of the sintered ceramics in which the resultant morphology is largely restricted by the shape and property of precursor particle, the morphology of sol-gel derived materials can be varied more flexibly. The gel films having tailored micropores have been applied for the membranes for gas separation [61, 62]. The macroporous films equipped with larger surface area, better material diffusivity, and higher mechanical strength are supposed to be desirable for the devices utilizing the electrical and chemical reactions on surface such as electrode materials, catalyst supports, sensors, chromatographies, and so on. Compared to the studies on the morphology from microscopic to mesoscopic scales, little attention has been given to the morphology of macroscopic scale although the formation of macroscopic domain was found on the films prepared both by dip-coating [63] and spin-coating [64, 65] methods even from simple solutions consisting only of alkoxides, alcohols, water, and acid catalysts. Recently, however several attempts have been made aiming at the active modification of film morphology by adding alkyl-substituted alkox-

ides [66] or organic polymers [67] to the precursor solution, and by immersing the gel films in hydrofluoric acid solution [68] or boiling water [69, 70] after the deposition. In the TiO_2-based systems, direct preparation of macroporous films by sol-gel dip-coating method have been reported for the system containing poly(ethylene glycol) (PEG) and diethanolamine (DEA) [29], while the mechanism of morphology formation as well as the morphology determining parameters are scarcely known. In addition, the effect of dipping environment such as temperature and humidity has not been considered seriously so far except for a few studies [65, 66], although it is supposed that the considerable material transport between the sol film and the ambient atmosphere is largely responsible for the physical and chemical reactions during the film deposition.

Perspective of this thesis

The present thesis describes the macroscopic morphology formation and the electrical property of the TiO_2 films prepared by sol-gel dip-coating method. In the former half of the thesis, the formation of macroscopic morphology is investigated under various and strictly controlled preparation conditions aiming at macroporous TiO_2 films having tailored morphology. In the latter half of the thesis, several attempts are made to apply the sol-gel derived TiO_2 films for electrical devices.

In Chapter 1, the general procedures and apparatuses used to fabricate TiO_2 films are first outlined. Subsequently, the variation of morphology with withdrawal speed and relative humidity is exhibited for the systems containing PEG, and the importance of material transport between the sol film and the ambient atmosphere during the deposition is pointed out. Several morphology determining parameters are presented to explain the variation of morphology. The influence of solution composition on morphology is also examined correlating with the effects of withdrawal speed and relative humidity.

In Chapter 2, the variation of morphology is examined by changing the molecular weight of PEG and dipping temperature. The results obtained are interpreted by using the morphology determining parameters presented in Chapter 1.

In Chapter 3, the variation of morphology is examined for the systems containing various types of chemical additives to obtain detailed information about the morphology

formation and to explore better solution compositions. Both the several organic solvents having different properties and the alcohols of which alkyl groups are larger than that of ethanol are incorporated as additives, and their influences on morphology formation are discussed individually.

In Chapter 4, the macroscopic morphology is investigated at various preparation conditions to understand the general principle of morphology formation. The mechanism of morphology formation is described comprehensively based on the results obtained through Chapters 1–4. Besides, the effect of heat treatment is studied on densification, crystallization, and morphology change behaviors of titania gel films.

In Chapter 5, the variations of morphology and thickness are investigated for the systems containing not only PEG but also poly(vinylpyrrolidone) (PVP) having higher molecular weight. To realize the thicker TiO_2 films having interconnected macroporous morphology, both the optimization of dipping condition and the repetition of depositions are attempted. Furthermore, the relationship between the ability of macroporous morphology formation and the dissolution behavior of polymer content is discussed.

In Chapter 6, sol-gel derived TiO_2 films having interconnected macroporous morphology are applied for the electrode materials of photoelectrochemical cells, and the effect of film morphology on photoelectrochemical properties is examined. Several organic dyes are employed to photosensitize the TiO_2 electrode, and the sensitization efficiency is interpreted in terms of the chemical and electronic structures of dye molecule.

In Chapter 7, the electrical property of sol-gel derived TiO_2 films doped with Ta is investigated as a material of which electrical conductivity is sensitive to ambient oxygen. The origin of oxygen sensitivity is discussed by correlating the results of DC conductivity measurement and complex impedance analysis with the information about the distribution state of Ta ion.

Finally, in Summary, the whole results and discussions of this thesis are summarized, and the future perspectives are pointed out.

References

[1] N. Tsuda, K. Nasu, A. Fujimori, and K. Siratori, *Electronic Conduction in Oxides*, 2 ed. (Shokabo, Tokyo, 1983).

[2] W. D. Kingery, H. K. Bowen, and D. R. Uhlmann, *Introduction to Ceramics*, 2 ed. (John Wiley & Sons, New York, 1976).

[3] J. F. Nye, *Physical Properties of Crystals: Their Representation by the Tensors and Matrices* (Oxford University Press, New York, 1985).

[4] K. Kobayashi, *Introduction to Electric Conduction in Solids*, 3 ed. (Syokabo, Tokyo, 1993).

[5] P. A. Cox, *The Electronic Structure and Chemistry of Solids* (Oxford University Press, Oxford, 1987).

[6] J. G. Bednorz and K. A. Müllar, Z. Phys. **B64**, 189 (1986).

[7] M. K. Wu, J. R. Ashburn, C. J. Torng, P. H. Hor, R. L. Meng, L. Gao, Z. J. Huang, Y. Q. Wang, and C. W. Chu, Phys. Rev. Lett. **58**, 980 (1987).

[8] H. Maeda, Y. Tanaka, M. Fukutomi, and T. Asano, Jpn. J. Appl. Phys. **27**, L209 (1988).

[9] H. Ohta, W.-S. Seo, and K. Koumoto, J. Am. Ceram. Soc. **79**, 2193 (1996).

[10] H. Hosono, N. Ueda, H. Kawazoe, and N. Matsunami, J. Non-Cryst. Solids **182**, 109 (1995).

[11] N. Kikuchi, H. Hosono, H. Kawazoe, K. Oyoshi, and S. Hishita, J. Am. Ceram. Soc. **80**, 22 (1997).

[12] T. Otabe, K. Ueda, A. Kudoh, H. Hosono, and H. Kawazoe, Appl. Phys. Lett. **72**, 1036 (1998).

[13] H. Kawazoe, M. Yasukawa, H. Hyodo, M. Kurita, H. Yanagi, and H. Hosono, Nature **389**, 939 (1997).

[14] A. Kudo, H. Yanagi, H. Hosono, and H. Kawazoe, Appl. Phys. Lett. **73**, 220 (1998).

[15] R. N. Blumenthal, J. Coburn, J. Baukus, and W. M. Hirthe, J. Phys. Chem. Solids **27**, 643 (1966).

[16] P. Odier, J. F. Baumard, D. Panis, and A. M. Anthony, J. Solid State Chem. **12**, 324 (1975).

[17] R. G. Breckenridge and W. R. Hosler, Phys. Rev. **91**, 793 (1953).

[18] F. A. Grant, Rev. Modern Phys. **31**, 646 (1959).

[19] L. Forro, O. Chauvet, D. Emin, L. Zuppiroli, H. Berger, and F. Lévy, J. Appl. Phys. **75**, 633 (1994).

[20] H. Tang, K. Prasad, R. Sanjinès, P. E. Schmid, and F. Lévy, J. Appl. Phys. **75**, 2042 (1994).

[21] in *CRC Handbook of Chemistry and Physics*, 76 ed., edited by D. R. Lide (CRC Press, Boca Raton, 1995), Chap. 5.

[22] A. Fujishima and K. Honda, Nature **238**, 37 (1972).

[23] T. Miyasaka, T. Watanabe, A. Fujishima, and K. Honda, Nature **277**, 638 (1979).

[24] B. O'Regan and M. Grätzel, Nature **353**, 737 (1991).

[25] M. K. Nazeeruddin, A. Kay, I. Rodicio, R. Humphry-Baker, E. Müller, P. Liska, N. Vlachopoulos, and M. Grätzel, J. Am. Chem. Soc. **115**, 6382 (1993).

[26] A. Kay and M. Grätzel, J. Phys. Chem. **97**, 6272 (1993).

[27] K. Hashimoto and A. Fujishima, Shokubai **36**, 524 (1994).

[28] K. Kato, A. Tsuzuki, H. Taoda, Y. Torii, T. Kato, and Y. Butsugan, J. Mater. Sci. **29**, 5911 (1994).

[29] K. Kato, A. Tsuzuki, Y. Torii, H. Taoda, T. Kato, and Y. Butsugan, J. Mater. Sci. **30**, 837 (1995).

[30] T. Y. Tien, H. L. Stadler, E. F. Gibbons, and P. J. Zacmanidis, Am. Ceram. Soc. Bull. **54**, 280 (1975).

[31] A. L. Micheli, Am. Ceram. Soc. Bull. **63**, 694 (1984).

[32] A. Takami, Am. Ceram. Soc. Bull. **67**, 1956 (1988).

[33] T. Takeuchi, Sens. Actuators **14**, 109 (1988).

[34] L. D. Birkefeld, A. M. Azad, and S. A. Akbar, J. Am. Ceram. Soc. **75**, 2964 (1992).

[35] K. Satake, A. Katayama, H. Ohkoshi, T. Nakahara, and T. Takeuchi, Sens. Actuators B, Chem. **20**, 111 (1994).

[36] G. Gusmano, G. Montesperelli, P. Nunziante, E. Traversa, A. Montenero, M. Braghini, G. Mattogno, and A. Bearzotti, J. Ceram. Soc. Jpn. **101**, 1095 (1993).

[37] K. Nagase, Y. Shimizu, N. Miura, and N. Yamazoe, J. Ceram. Soc. Jpn. **101**, 1032 (1993).

[38] Y. Yagi, M. Hibino, and T. Kudo, J. Electrochem. Soc. **144**, 4208 (1997).

[39] S. Y. Huang, L. Kavan, I. Exnar, and M. Grätzel, J. Electrochem. Soc. **142**, L142 (1995).

[40] T. Ohzuku, A. Ueda, and N. Yamamoto, J. Electrochem. Soc. **142**, 1431 (1995).

[41] S. Sakka, *Science of Sol-Gel Method* (Agune-Shofu-Sha, Tokyo, 1988).

[42] S. Sakka, *Application of Sol-Gel Method* (Agune-Shofu-Sha, Tokyo, 1997).

[43] C. J. Brinker and G. W. Scherer, *Sol-Gel Science: The Physics and Chemistry of Sol-Gel Processing* (Academic Press, New York, 1990).

[44] G. Philip and H. Schmidt, J. Non-Cryst. Solids **63**, 283 (1983).

[45] H. Schmidt, J. Non-Cryst. Solids **73**, 681 (1985).

[46] C. Sanchez and M. In, J. Non-Cryst. Solids **147&148**, 1 (1992).

[47] J. D. Mackenzie, J. Ceram. Soc. Jpn. **101**, 1 (1993).

[48] J. D. Mackenzie, J. Sol-Gel Sci. Technol. **2**, 81 (1994).

[49] T. Vicsek, *Fractal Growth Phenomena* (World Scientific, Singapore, 1989).

[50] T. Yazawa, A. Miyake, and H. Tanaka, J. Ceram. Soc. Jpn. **99**, 1094 (1991).

[51] T. Saegusa, J. Macromol. Sci.: Chem. A **28**, 817 (1991).

[52] A. Sayari and P. Liu, Microporous Mater. **12**, 149 (1997).

[53] R. Takahashi, S. Takenaka, S. Sato, T. Sodesawa, K. Ogura, and K. Nakanishi, J. Chem. Soc., Faraday Trans. **94**, 3161 (1998).

[54] H. Kozuka and S. Sakka, Chem. Mater. **1**, 398 (1989).

[55] K. Nakanishi, J. Porous Mater. **4**, 67 (1997).

[56] H. Kaji, K. Nakanishi, and N. Soga, J. Non-Cryst. Solids **181**, 16 (1995).

[57] H. Kaji, K. Nakanishi, and N. Soga, J. Non-Cryst. Solids **185**, 18 (1995).

[58] S. Sato, T. Murakata, T. Suzuki, and T. Ohgawara, J. Mater. Sci. **25**, 4880 (1990).

[59] K. Nakanishi and N. Soga, J. Am. Ceram. Soc. **74**, 2518 (1991).

[60] K. Nakanishi, H. Komura, R. Takahashi, and N. Soga, Bull. Chem. Soc. Jpn. **67**, 1327 (1994).

[61] T. Yazawa, H. Tanaka, H. Nakamichi, K. Eguchi, and O. Yamaguchi, J. Ceram. Soc. Jpn. **99**, 1271 (1991).

[62] C. J. Brinker, N. K. Raman, M. N. Logan, R. Sehgal, R. A. Assink, D. W. Hur, and T. L. Ward, J. Sol-Gel Sci. Technol. **4**, 117 (1995).

[63] I. Strawbridge and P. F. James, J. Non-Cryst. Solids **82**, 366 (1986).

[64] X. Orignac, H. C. Vasconcelos, X. M. Du, and R. M. Almeida, J. Sol-Gel Sci. Technol. **8**, 243 (1997).

[65] Y.-J. Kim and L. F. Francis, J. Am. Ceram. Soc. **76**, 737 (1993).

[66] K. Makita, Y. Akamatsu, S. Yamazaki, Y. Kai, and Y. Abe, J. Ceram. Soc. Jpn. **105**, 1012 (1997).

[67] A. Matsuda, Y. Matsuno, S. Katayama, T. Tsuno, N. Tohge, and T. Minami, J. Ceram. Soc. Jpn. **102**, 330 (1994).

[68] B. E. Yoldas and D. P. Partlow, Thin Solid Films **129**, 1 (1985).

[69] K. Tadanaga, N. Katata, and T. Minami, J. Am. Ceram. Soc. **80**, 1040 (1997).

[70] K. Tadanaga, N. Katata, and T. Minami, J. Am. Ceram. Soc. **80**, 3213 (1997).

Chapter 1

Effects of humidity and solution composition on morphology in system containing poly(ethylene glycol)

1.1 Introduction

Sol-gel method is a promising method for fabricating ceramics having controlled pore structure. In particular, the scale and morphology of resultant gels can be modified widely by inducing the phase separation concurrently with the gelation. Based on the concept, the domain formation mechanism and the technique of morphology control have been intensively studied especially for silica-based macroporous bulk gels prepared from the systems containing organic polymers [1–3].

Compared to the bulk systems, the overlap of solvent evaporation and polycondensation stages, the rapid deposition process, and the larger sensitivity to environmental conditions are characteristic features of the film systems. Partly due to such additional morphology determining parameters, the detailed mechanisms of macroscopic morphology formation have hardly been discussed in the film systems in spite of the importance.

The material exchange with the ambient atmosphere during the dipping operation should play important roles for the morphology formation because the considerable exchange of volatile materials is anticipated from the larger surface to volume ratio of the fluidic sol films. In the sol-gel processes, water is a key material to proceed with the hydrolysis and polycondensation. Then it is expected that the water adsorption from the ambient atmosphere influences significantly on the morphology formation. This supposition is verified clearly by the recent research that the morphology of organosilicate films prepared from the solution containing tetraethoxysilane (TEOS) and methyltrimethoxysi-

lane (MTMS) depends largely on ambient humidity [4].

The reaction chemistry and the morphology of resultant gels are also sensitive to the composition of alkoxide-based solution [5]. The chemical property of alkoxide-based solution is typically characterized by the concentrations of reactants and catalytic conditions. As expected from the role of water during the sol-gel reaction, the reactivity of solution depends greatly on water to alkoxide ratio (r). For example, a viscosity measurement of silica-based solutions revealed that the viscosity increases nonlinearly with time followed by the gelation at $r = 2$, whereas the viscosity saturates after the consumption of water at $r = 1$ [6]. The concentration of alkoxide is important as well. The dilute solution of alkoxide is no longer gelled homogeneously due to the lower crosslinking density even if its r is large enough to complete the hydrolysis. Such condition is sometimes useful to prepare monodispersed fine gel powders [7, 8]. Furthermore, the reaction rates and mechanisms are modified seriously by the addition of acid and base catalysts [9].

In the first section of this chapter, the common procedures for the preparation of the TiO_2 films are described together with the details of related experimental techniques used throughout the thesis. Then, the morphology formation under the variation of withdrawal speed and relative humidity is investigated for the TiO_2 films prepared from the system containing poly(ethylene glycol) (PEG; $HO[\text{-}CH_2CH_2O\text{-}]_nH$). Finally, the variation of macroscopic morphology is examined by changing the water and alkoxide concentrations relating to the effects of withdrawal speed and relative humidity.

1.2 General experimental procedure

Figure 1.1 schematically illustrates the dip-coating apparatus assembled in a thermostat-humidistat chamber (AE-215, ADVANTEC Ltd.) aiming at the precise control of temperature and humidity during the dipping operation. The driving unit of which maximum head speed was about $70\,\text{mm}\cdot\text{min}^{-1}$ consisted of a reversible moter (MSD206-411U, Oriental Motor Ltd.) with a slowdown gear module (2GN10XK) and a linearize gear module (2LF10N-1). The dipping operation was performed in a small compartment built in the chamber to ensure the stability of ambient condition, because the chamber was switched off during the dipping to stop the vibration mainly came from the built-in refrigerator

and air-circulator.

Figure 1.2 schematically illustrates the experimental procedure. Titanium tetraisopropoxide (TIP), product of Wako Pure Chemical Industries Ltd., was used as a titanium source as received. The PEGs having average molecular weights of 400, 1,000, 1,540, 2,000, 3,400, and 4,000 were used as polymer contents. In the following sentences, the number following the "PEG" prefix denotes the average molecular weight. The PEGs except for PEG3400, which was the product of Aldrich Chemical Ltd., were obtained from Hayashi Pure Chemical Industries Ltd. A half of the prescribed amount of solvent, water, and 60 wt% aqueous solution of nitric acid were mixed together and added to ice-cooled TIP dissolved in the reminder of solvent under vigorous stirring. After the mixing, prescribed amount of PEG was added to the solution. The container was sealed and moved to the dipping chamber in which the solution was stirred at 40–50°C for 1 h to dissolve PEG completely. Unless otherwise noted, the dissolution was done at 40°C. Then the temperature inside the chamber was lowered to 15–35°C, 30–70% RH at which the dipping operation was performed. A TiO_2 film was deposited on either a Corning #7059 alkali-ion-free borosilicate glass substrate (Kinoene Kogaku Kogyo Ltd.) or a commercial microscope glass substrate cut into 10–25 mm × 40 mm, immediately followed by heat treatment at 500°C for 10 min unless otherwise described. The #7059 substrate was typically employed when the film was subjected to ellipsometry or to heat treatment beyond 500°C.

Gelation tests were performed to estimate the polycondensation rate. The water concentration of the gelation test solution was set higher than that of the dipping solution because the dipping solution did not gel due to the lack of water. The gelation behavior was observed by holding the solution statically at 0, 40, or 50°C after the stirring as shown in Fig. 1.2. Gelation time (t_g) was determined simply by tilting the container as the time at which the macroscopic fluidity was lost since the preparation of the solution. For non-gelling systems due to the lower crosslinking density, precipitation time (t_{ps}) was measured as the time at which the precipitation first appeared.

The macroscopic morphology of the resultant TiO_2 film was observed by scanning electron microscopy (SEM; S-510, Hitachi Ltd.). The terms "smooth", "pits", "uneven

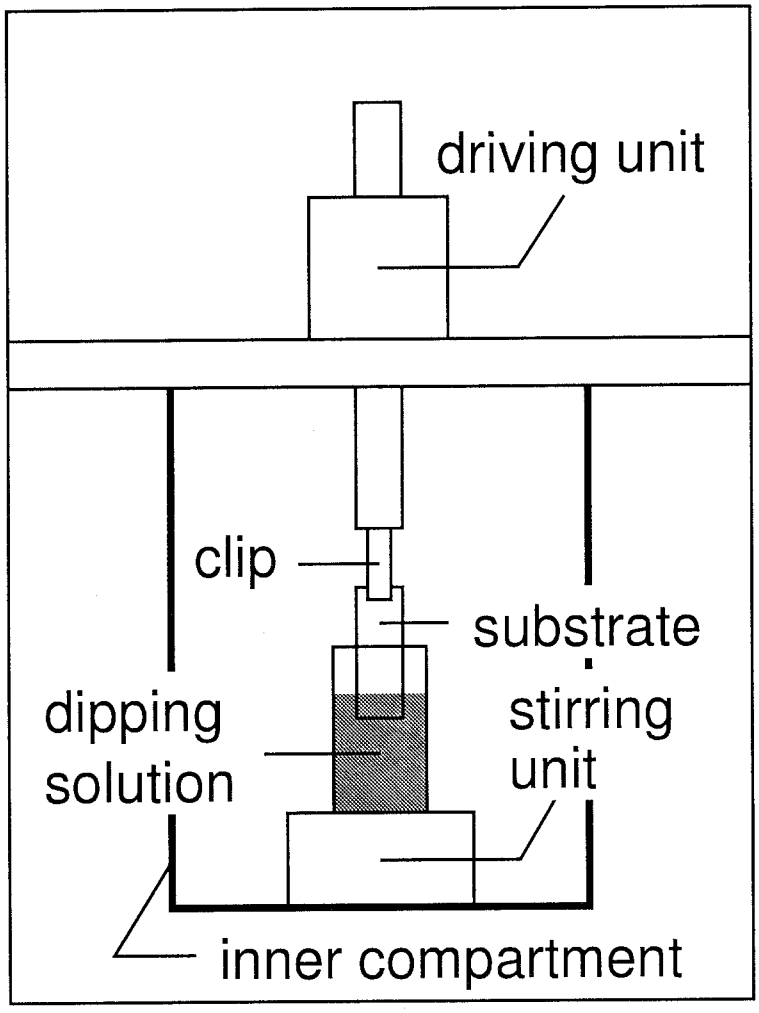

Fig. 1.1: Schematic illustration of the dip-coating apparatus built in a thermostat-humidistat chamber.

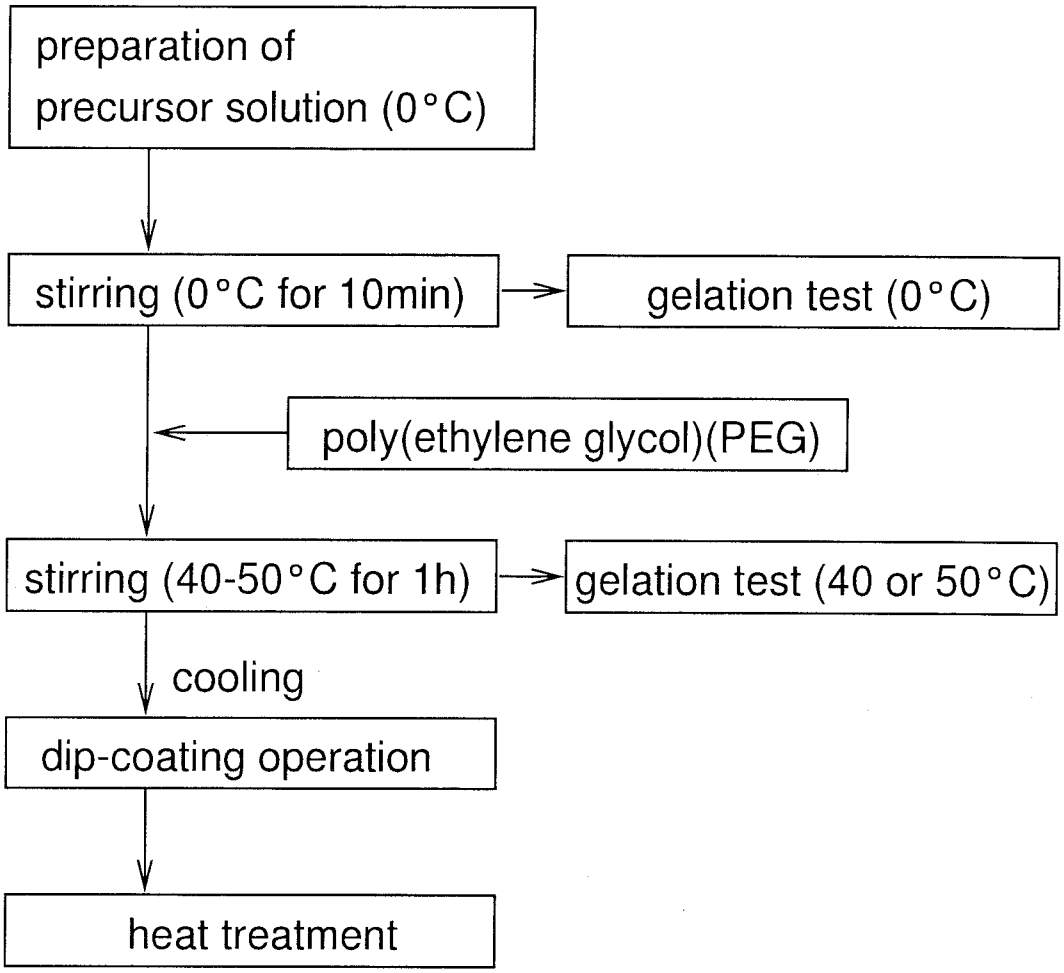

Fig. 1.2: Schematic illustration of experimental procedures.

surface", "macropores", and "macroscopic cracks" were employed to classify the morphology. The word "macropores" represents a morphology covered with well-developed macropores densely. On the other hand, "pits" represents a morphology covered with small and shallow pores, and "uneven surface" denotes a rough surface where pore outline is often not clear. The word "smooth" means flat surface without apparent macroscopic morphology. The cracks spreaded over the film are termed as "macroscopic cracks". The domain size of macroporous morphology was represented by average pore diameter (D), which was evaluated from SEM photographs by averaging the maximum horizontal diameter of fifty adjacent macropores. The standard deviation of D was indicated by error bars.

Thickness of the TiO_2 film was measured using an ellipsometer (DVA-36VW, Mizojiri Optical Ltd.). A He-Ne laser was used as a light source and the incident angle of laser (ϕ) and the azimuthal angle of incident polarizer (P) were set at 65° and 45°, respectively. The thickness measured using the ellipsometer was compared that obtained using a surface profile meter (SE-30D, Kosaka Lab. Ltd.). In general, those values agreed well. The thickness was evaluated using an another surface profile meter (Surfcom 112B, Tokyo Seimitsu Ltd.) for thicker films than about 100 nm. The crystallinity of the TiO_2 film and the lattice constant of the crystalline phases were examined using a thin-film X-ray diffractometer (XRD; RINT2500, Rigaku Ltd.) with Cu$K\alpha$ radiation. Thermogravimetry (TG) and differential thermal analysis (DTA) were performed using a TG-DTA system (8112BH, Rigaku Ltd.) to evaluate the thermal property of titania gel.

1.3 Effects of humidity and withdrawal speed

Effects of withdrawal speed and relative humidity on macroscopic morphology of the TiO_2 films were examined for the composition listed in Table 1.1. The PEG having average molecular weight of 2,000 was used as polymer content and the dipping was done at 25°C. Figure 1.3 shows a photograph of the TiO_2 films prepared at 30% RH. The appearance of the film changed from transparent to opaque with an increase in withdrawal speed because of the light scattering from the macroscopic structure formed uniformly on the film.

Table 1.1: Composition of the dipping solution (unit: mol).

H_2O	EtOH	TIP	HNO_3	PEG (g)
0.12	1.0	0.12	0.02	5.0

1.3.1 Basic factors for morphology determination

Figures 1.4 and 1.5 show the SEM photographs of the TiO_2 films prepared at 40% and 60% RH, respectively. At 40% RH, macroscopic cracks disappeared to be replaced by macropores with an increase in withdrawal speed. At 60% RH, in contrast, the films prepared at higher withdrawal speed were smooth whereas those prepared at lower withdrawal speed were macroporous. In addition, the macroscopic domain formation was less evident than that prepared at 40% RH. Table 1.2 summarizes the variation of morphology and indicates that the morphology depended considerably on both the withdrawal speed and relative humidity.

Table 1.2: Macroscopic morphology of the TiO_2 films under variations of relative humidity and withdrawal speed: -, smooth; ◡, pits; ●, macropores; ▲, uneven surface; C, macroscopic cracks.

Withdrawal speed	Relative humidity (%RH)				
($mm \cdot min^{-1}$)	30	40	50	60	70
7.5	C	◡C	◡	●	▲
15.0	◡C	●C	●	▲	◡
22.5	●C	●	●	◡	-
30.0	●	●	-	-	-

It is supposed that the enhancement of polycondensation and the suppression of solvent evaporation from the sol film can be the principal effects of ambient moisture during the dipping operation. In order to verify these suppositions, evaporation rates of water and ethanol were measured by recording the weight loss of liquid in a 200 ml beaker during a defined period at 25°C. As shown in Fig. 1.6, the evaporation rate of water decreased linearly with an increase in relative humidity, and is predicted to be zero at 100% RH

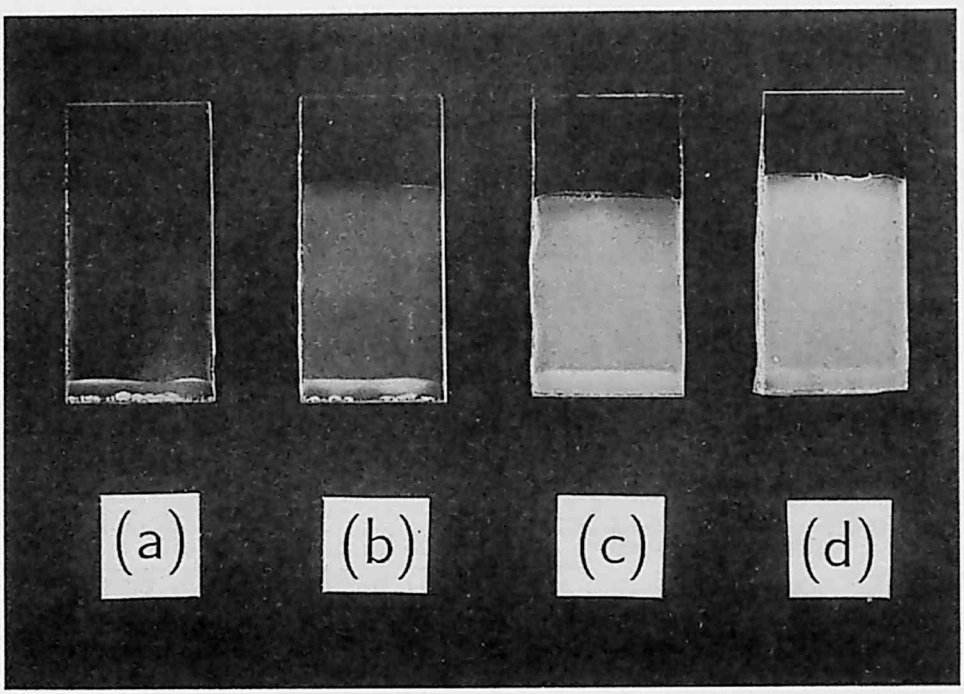

Fig. 1.3: Photograph of the TiO_2 films prepared at 30% RH. Withdrawal speed is (a) 7.5, (b) 15.0, (c) 22.5, (d) 30.0 mm·min^{-1}. The size of the substrate is 20 mm × 40 mm.

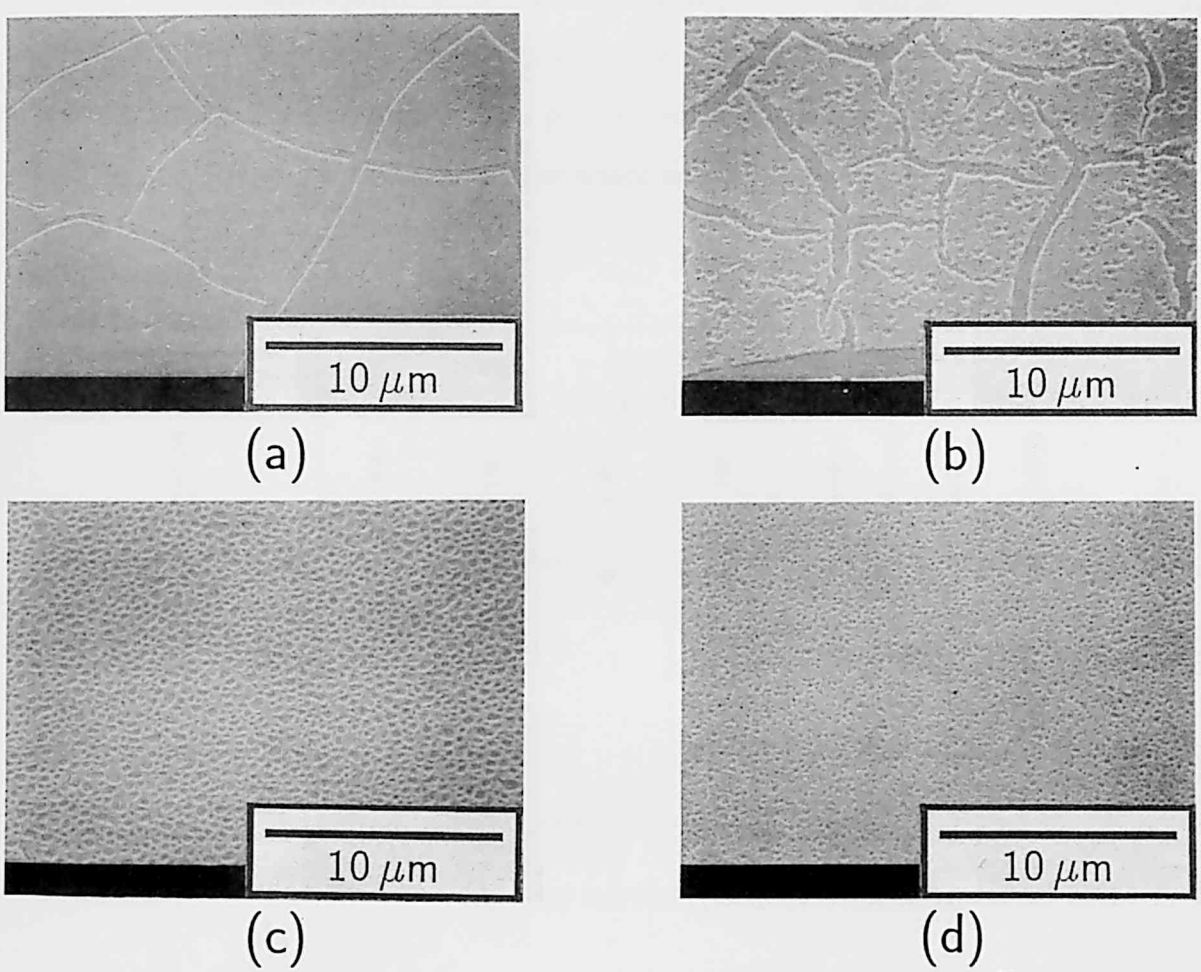

Fig. 1.4: SEM photographs of the TiO_2 films prepared at 40% RH. Withdrawal speed is (a) 7.5, (b) 15.0, (c) 22.5, (d) 30.0 mm·min^{-1}. View angle is 45°.

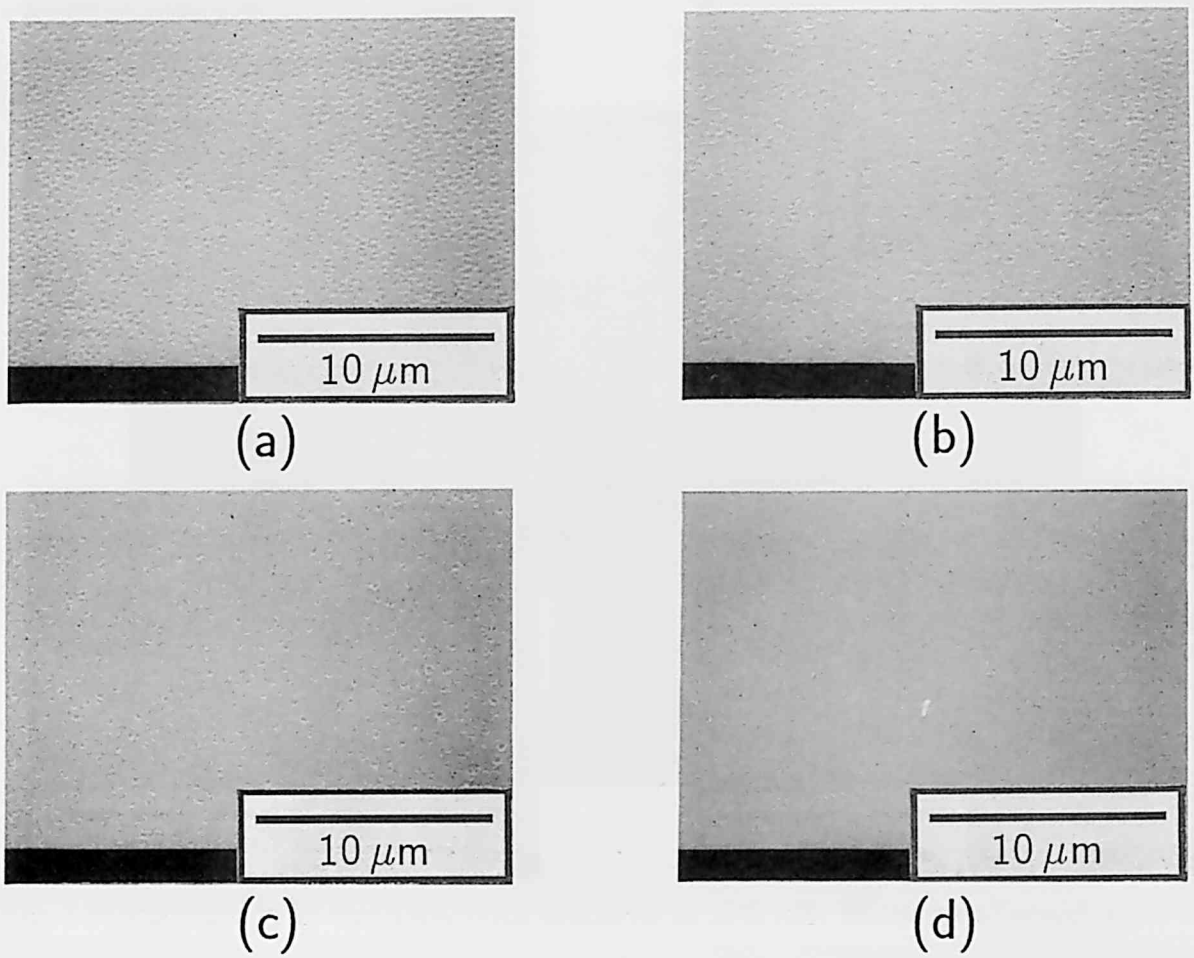

Fig. 1.5: SEM photographs of the TiO_2 films prepared at 60% RH. Withdrawal speed is (a) 7.5, (b) 15.0, (c) 22.5, (d) 30.0 mm·min^{-1}. View angle is 45°.

by extrapolating the data points. In contrast, the evaporation rate of ethanol was independent of relative humidity but decreased gradually with time owing to the increase in ethanol vapor pressure inside the chamber, because the evaporation rate is proportional to the difference between the current vapor pressure and the saturated vapor pressure of the relevant gas. Since the major component of the dipping solution is ethanol as listed in Table 1.1, the solvent evaporation rate seems to be irrelevant to relative humidity in the present case. On the other hand, it seems reliable that the water adsorption rate from the ambient atmosphere is proportional to the relative humidity. The typical application of this phenomenon is the exposure of precursor solutions containing reactive alkoxides to humid atmosphere so as to proceed with the hydrolysis and polycondensation mildly [6, 10, 11]. Consequently, only the water adsorption rate would be affected by the relative humidity.

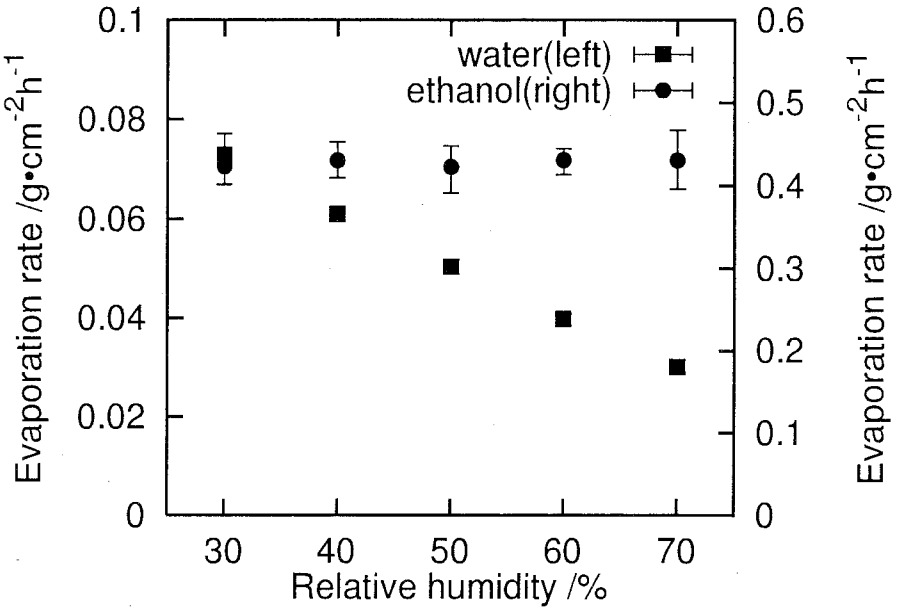

Fig. 1.6: Relative humidity dependence of the evaporation rates of water and ethanol.

The films prepared at higher withdrawal speed tend to be smooth. In addition, the withdrawal speed above which the smooth films are prepared decreases with an increase in relative humidity as listed in Table 1.2. Hence it is suggested that the morphology formation at higher withdrawal speed is dominated by the polycondensation resulting

from the water adsorption.

The fluidity reduction rate is assumed to be inversely proportional to the thickness of the sol film because the solvent evaporation rate across the top surface of the film is expected to be independent of the thickness. According to the theory of steady-state dip-coating process, the thickness profile with constant evaporation and no curvature effects can be expressed as follows [12,13]:

$$Sx = h(x)\left\{1 - \frac{h(x)^2}{3\lambda^2}\right\} \quad \text{where} \quad S = \frac{m}{\rho U_0}, \quad \lambda = \left(\frac{U_0\eta}{\rho g}\right)^{\frac{1}{2}}, \tag{1.1}$$

where $h(x)$ denotes the thickness at position x, m the evaporation rate, U_0 the withdrawal speed, g the gravity constant, η the viscosity, and ρ the density of the solution. The geometry of Eq. 1.1 is schematically shown in Fig. 1.7. Equation 1.1 predicts that the resultant thickness is proportional to λ and therefore proportional to $1/2$ power of withdrawal speed, although the actual thickness of gel film is reported to be proportional to 0.5–0.7 power of withdrawal speed probably due to the contribution from the surface energy term [14–17]. Thus it is suggested that the effect of fluidity reduction is significant in thinner films prepared at lower withdrawal speed. The effect of fluidity reduction due to the rapid solvent evaporation appears clearly at lower relative humidity as 30–40% RH, in which the film is smooth at lower withdrawal speed because the sol film is quickly dried out before the formation of macroscopic domain.

As the withdrawal speed increases, the rate of fluidity reduction slows down to give rise to the remarkable macroscopic domain formation. It is considered that the driving force for phase separation is the repulsive interaction between the titania oligomer modified by PEG and the solvent mixture. The mechanism of phase separation is discussed further in Chapters 2–4. Interestingly, the macroscopic domain formation is suppressed by increasing the withdrawal speed beyond a certain value. This result suggests that the polycondensation rate overcomes the phase separation rate at higher withdrawal speed, at which the polycondensation dominates the morphology.

Equation 1.1 indicates that the height of drying front is equal to $2\lambda/3S$ and the surface area of sol film exposed to the ambient atmosphere increases proportionally with $U_0^{3/2}$. The increase in surface area probably enhances the water adsorption and subsequent poly-

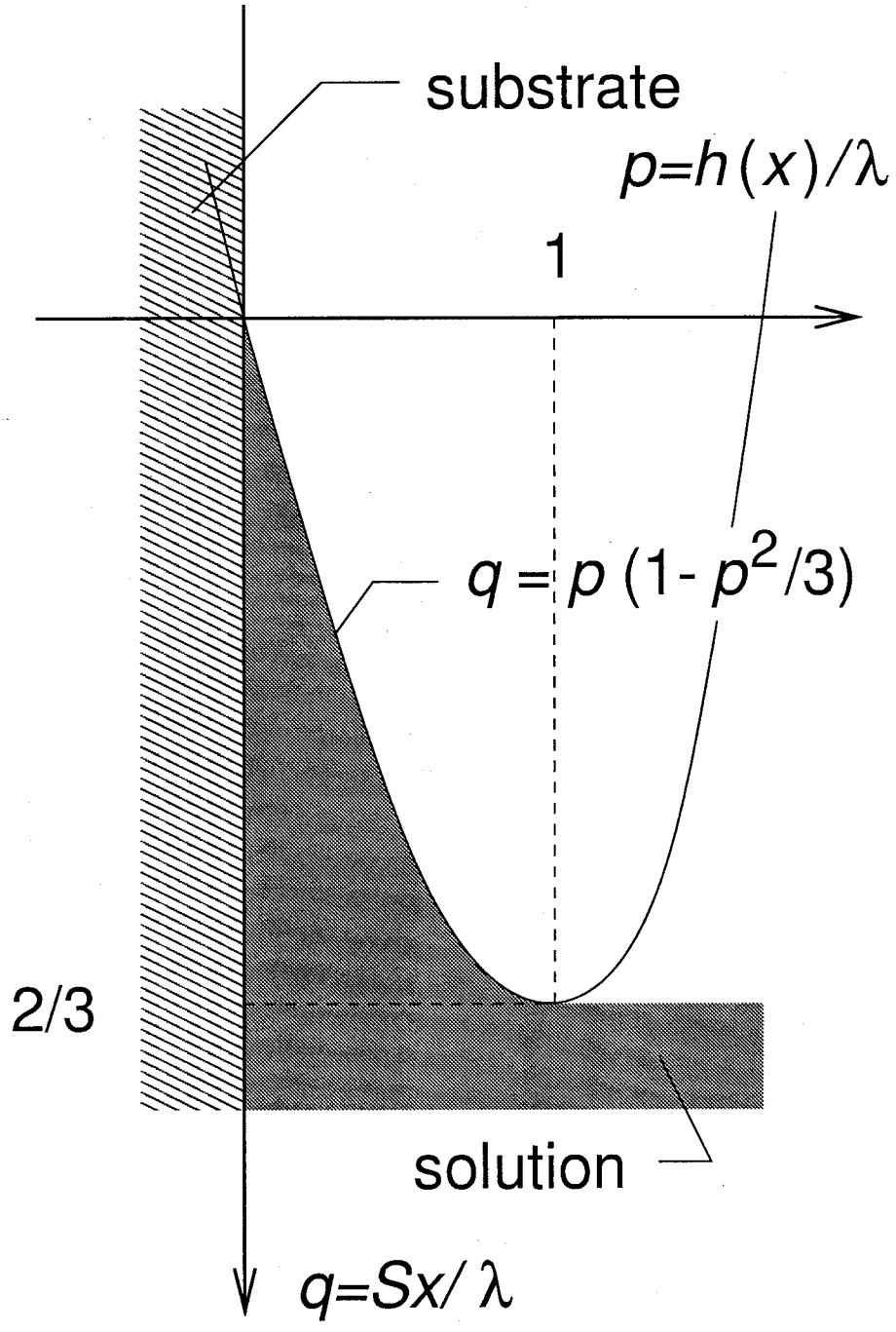

Fig. 1.7: Geometrical expression of Eq. 1.1.

condensation. Although the phase separation is also enhanced by the water adsorption as discussed later, the polycondensation of titanium-based highly-reactive alkoxide should overcome the phase separation at water-rich conditions. On the contrary, the phase separation seems to be suppressed at higher withdrawal speed because the slower reduction of solvent maintains the better compatibility among the constituents for a long time. Accordingly, both the accelerated polycondensation and the suppressed phase separation result in the reduction of domain formation at higher withdrawal speed.

From the discussion made so far, it is elucidated that the resultant morphology is dominated by the following three morphology determining parameters: (a) fluidity reduction due to solvent evaporation, (b) polycondensation of titania oligomer, and (c) phase separation between the titania oligomer adsorbed by PEG and the solvent mixture. The resultant morphology is determined by the competitive interaction among these parameters. The effect of solvent evaporation is the most important at lower withdrawal speed whereas the polycondensation dominates the morphology at higher withdrawal speed. Then the macroscopic domain formation can proceed at moderate withdrawal speed at which neither the polycondensation nor the fluidity reduction are remarkable.

1.3.2 Effect of humidity

The relationship between the phase separation rate and relative humidity is a subject to be discussed here. Assuming that the phase separation rate is independent of the relative humidity, the film prepared at 70% RH, 7.5 mm·min^{-1} should be smooth because the film prepared at 30% RH, 7.5 mm·min^{-1} is smooth and the fluidity reduction rate is irrelevant to relative humidity. Then it is suggested that the phase separation rate increases with an increase in relative humidity particularly at lower withdrawal speed. From the thermodynamics of the mixture of two chemically different polymeric components, the compatibility between the components can be expressed by Flory-Huggins formula as follows [18]:

$$\Delta G \sim RT \left\{ \left(\frac{\phi_1}{P_1} \right) \ln \phi_1 + \left(\frac{\phi_2}{P_2} \right) \ln \phi_2 + \chi_{12}(T) \phi_1 \phi_2 \right\}, \tag{1.2}$$

where ΔG represents the free energy change for mixing, ϕ_i and P_i $(i = 1, 2)$ respectively denote the volume fraction and polymerization degree of the component i, $\chi_{12}(T)$ the interaction parameter, R the gas constant, and T the absolute temperature. The $\chi_{12}(T)$ is

positive for the phase separating system in which the interaction between the components is repulsive. The reason of enhanced phase separation at higher relative humidity is possibly ascribable to the decreased compatibility between the titania oligomer and the solvent mixture due to the enhanced polycondensation of titania oligomer, namely, increase in P_1. However, increase of ΔG in such mechanism is suggested not to be appropriate to describe the phase separation in the systems containing strongly hydrogen-bonding polymers such as PEG [2]. The phase separation in such systems is explained by the solubility reduction of hydrolyzed oligomer after complexing with PEG. Similar discussion can be made for the present system by considering the enhanced hydrolysis owing to the accelerated water adsorption. The initial r of the dipping solution is not enough to finish the hydrolysis of TIP. However, the reminder alkoxy groups should be hydrolyzed promptly by the adsorbed water because the hydrolysis rate of titanium-based alkoxide is quite large [19]. The formation of hydroxy groups is supposed to accelerate the complexation of titania oligomer with PEG through hydrogen bond as described in Section 2.2. Considering that the driving force for phase separation is the repulsive interaction between the titania oligomer adsorbed by PEG and the solvent mixture, the moderate water adsorption probably accelerates the phase separation. This mechanism corresponds to $\chi_{12}(T)$ increase.

The macroscopic domain formation becomes less evident at higher relative humidity in the present study as typically seen from the comparison of Figs. 1.4 and 1.5. Such variation of morphology is contrary to the result of the system containing TEOS and MTES, in which both the distinctness and size of macroscopic domain increase linearly with an increase in relative humidity [4]. The above two systems are supposed to be different from the following standpoints. First, the hydrolysis and polycondensation rates of titanium-based alkoxides are generally far larger than that of silicon-based alkoxides [19]. Second, r is 1 in the present system whereas r of the TEOS-MTES system is 3–4. In the latter system, the water adsorption no longer accelerates the polycondensation considerably because the initial r is already enough to complete the hydrolysis theoretically, and such gradual acceleration of polycondensation with respect to relative humidity would be favorable for the phase separation. In the present titanium-based alkoxide system,

however, the macroscopic domain formation becomes difficult at higher relative humidity because of the drastic acceleration of polycondensation.

Figure 1.8 shows the change of the macroscopic morphology with the heat treatment at 500°C for 10 min. The heat treatment generated the macroscopic cracks whereas the macropores were already formed in the as-deposited film. It is considered that the macroscopic cracks are formed when the gel film is too soft to stand for the horizontal tensile stress emerged during the heat treatment, and the heat treatment is not responsible for the formation of macroporous morphology which is formed during the dipping operation. Such macroscopic cracks can also be created by the solvent evaporation and the following shrinkage of gel film just after the deposition but direct evidence was not found in the present experiment. The strength of gel film is expected to be increased by the enhanced water adsorption and the subsequent increase in metalloxane crosslinking density. Actually, the macroscopic cracks disappear at higher relative humidity due to the enhanced polycondensation as listed in Table 1.2. The macroscopic cracks are not found in the film prepared at higher withdrawal speed. It is supposed that the slower fluidity reduction increases the time during which the polycondensation proceeds and the tensile stress is relaxed by the formation of macropores. Furthermore, this result accords with the idea that the effect of polycondensation becomes significant at higher withdrawal speed.

Figure 1.9 exhibits the relative humidity and withdrawal speed dependence of thickness. The thickness of the films prepared by dip-coating methods has been reported to be proportional to 0.5–0.7 power of withdrawal speed [14–17]. The 0.5–0.7 power law seems to be acceptable for the dipping at higher relative humidity, while the thickness increases too steeply at lower relative humidity as shown in Fig. 1.9. It is noteworthy that the films having the macroscopic structure is thicker than the expected value. A careful observation of Fig. 1.9 reveals that the thickness at 7.5 mm·min^{-1} of withdrawal speed increases slightly with an increase in relative humidity simultaneously with the weakly formation of macroscopic structure. Consequently, it is considered that the vacant space formed in the gel film as a result of the macroscopic phase separation increases the thickness excessively.

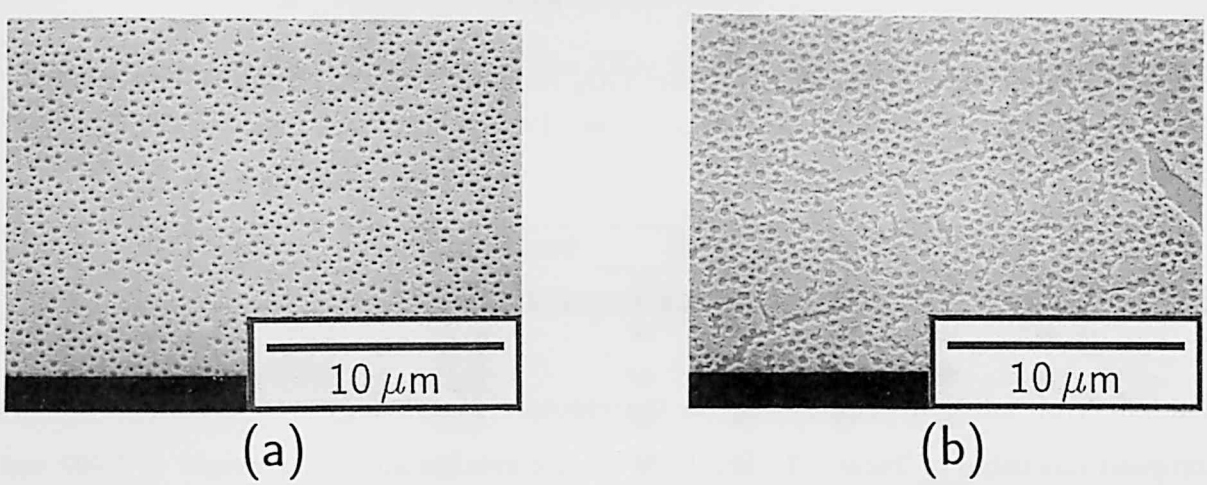

Fig. 1.8: SEM photographs of the TiO_2 films prepared at 30% RH, 22.5 mm·min^{-1}of withdrawal speed (a) without heat treatment, (b) with heat treatment at 500°C for 10 min. View angle is 45°.

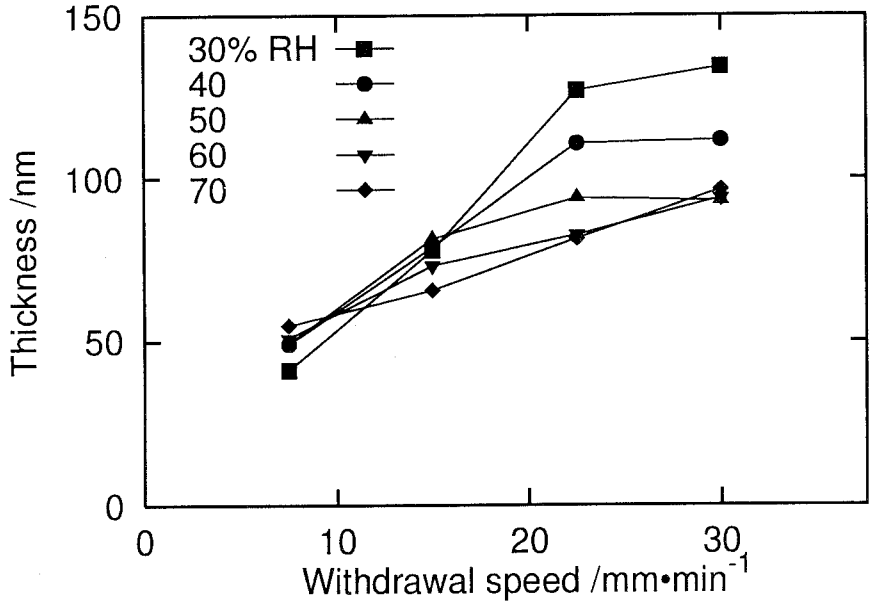

Fig. 1.9: Dependence of thickness of the TiO_2 films on relative humidity and withdrawal speed.

1.4 Effect of solution composition

The effect of solution composition on macroscopic morphology was examined for the compositions listed in Table 1.3. The PEG having average molecular weight of 2,000 was employed and the dipping was done at 25°C. Both water to TIP ratio ($r \equiv H_2O/TIP$) and TIP to ethanol ratio ($c \equiv TIP/EtOH$) are used to define the water and TIP concentrations, respectively.

Table 1.3: Compositions of the dipping and gelation test solutions (unit: mol).

	H_2O	EtOH	TIP	HNO_3	PEG (g)	H_2O/TIP, r
Dipping	0.10–0.14	1.0	0.12	0.02	5.0	0.83–1.17
	0.12	1.0	0.10–0.14	0.02	5.0	1.00
Gelation test A	0.15–0.30	1.0	0.12	0.02	0, 5.0	1.25–2.50
Gelation test B	0.22	0.7, 0.8	0.10–0.14	0.02	-	1.57–2.20
	0.24	1.0	0.10–0.14	0.02	-	1.71–2.40

1.4.1 Effect of water concentration

The morphology of the TiO_2 films was investigated at three water concentrations (r = 0.83, 1.00, and 1.17). The TIP concentration was fixed at $c = 0.12$. The variation of macroscopic morphology with r is summarized in Table 1.4. Figures 1.10 and 1.11 respectively show the SEM photographs of the films prepared at 15.0 and 30.0 mm·min^{-1} of withdrawal speeds at 30% RH. At lower relative humidity as 30% RH, the macroporous morphology became evident with an increase in r as also seen from Figs. 1.10 and 1.11. At high relative humidity as 70% RH, however, the morphology was quite smooth for the films prepared from the $r = 1.17$ system whereas the films were obviously macroporous particularly at lower withdrawal speed for the lower r systems as 0.83 and 1.00.

Table 1.4: Macroscopic morphology of the TiO_2 films under variation of water concentration at $c = 0.12$: -, smooth; ◡, pits; ●, macropores; ▲, uneven surface; C, macroscopic cracks.

H_2O/TIP, r	Withdrawal speed (mm·min^{-1})	Relative humidity (%RH)				
		30	40	50	60	70
0.83	7.5	◡	◡	◡	◡	◡
	15.0	◡	●	●	●	◡
	22.5	●	●	●	◡	-
	30.0	●	◡	-	-	-
1.00	7.5	C	◡C	◡	●	▲
	15.0	◡C	●C	●	▲	◡
	22.5	●C	●	●	◡	-
	30.0	●	●	-	-	-
1.17	7.5	◡C	●C	▲	▲	-
	15.0	●	◡	◡	◡	-
	22.5	●	◡	◡	-	-
	30.0	●	◡	-	-	-

Table 1.5 lists the variation of static gelation behavior with r at 40°C for the test solutions A, and exhibits that both the gelation time and the appearance of the test solution were quite sensitive to r. The appearance of the $r = 1.25$ solution did not change even after a week at 40°C. Then it is expected that the property of dipping solutions, all

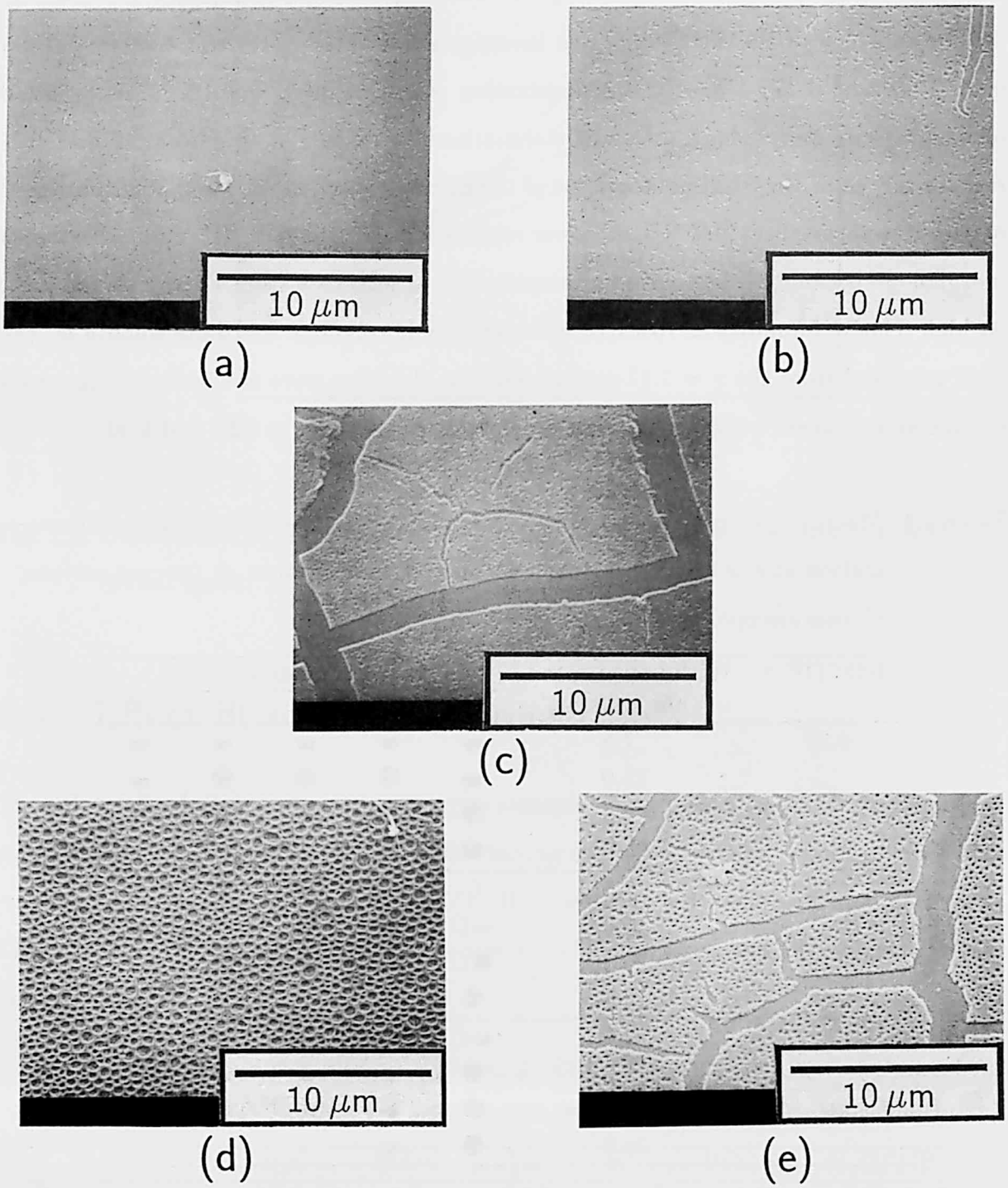

Fig. 1.10: SEM photographs of the TiO_2 films prepared at 30% RH, 15.0 mm·min^{-1} of withdrawal speed. (c, r) is (a) (0.10, 1.00), (b) (0.12, 0.83), (c) (0.12, 1.00), (d) (0.12, 1.17), (e) (0.14, 1.00). View angle is 45°.

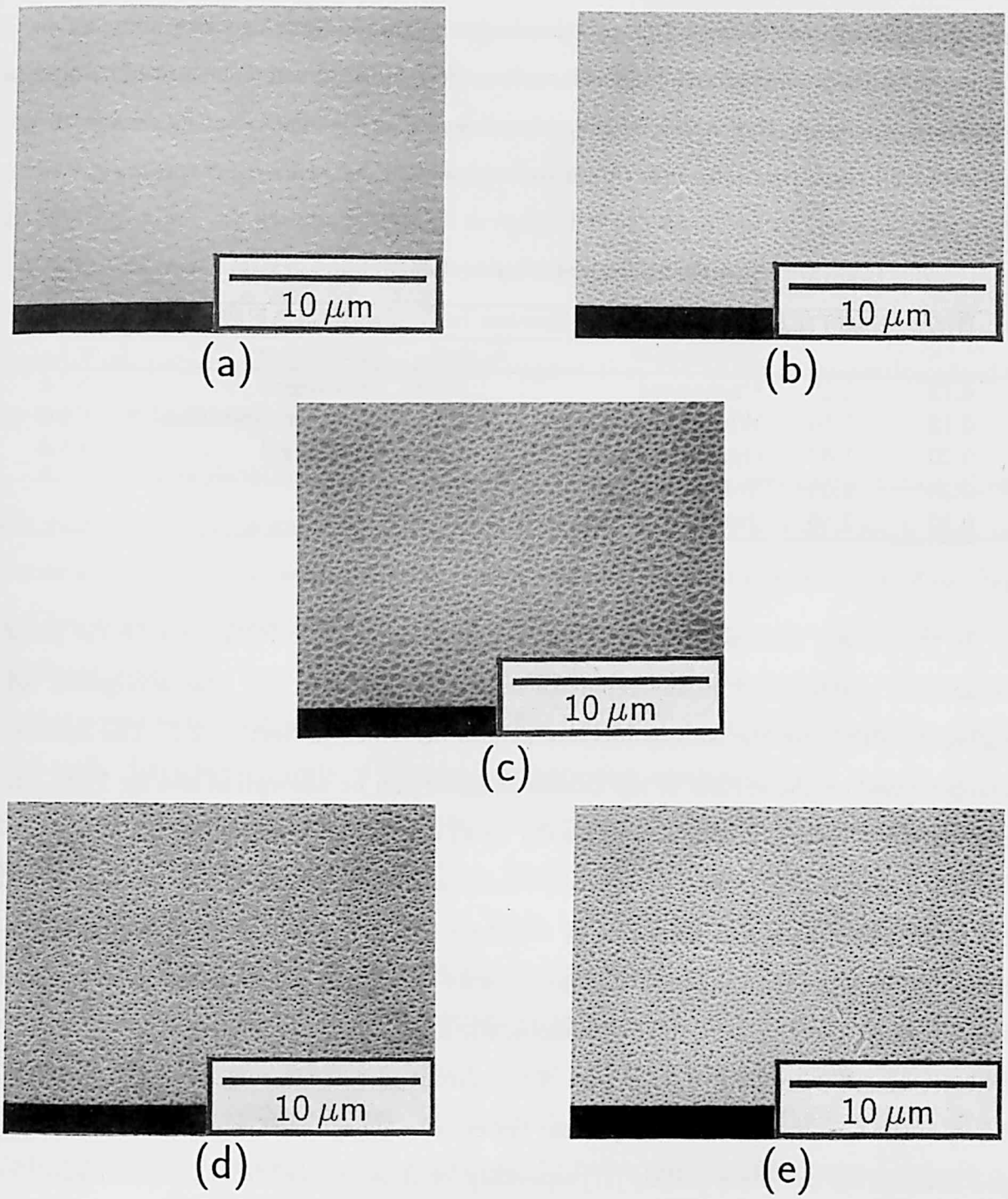

Fig. 1.11: SEM photographs of the TiO_2 films prepared at 30% RH, 30.0 mm·min^{-1} of withdrawal speed. (c, r) is (a) (0.10, 1.00), (b) (0.12, 0.83), (c) (0.12, 1.00), (d) (0.12, 1.17), (e) (0.14, 1.00). View angle is 45°.

of which r are smaller than 1.17, varies negligibly with time during the dipping operations at 25°C. In contrast, the $r = 1.50$ solution began to turbid within several hours at 40°C because the macroscopic particles which scatter the visible light were generated before the complete consumption of water by the polycondensation. It is noteworthy that both the gelation and the formation of precipitation were always delayed by incorporating PEG.

Table 1.5: Static gelation behavior at 40°C for the gelation test A.

H_2O	H_2O/TIP, r	PEG free		PEG 5.0	
		Appearance	t_g or t_{ps}	Appearance	t_g or t_{ps}
0.15	1.25	Unchanged	>7 d	Unchanged	>7 d
0.18	1.50	White precipitation	2.5 d	White precipitation	9 d
0.20	1.67	Opaque gel	1.5 d	Opaque gel	4.5 d
0.25	2.08	Transparent gel	<1 min	-	
0.30	2.50	Transparent gel	<1 min (0°C)	-	

In the present titania-based phase separating systems, the driving force for the phase separation is attributed to the repulsive interaction between the titania oligomer adsorbed by PEG and the solvent mixture as also described in Section 2.2. The hydroxy group formed on the surface of the titania oligomer can be adsorption site for PEG, but the number of hydroxy groups is originally small due to the smaller r as 1 and the consumption of hydroxy groups by the polycondensation. The relationship between r and the hydrolysis degree was examined by NMR for a TMOS-based system containing formamide [20], although the result may not directly be applied to the present titania-based system. In that experiment, the hydrophobic silica oligomer suddenly turns to hydrophilic by increasing r from 1.5 to 1.6 because of the abrupt increase in surface hydroxy density. Then on the assumptions that the present system also affords such change and the hydrolysis of alkoxides complete quickly [21] especially for those derived from the electropositive metals [19,22], the degree of water adsorption can be a dominant factor to determine the hydrophilicity of the titania oligomer. The phase separation is supposed to be accelerated by enhancing the hydrophilicity of titania oligomer and the following complexation with PEG. This supposition is consistent with the discussion made in Section 1.3 that the withdrawal speed for macroscopic domain formation decreases with an increase in rela-

tive humidity as listed in Table 1.4. In addition, the formation of titania-PEG complex achieves the relative enhancement of the phase separation because the hydroxy group adsorbed by PEG is inactivated to the polycondensation as listed in Table 1.5. At 30% RH, the macroscopic domain formation is most evident in the $r = 1.17$ system because the phase separation is preferentially accelerated at that water concentration. However, D at $30.0\,\mathrm{mm{\cdot}min^{-1}}$ of withdrawal speed is smaller than the other systems as shown in Fig. 1.11. Since the effect of water adsorption is greater at higher withdrawal speed, it is considered that the additionally adsorbed water accelerates not only the phase separation but also the polycondensation. These facts suggest that the water concentration should be moderate to enhance the domain formation.

An another explanation must be required for the macroscopic domain formation when the water adsorption is quite rapid. When r is small as 1, the sol is fluid enough because the smaller r in a highly acidic condition ensures the homogeneous distribution of smaller and less-branched titania oligomer [19]. However, the polycondensation degree increases nonlinearly against r near the percolation threshold at which the formation of spanning cluster gives rise to the gelation. The gelation test listed in Table 1.5 reflects such tendency very well. Since the viscosity of solution also increases nonlinearly with respect to the polycondensation degree [23], there should be a certain r at which the polycondensation is expected to overcome the phase separation. Besides, the great increase in PEG solubility by incorporating little water as listed in Table 5.8 in Chapter 5 can be an additional and probable reason for the suppressed phase separation. In the $r = 1.17$ system, the macroscopic domain formation is suppressed suddenly with a slight increase in relative humidity, because the orignal r is nearer to the critical r bringing about the smooth morphology than the other systems. The variation of morphology in the $r = 0.83$ system contrasts with that of the $r = 1.17$ system at the point that the macroscopic domain is formed even at higher relative humidity. However, the domain formation is not evident probably due to the weak interaction between the titania oligomer and PEG under a less-hydrolyzed condition.

The effect of water concentration is also discussed in Section 4.2.2 for extended solution compositions.

1.4.2 Effect of alkoxide concentration

The morphology of the TiO_2 films was examined at three TIP concentrations (c = 0.10, 0.12, and 0.14). Water concentration was fixed at r = 1.00 for all the dipping solutions. The variation of morphology with c is summarized in Table 1.6, and Figs. 1.10 and 1.11 show the relevant SEM photographs. In contrast to the variation with r listed in Table 1.4, the macroscopic domain formation became evident with an increase in c at almost all the dipping conditions. It is surprising that the resultant morphology is considerably varied by changing c slightly from 0.10 to 0.14 in spite of the same r as 1.00.

Table 1.6: Macroscopic morphology of the TiO_2 films under variation of TIP concentration at r = 1.00: -, smooth; ◡, pits; ●, macropores; ▲, uneven surface; C, macroscopic cracks.

TIP/EtOH, c	Withdrawal speed ($mm \cdot min^{-1}$)	Relative humidity (%RH)				
		30	40	50	60	70
0.10	7.5	-	-	-	▲	-
	15.0	◡	◡	▲	▲	-
	22.5	◡	▲	◡	-	-
	30.0	▲	●	-	-	-
0.12	7.5	C	◡C	◡	●	▲
	15.0	◡C	●C	●	▲	◡
	22.5	●C	●	●	◡	-
	30.0	●	●	-	-	-
0.14	7.5	C	●C	●C	●	●
	15.0	●C	●	●	●	◡
	22.5	●	●	●	◡	◡
	30.0	●	●	◡	-	-

Figures 1.12 and 1.13 show the solution composition and withdrawal speed dependence of the thickness. At 30% RH, the thickness increased considerably by increasing c and r as shown in Fig. 1.12. At 70% RH, in contrast, the thickness profile depended less on the solution composition as shown in Fig. 1.13. A careful observation revealed that the thickness is larger for the films having the macroscopic domain. These facts suggest that the thickness increases excessively not by the increase in solution viscosity but by the

macroscopic domain formation, and the viscosity would not be different largely among the present dipping solutions.

The variation of average pore diameter (D) with c and relative humidity is shown in Fig. 1.14. The D decreased with an increase in relative humidity. The morphology at an early stage of phase separation is frozen due to the rapid polycondensation when the relative humidity is raised at a fixed withdrawal speed. The D also decreased monotonically with an increase in c although the macroscopic domain became clear. Assuming that D reflects the degree of competitive interaction between the phase separation and the polycondensation, it is suggested that the phase separation is suppressed with an increase in c.

The upper limits of withdrawal speed and relative humidity for the macroscopic domain formation increase with an increase in c as listed in Table 1.6. Such tendency is particularly clear at 60% and 70% RH, at which the smooth film dominates the resultant morphology in the $c = 0.10$ system whereas the domain formation is considerable in the $c = 0.12$ and 0.14 systems. These results suggest that the polycondensation is more important at lower c. Both the enhanced phase separation and the suppressed polycondensation can explain the enhanced domain formation. However, the former mechanism is contradictory to the result that D decreases by increasing c as shown in Fig. 1.14. Therefore the polycondensation rate is supposed to be slowed down by increasing c.

Figure 1.15 shows the solution composition dependence of t_g at 0°C for the test solutions B. Transparent gel was always obtained indicating that the gelation proceeded homogeneously. The t_g exhibited a minimum at about $r = 2$ for all the series of compositions and decreased greatly by decreasing the amount of ethanol. In the solution of which r was larger than 2, an elastic behavior gradually appeared after the gelation because the reminder water continuously increased the crosslinking density of the gel. In contrast, the solution of which r is smaller than 2 had been viscous over the experimental period. The t_g could not be determined for the $r = 1.57$ (H_2O:TIP = 0.22:0.14) solutions of which viscosities were not high even after 1 d, although the initial onsets of viscosity were rapid due to the larger c.

When c is varied under fixed amounts of water and ethanol in the present TIP-based

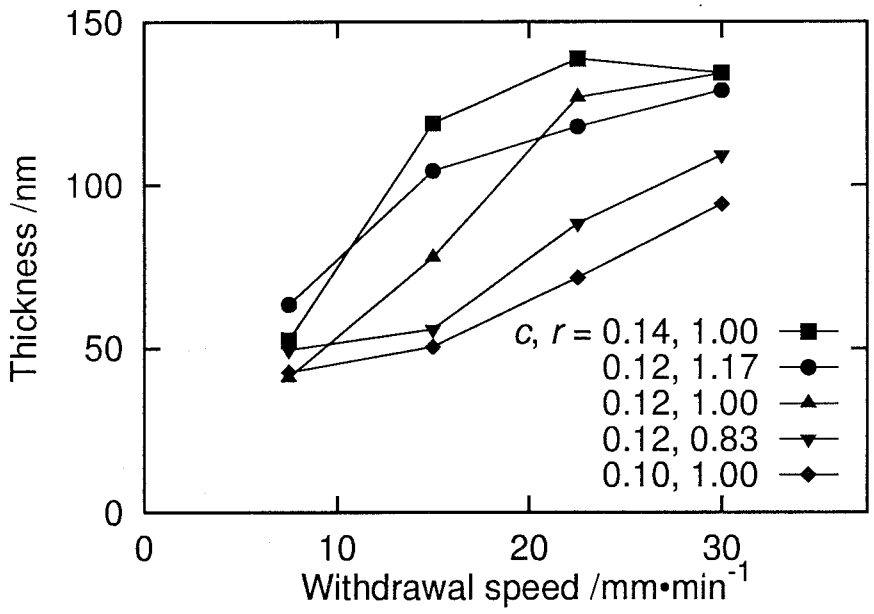

Fig. 1.12: Dependence of thickness on relative humidity and withdrawal speed for the TiO_2 films prepared at 30% RH.

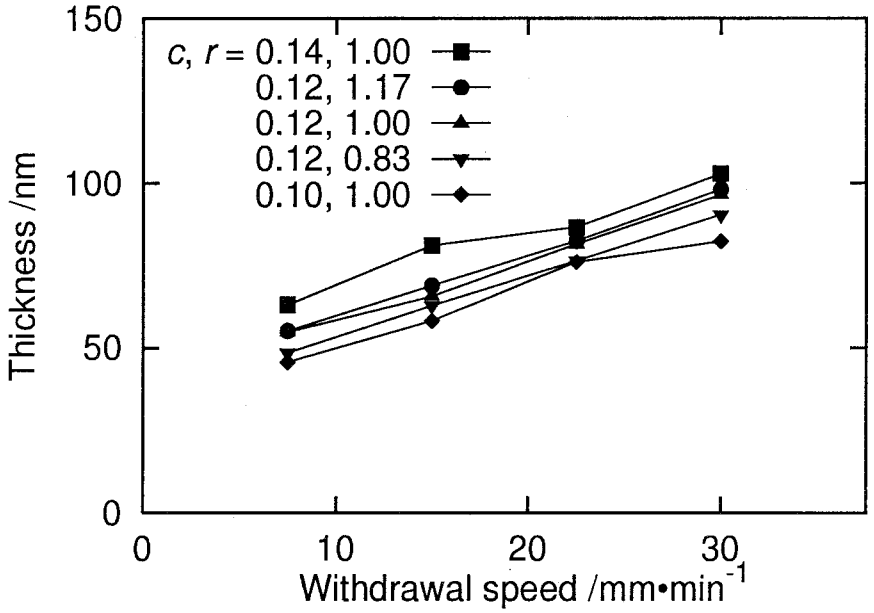

Fig. 1.13: Dependence of thickness on relative humidity and withdrawal speed for the TiO_2 films prepared at 70% RH.

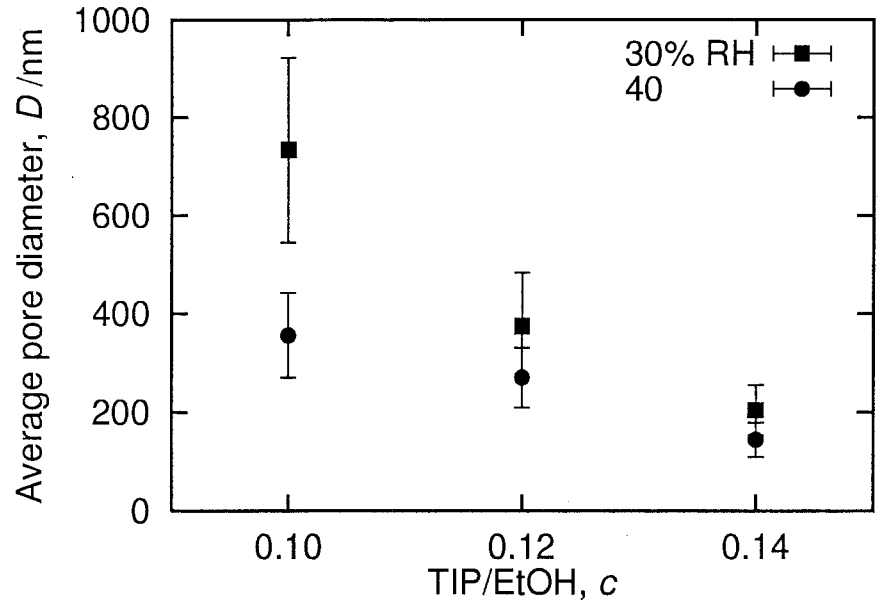

Fig. 1.14: Dependence of average pore diameter D on relative humidity and TIP concentration for the TiO_2 films prepared at 30.0 mm·min^{-1} of withdrawal speed. Water to TIP ratio r of the solution is fixed at 1.00.

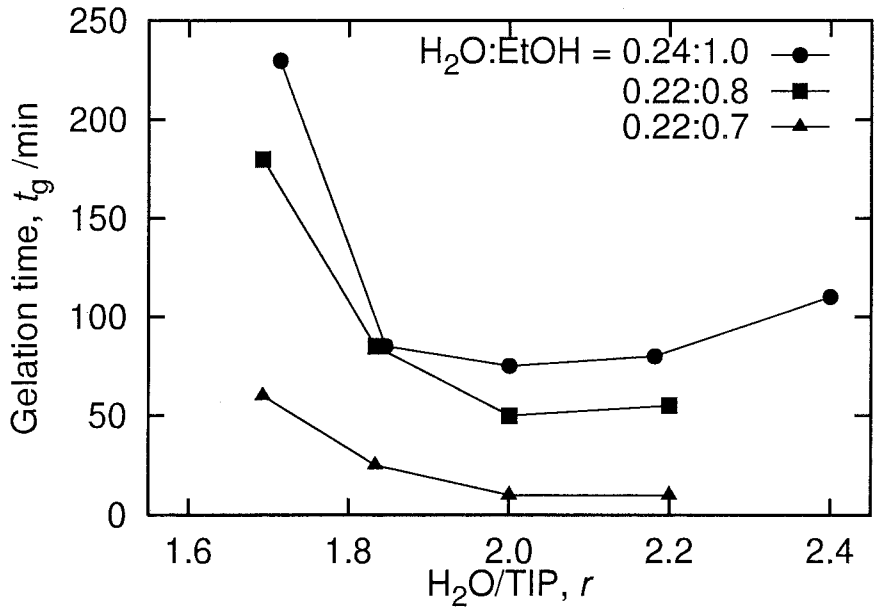

Fig. 1.15: Dependence of gelation time t_g at 0°C on solution composition for the gelation test B.

system, t_g is the shortest at around $r = 2$ and increases by separating r from 2 as shown in Fig. 1.15. When r becomes larger than 2, the polycondensation rate decreases because the collision frequency of the titania oligomer decreases with a decrease in c. However, the resultant gel turns to be elastic within the experimental period, because a lot of hydrolyzed precursors left unreacted among the loose network of spanning cluster realize the continuous increase in crosslinking density beyond the gelation. In such water-rich conditions, the polycondensation is expected to be accelerated by decreasing the amount of solvent phase, that is, by decreasing the average separation between the oligomers so as to increase the reaction probability. When r is smaller than 2, on the other hand, the viscosity increase saturates against time often before the gelation, because the exhaustion of water stops the polycondensation even before the bridging of less branched polymers formed preferentially in acidic conditions [19, 24]. Then decreasing the amount of the solvent phase is supposed to be ineffective to cause the gelation.

In the present system of which initial r is far smaller than 2, the polycondensation rate would be decreased with an increase in c because the amount of water necessary to cause the gelation increases with an increase in c. In addition, both the solution viscosity and thickness increase with an increase in c as shown in Fig. 1.13 possibly to slowdown the polycondensation although their increases are relatively small. Consequently due to the slower polycondensation, the number of the dipping conditions at which the domain formation occurs increases with an increase in c as shown in Fig. 1.6.

Another characteristic feature is the smooth morphology at $7.5\,\mathrm{mm{\cdot}min^{-1}}$ of withdrawal speed in the $c = 0.10$ system suggesting the rapid fluidity reduction. The smaller thickness is a possible candidate for the rapid drying because the thinner film dries rapidly. The fluidity of sol film may decrease abruptly if the rapid hydrolysis generates alcohol speedy, whereas the gradual release of alcohol under slower hydrolysis may extend the drying time of sol film. However, definite explanation can not be made at present.

The effect of TIP concentration is also discussed in Section 4.2.1 correlating with the effect of PEG concentration.

1.5 Conclusions

The variation of macroscopic morphology with withdrawal speed, ambient humidity, and solution composition particularly for water and alkoxide concentrations, was examined for the TiO_2 films prepared from the solution containing PEG. The results obtained are summarized as follows:

(1) For the TiO_2 films prepared from the solution containing PEG, the resultant morphology is determined by the competitive interaction among (a) fluidity reduction due to the evaporation of solvent, (b) network formation by the polycondensation of titania oligomer, and (c) macroscopic domain formation through the phase separation into the titania oligomer adsorbed by PEG and the solvent mixture. Since the effect of solvent evaporation is the most important at lower withdrawal speed whereas the polycondensation dominates the morphology at higher withdrawal speed, the macroscopic domain formation can be observed at moderate withdrawal speed at which neither the polycondensation nor the fluidity reduction are remarkable.

(2) The macroporous morphology becomes less evident with an increase in relative humidity, suggesting that the polycondensation is preferentially accelerated by the water adsorption at higher relative humidity.

(3) The optimum withdrawal speed for macroscopic domain formation decreases with an increase in relative humidity, suggesting that not only the polycondensation but also the phase separation are accelerated by increasing the water concentration. This result agrees well with the morphology change when the initial water concentration is increased, in which the macroscopic domain formation is enhanced at lower relative humidity but is suppressed at higher relative humidity. It is supposed that the phase separation is accelerated by the enhanced hydrolysis of titania oligomer and the subsequent complexation with PEG as long as the water concentration in the sol film is moderate. However, the polycondensation overcomes the phase separation when the water concentration is increased excessively.

(4) The macroscopic domain formation is enhanced with an increase in TIP concentration at almost all the dipping conditions. It is considered that the domain formation

becomes evident mainly due to the slowdown of the polycondensation at higher TIP concentration.

References

[1] K. Nakanishi and N. Soga, J. Am. Ceram. Soc. **74**, 2518 (1991).

[2] K. Nakanishi, H. Komura, R. Takahashi, and N. Soga, Bull. Chem. Soc. Jpn. **67**, 1327 (1994).

[3] K. Nakanishi, J. Porous Mater. **4**, 67 (1997).

[4] K. Makita, Y. Akamatsu, S. Yamazaki, Y. Kai, and Y. Abe, J. Ceram. Soc. Jpn. **105**, 1012 (1997).

[5] C. J. Brinker and G. W. Scherer, *Sol-Gel Science: The Physics and Chemistry of Sol-Gel Processing* (Academic Press, New York, 1990).

[6] S. Sakka, K. Kamiya, and T. Kato, Yogyo-Kyokai-Shi **90**, 555 (1982).

[7] G. L. Messing and W. T. Minehan, J. Ceram. Soc. Jpn. **99**, 1036 (1991).

[8] T. Ikemoto, K. Uematsu, N. Mizutani, and M. Kato, Yogyo-Kyokai-Shi **93**, 261 (1985).

[9] S. Sakka, H. Kozuka, and S.-H. Kim, in *Ultrastructure Processing of Advanced Ceramics*, edited by J. D. Mackenzie and D. R. Ulrich (John Wiley & Sons, New York, 1988), Chap. 10.

[10] T. Atarashi, A. Kishimoto, and K. Nakatsuka, J. Jpn. Soc. Powder and Powder Metallurgy **42**, 84 (1995).

[11] K. Kamiya, S. Sakka, and Y. Tatemichi, J. Mater. Sci. **15**, 1765 (1980).

[12] C. J. Brinker, A. J. Hurd, G. C. Frye, K. J. Ward, and C. S. Ashley, J. Non-Cryst. Solids **121**, 294 (1990).

[13] C. J. Brinker and G. W. Scherer, in *Sol-Gel Science: The Physics and Chemistry of Sol-Gel Processing* (Academic Press, New York, 1990), Chap. 13. See Ref. [5].

[14] I. Strawbridge and P. F. James, J. Non-Cryst. Solids **82**, 366 (1986).

[15] I. Strawbridge and P. F. James, J. Non-Cryst. Solids **86**, 381 (1986).

[16] S. Sakka and H. Kozuka, J. Non-Cryst. Solids **100**, 142 (1988).

[17] C. J. Brinker, A. J. Hurd, G. C. Frye, P. R. Schunk, and C. S. Ashley, J. Ceram. Soc. Jpn. **99**, 862 (1991).

[18] P. J. Flory, *Principles of Polymer Chemistry* (Cornell University Press, Ithaca, New York, 1971).

[19] C. J. Brinker and G. W. Scherer, in *Sol-Gel Science: The Physics and Chemistry of Sol-Gel Processing* (Academic Press, New York, 1990), Chap. 2. See Ref. [5].

[20] H. Kaji, K. Nakanishi, and N. Soga, J. Non-Cryst. Solids **181**, 16 (1995).

[21] K. C. Chen, T. Tsuchiya, and J. D. Mackenzie, J. Non-Cryst. Solids **81**, 227 (1986).

[22] J. Livage, M. Henry, and C. Sanchez, Prog. Solid State Chem. **18**, 259 (1988).

[23] C. J. Brinker and G. W. Scherer, in *Sol-Gel Science: The Physics and Chemistry of Sol-Gel Processing* (Academic Press, New York, 1990), Chap. 5. See Ref. [5].

[24] K. Kamiya, K. Tanimoto, and T. Yoko, J. Mater. Sci. Lett. **5**, 402 (1986).

Chapter 2

Effects of molecular weight and temperature on morphology in system containing poly(ethylene glycol)

2.1 Introduction

It is expected that the molecular weight of PEG is associated with the resultant morphology because the properties of organic polymers, such as melting point and solubility, usually depend on molecular weight. In the silica-based phase separating systems containing organic polymers, the resultant morphology of macroporous silica gel depends considerably on molecular weight of the polymer incorporated, because the type and degree of interactions among the constituents of the reaction mixture relate to the molecular weight [1]. Temperature is an another important factor which influences the reactivity of precursor as well as the compatibility among the constituents. In the film system, in particular, the fluidity reduction rate becomes an additional parameter which is sensitive to the dipping temperature and modifies the morphology formation during the dipping operation.

In this chapter, the variation of macroscopic morphology is examined by changing the molecular weight of PEG and the dipping temperature.

2.2 Effect of molecular weight

Table 2.1 lists the composition of dipping, gelation test, and viscosity test solutions. The PEGs having average molecular weights of 400, 1,000, 1,540, 2,000, 3,400, and 4,000 were used as polymer contents. The stirring temperature was raised to 45°C only when PEG

could not be dissolved completely under the stirring at 40°C for 1 h. The dipping temperature selected was high enough to avoid the reprecipitation of PEG. Figure 2.1 shows the variation of the saturated vapor pressures of water and ethanol with temperature. The relative humidity inside the chamber was set as listed in Table 2.2 so as to reproduce the water vapor pressure at 25°C, 40% RH assuming that the water adsorption rate from the ambient atmosphere is proportional to the water vapor pressure.

Table 2.1: Compositions of the dipping, gelation test, and viscosity test solutions (unit: mol).

	H_2O	EtOH	TIP	HNO_3	PEG (g)
Dipping	0.12	1.0	0.12	0.02	5.0
Gelation test	0.20	1.0	0.12	0.02	0–5.0
Viscosity test	0.10	1.0	-	-	0–10.0

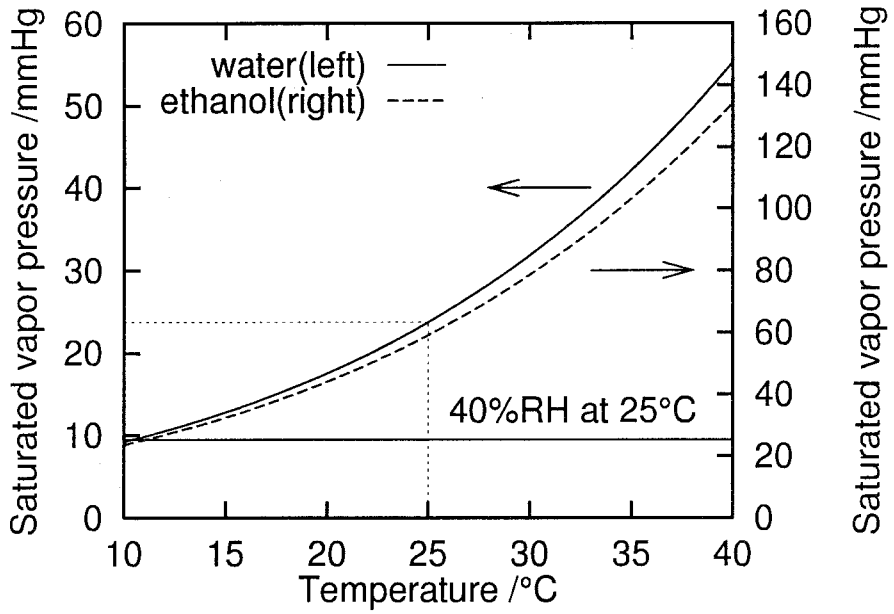

Fig. 2.1: Temperature dependence of saturated vapor pressures of water and ethanol.

Table 2.3 lists the variation of macroscopic morphology with molecular weight of PEG and dipping temperature. The SEM photographs of the TiO_2 films prepared at 30.0 and

Table 2.2: Temperature dependence of saturated water vapor pressure and relative humidity preserving the partial water vapor pressure at 25°C, 40% RH (9.5 mmHg).

Temperature (°C)	15	20	25	30	35
Saturated water pressure (mmHg)	12.8	17.5	23.8	31.8	42.2
Relative humidity (%RH)	74	54	40	30	23

60.0 mm·min^{-1} of withdrawal speeds are also shown in Figs. 2.2 and 2.3, respectively. The macroscopic domain formation was most apparent in the PEG2000 system. The domain formation exhibited maximum against the withdrawal speed in consistent with the results described in Section 1.3. The withdrawal speed for domain formation increased with an increase in dipping temperature. Macroscopic cracks were always observed in the PEG3400 system although the macropores were seen at higher withdrawal speed. In contrast, the film was always smooth in the PEG1540 system.

Table 2.3: Macroscopic morphology of the TiO_2 films under variations of molecular weight of PEG and dipping temperature: -, smooth; ◡, pits; ●, macropores; C, macroscopic cracks.

System	Dipping temperature (°C)	Withdrawal speed (mm·min^{-1})					
		7.5	15.0	22.5	30.0	45.0	60.0
PEG1540	20	-	-	-	-	-	-
	35	-	-	-	-	-	-
PEG2000	25	-	◡	●	●	◡	-
	30	-	◡	◡	●	●	◡
	35	-	◡	◡	◡	●	●
PEG3400	35	C	C	◡C	◡C	◡C	◡C

Figure 2.4 shows the variation of gelation time (t_g) for the gelation test solutions of which compositions are listed in Table 2.1. Each solution gradually increased its viscosity and turbidity, and finally transformed to a white, opaque, and homogeneous gel after several days. The PEG-free solution exhibited the shortest t_g. The t_gs of the PEG3400

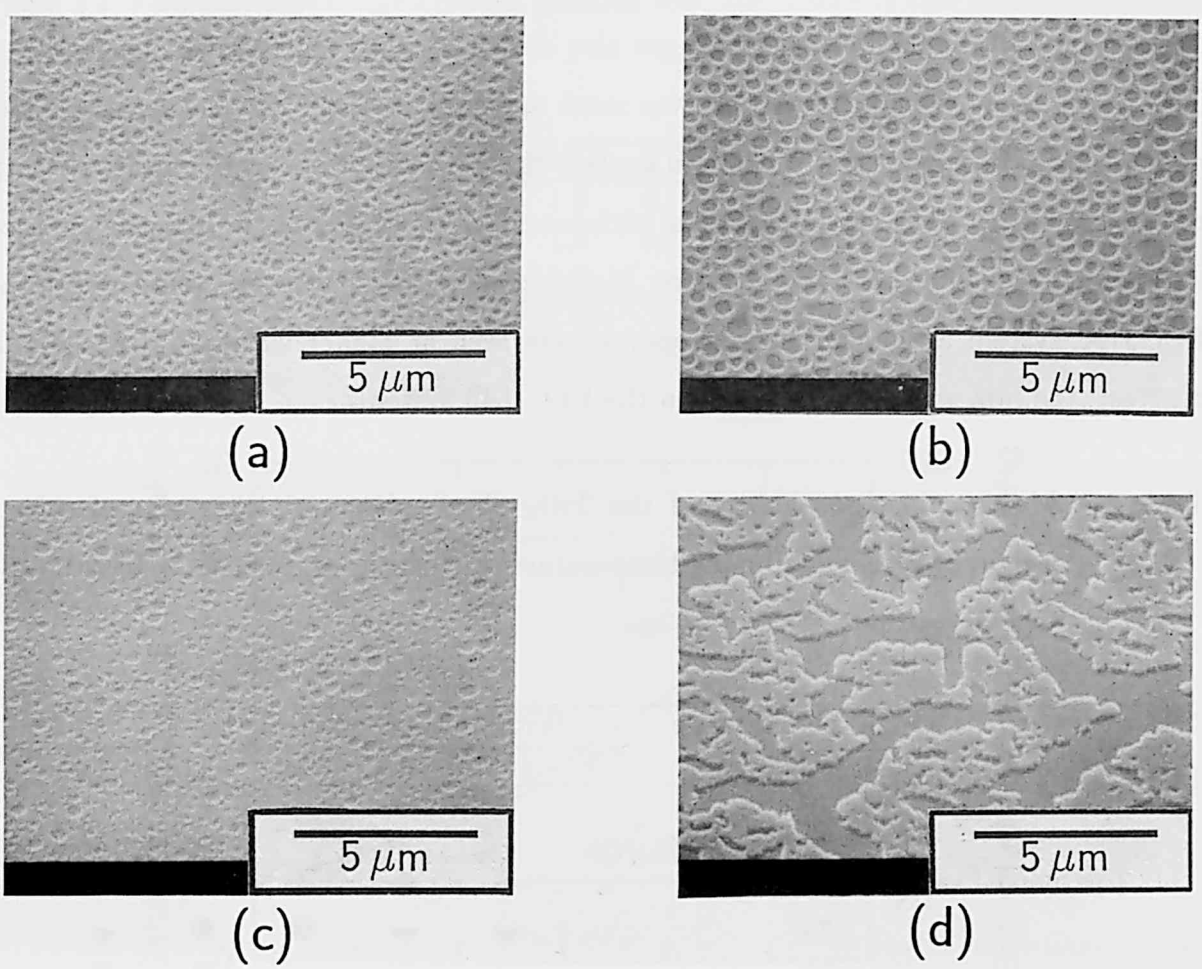

Fig. 2.2: SEM photographs of the TiO_2 films prepared at 30.0 mm·min^{-1} of withdrawal speed. Dipping temperature is (a) 25, (b) 30, (c) 35°C for the PEG2000 system, and (d) 35°C for the PEG3400 system. View angle is 45°.

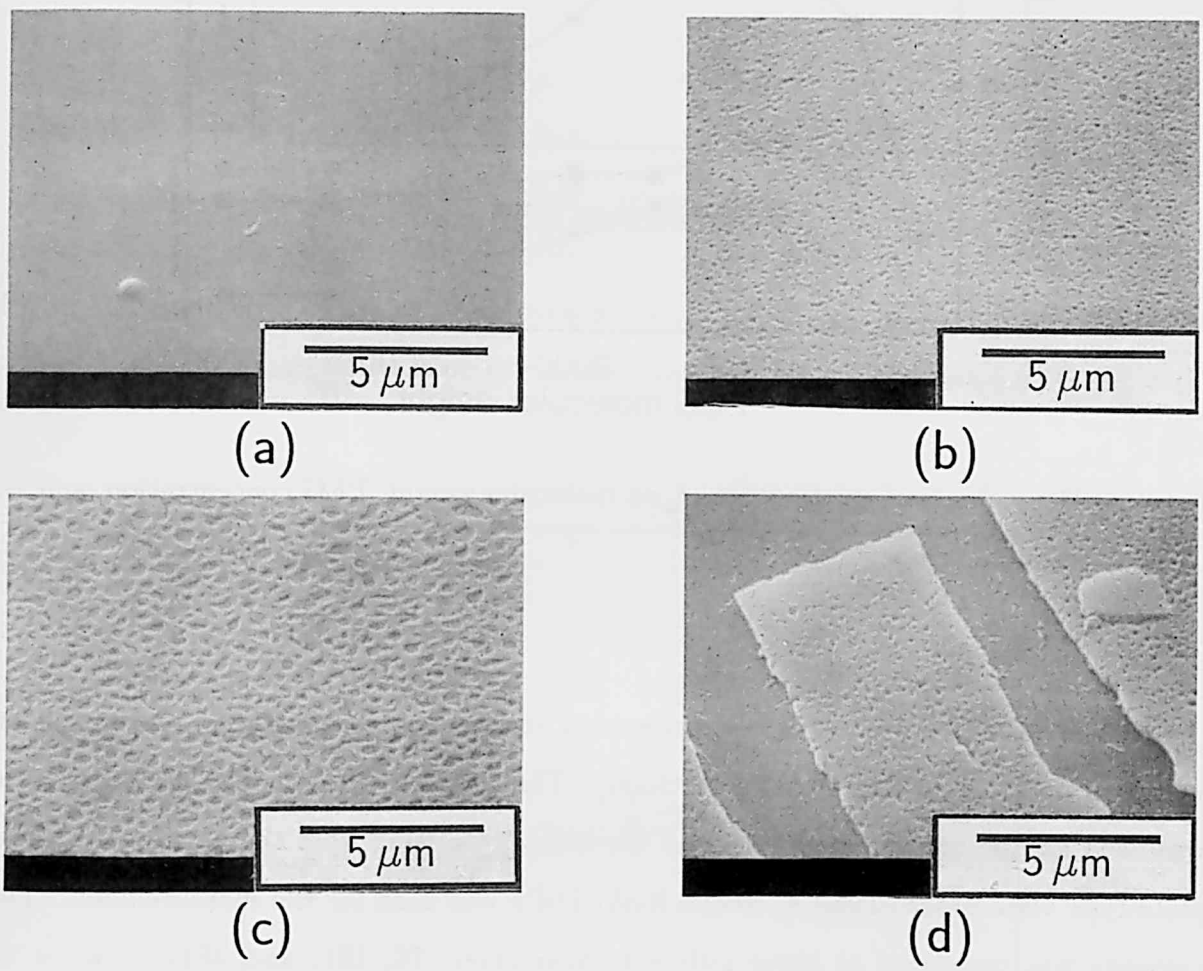

Fig. 2.3: SEM photographs of the TiO_2 films prepared at 60.0 mm·min^{-1} of withdrawal speed. Dipping temperature is (a) 25, (b) 30, (c) 35°C for the PEG2000 system, and (d) 35°C for the PEG3400 system. View angle is 45°.

and PEG4000 systems were considerably shorter than those of the other systems containing PEG having lower molecular weight. At all the molecular weights, t_g increased by increasing the PEG concentration but decreased by increasing the gelation temperature.

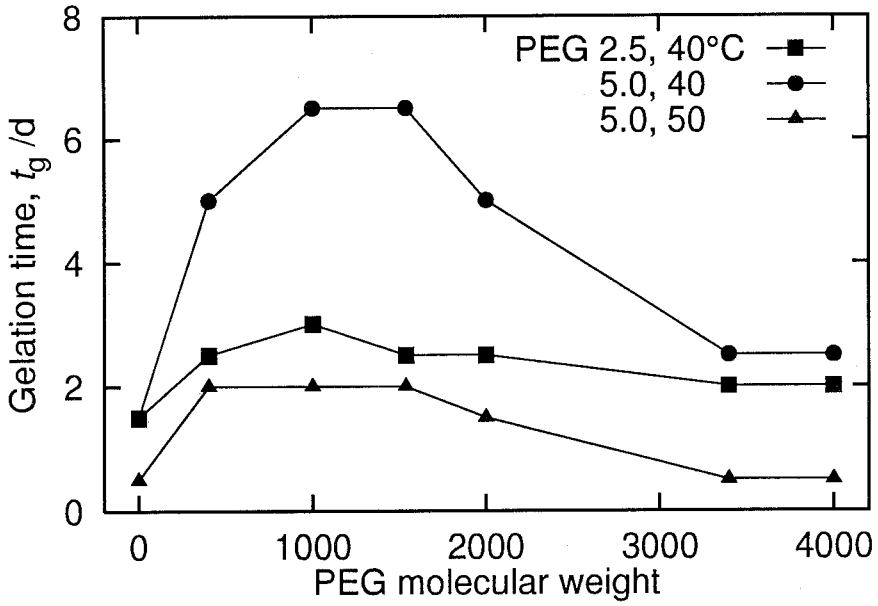

Fig. 2.4: Dependence of gelation time t_g on molecular weight, PEG concentration, and gelation temperature.

Figures 2.5 and 2.6 show the dependence of viscosity on concentration and molecular weight of PEG at 30 and 40°C, respectively. The solution without TIP and nitric acid was used for the measurement to avoid the difficulty arising from the gelation. A cone-plate-type viscometer (Type E, Tokyo-Keiki Ltd.) was used for the measurement.[1] The viscosity was measured at three different shear rates (76, 191, and 383 s^{-1}) while no apparent difference was found. The viscosity increased by increasing the concentration and molecular weight of PEG, and by decreasing the solution temperature.

Since PEG consists of hydrophilic terminal hydroxy groups and rather hydrophobic oxyethylene chain, solubility of PEG depends largely on molecular weight. In general, the solubility of organic polymer decreases with an increase in molecular weight owing to

[1] Viscosity measurements were carried out in cooperation with Prof. H. Kozuka of the Institute for Chemical Research, Kyoto University.

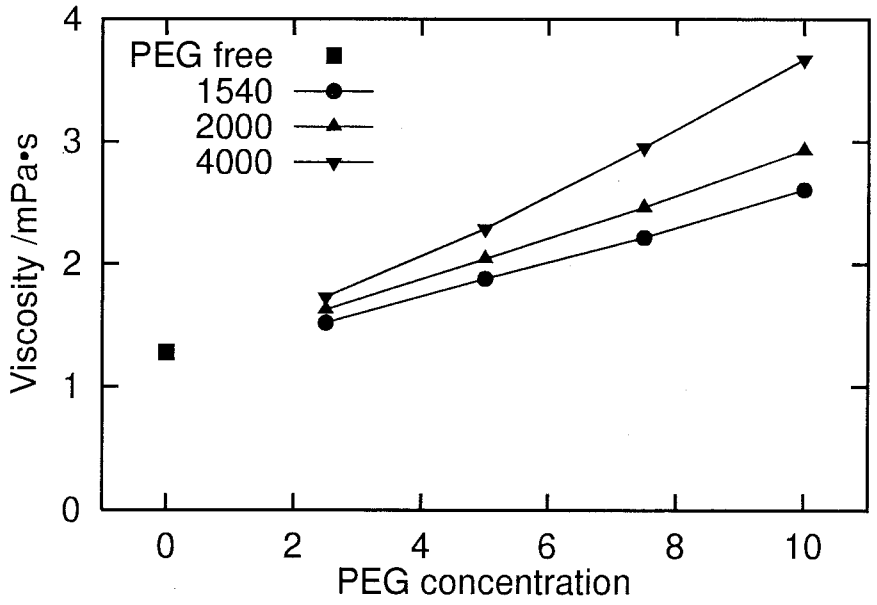

Fig. 2.5: Dependence of viscosity on concentration and molecular weight of PEG at 30°C for the test solution composed only of water, ethanol, and PEG.

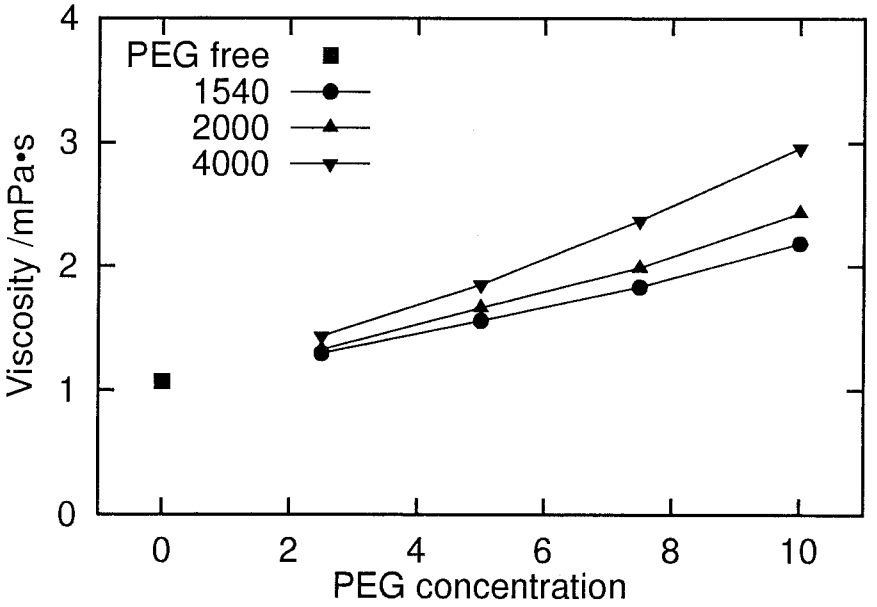

Fig. 2.6: Dependence of viscosity on concentration and molecular weight of PEG at 40°C for the test solution composed only of water, ethanol, and PEG.

the decrease in mixing entropy. Additionally, PEG having higher molecular weight tends to be less soluble in polar solvents, because the hydrophilic terminal effect is suppressed while the enhanced interaction between the oxyethylene units stabilizes the aggregates and the ordered helical structure [2–5]. The temperature-composition phase diagram of PEG-water system indicates that the compatibility between PEG and water decreases with an increase in molecular weight particularly when the molecular weight is smaller than 10,000 [6]. Such variation is consistent with the molecular weight dependence of interaction parameter (χ) between PEG and water [7]. Since several PEG-alcohol systems also exhibit similar variations of χ [8], it is reasonable to consider that the compatibility between PEG and the alcohol-based solvent mixture decreases largely by increasing the molecular weight from 400 to 4,000. Actually, the solubility of PEG in alcohols decreases considerably by increasing the molecular weight from 1,000 to 2,000 as listed in Table 3.10 of Chapter 3.

It is known that PEG adsorbs exothermically onto hydrolyzed oxides by forming hydrogen bonds between the ether oxygens of PEG and the hydroxy groups on oxides [9,10]. Similarly, PEG is also reported to adsorb on titania and zirconia surfaces [11]. Moreover, direct chelation of oxygen atoms of PEG to the metal atom of alkoxide seems to be probable for the system containing alkoxides consisting of electropositive atom and affording coordination expansion. The adsorbed amount of polymer usually increases with an increase in molecular weight as verified theoretically [12, 13] and experimentally [10, 11] because the complexation strength increases in proportion with the number of hydrogen bonds. In poor solvents, the polymer adsorption is enhanced excessively because the solvation of polymer is thermodynamically unfavorable [12]. In the silica-based sol-gel systems containing PEG, the driving force for phase separation is attributed to the repulsive interaction between the oligomeric alkoxide adsorbed by PEG and the solvent mixture, because the hydrated structure of silica oligomer is destroyed by PEG [14, 15]. Assuming that the titania oligomer modified by PEG inherits the dissolution property of PEG, the phase separation strength should become remarkable with an increase in molecular weight of PEG.

The smooth morphology in the PEG1540 system listed in Table 2.3 indicates that

the larger affinity between PEG1540 and the solvent mixture suppresses the macroscopic domain formation. Nonetheless, the domain formation is possible even in the PEG1540 system typically under the addition of long-chain alcohols such as 1-propanol and 1-butanol so as to decrease the solubility of PEG. The details are described in Section 3.3.

The t_g increase with an increase in PEG concentration shown in Fig. 2.4 suggests that the polycondensation is suppressed by the modification of titania oligomer with PEG. Considering that the interaction between the titania oligomer and PEG is stronger at higher molecular weight, the formation of macroscopic cracks in the PEG3400 system is attributed to the lower crosslinking density. However, t_gs in the PEG3400 and PEG4000 systems are considerably shorter than those in the systems containing PEG having lower molecular weight. Despite of the interfered polycondensation, the phase separation advances the apparent gelation in the PEG3400 and PEG4000 systems in which the titania oligomers are concentrated in the gel phase to increase the reaction probability [14]. This would be an another evidence of the enhanced phase separation at higher molecular weight. The macroporous morphology in the PEG3400 system is less striking compared to that in the PEG2000 system as shown in Figs. 2.2 and 2.3, and Table 2.3 especially at lower withdrawal speed. In the solution containing higher molecular weight of PEG, the viscosity increases more rapidly with an increase in PEG concentration as shown in Figs. 2.5 and 2.6. Then it is supposed that the higher viscosity of PEG3400 suppresses the macroscopic domain formation when the solvent evaporates rapidly.

2.3 Effect of dipping temperature

Figure 2.7 shows the dependence of average pore diameter (D) on withdrawal speed and dipping temperature. The withdrawal speed at which D shows maximum was shifted to higher withdrawal speed by increasing the dipping temperature in accordance with the variation of morphology listed in Table 2.3.

Figures 2.8 and 2.9 show the dependence of thickness on withdrawal speed and dipping temperature in the PEG1540 and PEG2000 systems, respectively. The thickness increased almost monotonically with an increase in withdrawal speed in the PEG1540 system. In contrast, the thickness always exhibited a maximum against the withdrawal speed in the

PEG2000 system. The withdrawal speed for maximum thickness almost conformed to that of maximum D shown in Fig. 2.7.

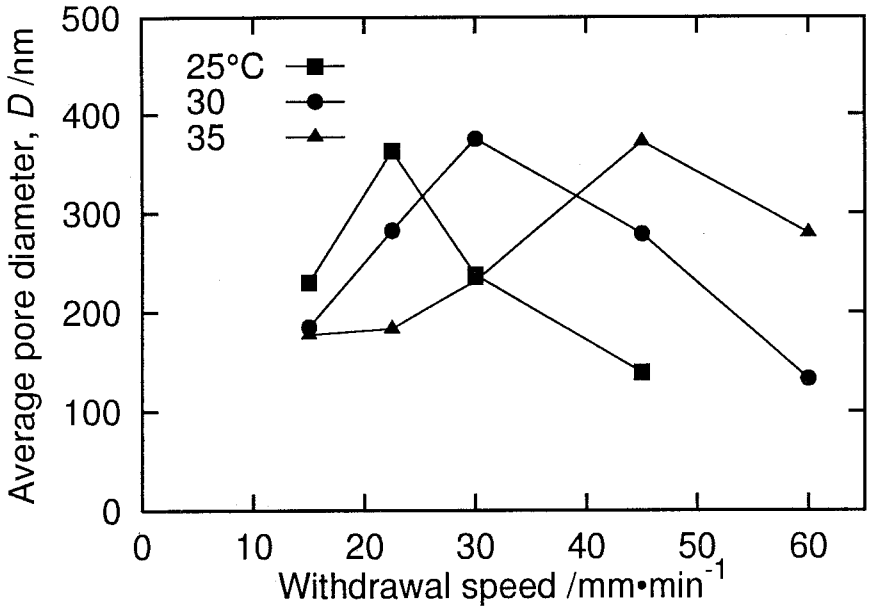

Fig. 2.7: Dependence of average pore diameter D on withdrawal speed and dipping temperature in the PEG2000 system.

It is considered that the macroscopic morphology is chiefly determined by the competition among (a) decrease in fluidity due to the evaporation of solvent, (b) polycondensation assisted by adsorption of ambient water, and (c) macroscopic domain formation simultaneously with the phase separation into gel and solvent phases triggered by the supersaturation of PEG as discussed in Section 1.3. The effect of solvent evaporation is important at lower withdrawal speed because the fluidity reduction of sol film is emphasized by the smaller thickness. On the contrary, the morphology at higher withdrawal speed is dominated by the polycondensation. Then the domain formation takes place only at moderate withdrawal speed at which neither the solvent evaporation nor the polycondensation are remarkable compared to the phase separation as listed in Table 2.3. In the case where both the polycondensation and the phase separation are more accelerated than the solvent evaporation typically by increasing the relative humidity, the withdrawal speed for macroscopic domain formation decreases as described in Section 1.3.

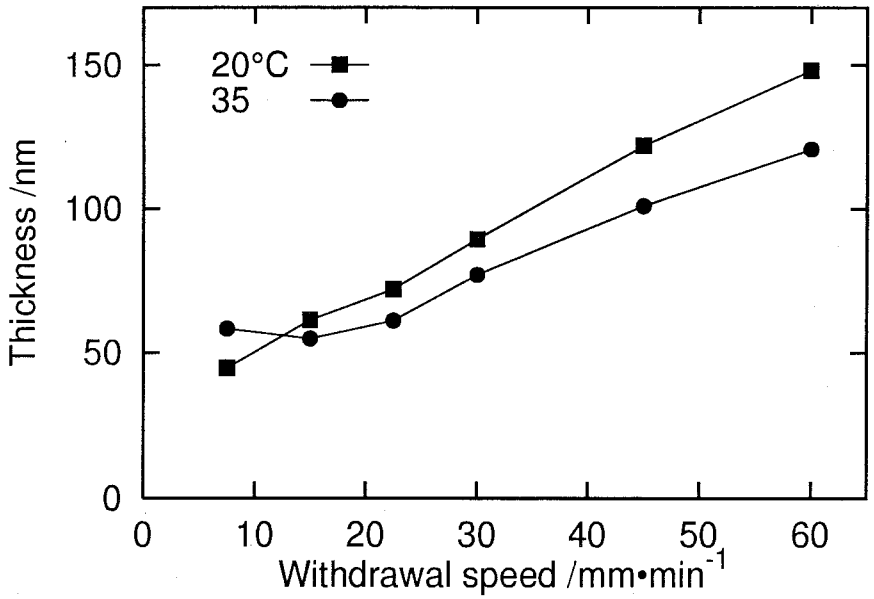

Fig. 2.8: Dependence of thickness on withdrawal speed and dipping temperature in the PEG1540 system.

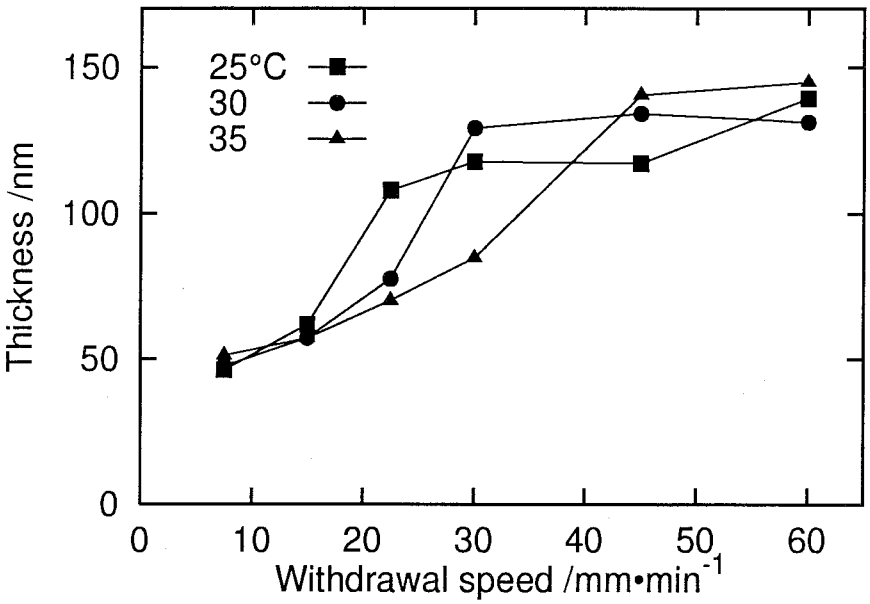

Fig. 2.9: Dependence of thickness on withdrawal speed and dipping temperature in the PEG2000 system.

The solvent evaporation rate is related to the saturated vapor pressure shown in Fig. 2.1 and increases with an increase in temperature. The polycondensation is also accelerated as experimentally shown in Fig. 2.4. The enhanced polycondensation at higher temperature is verified by the accelerated increase in solution viscosity [16] and by the almost exponential dependence of t_g on reciprocal temperature [17]. The solubility of PEG in the present precursor solution is better at higher temperature. Such the enhanced compatibility between PEG and the solvent mixture suppresses the phase separation in a closed system [15]. Against the supposition expected from above facts that the domain formation is suppressed at higher temperature, the withdrawal speed for macroscopic domain formation increases with an increase in dipping temperature as clearly shown in Figs. 2.7 and 2.9. These results suggest that the solvent evaporation and the phase separation are more accelerated than the polycondensation. The decrease in thickness at higher temperature shown in Fig. 2.8 can also highlight the effect of solvent evaporation. The enhanced compatibility at higher temperature would not be important in the present system similarly to the case when the external solvent of which boiling point is lower than ethanol is added, in which the phase separation is accelerated even if the external solvent increases the solubility of PEG to some extent as discussed in Section 3.2. The rapid removal of solvent would accelerate the supersaturation and exsolution of the titania-PEG complex. Consequently, it can be concluded that the increase in withdrawal speed for macroscopic domain formation at higher temperature in the PEG2000 system is owing to the accelerated solvent evaporation and results in thicker macroporous films. Nevertheless, the resultant film is smooth as ever even at 35°C in the PEG1540 system.

2.4 Conclusions

The variation of macroscopic morphology with molecular weight of PEG and dipping temperature was investigated for the TiO_2 films prepared from the solution containing PEG. The results obtained are summarized as follows:

(1) The macroporous morphology is formed only within the narrow range of molecular weight because the compatibility between PEG and the solvent mixture depends significantly on molecular weight of PEG. The morphology is always smooth at lower molecular

weight due to the good solubility of PEG, while the suppressed polycondensation enhances the formation of macroscopic cracks at higher molecular weight.

(2) The withdrawal speed for macroscopic domain formation increases with an increase in dipping temperature because the fluidity reduction and the phase separation are more accelerated than the polycondensation because of the enhanced solvent evaporation.

References

[1] K. Nakanishi, J. Porous Mater. **4**, 67 (1997).

[2] K.-J. Liu and J. L. Parsons, Macromolecules **2**, 529 (1969).

[3] J. Maxfield and I. W. Shepherd, Polymer **16**, 505 (1975).

[4] H. Daoust and D. St-Cyr, Macromolecules **17**, 596 (1984).

[5] K. Devanand and J. C. Selser, Nature **343**, 739 (1990).

[6] S. Saeki, N. Kuwahara, M. Nakata, and M. Kaneko, Polymer **17**, 685 (1976).

[7] A. Kagemoto, S. Murakami, and R. Fujishiro, Makromol. Chem. **105**, 154 (1967).

[8] A. Kagemoto, Y. Itoi, Y. Baba, and R. Fujishiro, Makromol. Chem. **150**, 255 (1971).

[9] J. Rubio and J. A. Kitchener, J. Colloid Interface Sci. **57**, 132 (1976).

[10] G. L. Howard, C. C. Ma, and C. W. Yip, Polym. Commun. **24**, 182 (1983).

[11] B. Siffert and J. F. Li, Colloid. Surf. **40**, 207 (1989).

[12] J. M. H. M. Scheutjens and G. J. Fleer, J. Phys. Chem. **83**, 1619 (1979).

[13] J. M. H. M. Scheutjens and G. J. Fleer, J. Phys. Chem. **84**, 178 (1980).

[14] K. Nakanishi, H. Komura, R. Takahashi, and N. Soga, Bull. Chem. Soc. Jpn. **67**, 1327 (1994).

[15] K. Nakanishi and N. Soga, Bull. Chem. Soc. Jpn. **70**, 587 (1997).

[16] S. Sakka and H. Kozuka, J. Non-Cryst. Solids **100**, 142 (1988).

[17] C. J. Brinker and G. W. Scherer, in *Sol-Gel Science: The Physics and Chemistry of Sol-Gel Processing* (Academic Press, New York, 1990), Chap. 5.

Chapter 3

Effect of chemical additives on morphology in system containing poly(ethylene glycol)

3.1 Introduction

It has been known that the reaction mechanism as well as the resultant morphology of gels can be modified by adding chemical compounds in sol-gel processes. The physical effects of external additives are to modify the surface tention and volatility of the solvent phase in the gel [1,2], and to vary the compatibility among the oligomeric alkoxide, solvent mixture, and additionally incorporated materials such as organic polymers [3–5]. On the other hand, the chemical reactions in the sol-gel processes such as hydrolysis and polycondensation can directly be modified by the functional groups of chemical additives [6–8]. Although the effect of chemical additives is often not simple, it is anticipated that a lot of information about the detail of sol-gel reactions can be obtained by examining the effects of chemical additives intensively. In addition, the resultant morphology is expected to be varied more widely by incorporating chemical additives.

The macroscopic domain formation is difficult at higher relative humidity in the ethanol-based system due to the rapid polycondensation in water-rich conditions as described in Chapter 1. Conversely, that result also suggests that the incorporation of chemical additives which slow down the polycondensation would permit the macroscopic domain formation even in a humid atmosphere. One of the empirical way to reduce the reactivity of alkoxides is to exchange the alkoxy groups with the longer ones. If the effect of humidity becomes negligible, it is additionally expected that the severe control of ambient humidity is no longer necessary to reproduce the desired morphology. The phase separation strength is another important factor affecting the resultant morphology. In

general, the solubility of PEG in alcohols decreases with an increase in the size of alkyl groups [9]. Considering that the dissolution property of titania oligomer adsorbed by PEG inherits that of PEG, the enhanced phase separation is also anticipated by incorporating such less-polar alcohols.

In the former section of this chapter, the variation of macroscopic morphology is investigated under the addition of various types of chemical additives of which properties are not similar to each other. In the latter section, the effect of chemical additives on macroscopic morphology is examined particularly for the systems incorporated alcohols having larger alkyl groups than ethanol.

3.2 System containing various types of organic solvents

Various organic solvents of which boiling points (T_b) and molecular weights (M.W.) are listed in Table 3.1 were employed as additives. The values of solubility parameter (δ_s), which is a measure of solvent polarity and is defined as a square root of cohesive energy density of a solvent, are also listed. In all the experiments, 20 wt% of ethanol was replaced by equivalent weight of an external solvent as listed in Table 3.2. The mixture of ethanol, water, and 60 wt% aqueous solution of nitric acid were added to ice-cooled TIP dissolved in the reminder ethanol and external solvent except for the case of the MeOH system. Since a large amount of white precipitation formed, probably oligomeric compound of methoxy-substituted TIP, prevented the stirring in the above described procedure, methanol was incorporated in the opposite solution. The PEG having average molecular weight of 2,000 was employed. The film was deposited at 25°C, 30% RH.

Figure 3.1 shows the SEM photographs of the TiO_2 films prepared from the EtOH system under the variation of withdrawal speed. The macroscopic domain formation exhibited a maximum against the withdrawal speed in consistent with the results shown in Section 1.3. Figures 3.2 and 3.3 respectively show the SEM photographs of the films prepared at 15.0 and 30.0 $mm \cdot min^{-1}$ of withdrawal speeds from the systems containing external solvents. It is noteworthy that the morphology was quite similar among the EtOH, PrOH, and HEX systems. In the DMK and MeOH systems, the domain formation

Table 3.1: Abbreviations and physical properties of various solvents employed.

Solvent (Abbreviation)		Solubility parameter, $\delta_s(\mathrm{cal}^{1/2}\cdot\mathrm{cm}^{-3/2})$	Boiling point, $T_b(°\mathrm{C})$	M.W.
n-Hexane	(HEX)	7.3	69	86.18
Diethylketone	(DEK)	8.8	102	86.13
Cyclohexanone	(CHK)	9.9	155	98.14
Dimethylketone (acetone)	(DMK)	9.9	56	58.08
1-Propanol	(PrOH)	11.9	97	60.10
Ethanol	(EtOH)	12.7	78	46.07
Methanol	(MeOH)	14.5	65	32.04
N,*N*-Dimethylformamide	(DMF)	12.1	153	73.09
Formamide	(FA)	19.2	110	45.04
2-Propanol			82	60.10

Table 3.2: Compositions of the dipping, gelation test, and compatibility test solutions (unit: mol).

	TIP	H_2O	EtOH	External solvent	HNO_3	PEG (g)
Dipping	0.12	0.12	0.8	$(0.2)^{(a)}$	0.02	5.0
Gelation test	0.12	0.20	0.8	$(0.2)^{(a)}$	0–0.02	0, 5.0
Compatibility test	-	-	8.0 g	2.0 g	-	0.1–10.0 g

(a) Equal weights of ethanol and external solvent are substituted. The parenthesized value indicates the molar of external solvent in terms of ethanol.

was most apparent at 15.0 mm·min^{-1} of withdrawal speed, which is slower than that in the EtOH system. The morphology was almost smooth in the CHK, DMF, and FA systems. The whole variation of morphology is summarized in Table 3.3.

Table 3.3: Macroscopic morphology of the TiO_2 films under variations of type of external solvent and withdrawal speed: -, smooth; ◡, pits; ●, macropores; ▲, uneven surface; C, macroscopic cracks.

Withdrawal speed (mm·min^{-1})	External solvent								
	HEX	PrOH	EtOH	DEK	DMF	CHK	MeOH	DMK	FA
15.0	◡C	◡C	◡C	◡	-	◡	●	▲	-
30.0	●	●	●	●	-	-	●	●	-
45.0	◡	●	●	●	-	-	◡	●	-
60.0	-	◡	◡	-	-	-	-	◡	-

3.2.1 Variation of morphology with solubility of poly(ethylene glycol)

Figure 3.4 shows the solubility of PEG in the ethanol solution of external solvent at 25°C. The solubility of PEG, which was judged from the transparency of the test solution after stirring at 25°C for 1 h, was greatly influenced by incorporating only 20 wt% of external solvent. The FA system dissolved PEG very well because the solvents having strongly hydrogen bonding character, such as water and formamide, usually solvate PEG well by forming hydrogen bond to the ether oxygen of PEG [10–12]. However, definite relationship was not found between the solubility of PEG and δ_s of external solvent particularly at lower δ_s. One of the possible reasons is that δ_s involves the various properties of solvent, such as dispersive effect, dielectric effect, and hydrogen bonding effect. On the other hand, PEG dissolves well in benzene [11–13] but is insoluble in alkanes although both of them are non-polar hydrocarbons. Therefore hydrophobic interaction between the ethylene group of PEG and solvent molecules is suggested to be important in some cases for the solvation of PEG.

It is considered that water in the reaction mixture is consumed quickly due to the

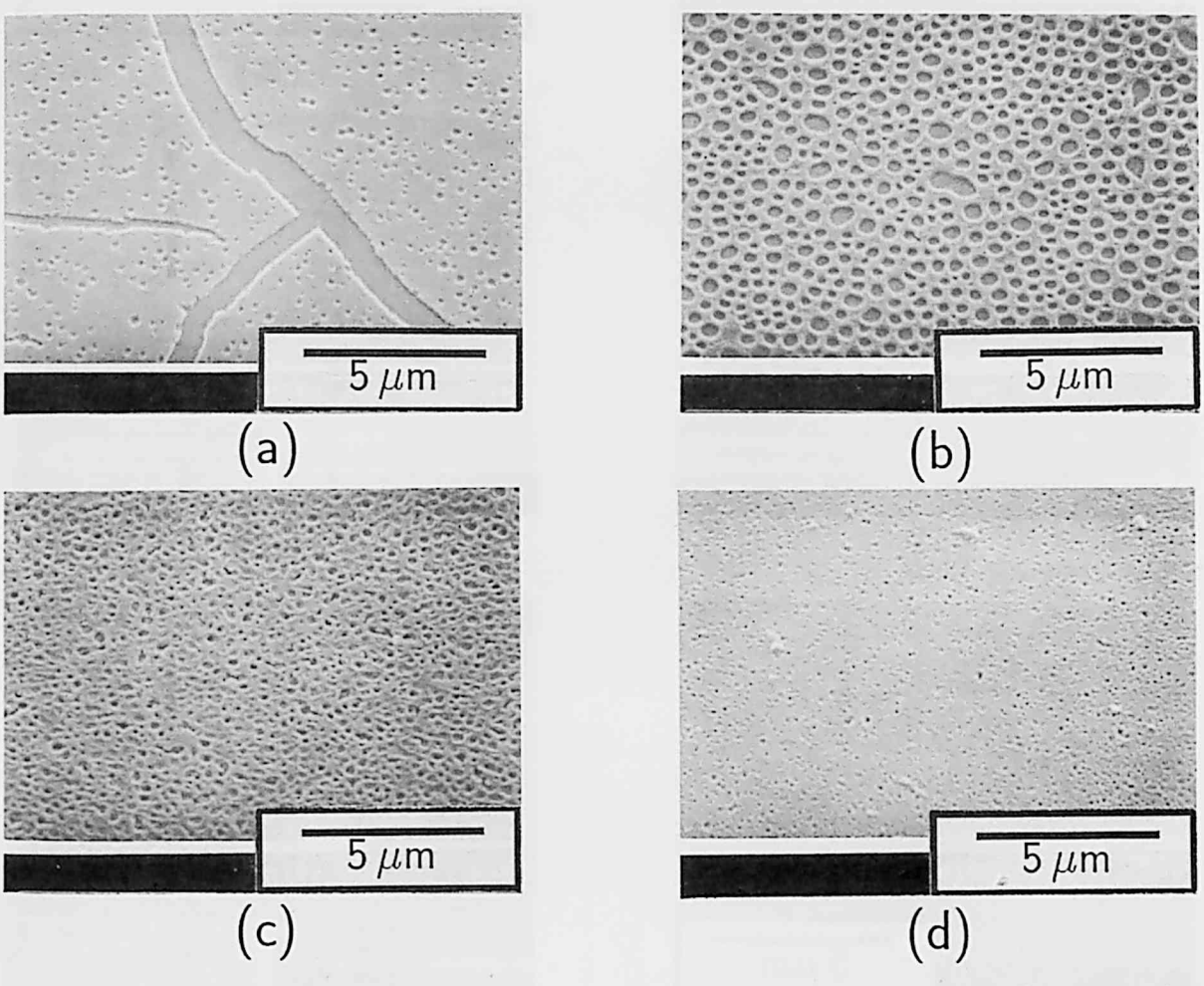

Fig. 3.1: SEM photographs of the TiO_2 films prepared from the EtOH system. Withdrawal speed is (a) 15.0, (b) 30.0, (c) 45.0, (d) 60.0 mm·min^{-1}. View angle is 45°.

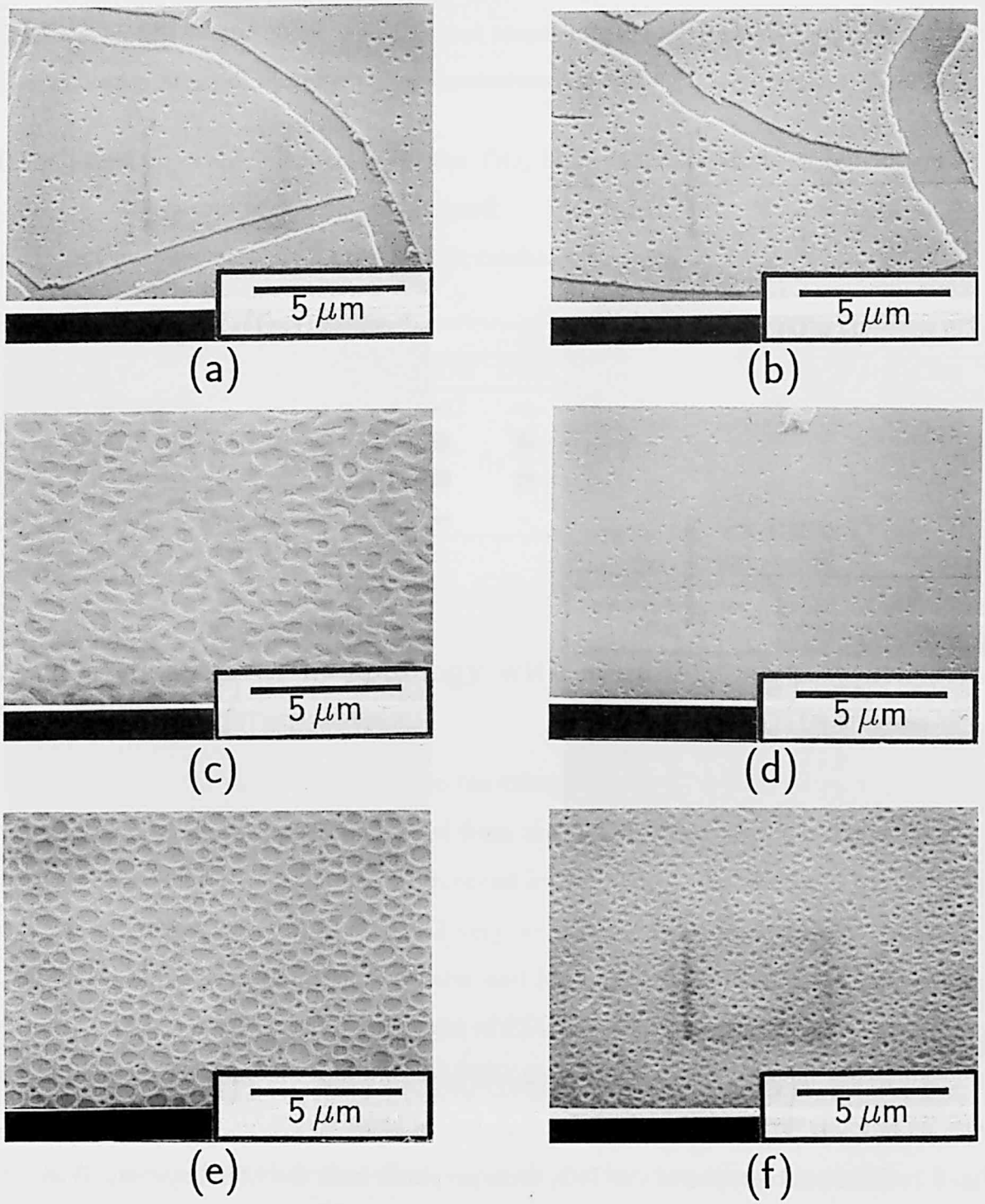

Fig. 3.2: SEM photographs of the TiO_2 films prepared at 15.0 mm·min^{-1} of withdrawal speed under the addition of (a) HEX, (b) PrOH, (c) DMK, (d) DEK, (e) MeOH, (f) CHK. View angle is 45°.

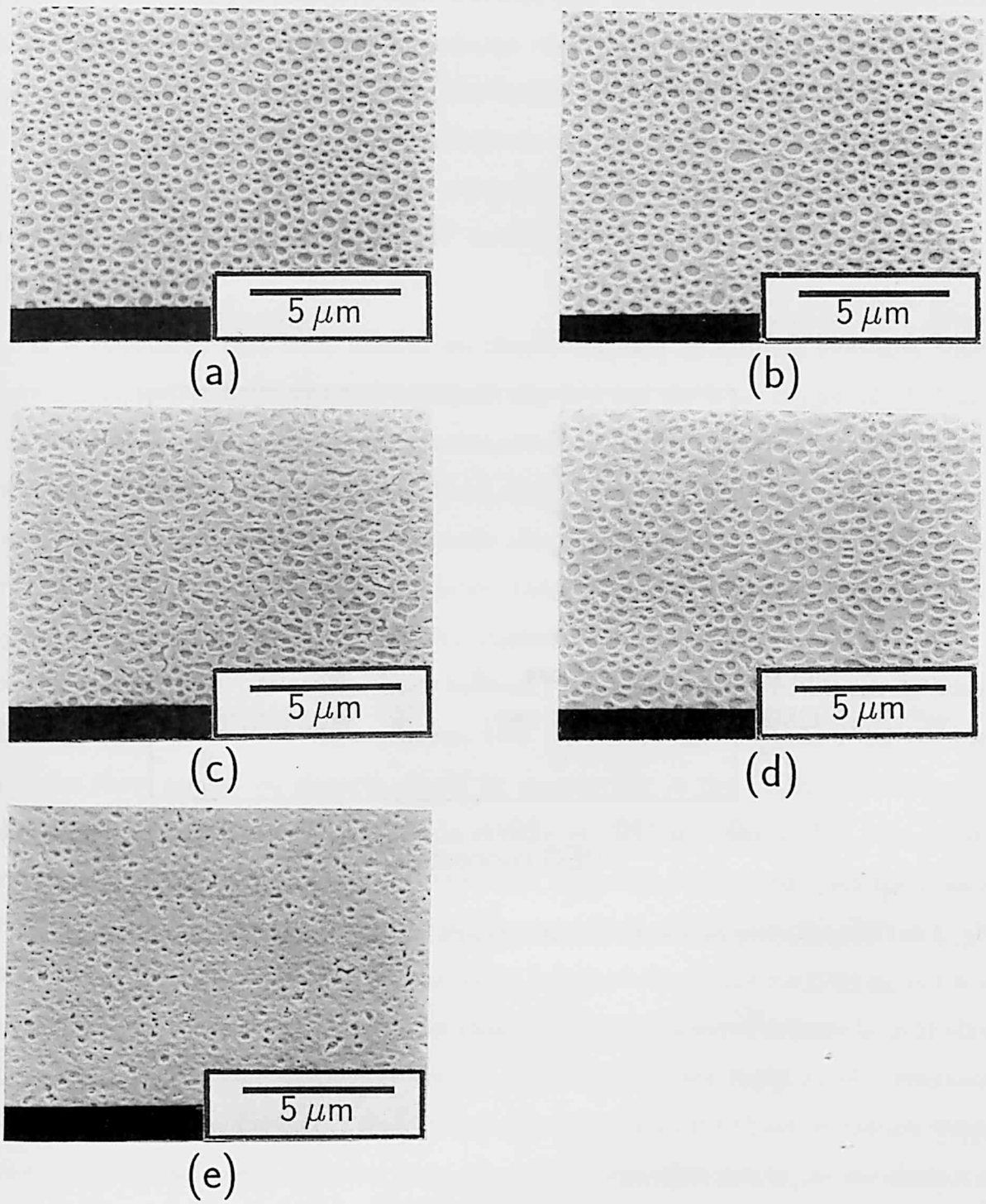

Fig. 3.3: SEM photographs of the TiO_2 films prepared at 30.0 mm·min^{-1} of withdrawal speed under the addition of (a) HEX, (b) PrOH, (c) DMK, (d) DEK, (e) MeOH. View angle is 45°.

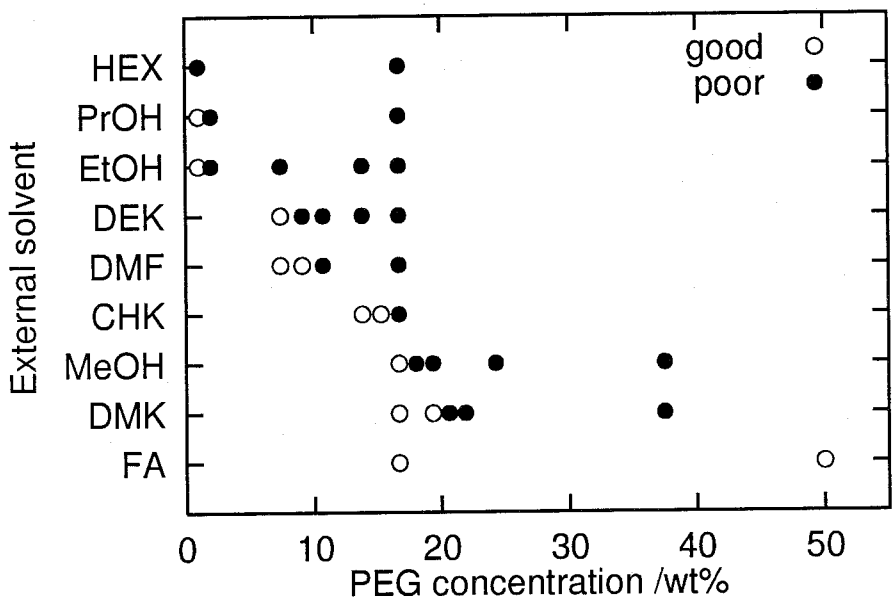

Fig. 3.4: Compatibility between PEG and 20 wt% ethanol solution of external solvent at 25°C.

higher hydrolysis rate of titanium-based alkoxide [14]. On the other hand, the generation of 2-propanol through the alcohol interchange reaction [6] is implied by the exothermic mixing between TIP and ethanol, and the athermal mixing between TIP and 2-propanol. Therefore, the major constituents of the solvent mixture of the present dipping solution should be ethanol and 2-propanol. The proportion of 2-propanol can be almost 50 mol% assuming that 2-propoxy groups on TIP are completely replaced with ethoxy groups in the EtOH system.

It is considered that PEG adsorbs on titania oligomer by forming hydrogen bonds between the surface hydroxy group of titania oligomer and the ether oxygen of PEG, and the dissolution behavior of titania oligomer adsorbed by PEG approximates to PEG as described in Section 2.2. On the other hand, the driving force for phase separation is the repulsive interaction between the oligomeric alkoxide adsorbed by PEG and the solvent mixture as clearly seen from the intensive study on the silica-based phase separating systems containing PEG [15,16]. Then it is suggested that the phase separation strength is largely determined by the compatibility between PEG and the solvent mixture. Although the dipping solution looks homogeneous, both the formation of titania-PEG complex and the phase separation strength should be considerable in the EtOH system because the solubility of PEG is relatively low in ethanol at 25°C as shown in Fig. 3.4. As the solvent evaporates during the dipping, the phase separation is initiated when the titania-PEG complex is supersaturated in the sol film and is exsoluted from the mixture. The solubility of PEG decreases with an increase in length of alkyl chain for the case of linear alcohols [9], and 2-propanol is less polar than 1-propanol because the branching of alkyl chain decreases the cohesive energy density as reflected by the lower T_b of 2-propanol. Since T_b of 2-propanol is higher than that of ethanol by 4°C, the phase separation would be enhanced to some extent at the later stage of the deposition due to the enrichment of 2-propanol.

In a good solvent, a polymer molecule is solvated as a flexible chain and the adsorption of polymer on solid surface is suppressed as predicted experimentally [17] and theoretically [18,19]. Since formamide is one of the good solvents of PEG as shown in Fig. 3.4, the formation of titania-PEG complex is suppressed by the higher compatibility among the

titania oligomer, PEG, and the solvent mixture resulting in the suppressed phase separation. It is noteworthy that the macroscopic domain formation was completely inhibited in the FA system containing only 5 wt% of formamide. In contrast, the formation of titania-PEG complex and the subsequent domain formation should be enhanced by the larger repulsive interaction between PEG and the solvent mixture in the systems containing poor solvents, such as hexane.

3.2.2 Variation of morphology with volatility of external solvent

As shown in Figs. 3.1–3.3 and Table 3.3, macroscopic morphology is quite similar among the EtOH, PrOH, and HEX systems at most of the dipping conditions. These results are contradictory to the expectation that the phase separation is more enhanced in the HEX system because of the lower solubility of PEG. During the dipping operation, hexane evaporates first because its T_b is lower than those of ethanol and 2-propanol, both of which are the major constituents of the solvent phase. Allowing for the rapid removal of hexane, the difference between the HEX and EtOH systems is supposed to be little at the moment when the macroscopic domain formation begins. In the PrOH system, 1-propanol evaporates last due to the highest T_b. However, the apparent polarity of solvent mixture and the phase separation strength would depend less on the proportion of 1-propanol because the polarity of 1-propanol is between those of ethanol and 2-propanol. Consequently, the macroscopic morphology is also similar between the EtOH and PrOH systems.

Macroscopic domain formation is observed at almost all the dipping conditions in the MeOH, DMK, and DEK systems. The solubility of PEG is initially high both in the MeOH and DMK systems as shown in Fig. 3.4, whereas T_b of methanol and acetone are quite low. Hence it is supposed that the compatibility between the titania-PEG complex and the solvent mixture decreases quickly as the solvent phase evaporates during the dipping. This presumption is partly confirmed from the morphology named "uneven surface" shown in Fig. 3.2(c) that appears at 15.0 mm·min^{-1} of withdrawal speed in the DMK system. Such morphology is formed as a result of the accelerated phase separation as discussed in Section 4.2, but was not observed in the present EtOH system. Considering that the

evaporation of solvent is important at lower withdrawal speed as shown in Section 1.3, it can be said that the phase separation is accelerated by the rapid evaporation of solvent particularly in the DMK system. In the DEK system, the solubility of PEG is lower than that in the DMK and MeOH systems, whereas DEK which is less volatile than 2-propanol should remain until the later stage of the deposition. Since the solubility of PEG is higher than that in the EtOH system, the macroscopic domain formation is possible but is not enhanced greatly in the DEK system.

In the DMF and CHK systems at which T_bs of the external solvents are quite high, the solubility of PEG in the later stage of the deposition would be dominated by the external solvent. Since both DMF and CHK are good solvents of PEG, the driving force for phase separation should be small and therefore the domain formation is not significant as shown in Table 3.3.

Taking these results into consideration, it can be concluded that the macroscopic domain formation becomes apparent with a decrease in compatibility between PEG and the solvent mixture, but is also possible as long as the external solvent is highly volatile even if the solubility of PEG is relatively high. The relationship between the solubility limit of PEG and T_b of the external solvent is summarized in Fig. 3.5, in which the domain formation is expected to be enhanced in the direction left-downward.

3.2.3 Effect of external solvent on polycondensation rate

The gelation test was performed at 40°C and the static gelation behavior of various test solutions are listed in Table 3.4. Opaque gels were commonly obtained but t_g was quite different. The test solution gradually lost the transparency parallel to the viscosity increase and finally gelled. There were some exceptions of the common behavior. In the CHK system, the solution had been transparent even after the gelation but the color changed from yellow to red accompanied with the increase in absorbance. Transparent gels were also obtained both in the FA and DMF systems but the former t_g was far shorter than the latter. The addition of PEG always increased t_g similarly to the results listed in Table 1.5 of Chapter 1 and shown in Fig. 2.4 of Chapter 2. In the MeOH system, the test solution containing PEG could not be prepared since the solution gelled during the

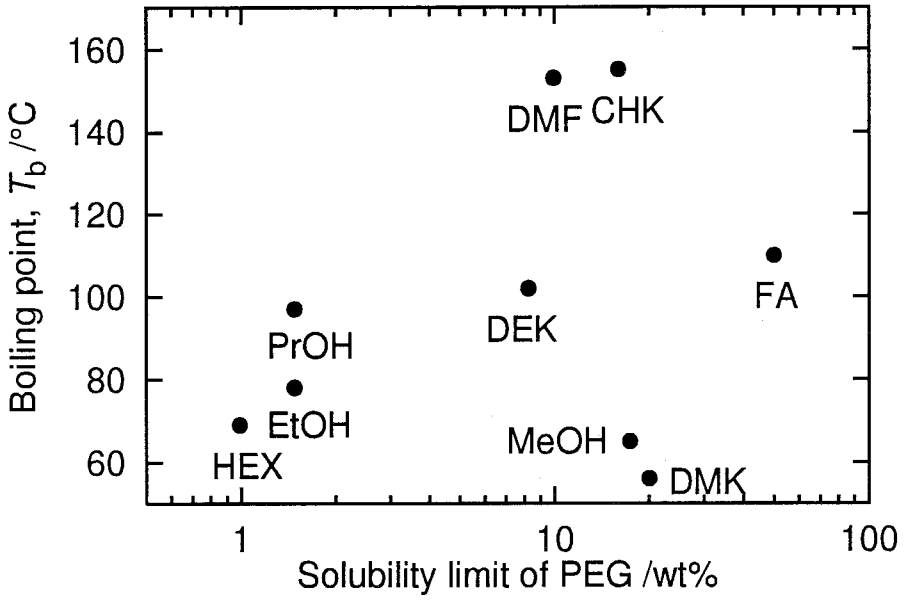

Fig. 3.5: Distributions of solubility limit of PEG in 20 wt% ethanol solution of external solvent and boiling point T_b of external solvent.

stirring at 0°C. The solution having lower acid concentration (TIP:HNO_3 = 0.12:0.002) gelled immediately after the preparation at 0°C. On the other hand, the solution without nitric acid did not gel but instantly generated white precipitation.

Table 3.4: Static gelation behavior at 40°C for various test solutions.

System	HNO_3	PEG free		PEG 5.0	
		Appearance	Gelation time, t_g	Appearance	Gelation time, t_g
HEX	0.02	Opaque gel	2 h	Opaque gel	10 h
PrOH	0.02	Opaque gel	1.5 d	Opaque gel	4.0 d
EtOH	0.02	Opaque gel	1.5 d	Opaque gel	4.5 d
DEK	0.02	Opaque gel	4.5 d	Opaque gel	16 d
DMF	0.02	Transparent sol	>20 d	Transparent sol	>20 d
CHK	0.02	Red transparent gel	1.5 d	Red transparent gel	2.0 d
MeOH	0.02	Transparent gel	<1 min (0°C)	-	
DMK	0.02	Pale-yellow opaque gel	6.5 d	Yellow transparent sol	>20 d
FA	0.02	Transparent gel	1.5 h	Translucent gel	2 h
EtOH	0.002	Transparent gel	<1 min (0°C)	-	
EtOH	0	Precipitation	<1 min (0°C)	-	

The resultant sample without special notation was colorless.

The variation of macroscopic morphology of the TiO_2 film is not explained well by only considering the solubility of PEG and the volatility of external solvent. As shown in Figs. 3.2 and 3.3, the average pore diameter in the DMK system is generally larger than that in the MeOH system, although both the solubility of PEG and T_b are comparable in these systems. The difference between the DMF and CHK systems is an another example, at which only the CHK system affords the macroscopic domain formation. An acceptable reason for such differences is the modification of polycondensation process by the external solvent. The polycondensation rate is one of the principal morphology determining parameters and can be evaluated by observing the static gelation behavior.

The hydrolysis rate of metal alkoxide generally increases with a decrease in size of alkoxyl group attached to the central metal because both the steric hindrance for ligand substitution and the electron donating power of alkoxyl group decrease [6,20,21]. Indeed, t_g is shorter in a tetramethoxysilane (TMOS)-methanol system than in a tetraethoxysilane (TEOS)-ethanol system, and t_g of the latter system is decreased by using methanol as a

solvent [22,23]. Assuming that the present TIP system exhibits the similar tendency, the rapid gelation of the MeOH system is ascribable to be the fast hydrolysis of methoxy-substituted TIP. The withdrawal speed for macroscopic domain formation is decreased from 30.0 mm·min^{-1} to 15.0 mm·min^{-1} by incorporating methanol as listed in Table 3.3. An analogous variation is observed when the relative humidity is increased in the EtOH system, at which both the phase separation and the polycondensation are accelerated by the water adsorption as shown in Section 1.3. Therefore the withdrawal speed for domain formation decreases by increasing the reactivity of TIP in the MeOH system, instead of increasing the water concentration.

It has been known that formamide is hydrolyzed to form ammonia and formic acid under a strongly acidic condition and increases the pH of the solution. For example in a system consisting of TMOS, formamide, water, and nitric acid, the pH of the solution is reported to increase from 0–1 to 4–5 within several minutes at 40°C even by the small addition of formamide [3]. In the present TIP system, reduction of the nitric acid concentration by 1/10 significantly decreases t_g as listed in Table 3.4. Under a highly acidic conditions ($[H^+] \sim [Ti]$), the polycondensation process is strongly inhibited [21] probably because the reduced negative charge on hydroxy oxygen suppresses the nucleophilic polycondensation. In addition, the isoelectric point of titania at which the electrostatic repulsion between the titania oligomers disappears is reported to be about pH 6 [24]. Therefore, it is reasonable to consider that the polycondensation is enhanced with an increase in pH in the FA system. This result is consistent with the report that the generation of colloidal titania particle is greatly accelerated in basic conditions [25]. Additionally, formamide may catalytically accelerate the polycondensation by deprotonating the hydroxy group [7].

In the DMF system, gelation did not occur during the experimental period. Furthermore, the test solution did not lose the transparency although most of the test solutions turned opaque before the gelation. A research on TMOS-based system indicates that DMF suppresses the polycondensation in contrast to formamide which accelerates the polycondensation [26]. It is considered that the higher stability of DMF against the hydrolysis preserves the pH of the solution almost constant in the DMF system. Fur-

thermore, the lone pair on nitrogen atom in DMF is able to coordinate directly with the electropositive titanium atom. Such nitrogen-metal interaction is capable of interfering the polycondensation as has been demonstrated by the system containing diethanolamine (DEA) as an amine-based stabilizing agent [27]. A research on silica-based system containing poly(acrylic acid) (HPAA) suggests that not only the polycondensation but also the phase separation can be suppressed by incorporating DMF [5]. It is supposed that the structure and property of DMF molecule are effective to maintain the miscibility of components for a long time. Considering that the solution is also transparent in the CHK system, the difference in macroscopic morphology between the DMF and CHK systems would be attributed to the larger difference in t_g.

The polycondensation is quite slow in the DMK and DEK systems as listed in Table 3.4. Although the detailed mechanism is not known yet, the yellow coloration in the DMK system implies some direct interaction between the acetone molecule and the titanium ion. It should be noted that the degree of coloration increases in the order of the DEK, DMK, and CHK systems, and the order is consistent with that of Lewis basicity of the corresponding carbonyl compounds. Such Lewis bases are reported to form a 1:1 complex with a Lewis acid such as phenol [28]. Therefore, suppressed polycondensation due to the formation of hydrogen bond to the hydroxy group on TIP, and due to the alcoxolation between the carbonyl compound and TIP [29] might be suggested. A rough estimation from the shadow of macropores in Figs. 3.1–3.3 indicates that the thickness in the DMK system is thinner than those in the EtOH and PrOH systems. Furthermore, several small cracks are recognized in the films prepared from the DMK system. The slower polycondensation in the DMK system is supposed to decrease both the viscosity of the dipping solution and the crosslinking density of the resultant film compared to the EtOH system.

The mixture of TIP and CHK gives rise to a yellow solution, suggesting a strong interaction between the titanium ion and CHK. In the CHK system, the color of the solution turns to orange by adding water and nitric acid, followed by the gradual increase in absorbance and wavelength of absorption throughout the sol-gel reaction. Although the direct reaction between TIP and CHK, which might be the origin of the enhanced

coloration and rapid gelation, is supposed [29], the detailed mechanism is currently left unknown. The faster polycondensation in the CHK system compared to the DMF system would contribute to the macroscopic domain formation at lower withdrawal speed. However, the domain formation is suppressed greatly compared to the other systems due to the suppressed phase separation as expected from the considerable solubility of PEG and the transparency of the gelation test solution.

3.3 System containing long-chain alcohols

Three types of alcohols, 1-propanol, 2-propanol, and 1-butanol of which T_bs are listed in Table 3.5, were employed as external alcohols which are less polar than ethanol. The compositions of the solutions prepared are listed in Table 3.6. The PEGs having average molecular weights of 1,000, 1,540, and 2,000 were employed, and PEG1540 was used as polymer content for the dipping solution. Part of ethanol was replaced by the equivalent weight of external alcohol so as not to change the total weight of alcohol content. Prescribed amounts of ethanol and external alcohol were firstly mixed before the addition of water or TIP. Proportion of external alcohol (x) is defined as the ratio of external alcohol to the sum of ethanol and external alcohol in weight. The film was deposited at 25°C.

Table 3.5: Boiling point T_b of various alcohols employed.

	Ethanol	1-Propanol	1-Butanol	2-propanol
Boiling point, T_b(°C)	78	97	118	82

3.3.1 Structure and reactivity of titanium alkoxides

The gelation test was performed at 0°C and the solution composition dependence of t_g is shown in Fig. 3.6. In the 1-propanol and 1-butanol systems, t_g increased monotonically with an increase in x. The increase in t_g was prominent at $x \geq 0.5$, and the solutions did not gel even after 500 min at $x = 1.0$. In the 2-propanol system, in contrast, t_g decreased abruptly even by the small increase in x. All the test solutions had been transparent until

Table 3.6: Compositions of the dipping, gelation test, and compatibility test solutions (unit: mol).

	H_2O	EtOH	External alcohol	TIP	HNO_3	PEG (g)
Dipping	0.12	1.0–0	(0–1.0)[a]	0.12	0.02	5.0
Gelation test	0.24	0.8–0	(0–0.8)[a]	0.12	0.02	-
	0.24	1.0–0	(0–1.0)[a]	0.12	0.02	-
Compatibility test	-	-	10.0 g	-	-	0.1–10.0 g

(a) Equal weights of ethanol and external alcohol are substituted. The parenthesized value indicates the molar of external alcohol in terms of ethanol.

the gelation except for the cases resulting in translucent gel at $x = 0.6$ and opaque gels $x \geq 0.8$ in the 2-propanol system.

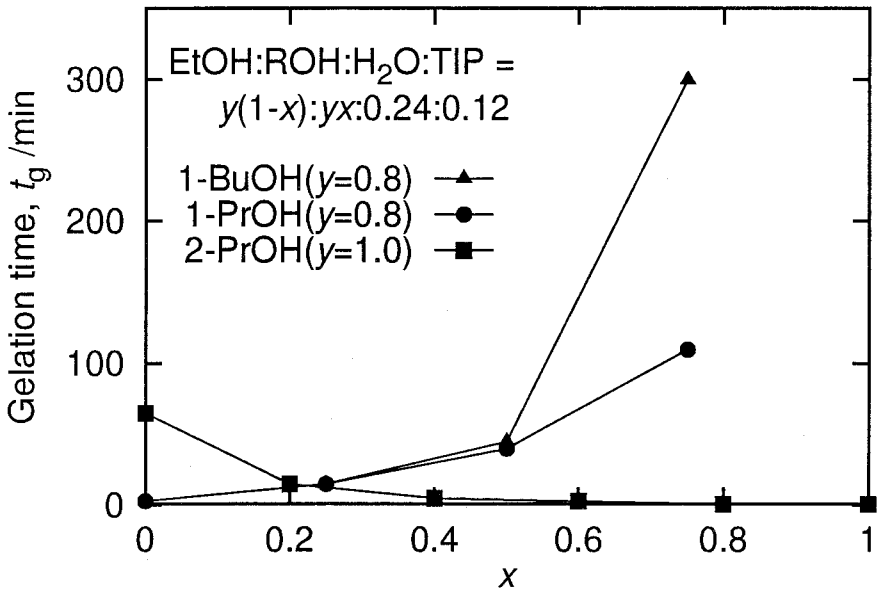

Fig. 3.6: Dependence of gelation time t_g at 0°C on solution composition.

Although the reactivity of metal alkoxide is largely determined by the electronegativity of central atom, the hydrolysis and polycondensation rates of alkoxides are strongly affected by the types of functional groups attached to the central atom [6,14]. In general, the hydrolysis rate of alkoxide consisting of linear alkoxy groups decreases with an increase

in length of alkyl chain as typically seen from the reactivity of silicon alkoxides [22, 30]. Charge distribution calculations performed for silicon and titanium alkoxides also support such tendency [21]. It is considered that both the reduced positive partial charge on the central atom and the steric hindrance of alkoxy groups suppress the reactivity of alkoxides derived from long-chain alcohols.

The coordination number of Si in silicon alkoxides is always 4 due to the strong sp^3 bonding nature of Si, while the coordination number of Ti in titanium alkoxides can be increased up to 6 [6,21]. The reactions of titanium alkoxides are more complicated because such coordination expansion enables the formation of oligomeric alkoxides bridged by the alkoxy oxygens and the additional solvent donor molecules [6, 20, 21]. The formation of oligomeric alkoxides is normally easier for the alkoxides derived from linear alcohols. It is reported that the oligomerization degrees of titanium tetramethoxide (TM) and titanium tetraethoxide (TE) are respectively 4 and 3, and such oligomeric structure is partly maintained even after the dilution by their parent alcohols [14, 21]. On the other hand, TIP is reported to remain monomeric due to the steric hindrance of 2-propoxy groups [14]. Direct evidences of oligomerization are provided by X-ray absorption fine structure (XAFS) measurements [31, 32]. The coordination numbers of Ti in TIP and titanium tetra-*tert*-amyloxide (TTA) ($Am^t = CH_3CH_2(CH_3)_2C$) remain 4 whereas those in TE and titanium tetrabutoxide (TNB) increase up to 5 as well as a Ti–Ti correlation having a distance of 3.1 Å is found. It is considered that the less-flexible and more-bulky alkoxy groups hinder the extra ligand from entering and disturb the oligomerization of TIP and TTA.

In general, the oligomerization decreases the solubility and reactivity of alkoxides [14, 21, 33]. The decrease in hydrolysis and polycondensation rates in oligomeric titanium-based alkoxides is confirmed from the results that monodispersed titania powders can be prepared by the controlled hydrolysis of TE dissolved in ethanol [6, 34, 35], but the monodispersity is lost when TIP is dissolved in 2-propanol [21] and TE is dissolved in *tert*-butyl alcohol [35]. Although TIP is monomeric itself, oligomerization of TIP is anticipated by dissolving TIP in ethanol and replacing part of 2-propoxy groups with ethoxy groups. This expectation does not contradict the result that white precipitation, proba-

bly oligomeric compound of methoxy-substituted TIP, is formed when TIP is mixed with methanol as shown in Section 3.2. The solution composition dependence of t_g shown in Fig. 3.6 indicates that t_g increases with an increase in x in the 1-propanol and 1-butanol systems. It is supposed that incorporated 1-propanol or 1-butanol not only decreases the reactivity of alkoxide but also preserves the oligomeric structure of ethoxy-substituted TIP. The prominent increase in t_g at $x \geq 0.5$ would be attributed to the significant reduction of ethoxy groups assuming that ethoxy group is the most reactive and dominates the polycondensation rate. In the 2-propanol system, in contrast, t_g decreases with an increase in x. It is suggested that the addition of 2-propanol destructs the oligomeric structure and increases the reactivity of alkoxide even if x is rather small.

3.3.2 Morphology formation in system containing long-chain alcohols

Table 3.7 lists that the variation of macroscopic morphology with solution composition at 30% RH. The resultant film was always non-porous and smooth when ethanol was the only constituent of alcohol content in consistent with the results in Section 2.2. The macroporous morphology appeared when 1-propanol or 1-butanol was added, while the morphology was smooth as ever under the addition of 2-propanol. Homogeneous solution could not be prepared at $x \geq 0.8$ in the 2-propanol system due to the lower solubility of PEG.

Table 3.7: Macroscopic morphology of the TiO_2 films at 30% RH: -, smooth; ◡, pits; ●, macropores.

External alcohol	Withdrawal speed ($mm \cdot min^{-1}$)	Proportion of external alcohol (x)					
		0	0.2	0.4	0.6	0.8	1.0
1-Propanol	15.0	-	-	-	●	●	●
	30.0	-	-	-	◡	◡	●
1-Butanol	15.0	-	●	●	●	●	●
	30.0	-	●	●	●	●	●
2-Propanol	15.0	-	-	-	-		
	30.0	-	-	-	-		

Tables 3.8 and 3.9 list the relative humidity dependence of macroscopic morphology in the 1-propanol and 1-butanol systems at $x = 1.0$, respectively. The corresponding SEM photographs of the TiO_2 films prepared at 30% RH are shown in Figs. 3.7 and 3.8. The SEM photographs of the films prepared at 70% RH are also shown in Fig. 3.9. The suppressed macroscopic domain formation at higher relative humidity was notable in the 1-propanol system as listed in Table 3.8. On the other hand, the morphology depended less on relative humidity in the 1-butanol system as listed in Table 3.9.

Table 3.8: Macroscopic morphology of the TiO_2 films in the 1-propanol system at $x = 1.0$: -, smooth; ◡, pits; ●, macropores; ▲, uneven surface.

Withdrawal speed	Relative humidity (%RH)				
($mm \cdot min^{-1}$)	30	40	50	60	70
7.5	◡	◡	◡	●	●
15.0	●	●	◡	◡	▲
22.5	●	◡	-	-	-
30.0	●	-	-	-	-

Table 3.9: Macroscopic morphology of the TiO_2 films in the 1-butanol system at $x = 1.0$: ◡, pits; ●, macropores; C, macroscopic cracks.

Withdrawal speed	Relative humidity (%RH)				
($mm \cdot min^{-1}$)	30	40	50	60	70
7.5	◡C	◡C	◡C	◡C	◡
15.0	●	●	●	●	●
22.5	●	●	●	●	●
30.0	●	●	●	●	◡

Figure 3.10 shows the variation of average pore diameter (D) with relative humidity at $15.0\,mm \cdot min^{-1}$ of withdrawal speed in the 1-propanol and 1-butanol systems. In both the systems, D decreased monotonically with an increase in relative humidity. Figure 3.11 shows the variation of D with withdrawal speed. At 30% RH, D exhibited a maximum at $15.0\,mm \cdot min^{-1}$ in the 1-propanol system while remained almost constant

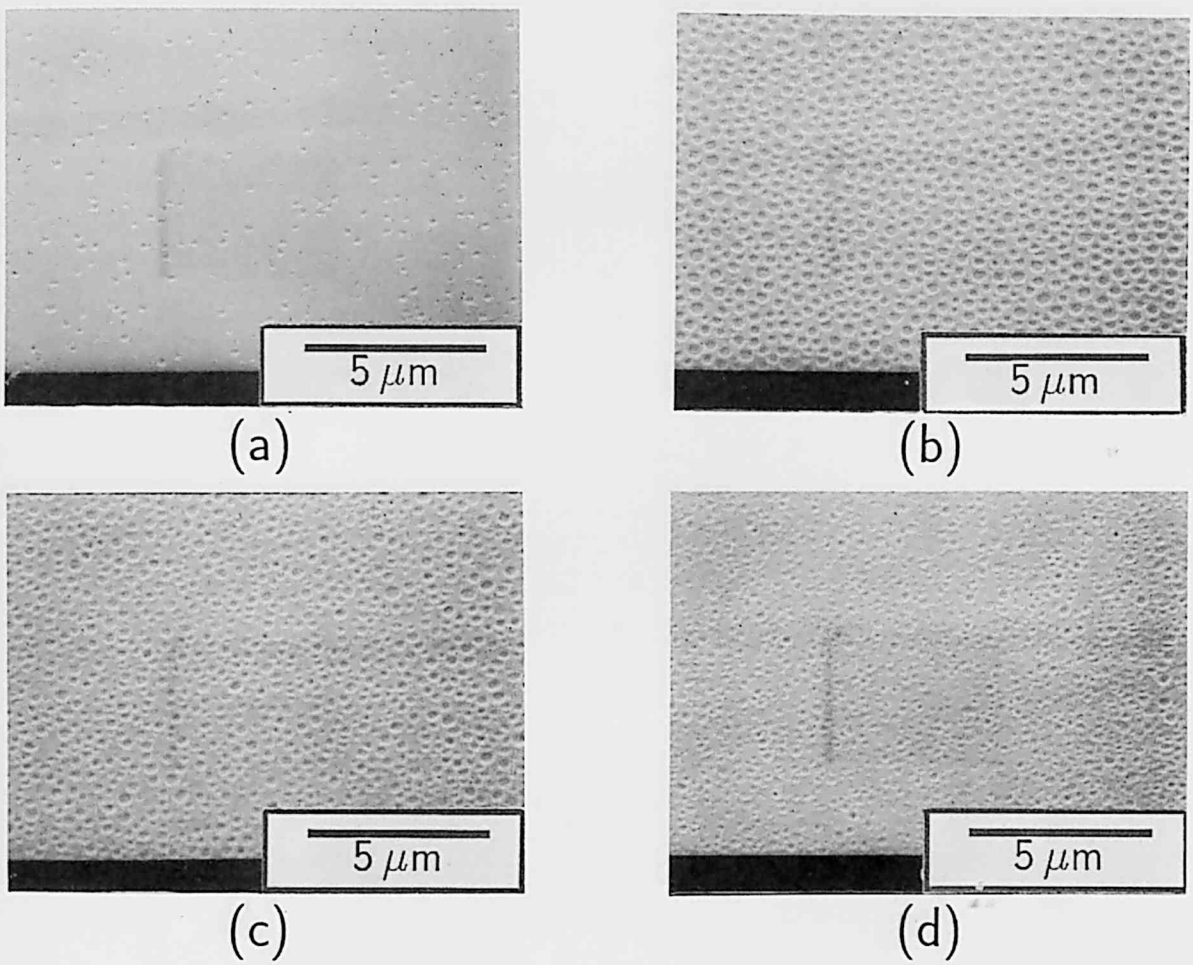

Fig. 3.7: SEM photographs of the TiO_2 films prepared from the 1-propanol system at $x = 1.0$, 30% RH. Withdrawal speed is (a) 7.5, (b) 15.0, (c) 22.5, (d) 30.0 mm·min^{-1}. View angle is 45°

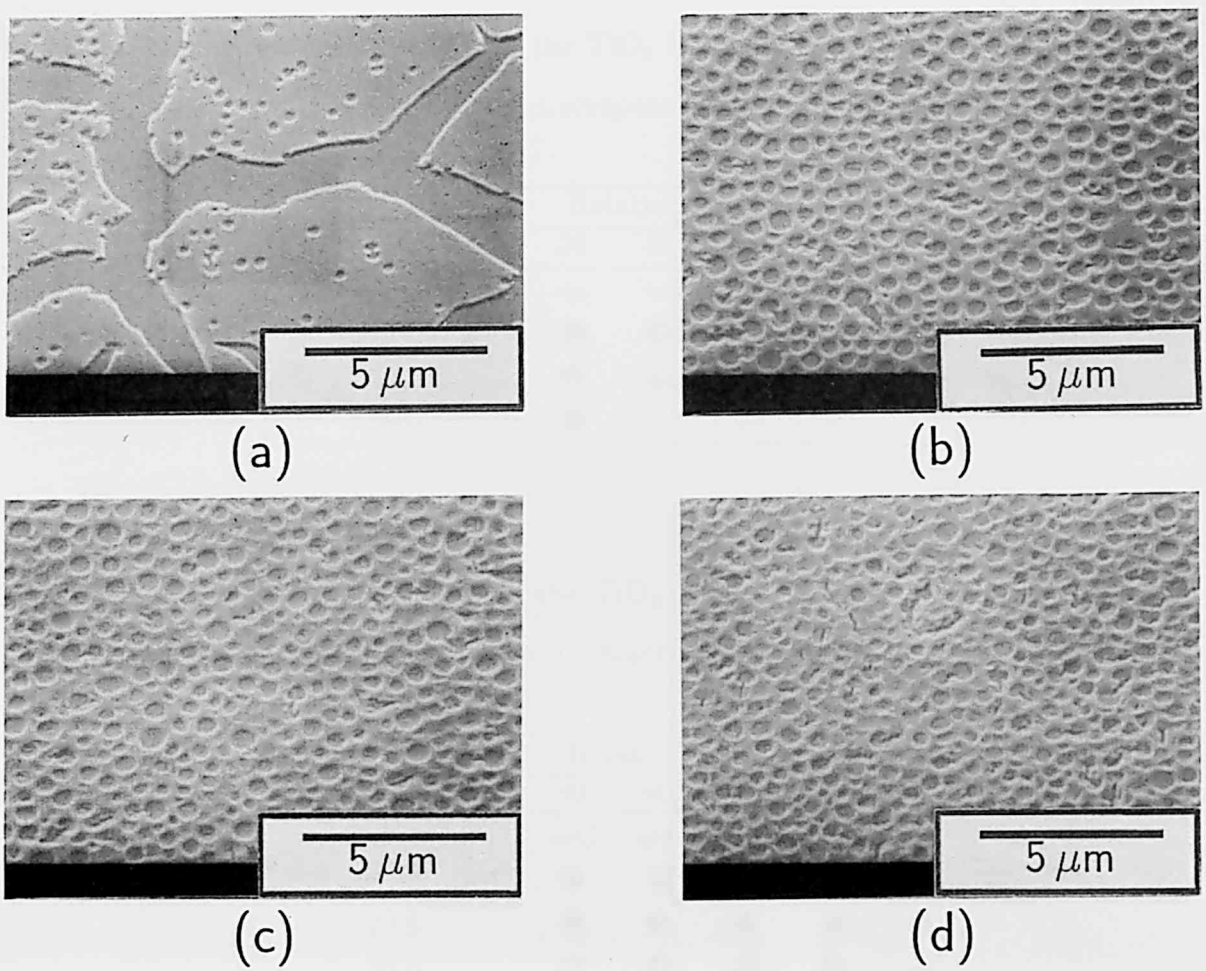

Fig. 3.8: SEM photographs of the TiO_2 films prepared from the 1-butanol system at $x = 1.0$, 30% RH. Withdrawal speed is (a) 7.5, (b) 15.0, (c) 22.5, (d) 30.0 mm·min^{-1}. View angle is 45°.

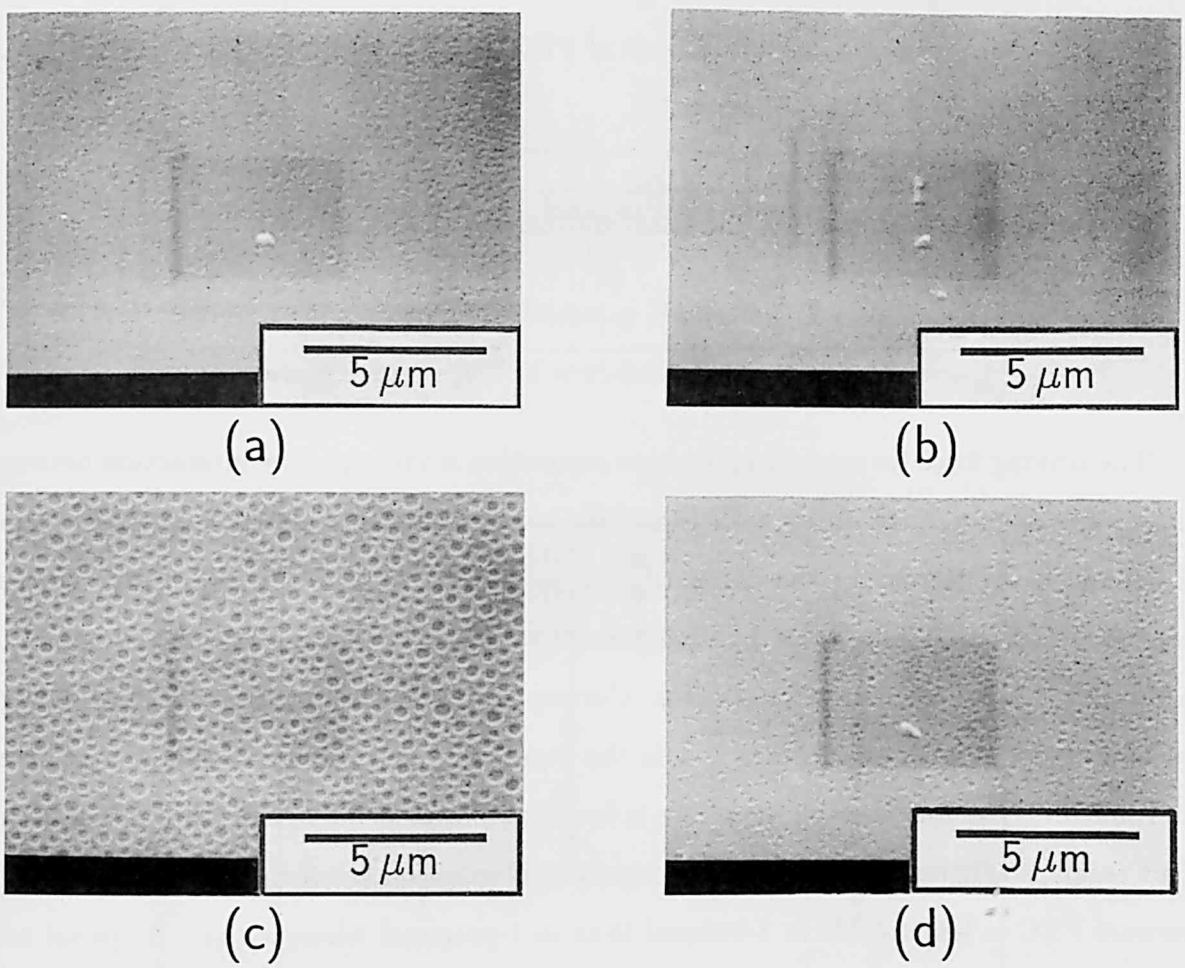

Fig. 3.9: SEM photographs of the TiO_2 films prepared at $x = 1.0$, 70% RH. Withdrawal speed is (a) 15.0, (b) 30.0 mm·min^{-1} for the 1-propanol system, and (c) 15.0, (d) 30.0 mm·min^{-1} for the 1-butanol system. View angle is 45°.

above 15.0 mm·min^{-1} in the 1-butanol system. The variations of D were quite similar between the 1-propanol system at 30% RH and the 1-butanol system at 70% RH.

Table 3.10 lists the solubility limit of PEG in various types of alcohols after stirring at 25°C for 1 h. The solubility of PEG decreased with an increase in the size of alkyl group for the linear alcohols. However, the solubility of PEG in 2-propanol was much lower than that in 1-butanol although 2-propanol has smaller alkyl group than 1-butanol. The solubility of PEG decreased steeply by increasing the molecular weight of PEG.

Table 3.10: Dependence of solubility limit of PEG at 25°C on molecular weight of PEG and alcohol type (unit: wt%).

	Ethanol	1-Propanol	1-Butanol	2-Propanol
PEG1000		>50	45	21
PEG1540	19	7	2	<1
PEG2000	1	<1		

The driving force for macroscopic phase separation is the repulsive interaction between the titania oligomer adsorbed by PEG and the solvent mixture, and the phase separation is enhanced by decreasing the compatibility between PEG and the solvent mixture as described in Section 3.2. Table 3.10 indicates that the solubility of PEG in 1-propanol or 1-butanol is lower than that in ethanol. Correspondingly, the macroporous morphology becomes evident with an increase in x in the 1-propanol and 1-butanol systems as listed in Table 3.7. The macroscopic structure is found even at $x = 0.2$ in the 1-butanol system. This result is attributable to the larger repulsive interaction between PEG and 1-butanol because PEG is less soluble in 1-butanol than in 1-propanol whereas the 1-propanol and 1-butanol systems exhibit almost comparable t_gs at $x = 0.2$ as shown in Fig. 3.6.

In the 1-propanol system at 30% RH, D shows a maximum at 15.0 mm·min^{-1} as shown in Fig. 3.11 because the fluidity reduction and the polycondensation respectively suppress the phase separation at lower and higher withdrawal speeds as discussed in Section 1.3. In the 1-butanol system, however, D is almost constant above 15.0 mm·min^{-1} at 30% RH. It is supposed that the phase separation still overcomes the polycondensation even at 30.0 mm·min^{-1} because of the decreased reactivity of alkoxide. The slower polycondensa-

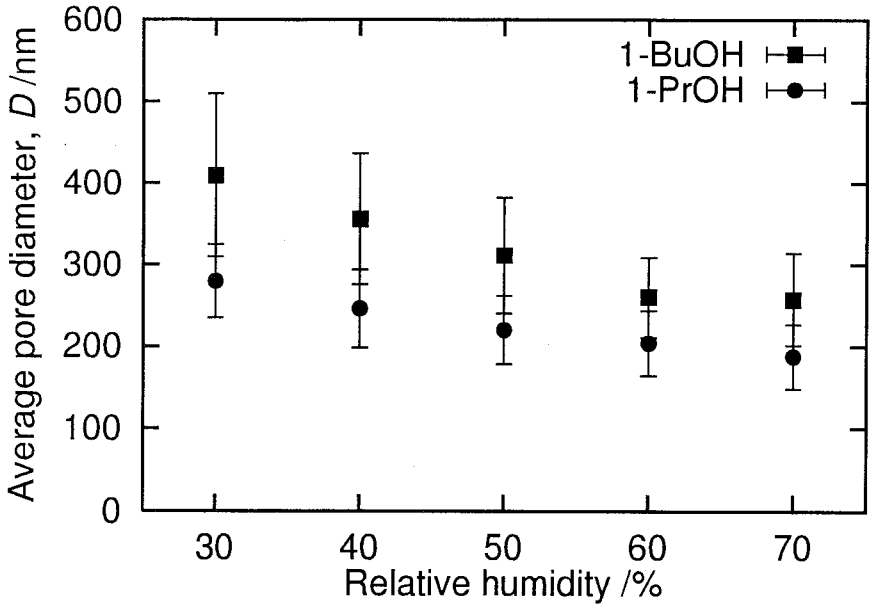

Fig. 3.10: Dependence of average pore diameter D on solution composition and relative humidity at 15.0 mm·min^{-1} of withdrawal speed.

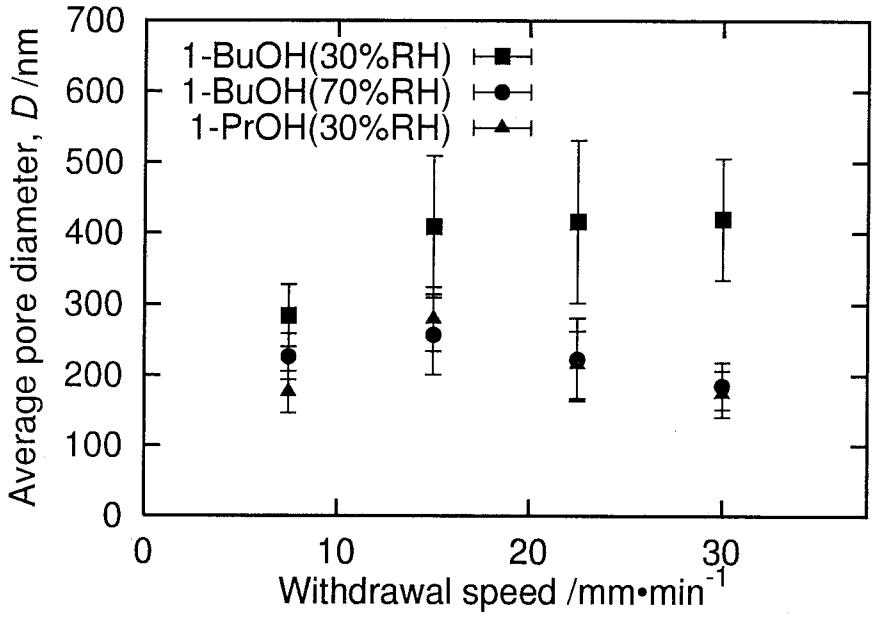

Fig. 3.11: Dependence of average pore diameter D on solution composition and withdrawal speed.

tion gives rise to the evident formation of macroscopic domain even at 70% RH as well as the formation of macroscopic cracks at lower relative humidity at 7.5 mm·min^{-1} as listed in Table 3.9 in the 1-butanol system. Despite of the increased stability against the water attacks, the polycondensation is accelerated with an increase in relative humidity even in the 1-butanol system as shown in Fig. 3.10. Then the withdrawal speed dependence of D at 70% RH in the 1-butanol system becomes similar to that at 30% RH in the 1-propanol system. In the 1-propanol system, the domain formation is more sensitive to relative humidity and therefore the withdrawal speed for macroscopic domain formation decreases with an increase in relative humidity. Such variation is consistent with the behavior of the ethanol-based system containing PEG2000 shown in Section 1.3.

The resultant films are always smooth in the 2-propanol system as listed in Table 3.7. This result seems contradictory to the result of compatibility test listed in Table 3.10, which indicates that the phase separation strength is largest in the 2-propanol system. Actually, PEG does not dissolve completely in the precursor solution at $x = 0.8$ in the 2-propanol system, and opaque gels are obtained in the gelation test owing to the larger exsolution strength of PEG. Furthermore, it is considered that the lower T_b of 2-propanol than T_bs of 1-propanol and 1-butanol is preferable for the macroscopic domain formation because the supersaturation of PEG in the sol film is accelerated by the enhanced solvent evaporation as shown in Section 3.2. Such contradiction can be explained by taking the polycondensation rate into account. As shown in Fig. 3.6, 2-propanol affects t_g in completely reversed way as 1-propanol and 1-butanol. The polycondensation rate in the former system is far larger than the latter systems. In consequence, it is supposed that the macroscopic domain formation in the 2-propanol system is entirely inhibited by the extremely rapid polycondensation and the subsequent gelation in spite of the larger phase separation strength.

3.4 Conclusions

The variation of macroscopic morphology and the mechanism of morphology formation were investigated for the TiO_2 films prepared from the solution containing PEG and the various types of chemical additives. The results obtained are summarized as follows:

(1) The macroscopic domain formation is enhanced considerably when the compatibility between the titania-PEG complex and the solvent mixture is poor. When the external solvent enhances the compatibility among the titania oligomer, PEG, and the solvent mixture, the external solvent should be highly volatile to cause the macroscopic phase separation. It is considered that the polycondensation rate of titania oligomer, which is greatly influenced by the addition of external solvent, should be moderate to enhance the macroscopic domain formation.

(2) The macroscopic domain formation is realized even if the molecular weight of PEG is as small as 1,540 by decreasing the compatibility between PEG and the solvent mixture, but is inhibited when the polycondensation is greatly accelerated by the addition of external alcohol.

(3) The macroporous morphology is clearly formed even at higher relative humidity as 70% RH by incorporating external alcohol such as 1-butanol which not only slows down the polycondensation but also increases the phase separation strength.

References

[1] T. Adachi and S. Sakka, J. Non-Cryst. Solids **99**, 118 (1988).

[2] T. Adachi, S. Sakka, and M. Okada, Yogyo-Kyokai-Shi **95**, 970 (1987).

[3] H. Kaji, K. Nakanishi, and N. Soga, J. Non-Cryst. Solids **181**, 16 (1995).

[4] H. Kaji, K. Nakanishi, and N. Soga, J. Non-Cryst. Solids **185**, 18 (1995).

[5] K. Nakanishi and N. Soga, J. Non-Cryst. Solids **142**, 45 (1992).

[6] C. Sanchez, J. Livage, M. Henry, and F. Babonneau, J. Non-Cryst. Solids **100**, 65 (1988).

[7] G. Orcel and L. Hench, J. Non-Cryst. Solids **79**, 177 (1986).

[8] G. Orcel, L. L. Hench, I. Artaki, J. Jonas, and T. W. Zerda, J. Non-Cryst. Solids **105**, 223 (1988).

[9] A. Kagemoto, Y. Itoi, Y. Baba, and R. Fujishiro, Makromol. Chem. **150**, 255 (1971).

[10] K. Devanand and J. C. Selser, Nature **343**, 739 (1990).

[11] K.-J. Liu and J. L. Parsons, Macromolecules **2**, 529 (1969).

[12] J. Maxfield and I. W. Shepherd, Polymer **16**, 505 (1975).

[13] S. Bluestone, J. E. Mark, and P. J. Flory, Macromolecules **7**, 325 (1974).

[14] C. J. Brinker and G. W. Scherer, in *Sol-Gel Science: The Physics and Chemistry of Sol-Gel Processing* (Academic Press, New York, 1990), Chap. 2.

[15] K. Nakanishi, H. Komura, R. Takahashi, and N. Soga, Bull. Chem. Soc. Jpn. **67**, 1327 (1994).

[16] K. Nakanishi and N. Soga, Bull. Chem. Soc. Jpn. **70**, 587 (1997).

[17] J. Koral, R. Ullman, and F. R. Eirich, J. Phys. Chem. **62**, 541 (1958).

[18] J. M. H. M. Scheutjens and G. J. Fleer, J. Phys. Chem. **83**, 1619 (1979).

[19] J. M. H. M. Scheutjens and G. J. Fleer, J. Phys. Chem. **84**, 178 (1980).

[20] M. Guglielmi and G. Carturan, J. Non-Cryst. Solids **100**, 16 (1988).

[21] J. Livage, M. Henry, and C. Sanchez, Prog. Solid State Chem. **18**, 259 (1988).

[22] K. C. Chen, T. Tsuchiya, and J. D. Mackenzie, J. Non-Cryst. Solids **81**, 227 (1986).

[23] S. Sakka, H. Kozuka, and S.-H. Kim, in *Ultrastructure Processing of Advanced Ceramics*, edited by J. D. Mackenzie and D. R. Ulrich (John Wiley & Sons, New York, 1988), Chap. 10. See Ref. [36].

[24] K. W. Busch, M. A. Busch, S. Gopalakrishnan, and E. Chibowski, Colloid. Polym. Sci. **273**, 1186 (1995).

[25] T. Ikemoto, K. Uematsu, N. Mizutani, and M. Kato, Yogyo-Kyokai-Shi **93**, 261 (1985).

[26] J. Jonas, in *Science of Ceramic Chemical Processing*, edited by L. L. Hench and D. R. Ulrich (John Wiley & Sons, New York, 1986), Chap. 5.

[27] Y. Takahashi and Y. Matsuoka, J. Mater. Sci. **23**, 2259 (1988).

[28] M.-L. H. Jeng and Y.-S. Li, Spectrochim. Acta **45A**, 525 (1989).

[29] R. J. P. Corriu, D. Leclercq, A. Vioux, M. Pauthe, and J. Phalippou, in *Ultrastructure Processing of Advanced Ceramics*, edited by J. D. Mackenzie and D. R. Ulrich (John Wiley & Sons, New York, 1988), Chap. 7. See Ref. [36].

[30] H. Schmidt, H. Scholze, and A. Kaiser, J. Non-Cryst. Solids **63**, 1 (1984).

[31] C. Sanchez, F. Babonneau, S. Doeuff, and A. Leaustic, in *Ultrastructure Processing of Advanced Ceramics*, edited by J. D. Mackenzie and D. R. Ulrich (John Wiley & Sons, New York, 1988), Chap. 4. See Ref. [36].

[32] F. Babonneau, S. Doeuff, A. Leaustic, C. Sanchez, C. Cartier, and M. Verdaguer, Inorg. Chem. **27**, 3166 (1988).

[33] R. W. Adams, E. Bishop, R. L. Martin, and G. Winter, Aust. J. Chem. **19**, 207 (1966).

[34] E. A. Barringer and H. K. Bowen, Langmuir **1**, 414 (1985).

[35] M. T. Harris and C. H. Byers, J. Non-Cryst. Solids **103**, 49 (1988).

[36] *Ultrastructure Processing of Advanced Ceramics*, edited by J. D. Mackenzie and D. R. Ulrich (John Wiley & Sons, New York, 1988).

Chapter 4

General principle of morphology formation in system containing poly(ethylene glycol)

4.1 Introduction

As has been discussed in Chapters 1–3, the resultant morphology of TiO_2 films is quite sensitive to the variation of dipping conditions, such as ambient humidity, water and alkoxide concentrations, withdrawal speed, and chemical additives. In these studies, the variation of morphology concerning each dipping parameter is interpreted almost individually although the films of similar morphology can be prepared even if the dipping conditions are different. It is valuable to clarify the similarity and correlation between the dipping parameters and explore the generalized mechanism of morphology formation because they should provide advanced insights for the morphology control of macroporous TiO_2 films.

An as-deposited titania gel film is soft and amorphous, and contains a lot of organic substances such as residual alkoxy groups, unevaporated solvents, and additives such as polymers incorporated in the reaction mixture, all of which generally restrict the application of titania gel film as practical ceramics. The gel film is easily converted into dense oxide film by heat treatment accompanied by the removal of organic materials. However, both the shrinkage of the gel resulting from the evaporation and decomposition of organic substances and the displacement of atoms owing to the crystallization induce considerable stress in the resultant ceramic body. The morphology is varied to reduce the stress but the macroscopic cracks are sometimes created as exhibited previously when the induced stress is too large to be compensated enough by the plastic deformation of the film. Not only the macroscopic morphology but also the microscopic structure such as crystallinity usually

depend largely on the heat treatment conditions such as time and temperature. Therefore it is significant to investigate the relationship between the properties of resultant TiO_2 film and the heat treatment condition.

In the former section of this chapter, the morphology of the TiO_2 film is examined under the wide variation of water, alkoxide, and PEG concentrations of the dipping solution at several relative humidity. The variation of morphology is discussed correlating with the mechanism of phase separation during the dipping operation. In the latter section, the influence of heat treatment is described on the macroscopic morphology and the characteristics of the resultant TiO_2 films.

4.2 Morphology formation through sol-gel dip-coating method

The variation of morphology was examined for the compositions listed in Table 4.1. The PEG having average molecular weight of 2,000 was employed. Water to TIP ratio ($r \equiv H_2O/TIP$), TIP to ethanol ratio ($c \equiv$ TIP/EtOH), and PEG to ethanol ratio ($p \equiv$ PEG/EtOH) are respectively used to denote the water, TIP, and PEG concentrations.

Table 4.1: Compositions of the dipping solutions (unit: mol).

Solution	H_2O	EtOH	TIP	HNO_3	PEG (g)	H_2O/TIP, r
A1	0.10–0.18	1.0	0.10–0.18	0.02	4.0–7.0	1.00
A2	0.14	1.0	0.14	0.02	4.0–7.0	1.00
B1	0.08–0.16	1.0	0.12	0.02	5.0	0.67–1.33
B2	0.14–0.22	1.0	0.16	0.02	7.0	0.88–1.38
B3	0.14	1.0	0.12	0.02	4.0–7.0	1.17

The phase separation occurs when the system having a miscibility gap in its temperature-composition phase diagram is quenched, physically or chemically, from a single-phase region into a two-phase region surrounded by binodal line. In the two-phase region, the system is thermodynamically the most stable as a non-uniform mixture of the end-compositions of which amounts are determined by the binodal line. Two typical mechanisms of phase separation, nucleation-growth and spinodal decomposition, are generally

known, and either of which occurs depending on the stability of the quenched system [1,2]. The nucleation-growth takes place when the system is quenched inside the binodal line but outside the spinodal line. In that region, the system is metastable, that is, stable against the small fluctuation of composition because the second derivative of Gibbs free energy on mixing is positive. The growth of nuclei is proportional to the square root of time since the rate limiting process of domain formation is the material diffusion to nuclei. In principle, the nucleation-growth can be observed in every phase separating system because the quenching path always intersects the metastable region before reaching the unstable region, but is suppressed when the quench is rapid and the constituents of the mixture are less mobile. In the present system, it is supposed that the quench depth increases continuously by proceeding with the solvent evaporation within a short time, because the solvent evaporation is essential to cause the phase separation by decreasing the compatibility among the constituents. On the other hand, it is confirmed that the macroporous structure is formed via spinodal decomposition using a light scattering technique in several silica-based phase separating systems containing organic polymers [3, 4]. Considering the similarity among the phase separating system containing organic polymers, the type of phase separation in the present titania dip-coating system is likely to be spinodal decomposition.

At a definite quench depth, the spinodal decomposition proceeds through the successive three stages [4–6]. In the initial stage described by the linearized theory of Cahn [7,8], the composition fluctuation of particular wavelength increases its amplitude exponentially with time. Then the wavelength begins to increase with also increasing its amplitude during the intermediate stage. In the late stage, the composition fluctuation is saturated at the end-compositions to form the definite interface between the phases. However the domain continues growing so as to reduce the surface energy, and finally the fragmented structure and the dispersed minor-phase domains are observed especially at an off-critical composition. Accordingly, it is supposed that the resultant morphology of macroporous TiO_2 film preserves the structure formed during the intermediate or late stages of spinodal decomposition where the boundary between the phases becomes sharp. Basically, it is considered that the morphology varies in the order of smooth, pits, macropores, and

uneven surface as the phase separation proceeds in the present system.

4.2.1 Effects of alkoxide and polymer concentrations

Table 4.2 shows the macroscopic morphology of the TiO_2 films prepared from the solution A1 at 30% RH. The solution of which c was 0.20 could not be prepared due to the lower solubility of PEG. The SEM photographs of the TiO_2 films prepared at 30% RH from the solution A2, which is identical to the solution A1 at $c = 0.14$, are also shown in Fig 4.1. The morphology varied in the order of pits, macropores, and uneven surface with an increase in p, whereas the morphology varied in the reversed order with an increase in c. Figure 4.2 shows the solution composition dependence of average pore diameter (D). In general, D increased as the morphology changed from pits to uneven surface, and increased considerably when the morphology changed from macropores to uneven surface.

Table 4.2: Macroscopic morphology of the TiO_2 films prepared from the solution A1 at 30% RH: ◡, pits; ●, macropores; ▲, uneven surface. r is 1.00 for all the dipping solutions.

PEG/EtOH, p	TIP/EtOH, c				
	0.10	0.12	0.14	0.16	0.18
4.0	●	●	◡		
5.0	▲	●	●	●	◡
6.0	▲	▲	●	●	●
7.0		▲	▲	●	●

The macroscopic domain formation is enhanced with an increase in p as shown in Fig. 4.1 and Table 4.2 accompanied by the increase in D as shown in Fig. 4.2. The D also increases by increasing p for the system containing PEG and DEA [9]. It is pointed out that the dissolution property of titania oligomer approximates to that of PEG after being adsorbed by PEG on its surface as discussed in Section 2.2, and the phase separation is enhanced when the solubility of PEG is relatively low as described in Section 3.2. These facts suggest that the cause of phase separation is the supersaturation of PEG in the solvent mixture. Assuming that the evaporation rate of solvent during the

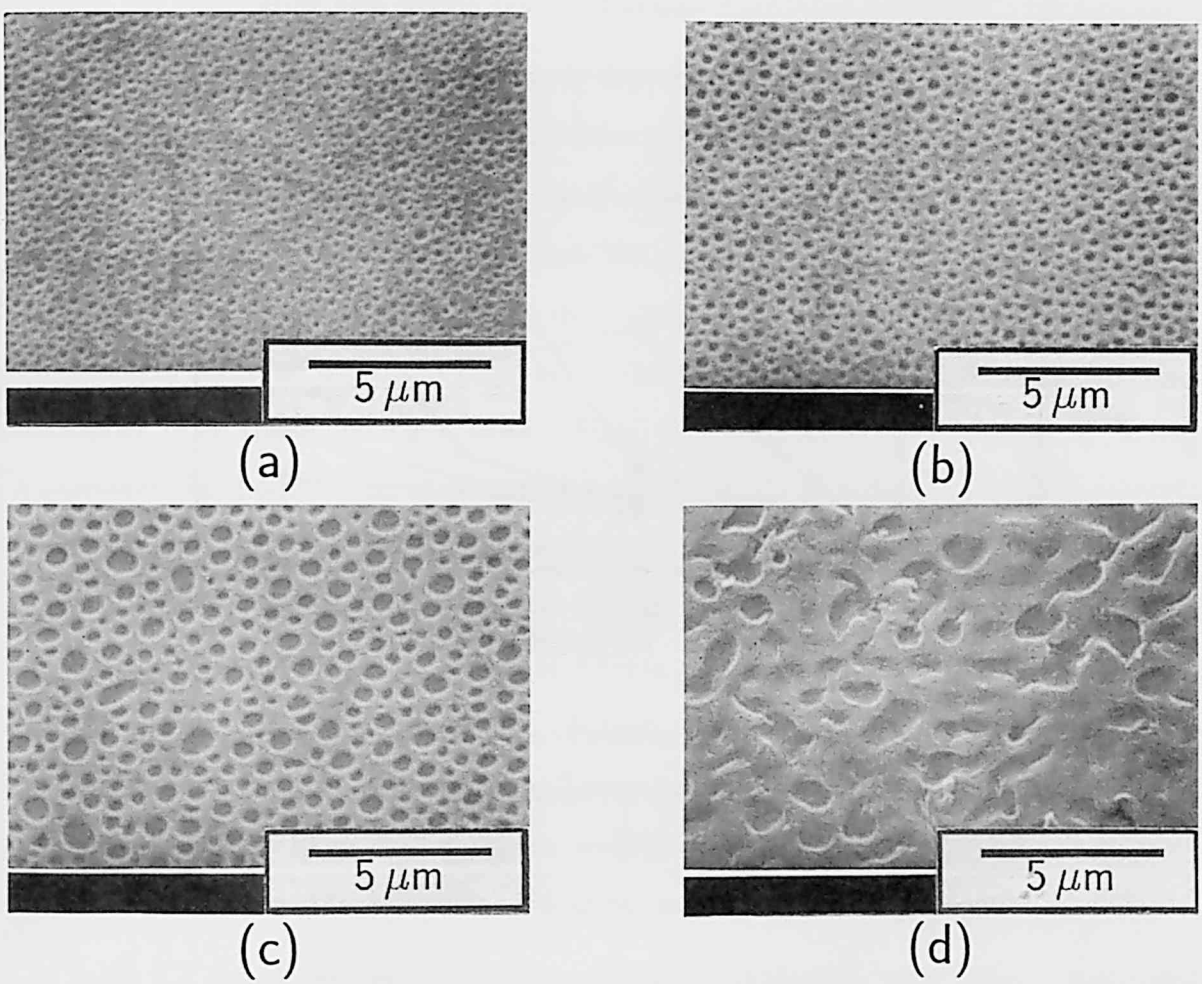

Fig. 4.1: SEM photographs of the TiO_2 films prepared from the solution A2 ($c = 0.14$) at 30% RH. p is (a) 4.0, (b) 5.0, (c) 6.0, (d) 7.0. View angle is 45°.

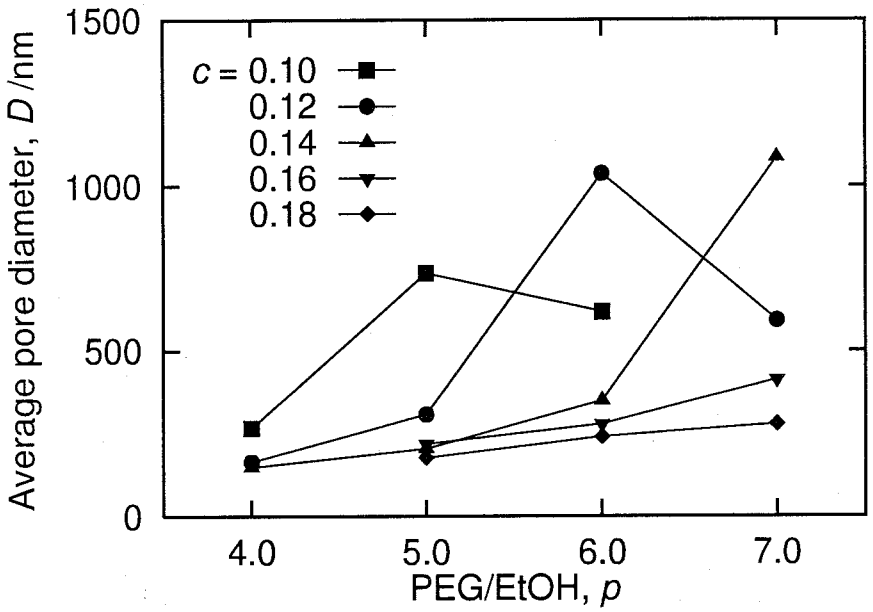

Fig. 4.2: Dependence of average pore diameter D on solution composition for the TiO_2 films prepared from the solution A1 at 30% RH.

dipping is independent of p, the supersaturation of PEG owing to the solvent evaporation occurs earlier at larger p. Then the phase separation is accelerated with an increase in p. Furthermore, the interfered polycondensation by PEG shown in Fig. 2.4 of Chapter 2 could enhance the domain formation additionally by delaying the gelation. The excess incorporation of PEG decreases D in the $c = 0.10$, $p = 6.0$ and the $c = 0.12$, $p = 7.0$ systems as shown in Fig. 4.2. Since the boundary of macropores is no longer clear at these compositions, it is supposed that the surface structure is macroscopically homogenized due to the rapid grow and coalescence of domain.

The macroscopic domain formation is suppressed with an increase in c at a fixed p as listed in Table 4.2. There are two possibilities to explain the result, that is, the accelerated polycondensation and the suppressed phase separation. The accelerated polycondensation does not seem to be acceptable because the gelation is delayed by increasing c when the upper limit of polycondensation rate is determined by the water adsorption rate as discussed in Section 1.4. On the other hand, the suppressed phase separation is anticipated at higher c by the following reasons. First, the lower PEG to TIP ratio at higher c suppresses the modification of titania oligomer by PEG. Second, the decrease in PEG to alcohol ratio owing to the release of additional alcohol by the hydrolysis of TIP increases the compatibility. Furthermore, considering that the thickness is increased to some extent by increasing c, the slower reduction of solvent phase should additionally be responsible for the suppressed phase separation. Indeed, the variation of morphology when c is increased is similar to that when the withdrawal speed is increased. In the latter case, the suppressed domain formation at higher withdrawal speed is interpreted by the decrease in solvent reduction rate due to the thickness increase as discussed in Section 1.3.

Table 4.3 shows the variation of macroscopic morphology with relative humidity in the A2 system. The SEM photographs of the films prepared at 50% RH and the variation of D with relative humidity in the A2 system are respectively shown in Figs. 4.3 and 4.4. The D decreased greatly with an increase in relative humidity at higher p but decreased little at lower p. Therefore all the systems exhibited similar Ds at 50% RH irrespective of the morphology in spite of the larger variation of D at 30% RH. The macropores were isolated at lower p while rather interconnected at higher p as shown in Figs. 4.1 and 4.3.

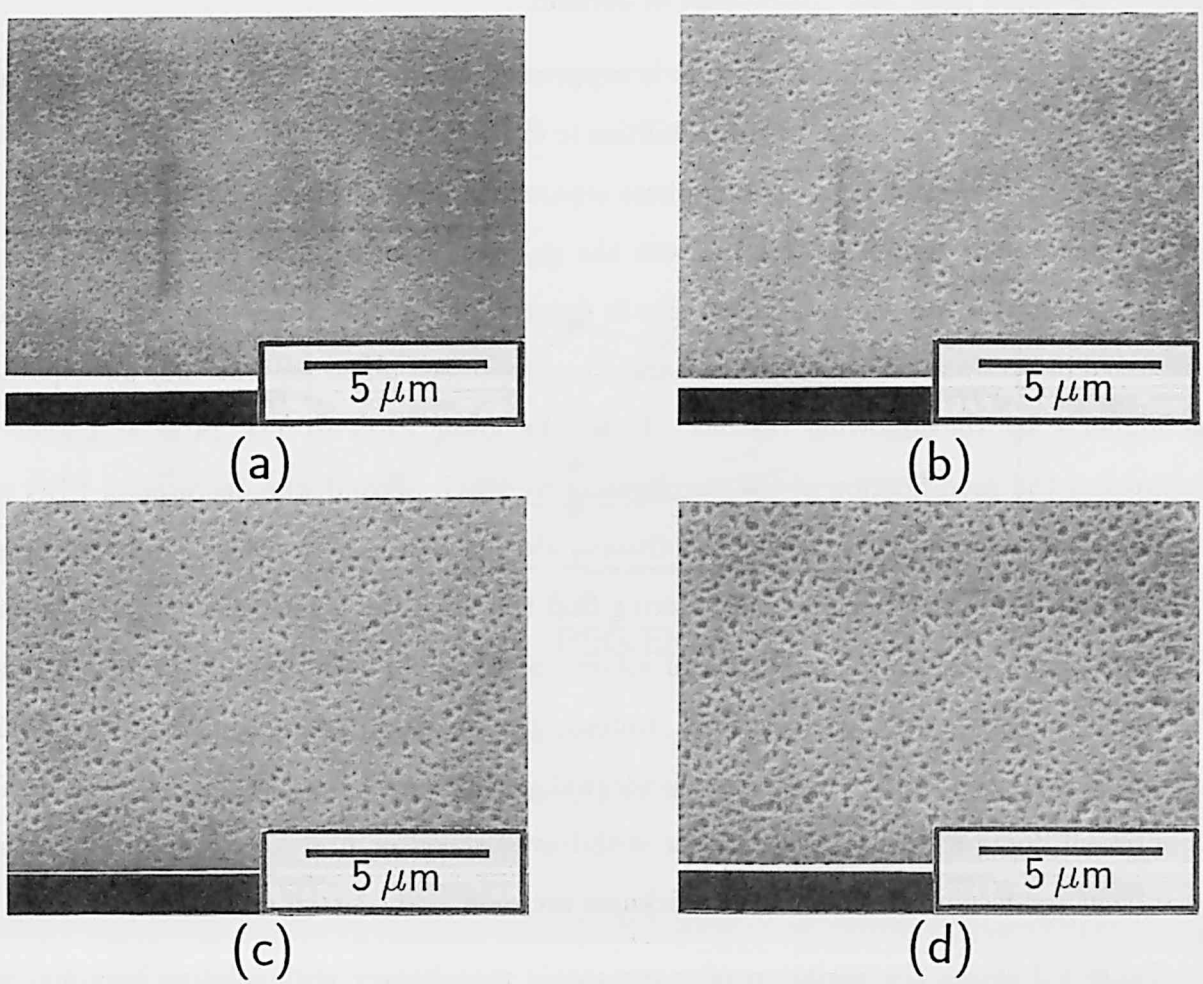

Fig. 4.3: SEM photographs of the TiO_2 films prepared from the solution A2 ($c = 0.14$) at 50% RH. p is (a) 4.0, (b) 5.0, (c) 6.0, (d) 7.0. View angle is 45°.

Table 4.3: Macroscopic morphology of the TiO_2 films prepared from the solution A2: ◡, pits; ●, macropores; ▲, uneven surface.

Relative humidity	PEG/EtOH, p			
(%RH)	4.0	5.0	6.0	7.0
30	◡	●	●	▲
40	◡	●	●	●
50	◡	◡	●	●

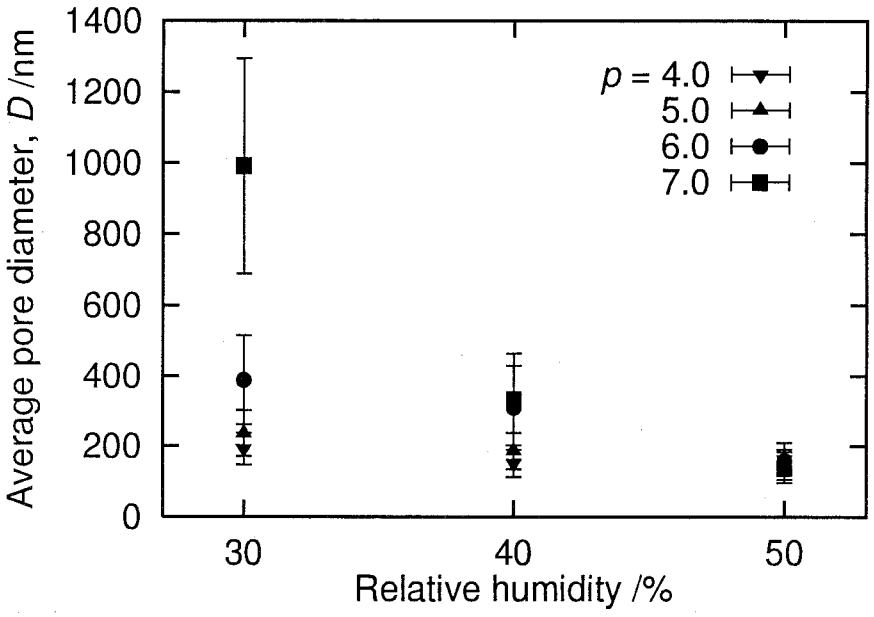

Fig. 4.4: Dependence of average pore diameter D on relative humidity for the TiO_2 films prepared from the solution A2 ($c = 0.14$).

As shown in Fig. 4.4, relative humidity dependence of D is varied greatly by changing p. Although both the polycondensation and the phase separation rates are accelerated with an increase in relative humidity, the polycondensation is preferentially accelerated when the relative humidity is increased at higher withdrawal speed as $30.0\,\mathrm{mm{\cdot}min^{-1}}$ as suggested in Section 1.3. Therefore, the morphology at an early stage of phase separation should be frozen at higher relative humidity. Since Ds at 50% RH are similar irrespective of p, it is supposed that the wavelength of composition fluctuation at an early stage of phase separation depends less on p. In the $p = 7.0$ system, both the nonlinear increase in D with a decrease in relative humidity shown in Fig. 4.4 and the rather interconnected morphology shown in Figs. 4.1(d) and 4.3(d) coincide well with the feature of macroscopic domain formation via spinodal decomposition. On the other hand, D increases little with a decrease in relative humidity in the $p = 4.0$ system. Furthermore, the volume fraction of solvent phase is decreased by decreasing p accompanied by the change of pore shape from interconnected-type to droplet-type as shown in Figs. 4.1 and 4.3. Such variation is reasonable because the volume fraction of solvent phase at which PEG is supersaturated to initiate the phase separation should be almost proportional to p. In general, the phase separation is most enhanced at the critical composition at which the volume fractions of both phases are comparable. Assuming that the present system exhibits an off-critical behavior at lower p, the slowdown of phase separation due to the shallower quench depth and the formation of isolated domains at the later stages are anticipated. Furthermore, the mechanism of phase separation could approach the nucleation-growth type when the quenching path is located almost on the edge of the unstable region surrounded by the spinodal line. These suppositions do not contradict the above results.

4.2.2 Effect of water concentration

Tables 4.4 and 4.5 show the variation of macroscopic morphology with r. Two dipping solutions B1 ($c = 0.12$, $p = 5.0$) and B2 ($c = 0.16$, $p = 7.0$) listed in Table 4.1 were selected as the base compositions at which the macroporous morphology was most apparent as shown in Table 4.2. The SEM photographs of the films prepared from the solution B1 are also shown in Fig. 4.5. Figure 4.6 shows the D–r relationships in the B1 and B2 systems.

In both the systems, D exhibited a maximum at around $r = 1.1$ but the macroporous morphology almost disappeared when r exceeded 1.3. The dipping solution of which r was larger than 1.5 was not stable because the solution originally contained too much water to avoid the macroscopic polycondensation. On the other hand, homogeneous solution could not be prepared at lower r due to the lower solubility of PEG.

As shown in Fig. 4.5, Tables 4.4 and 4.5, the morphology varies from macropores to smooth with an increase in r, because the polycondensation is more accelerated than the phase separation by increasing the water concentration and therefore the sol-gel transition occurs at an early stage of phase separation. However, D exhibits a maximum at about $r = 1.1$ as shown in Fig. 4.6, indicating that the increase in water concentration preferentially accelerates the phase separation below the certain r. Similar phenomenon occurs when the relative humidity is increased. Especially at lower withdrawal speed, the macroscopic domain formation is once enhanced with an increase in relative humidity but is suppressed with a further increase in relative humidity as shown in Section 1.3. It is supposed that the hydrophobic modification of titania oligomer by PEG decreases the solubility of titania oligomer in spite of the good compatibility between the hydrolyzed titania oligomer and the solvent mixture. The enhanced hydrolysis of titania oligomer would be preferable for the adsorption of PEG because the surface hydroxy group is important to form the hydrogen bond to ether oxygen of PEG. In addition, the titania oligomer has to grow into moderate size to enhance the adsorption and chelation of PEG because the complex formation is thermodynamically promoted as the number of hydrogen bonds increases. Then mainly due to the enhanced formation of the titania-PEG complex, the phase separation is accelerated with an increase in r below $r = 1.1$.

The D decreases rapidly with a further increase in r. As listed in Table 1.5 of Chapter 1, solution of which r is smaller than 1.25 is stable more than a week under a closed condition due to the exhaustion of water. On the contrary, macroscopic polycondensation is observed when r is larger than 1.5 and the solution gels immediately after the preparation when r is larger than 2.0. Therefore it may be enough for the polycondensation to inhibit the phase separation if the water adsorption increases r of the sol film to about 2.0 during the dipping. Moreover, dissolution behavior of PEG listed in Table 5.8 of

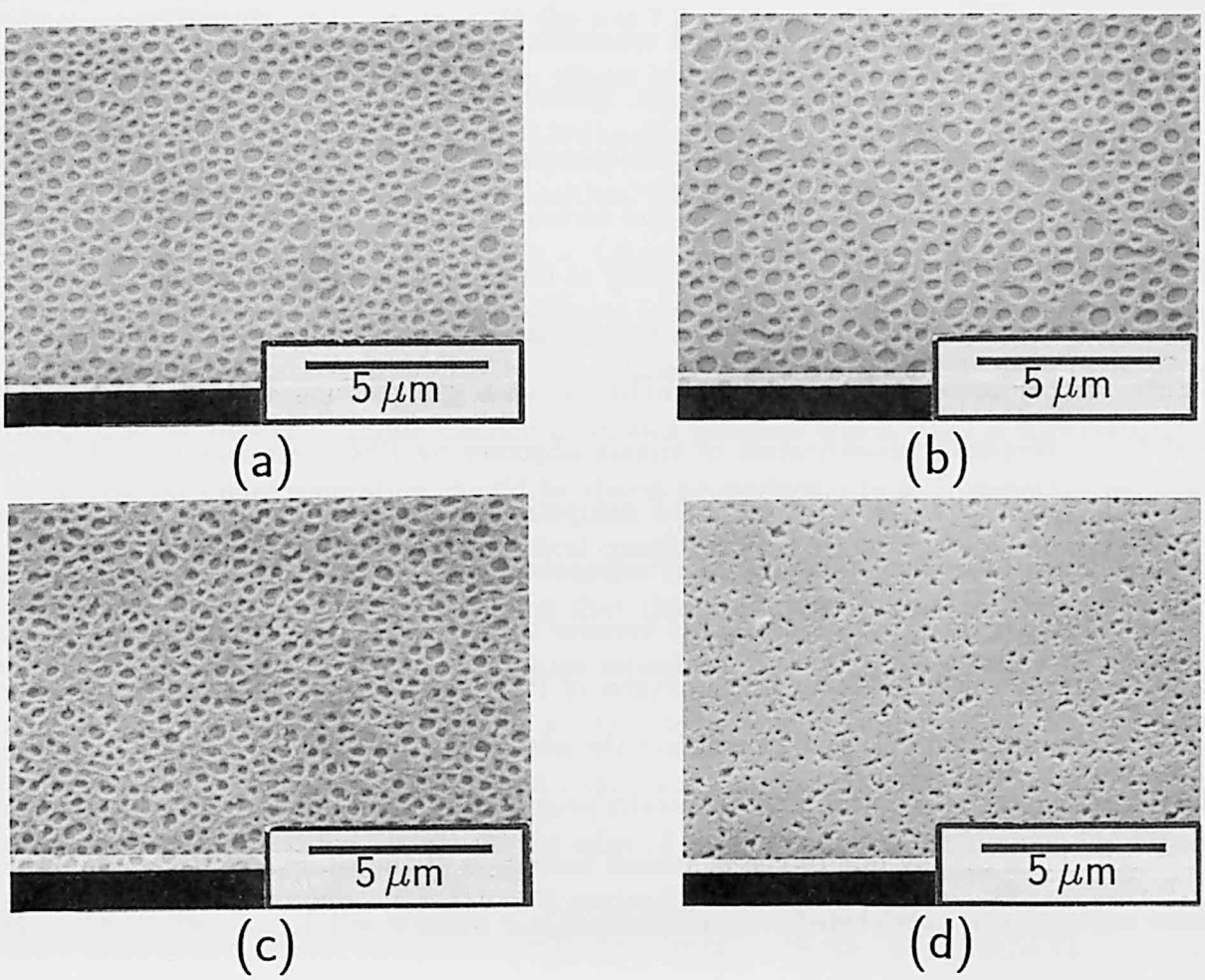

Fig. 4.5: SEM photographs of the TiO_2 films prepared from the solution B1 ($c = 0.12$, $p = 5.0$) at 30% RH. r are (a) 1.00, (b) 1.08, (c) 1.17, (d) 1.25. View angle is 45°.

Table 4.4: Macroscopic morphology of the TiO_2 films prepared from the solution B1 (c = 0.12, p = 5.0) at 30% RH: -, smooth; ◡, pits; ●, macropores.

H_2O	0.08	0.10	0.12	0.13	0.14	0.15	0.16
H_2O/TIP, r	0.67	0.83	1.00	1.08	1.17	1.25	1.33
Morphology	◡	●	●	●	●	●	-

Table 4.5: Macroscopic morphology of the TiO_2 films prepared from the solution B2 (c = 0.16, p = 7.0) at 30% RH: -, smooth; ◡, pits; ●, macropores.

H_2O	0.14	0.16	0.17	0.18	0.19	0.20	0.21	0.22
H_2O/TIP, r	0.88	1.00	1.06	1.13	1.19	1.25	1.31	1.38
Morphology	●	●	●	●	●	●	◡	-

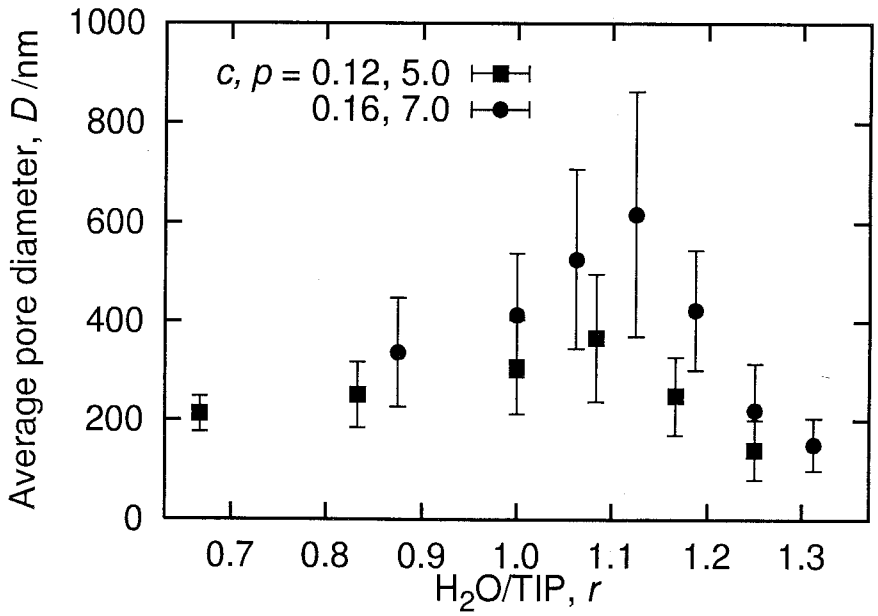

Fig. 4.6: Dependence of average pore diameter D on water to TIP ratio r for the TiO_2 films prepared from the solutions B1 (c = 0.12, p = 5.0) and B2 (c = 0.16, p = 7.0) at 30% RH.

Chapter 5 strongly suggests that the appearance of free water in the dipping solution can suppress the phase separation by increasing the compatibility among the constituents.

Both the macroscopic morphology and D can be similar between the films prepared at lower r and higher r as typically shown in Figs. 4.1(b) ($r = 1.00$) and 4.5(c) ($r = 1.17$), but the morphology is slightly different. The formation of rather stereoscopically interconnected macropores in the latter can be explained in several ways. One possibility is the longer metalloxane chain length in the water-rich system. It is reported that the linear metalloxane polymers are formed under acid-catalyzed conditions when r is lower than 2 [10–13]. Therefore, the polycondensation degree of linear or loosely branched titania oligomer is expected to increase with an increase in r as long as r is not too large. Such a spinnable sol is supposed to suppress the fragmentation of domain even if the pore wall becomes thin during the phase separation compared to water-poor sols with lower dynamic viscosity. Another possibility is the enhanced hydrolysis accompanied by the release of alcohol, which not only enhances the formation of titania-PEG complex but also could increase the volume fraction of solvent phase. Thus the phase separation could proceed near the critical composition at which the interconnected morphology is preserved for a long time. The films having interconnected pore structure are expected to be desirable in enhancing the surface area and material transport in the film. Figure 4.7 shows the SEM photographs of the TiO_2 films prepared from the solution B3 ($c = 0.12$, $r = 1.17$) under the variation of p. In that condition, D can be increased by increasing p with maintaining the interconnected macroporous morphology.

It is considered that the dip-coating method is not favorable as an industrial sol-gel film depositing process because this method is a batch process and essentially requires a solution bath as large as the substrate. Recently, however, a procedure named "laminar flow coating" has been proposed as a technique to fabricate sol-gel thin film, in which gel films are deposited using tubular solution dispenser units gently slid under the surface of the substrate [14]. This method is supposed to be advantageous from the standpoints that (a) larger film can be deposited continuously without using solution baths, (b) solvent evaporation during the deposition is uniform and mild in contrast to the spin-coating method, and (c) multi-layered films can be prepared with ease by sliding multiple dispenser

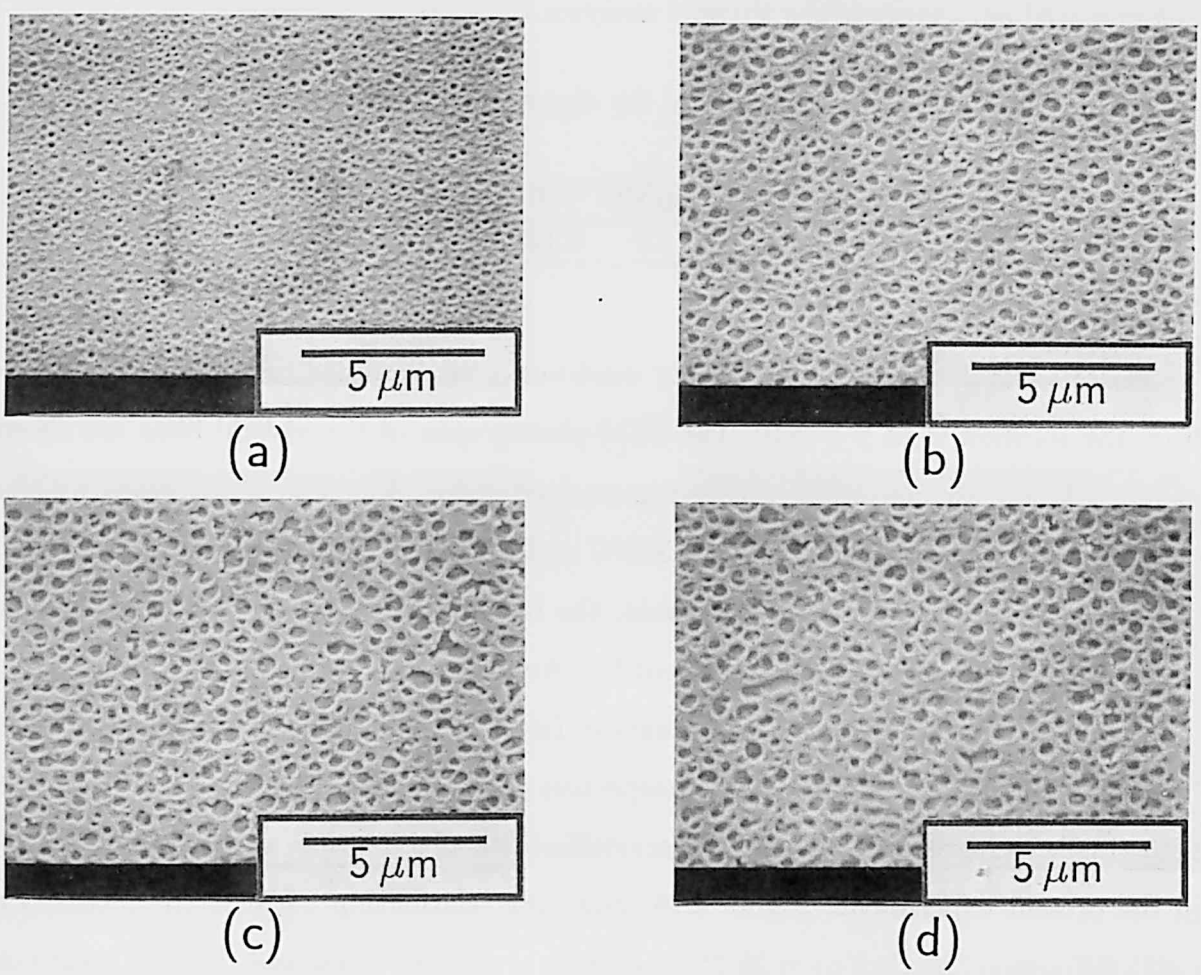

Fig. 4.7: SEM photographs of the TiO_2 films prepared from the solution B3 ($c = 0.12$, $r = 1.17$) at 30 %RH. p is (a) 4.0, (b) 5.0, (c) 6.0, (d) 7.0. View angle is 45°.

units successively. Since the deposition dynamics of the dip-coating and the laminar flow coating methods seem to be similar in many points, the macroporous films would be prepared at analogous conditions.

4.3 Effect of heat treatment

The effect of heat treatment was examined for the composition listed in Table 4.6. The PEG having average molecular weight of 2,000 was incorporated. The PEG-free solution was prepared only to serve the thermal analyses.

Table 4.6: Compositions of the dipping solutions C (unit: mol).

Solution	H_2O	EtOH	TIP	HNO_3	PEG (g)
C	0.12	1.0	0.12	0.02	0, 5.0

Variation of D with heat treatment condition was examined for the films prepared from the solution C at $p = 5.0$. The SEM photographs of the several films are shown in Fig. 4.8, and the variation of D is summarized in Fig. 4.9. The D increased with an increase in heating temperature below 300°C under the heat treatment for 10 min. When the heating time was extended to 60 min, the increase in D at 200°C was noteworthy compared to D under the heat treatment for 10 min.

The XRD analysis revealed that anatase TiO_2 crystalline phase was always formed by the heat treatment above 400°C irrespective of the heating time but the film heated below 300°C remained amorphous. No crystalline phases other than anatase were detected in the present experiment. Figure 4.10 shows the relationship between the intensity of (101) diffraction ($2\theta(\mathrm{Cu}K\alpha) = 25.3°$) of anatase crystalline phase and the heat treatment condition. The diffraction intensity increased with an increase in heating temperature and time, but was saturated by the heat treatment at 600°C for 60 min and 700°C.

The dried titania gel prepared by simply evaporating the solvent component of the dipping solution was subjected to TG-DTA. Figure 4.11 shows the TG and DTA curves of titania gels derived from the solutions C listed in Table 4.6. The gradual weight loss below 300°C was ascribable to the evaporation of residual solvent and the combustion of

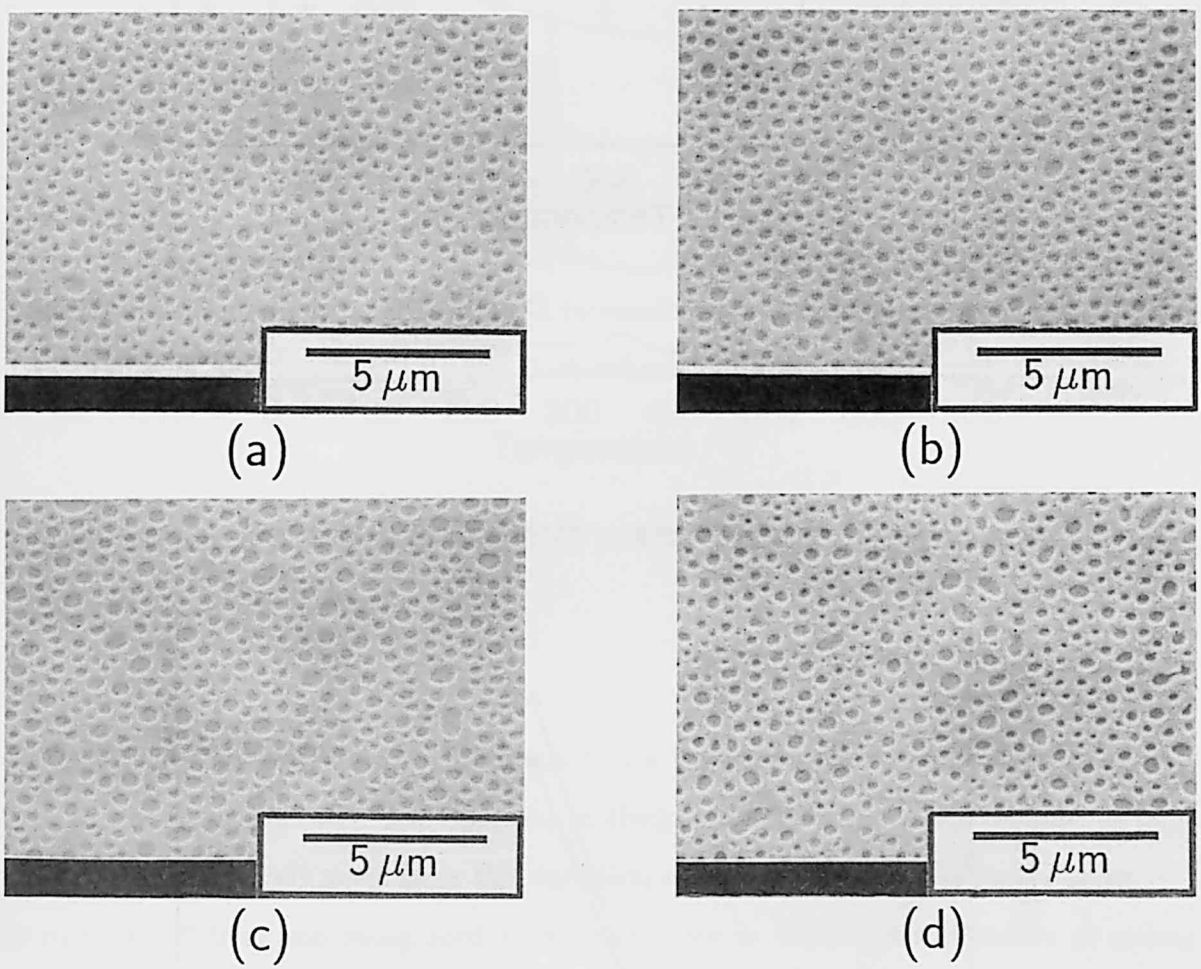

Fig. 4.8: SEM photographs of the TiO_2 films prepared from the solution C ($c = 0.12$) at $p = 5.0$, 30% RH. Heat treatment condition is at (a) 100, (b) 200, (c) 300°C for 10 min, and at (d) 200°C for 60 min. View angle is 45°.

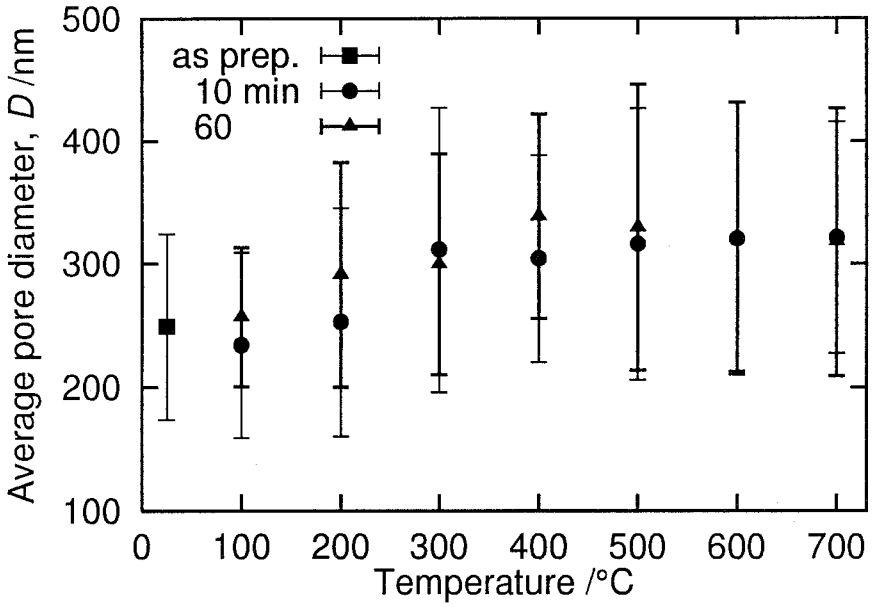

Fig. 4.9: Dependence of average pore diameter D on heat treatment condition for the TiO_2 films prepared from the solution C ($c = 0.12$) at $p = 5.0$, 30% RH.

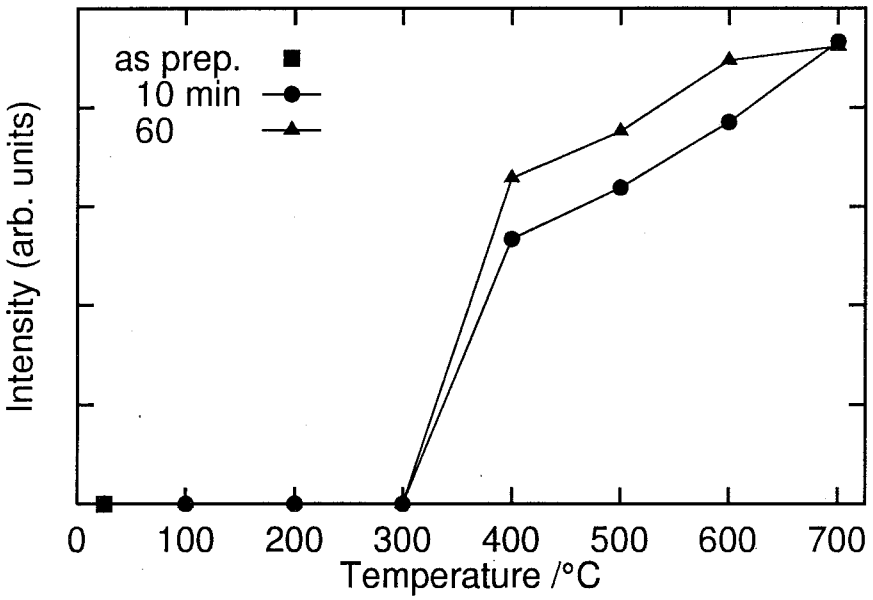

Fig. 4.10: Dependence of anatase (101) diffraction intensity on heat treatment condition for the TiO_2 films prepared from the solution C ($c = 0.12$) at $p = 5.0$, 30% RH.

organic substances. The PEG was thermally decomposed at about 280°C accompanied by an abrupt weight loss and a large exothermic peak in the $p = 5.0$ system. A small exothermic peak at about 350°C in the PEG-free gel was attributed to the crystallization of amorphous titania gel into anatase.

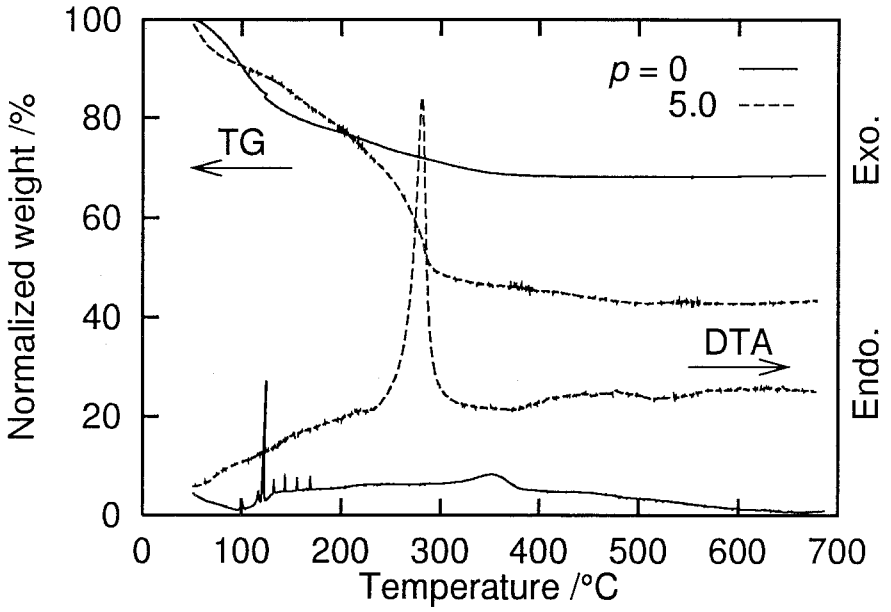

Fig. 4.11: TG and DTA curves of titania gel powders derived from the solution C ($c = 0.12$, $p = 0$ or 5.0).

The morphology of resultant titania gel film is influenced by the heat treatment condition as shown in Fig. 4.8. The decrease in thickness with an increase in heating temperature is qualitatively seen from the variation of the shadow of macroporous region. The increase in D is also recognized with an increase in heating temperature as shown in Fig. 4.9. The increase in D is most apparent between 100 and 300°C under the heat treatment for 10 min. The TG and DTA curves of the $p = 5.0$ system shown in Fig. 4.11 respectively exhibit a pronounced weight loss and a large exothermic reaction at about 280°C because of the combustion of PEG. A simple calculation shows that the amount of PEG incorporated is about the half of the amount of titania content in terms of TiO_2, and the calculation seems to be comparable to the TG result by considering the evaporation of residual solvent. In addition, when the heating time is extended to 60 min, significant

increase in D is observed at 200°C, at which the TG curve begins to bend downward as shown in Fig. 4.11. Consequently, the decomposition of PEG is the most responsible for the variation of macroscopic morphology.

A small exothermic peak is observed at about 350°C in the DTA curve for the PEG-free system corresponding to the crystallization of titania gel. Although the system containing PEG does not show such an exothermic peak apparently in its DTA curve, the present titania gel film is supposed to crystallize at about 350°C irrespective of the addition of PEG, because the heat treatment above 400°C is always required to crystallize the gel film as shown in Fig. 4.10. Then the decomposition of PEG seems to be less important for the formation of anatase. The rutile phase is not formed even by the heat treatment at 700°C for 60 min. Similarly, the crystalline phase of the TiO_2 film prepared from the solution consisting of TIP, water, ethanol, and hydrochloric acid is reported to remain anatase by the heat treatment up to 800°C [15]. However, the formation of rutile is reported at 600°C for the film prepared from the solution consisting of TIP, water, 2-propanol, and DEA although the anatase crystallization temperature remains between 300 and 400°C [16].

4.4 Conclusions

The macroscopic morphology was investigated at various preparation conditions to elucidate the general principle of morphology formation on the TiO_2 films prepared from the solution containing PEG. Besides, the effect of heat treatment on morphology was examined. Based on the results, the correlation between the morphologies was discussed. The results obtained are summarized as follows:

(1) The variation of macroscopic morphology is consistently explained by considering both the volume fraction of solvent phase during the phase separation and the water to TIP ratio in the sol film. The volume fraction of solvent phase mainly determines the type and rate of phase separation. On the other hand, the water to TIP ratio not only determines the period during which the macroscopic domain formation can progress but also modifies the phase separation rate. It is pointed out that laminar flow coating method can be an advantageous method in depositing macroporous films continuously on one side of the larger substrate through sol-gel route.

(2) The thermal decomposition of PEG dominates the shrinkage of the gel film accompanied by the increase in average pore diameter, while is responsible for little of the crystallization of titania gel film.

References

[1] J. W. Cahn and R. J. Charles, Phys. Chem. Glasses **6**, 181 (1965).

[2] W. D. Kingery, H. K. Bowen, and D. R. Uhlmann, in *Introduction to Ceramics*, 2 ed. (John Wiley & Sons, New York, 1976), Chap. 8.

[3] K. Nakanishi, Y. Yamasaki, H. Kaji, N. Soga, T. Inoue, and N. Nemoto, J. Sol-Gel Sci. Technol. **2**, 227 (1994).

[4] K. Nakanishi, J. Porous Mater. **4**, 67 (1997).

[5] T. Hashimoto, M. Itakura, and H. Hasegawa, J. Chem. Phys. **85**, 6118 (1986).

[6] T. Hashimoto, M. Itakura, and N. Shimidzu, J. Chem. Phys. **85**, 6773 (1986).

[7] J. W. Cahn, Acta Metal. **9**, 795 (1961).

[8] J. W. Cahn, J. Chem. Phys. **42**, 93 (1965).

[9] K. Kato, A. Tsuzuki, Y. Torii, H. Taoda, T. Kato, and Y. Butsugan, J. Mater. Sci. **30**, 837 (1995).

[10] S. Sakka and H. Kozuka, J. Non-Cryst. Solids **100**, 142 (1988).

[11] K. Kamiya, K. Tanimoto, and T. Yoko, J. Mater. Sci. Lett. **5**, 402 (1986).

[12] T. Yoko, K. Kamiya, and K. Tanaka, J. Mater. Sci. **25**, 3922 (1990).

[13] C. J. Brinker and G. W. Scherer, in *Sol-Gel Science: The Physics and Chemistry of Sol-Gel Processing* (Academic Press, New York, 1990), Chap. 2.

[14] P. F. Belleville and H. G. Floch, J. Sol-Gel Sci. Technol. **3**, 23 (1994).

[15] T. Yoko, A. Yuasa, K. Kamiya, and S. Sakka, J. Electrochem. Soc. **138**, 2279 (1991).

[16] Y. Takahashi and Y. Matsuoka, J. Mater. Sci. **23**, 2259 (1988).

Chapter 5

Morphology formation in system containing poly(ethylene glycol) and poly(vinylpyrrolidone)

5.1 Introduction

Poly(vinylpyrrolidone) (PVP; [-$CH_2CH($ $\underline{NCOCH_2CH_2CH_2}$$)$-$]_n$) is an organic polymer having amide-carbonyl group, and is quite soluble in water and alcohols even if the molecular weight is quite large as several million. Such property of PVP has been utilized to increase the thickness of sol-gel derived films. Crack-free TiO_2 and $BaTiO_3$ films as thick as 1 μm have been fabricated from the solution containing PVP after a single dipping and subsequent heat treatment at 700°C because the structural relaxation caused by PVP reduces the tensile stress emerged during the heat treatment [1].

The recent development of sol-gel derived organic-inorganic composite materials reveals the importance to investigate the molecular-level interactions among the constituents of the reaction mixture [2–5]. It seems that most of works were done at higher water to alkoxide ratio (r), typically $r \geq 2$ [3,6,7], probably because the supplement of water usually enhances the compatibility among the constituents and results in homogeneous gels. However, the research at lower r as 1–2 is also important particularly for the film and fiber fabrications, because the long term stability of the precursor solution is anticipated whereas alkoxides are often not stable at higher water concentration.

In the present chapter, variations of morphology and thickness are examined for the macroporous TiO_2 films prepared from the solution containing PVP together with PEG primarily aiming at thicker macroporous films. The mechanism of domain formation is discussed correlating with the interactions among the constituents.

5.2 Variations of morphology and thickness

Table 5.1 lists the compositions of the dipping solutions. The PEG having average molecular weight of 2,000, and PVPs having average molecular weights of 360,000 and 1,300,000 (Aldrich Chemical Ltd.) were used. The PEG and PVP concentrations are respectively indicated by p_{PEG} and p_{PVP} as polymers to ethanol ratios.

Table 5.1: Compositions of the dipping solutions (unit: mol).

H_2O	EtOH	TIP	HNO_3	PEG (g)	PVP (g)
0.12	1.0	0.12	0.02	0, 3.0–5.0	0–2.0

5.2.1 Effect of polymer concentration

The PVP360000 was used as PVP content. Table 5.2 shows the macroscopic morphology of the TiO_2 films prepared at 25°C, 30% RH. The SEM photographs of the films prepared from the (p_{PEG}, p_{PVP}) = (5.0, 0.5) and (5.0, 1.0) systems are also shown in Figs. 5.1 and 5.2. The stereoscopic interconnection of macroporous morphology has been realized because the thickness was increased by incorporating PVP. Since similar morphology was observed even before the heat treatment, the macroporous morphology is suggested to be formed during the dipping operation. The thickness increased whereas the domain size decreased with an increase in withdrawal speed.

In the $p_{PVP} = 0.5$ system, the macroscopic domain formation was significant at lower withdrawal speed while the domain size decreased quickly with an increase in withdrawal speed. On the contrary, the domain size was relatively small and was varied little with withdrawal speed in the $p_{PVP} = 1.0$ system. In addition, several small cracks were observed in the $p_{PVP} = 1.0$ system. In the $p_{PVP} = 1.5$ and 2.0 systems, the formation of macroscopic cracks became evident instead of the formation of macroporous morphology. The solution without PEG did not afford the formation of macroscopic domain.

Figure 5.3 shows the SEM photographs of the TiO_2 films prepared from the $p_{PVP} = 0.5$ system at 22.5 mm·min^{-1} of withdrawal speed under the variation of p_{PEG}. The domain

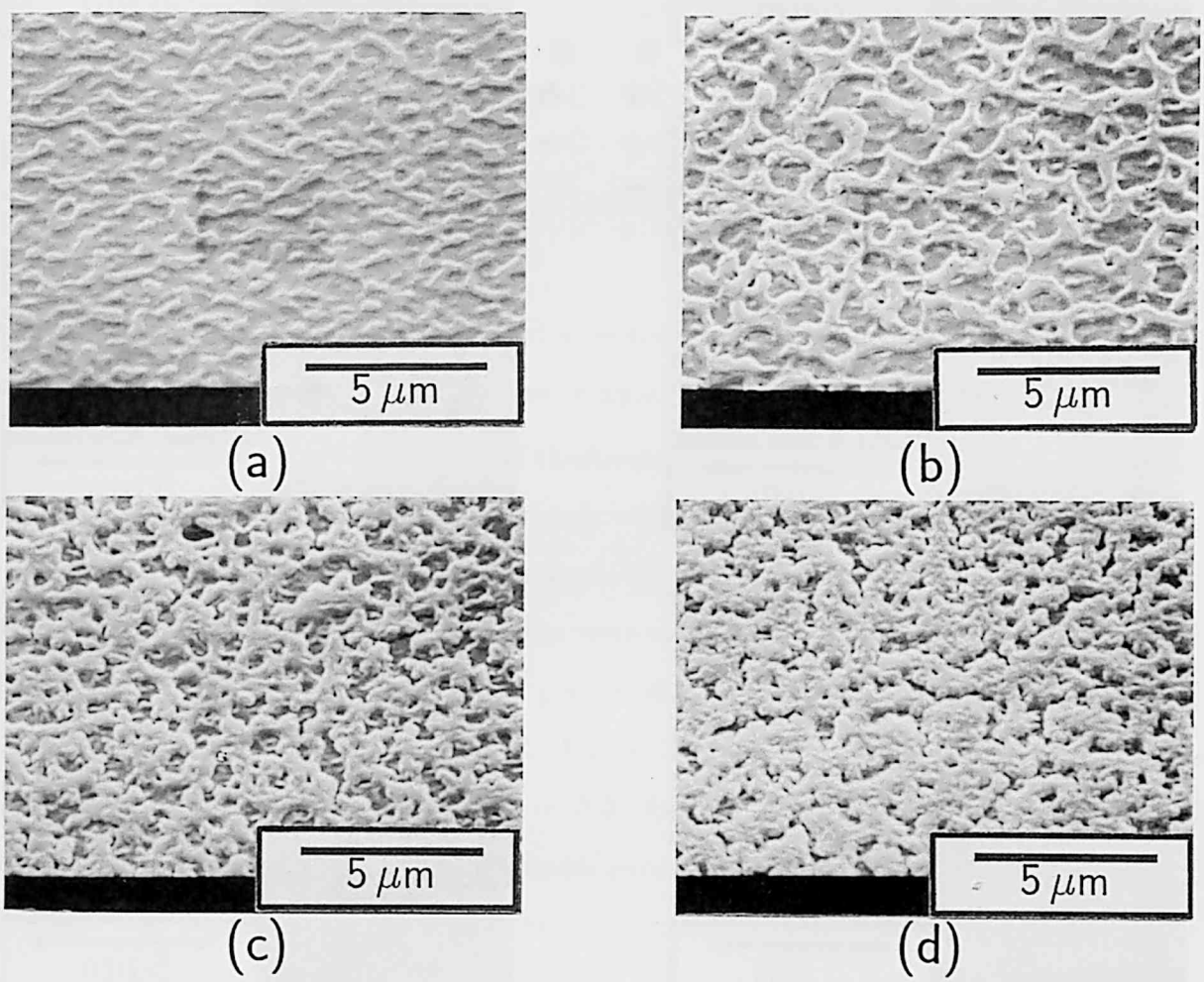

Fig. 5.1: SEM photographs of the TiO_2 films prepared from the PEG2000-PVP360000 system at (p_{PEG}, p_{PVP}) = (5.0, 0.5). Withdrawal speed is (a) 7.5, (b) 15.0, (c) 22.5, (d) 30.0 mm·min^{-1}. View angle is 45°.

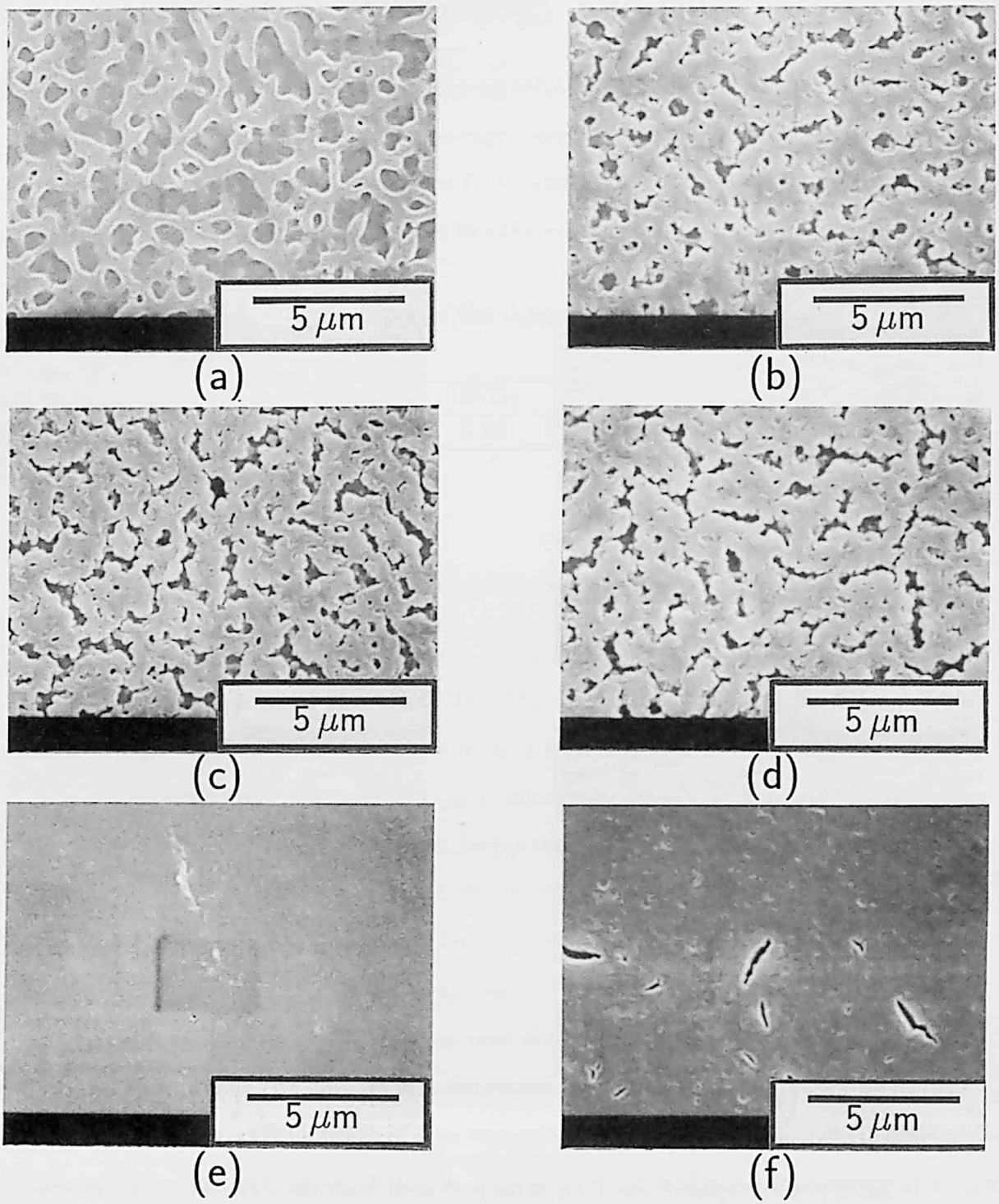

Fig. 5.2: SEM photographs of the TiO_2 films prepared from the PEG2000-PVP360000 system at $p_{PEG} = 5.0$. p_{PVP} and withdrawal speed ($mm \cdot min^{-1}$) are (a) (0.5, 15.0), (b) (1.0, 15.0), (c) (0.5, 30.0), (d) (1.0, 30.0), (e) (0.5, 60.0), (f) (1.0, 60.0). View angle is 0°.

Table 5.2: Macroscopic morphology of the TiO_2 films prepared from the PEG2000-PVP360000 system at 25°C, 30% RH: -, smooth; ◡, pits; ●, macropores; ▲, uneven surface; C, macroscopic cracks.

p_{PEG}	p_{PVP}	Withdrawal speed ($mm \cdot min^{-1}$)					
		7.5	15.0	22.5	30.0	45.0	60.0
0	0	-	-	-	-	-	-
0	1.0	-	-	-	-	C	C
0	2.0	-	-	-	-	C	C
5.0	0.5	▲	●	●	●	◡C	-
5.0	1.0	◡	●C	●C	◡C	◡C	◡
5.0	1.5	◡	◡C	◡C	◡C	◡C	◡C
5.0	2.0	C	C	◡C	◡C	◡C	C

size and the macropore volume increased monotonically with an increase in p_{PEG} from 3.0 to 6.0 with maintaining the macroporous morphology.

Figure 5.4 shows the dependence of thickness on withdrawal speed and p_{PVP} at p_{PEG} = 0. The thickness increased almost linearly with an increase in withdrawal speed. The resultant film was smooth and no macroscopic domain was observed. Although the adhesion and transparency of as-deposited film were always good, the film prepared at higher withdrawal speed and larger p_{PVP} was peeled off after the heat treatment as indicated by the open symbols and dotted lines. Figure 5.5 shows the dependence of thickness on withdrawal speed and p_{PVP} at p_{PEG} = 5.0. In contrast to Fig. 5.4, the formation of macroscopic domain increased the thickness excessively at around 15.0–30.0 $mm \cdot min^{-1}$. The film also peeled off by increasing the withdrawal speed and p_{PVP} too much.

Figure 5.6 shows the TG and DTA curves of the dried gel derived from the p_{PVP} = 1.0 dipping solution. The decomposition of PEG caused the considerable weight loss accompanied by the large exothermic peak at about 280°C similarly to the result of the PVP-free system shown in Fig. 4.11 of Chapter 4. The weight loss at about 500°C due to the decomposition of PVP was roughly estimated to be one fifth of that at about 280°C. This ratio agrees well with the PVP to PEG ratio of the dipping solution.

It is well known that both PEG and PVP are water-soluble organic polymers having

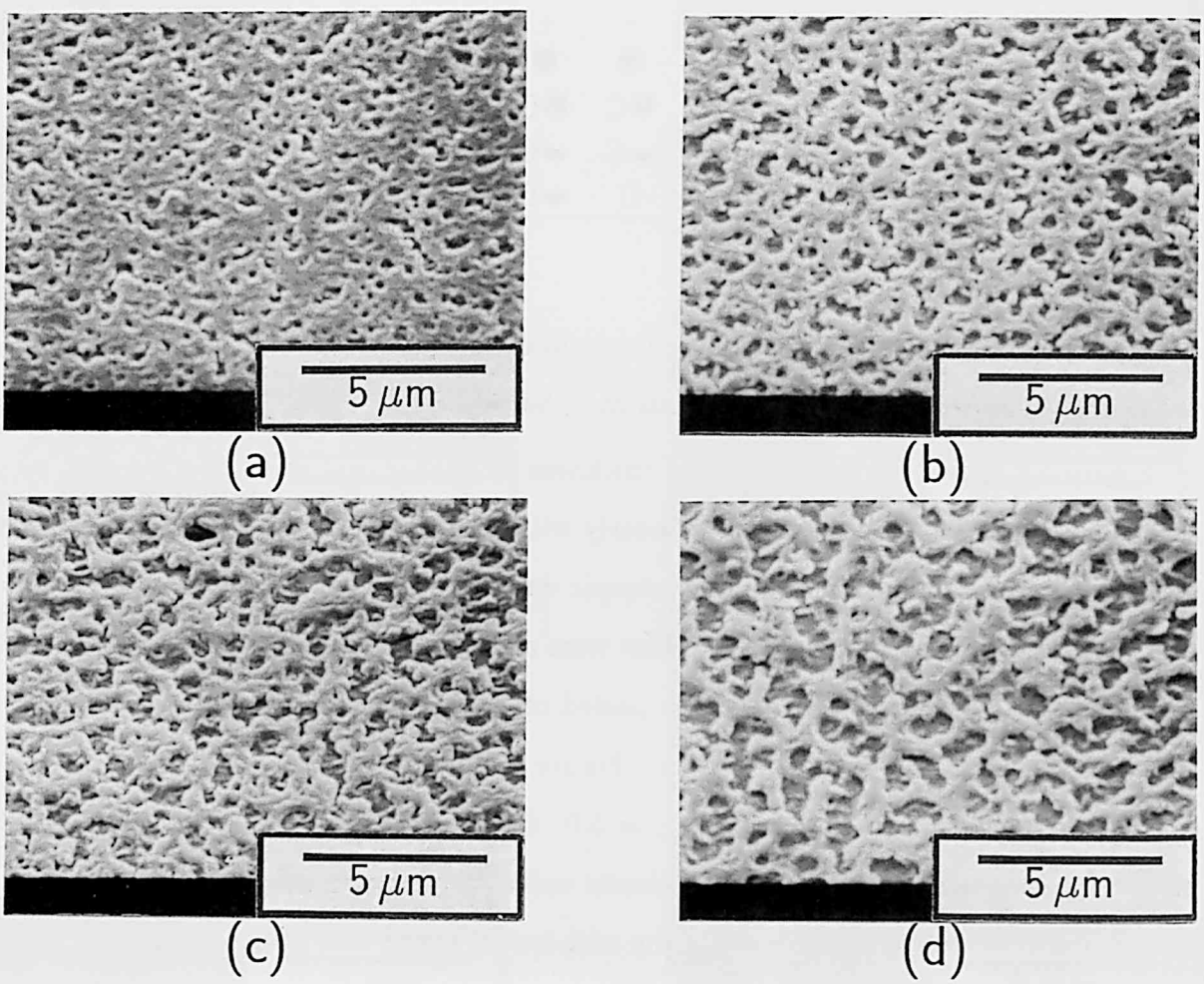

Fig. 5.3: SEM photographs of the TiO_2 films prepared from the PEG2000-PVP360000 system at p_{PVP} = 0.5, 22.5 mm·min^{-1} of withdrawal speed. p_{PEG} is (a) 3.0, (b) 4.0, (c) 5.0, (d) 6.0. View angle is 45°.

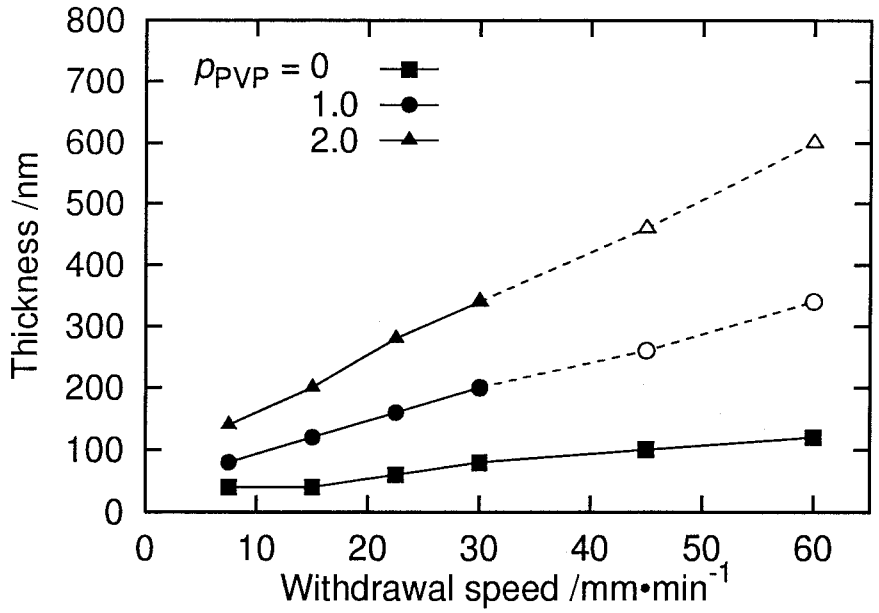

Fig. 5.4: Dependence of thickness on withdrawal speed and p_{PVP} at $p_{PEG} = 0$. Open symbol denotes the thickness of the peeled-off TiO_2 film.

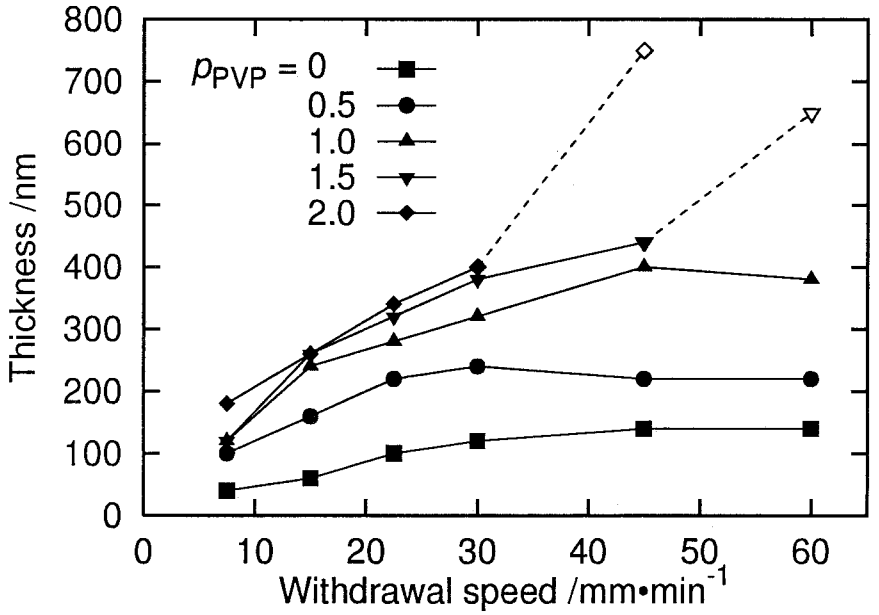

Fig. 5.5: Dependence of thickness on withdrawal speed and p_{PVP} at $p_{PEG} = 5.0$. Open symbol denotes the thickness of the peeled-off TiO_2 film.

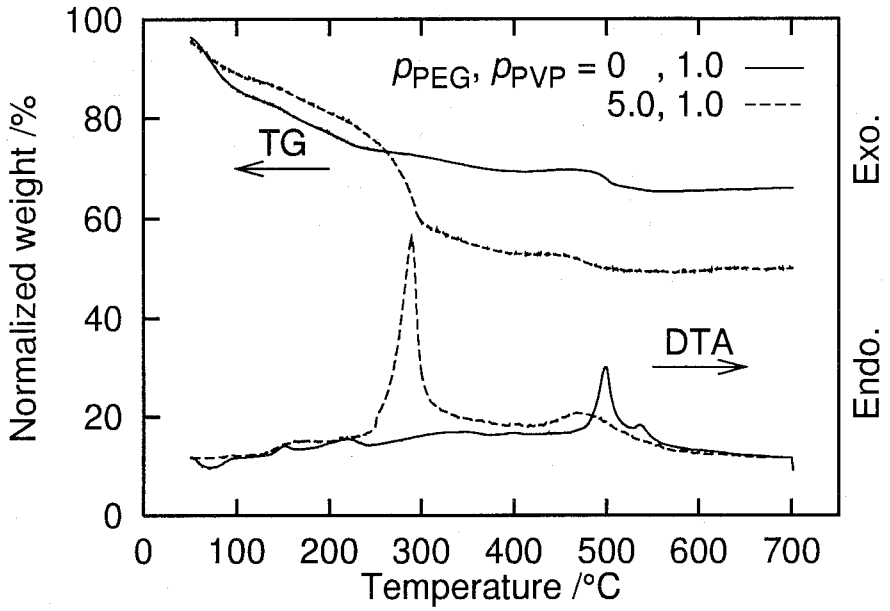

Fig. 5.6: TG and DTA curves of titania gel powders derived from the (p_{PEG}, p_{PVP}) = (5.0, 0) and (5.0, 1.0) solutions.

proton-accepting ability. The PEG is reported not only to adsorb on hydrolyzed oxides [8–10] but also to complex with poly(carboxylic acid) such as poly(acrylic acid) (HPAA) [11–13], because ether oxygen of PEG can be electron donor for electropositive atoms such as hydrogen and metal atoms. The complexation strength of PVP with poly(carboxylic acid) is larger than that of PEG because of the electronegative amide-carbonyl group [12, 14]. Since the types of hydrogen bonding character are similar between PEG and PVP, direct complexation between PEG and PVP is considered to be less important. This assumption seems to be valid because the results of TG-DTA shown in Fig. 5.6 suggest that the decompositions of PEG and PVP are almost independent.

Table 5.3 shows the compatibility between polymer contents and several solvents. Good compatibility between PVP and alcohol is noteworthy although the molecular weight of PVP is considerably large as 360,000. The considerable solvation of the amide-carbonyl group with polar solvent molecules and the lower crystallinity of PVP would be the main reasons of higher solubility. Since the solvent phase of the present system mainly consists of ethanol and 2-propanol, the compatibility between PVP and the solvent mixture would be better than that of PEG.

Table 5.3: Dependence of solubility limit of polymer content on solvent type (unit: wt%).

	H_2O	EtOH	2-PrOH	TIP
PEG2000	>50	1	<1	<1
PVP360000	>25	>25	>25	<1

It is considered that the phase separation is induced by the solvent evaporation during the dipping operation followed by the supersaturation and exsolution of the titania-PEG complex, because the solubility of PEG to the dipping solution is relatively low as listed in Table 3.10 of Chapter 3. The interconnected macroporous morphology typically shown in Figs. 5.1(b) and (c), and 5.2(a) suggests that the phase separation proceeds via spinodal decomposition. The domain size and macropore volume increase monotonically with an increase in p_{PEG} as shown in Fig. 5.3, similarly to the variation of the PVP-free PEG2000

systems shown in Section 4.2. Furthermore, the formation of macroscopic domain increases the thickness excessively at about 15.0–30.0 mm·min^{-1} as shown in Fig. 5.5. The macroscopic domain formation could not be seen in the systems containing PVP as an only polymer content as shown in Table 5.2. Then it is suggested that only PEG is responsible for the formation of macroporous morphology and PVP does not contribute to the phase separation due to the higher solubility. In contrast, the thickness depends significantly on p_{PVP} as shown in Figs. 5.4 and 5.5 because PVP greatly increases the solution viscosity.

The macroporous morphology almost disappears at higher p_{PVP} as listed in Table 5.2. Since the domain formation occurs under the rapid supersaturation of the titania-PEG complex and the slower fluidity reduction or gelation, two different mechanisms can be considered. First, the higher solution viscosity interferes the domain formation at higher p_{PVP}. Second, the slower fluidity reduction in a thicker film allows the dissolution of the titania-PEG complex for a long time and suppresses the phase separation. The suppressed domain formation at higher withdrawal speed is explained by the latter mechanism as discussed in Section 1.3. Although the fluidity of sol film decreases with an increase in p_{PVP}, the fluidity reduction rate also decreases due to the thickness increase. Hence the latter mechanism seems to explain well the suppressed domain formation at higher p_{PVP}. The enhanced crack formation at thicker films is attributed to the larger film deformation during the drying and the heating stages. The films having macroscopic cracks are often thicker than the expected because of the suppressed vertical shrinkage and the warp of the film pieces.

5.2.2 Effect of dipping temperature

The PVP1300000 was used as PVP content. Table 5.4 shows the macroscopic morphology of the TiO_2 films prepared at $p_{\mathrm{PEG}} = 5.0$, 30% RH. Since the excess incorporation of PVP enhances the formation of macroscopic cracks as listed in Table 5.2, $p_{\mathrm{PVP}} = 0.5$ was selected as the optimum PVP concentration. Figure 5.7 shows the SEM photographs of several specimens. Figure 5.8 shows the withdrawal speed dependence of thickness. The thickness of the macroporous film was increased from about 100 nm to 200–300 nm by

incorporating PVP.

Table 5.4: Macroscopic morphology of the TiO_2 films prepared from the PEG2000-PVP1300000 system at $p_{PEG} = 5.0$, 30% RH: -, smooth; ◡, pits; ●, macropores; ▲, uneven surface.

p_{PVP}	Temp.	Withdrawal speed ($mm \cdot min^{-1}$)					
	(°C)	7.5	15.0	22.5	30.0	45.0	60.0
0	25	-	◡	●	●	◡	-
0.5	25	▲	●	●	●	◡	-
0.5	40	▲	▲	●	●	●	●

In the PEG system, the withdrawal speed for macroscopic domain formation increases with an increase in dipping temperature as shown in Table 2.3 and Fig. 2.7 of Chapter 2 because both the fluidity reduction and the phase separation are more accelerated than the polycondensation. In the present PEG-PVP system, similarly, the withdrawal speed for macroscopic domain formation shifts to higher withdrawal speed by increasing the dipping temperature as listed in Table 5.4. As shown in Fig. 5.7, the morphologies observed at 15.0 (a) and 30.0 $mm \cdot min^{-1}$ (c) of withdrawal speeds at 25°C are quite similar to those observed at 30.0 (d) and 60.0 $mm \cdot min^{-1}$ (f) at 40°C, respectively. In addition, the position of maximum thickness shown in Fig. 5.8 shifts to higher withdrawal speed in accordance with the formation of macroporous morphology. The deposition speed became twice but the thickness increased only little because the advantage of domain formation at higher withdrawal speed was canceled by the viscosity decrease.

The total thickness can be increased by repeating the deposition process in the dip-coating method. The macropores are not filled by the repetitive dippings. Therefore macroporous TiO_2 film as thick as 1 μm has been successfully prepared by only five times repetition of dipping and heat treatment at 500°C for 10 min as shown in Figs. 5.9 and 5.10. It is noteworthy that r of the dipping solution is 1 then the solution is free from the gelation. The solution left at 40°C for a week under a sealed condition also provides the macroporous films. Such stability of dipping solution would be preferable for practical uses.

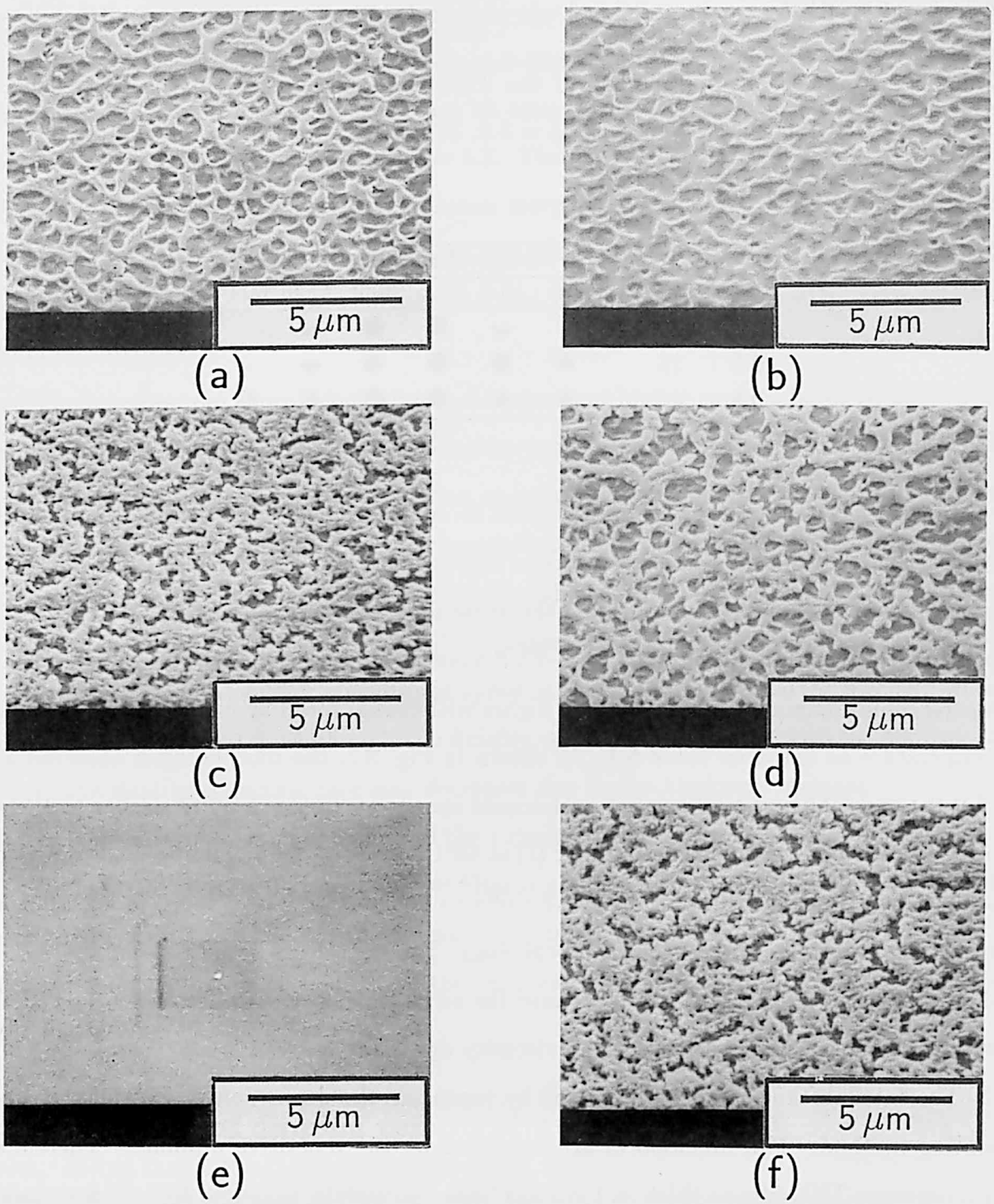

Fig. 5.7: SEM photographs of the TiO_2 films prepared from the PEG2000-PVP1300000 system at $p_{PEG} = 5.0$. Dipping temperature (°C) and withdrawal speed ($mm \cdot min^{-1}$) are (a) (25, 15.0), (b) (40, 15.0), (c) (25, 30.0), (d) (40, 30.0), (e) (25, 60.0), (f) (40, 60.0). View angle is 45°.

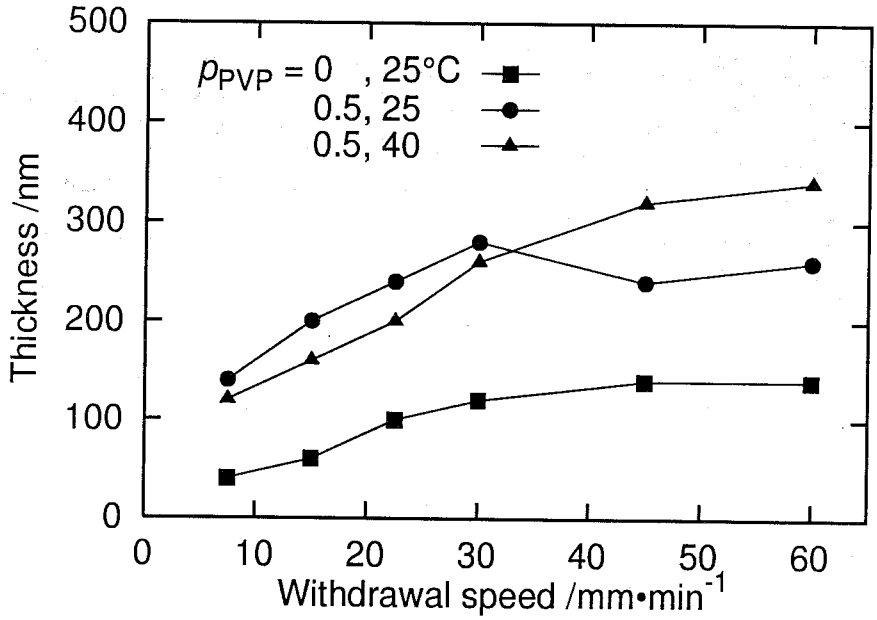

Fig. 5.8: Dependence of thickness on withdrawal speed and dipping condition.

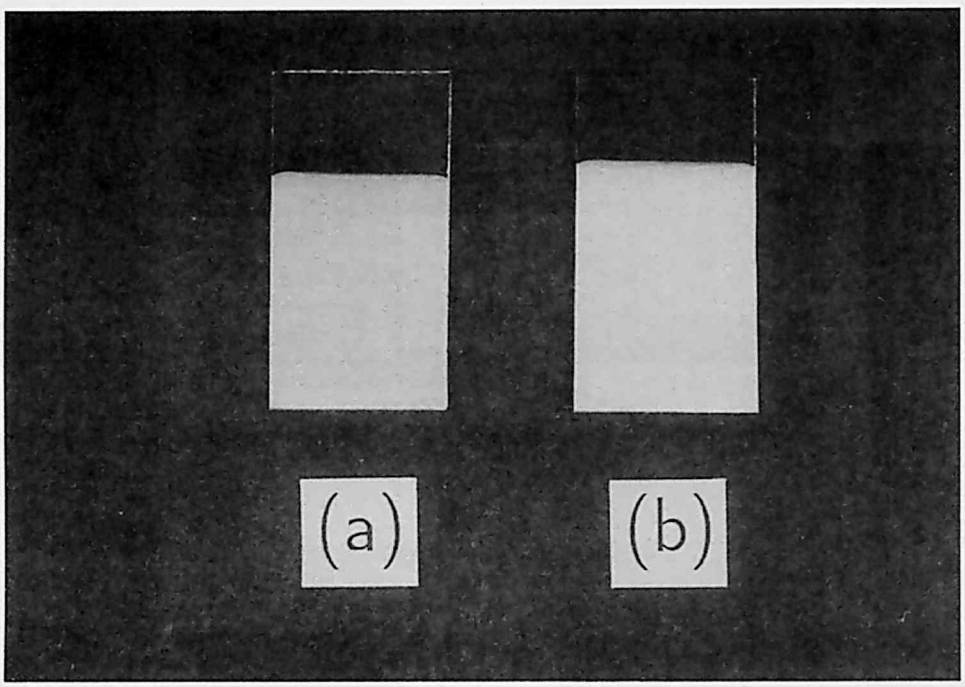

Fig. 5.9: Photograph of the TiO_2 films prepared from the PEG2000-PVP1300000 system at 40°C, 30% RH, and 30 mm·min^{-1} of withdrawal speed. Number of depositions is (a) one, and (b) five. The size of the substrate is 25 mm × 40 mm.

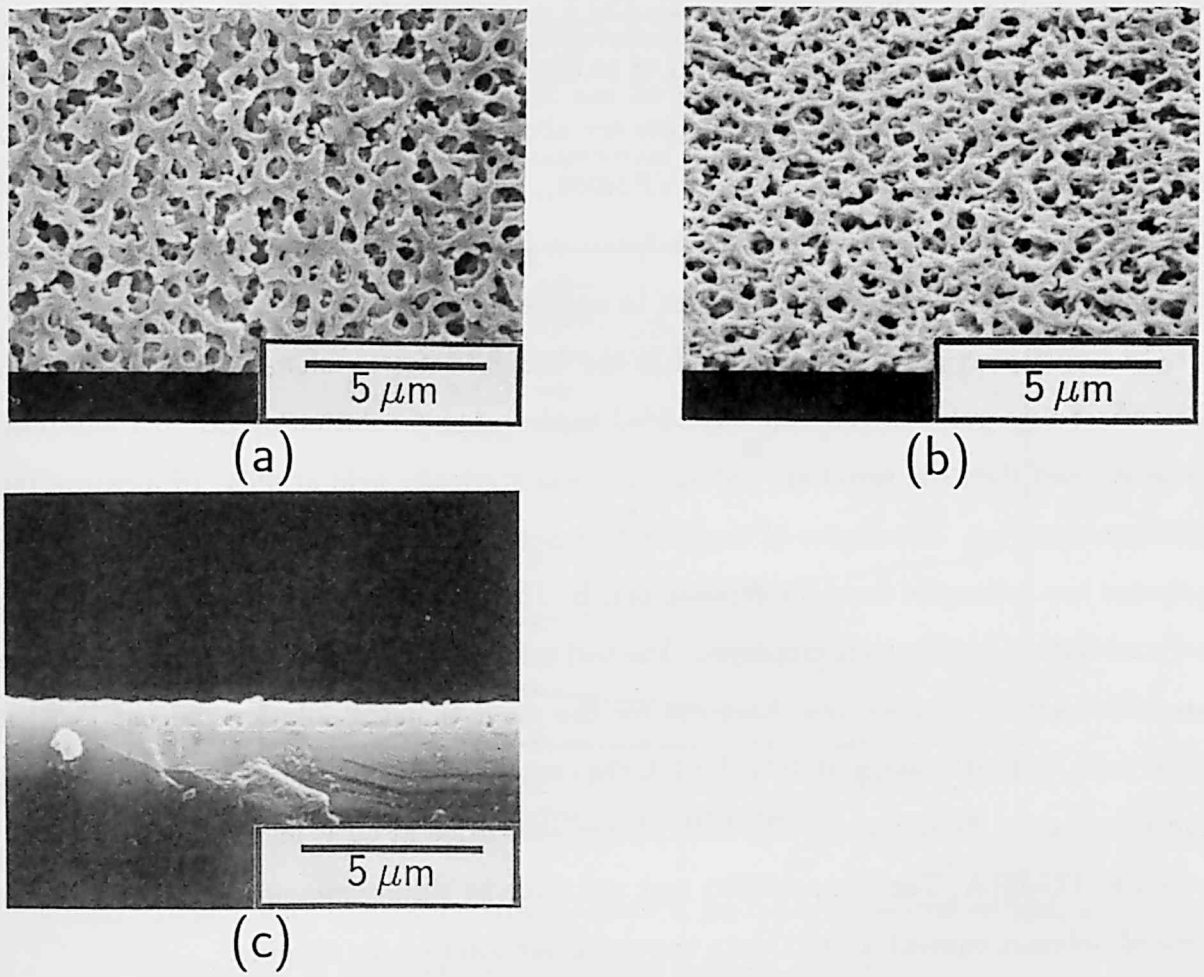

Fig. 5.10: SEM photographs of the TiO_2 films prepared from the PEG2000-PVP1300000 system and deposited five times at 40°C, 30%RH, and 30.0 mm·min^{-1} of withdrawal speed. View angle is (a) 0°, (b) 45°, (c) 90°.

5.3 Dissolution behavior of polymer contents

Gelation tests and some related experiments were performed for the solutions of which compositions are listed in Table 5.5 to investigate the physical and chemical interactions among the constituents. The PEGs having average molecular weights of 2,000, 4,000 (Hayashi Pure Chemical Industries Ltd.), and 10,000 (Aldrich Chemical Ltd.), and PVPs having average molecular weights of 10,000, 24,000, and 360,000 (Aldrich Chemical Ltd.) were used. Polymerization degrees are about 45 (PEG2000), 91 (PEG4000), 222 (PEG10000), 101 (PVP10000), 242 (PVP24000), and 3,636 (PVP360000). For the gelation test A, r was increased to 1.67 as listed in Table 5.5 because the dipping solution of which r is 1.00 did not gel. In order to ensure the homogeneity of starting solution, PEG or PVP was previously dissolved in the ethanol solution of water and nitric acid. The water-acid-polymer solution was added to the ethanol solution of TIP at room temperature and then the resultant test solution was statically held at 40°C to measure the gelation time (t_g). The degree of complexation between the titania oligomer and organic polymer was estimated from the gelation test B. The PEGs and PVPs having comparable polymerization degrees were employed. The test solution was prepared by almost the same procedure as the gelation test A except for the point that the solution did not contain nitric acid. After the aging at 40°C for 1 d, the content was separated into precipitated gel and supernatant fluid phases. The both phases were dried at 60°C and subsequently subjected to TG-DTA. The compatibility test was done by simply measuring the dissolution time of polymer content at 40°C into the precursor solution for dipping.

Table 5.5: Compositions of the test solutions (unit: mol).

	H_2O	EtOH	TIP	HNO_3	Polymer (g)
Gelation test A	0.20	1.0	0.12	0.02	0–6.0
Gelation test B	0.10	1.0	0.05	-	0.5, 1.0
Compatibility test	0.12–0.20	1.0	0.12	0.02	1.0

Figure 5.11 shows the dependence of t_g at 40°C on concentration and molecular weight of polymer content for the gelation test A. The solution was homogeneous and transparent

throughout the mixing for the PEG systems. In contrast, gradual mixing and vigorous stirring were required for the PVP systems to redissolve the precipitation temporarily generated accompanied by the mixing. The resultant gel was always opaque for all the systems. In the PEG2000 system, t_g increased with an increase in p_{PEG}. However, the gradient of the p_{PEG}–t_g curve changed from positive to negative by increasing the molecular weight of PEG. On the other hand, incorporation of PVP always reduced t_g significantly. The t_g of the PVP360000 system could not be measured because the solution did not show definite gelation due to the inhomogeneous gelation.

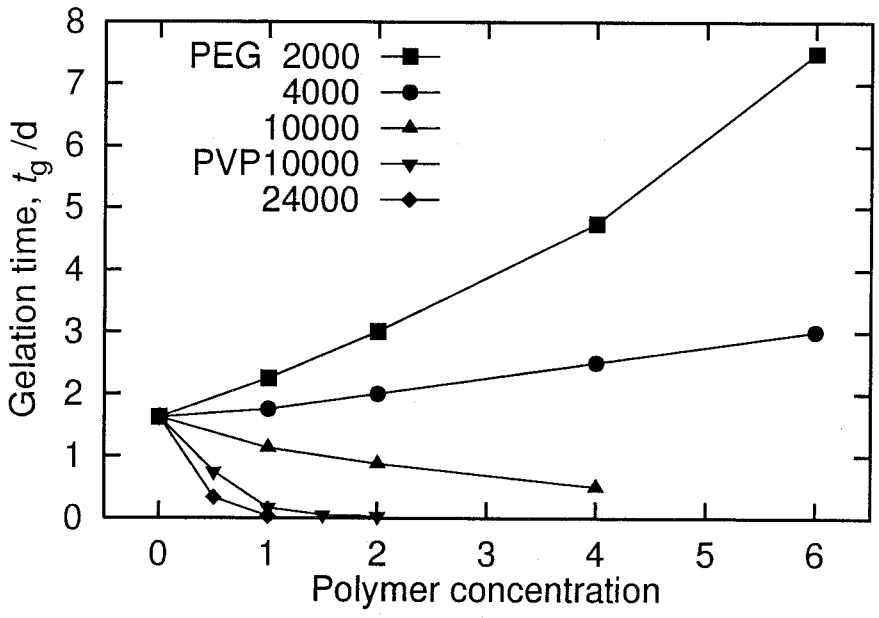

Fig. 5.11: Dependence of gelation time t_g at 40°C on type, molecular weight, and concentration of polymer content for the gelation test A.

Table 5.6 lists the results of the gelation test B. The $R_{fluid,wet}$ denotes the weight ratio of as separated fluid phase after the aging at 40°C with respect to the total weight of the test solution. Similarly, the weight ratio after drying at 60°C is described as $R_{fluid,dried}$. The $R_{fluid,wet}$ of the PEG systems was usually smaller than that of the PVP systems. The $R_{TG,gel/fluid}$ denotes the ratio of TG weight loss of the dried gel phase to that of the dried fluid phase between 200 and 600°C assuming that the weight loss at this temperature range is dominated by the thermal decomposition of organic polymer. Figures 5.12 and 5.13

shows the TG and DTA curves of the PEG10000 and PVP24000 systems, respectively. In the PEG10000 system, significant amount of PEG existed in the gel phase.

Table 5.6: Results of the gelation test B.

	p	System			
		PEG4000	PEG10000	PVP10000	PVP24000
$R_{\text{fluid,wet}}$	0.5	0.343	0.239	0.381	0.379
	1.0	0.253	0.176	0.355	0.405
$R_{\text{fluid,dried}}$	0.5	0.016	0.011	0.020	0.020
	1.0	0.024	0.008	0.032	0.032
$R_{\text{TG,gel/fluid}}$	0.5	0.19	0.55	0.30	0.29
	1.0	0.23	1.03	0.35	0.24

Table 5.7 shows the dissolution time of polymer content at 40°C for the compatibility test. The solubility of PEG increased with an increase in r whereas that of PVP decreased. Table 5.8 shows the solubility of PEG in ethanol containing smaller amount of water after stirring at 25°C for 1 h. The solubility of PEG increased drastically with a little increase in water concentration.

Table 5.7: Dissolution time of polymer content at 40°C (unit: min).

System	H_2O/TIP, r				
	1.00	1.17	1.33	1.50	1.67
PEG2000	20	15	15	15	
PEG4000	>60	45	35	30	25
PVP10000			10	10	25
PVP360000	10	10	>60		

Table 5.8: Dependence of solubility limit of PEG2000 at 25°C on water concentration for the ethanol solution of water.

Water concentration (wt%)	0	1	2	3
PEG2000 solubility (wt%)	1	5	12	17

The solubility of PEG increases with an increase in r as listed in Table 5.7. On the

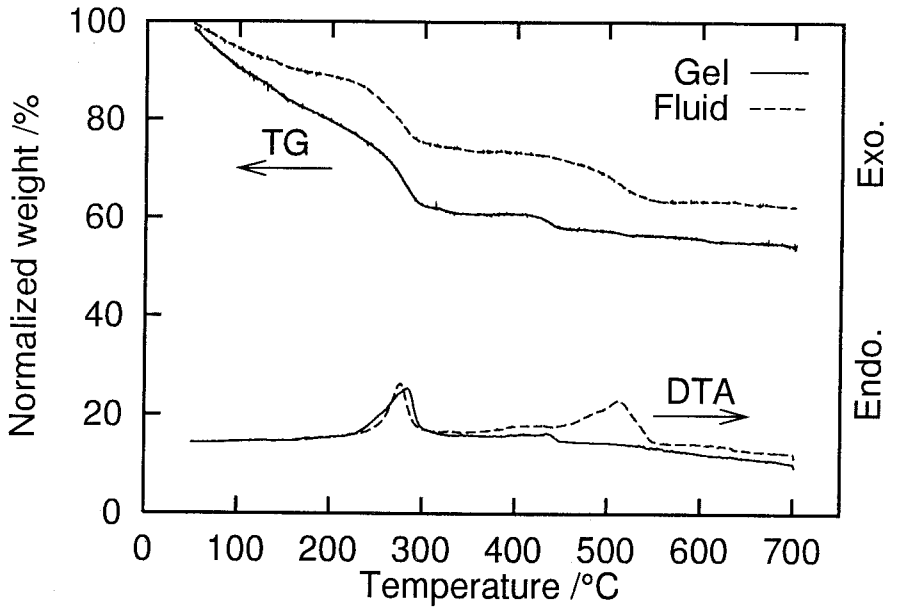

Fig. 5.12: TG and DTA curves of the dried gel and fluid phases for the PEG10000 system at $p_{\mathrm{PEG}} = 1.0$.

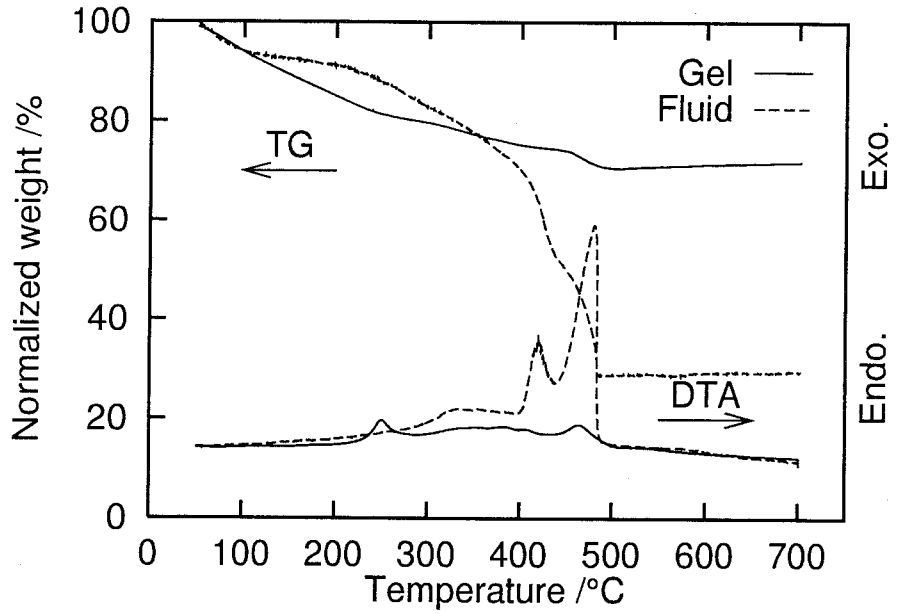

Fig. 5.13: TG and DTA curves of the dried gel and fluid phases for the PVP24000 system at $p_{\mathrm{PVP}} = 1.0$.

assumption that little portion of water escapes from the hydrolysis, it is considered that the increase in r not only accelerates the polycondensation of titania oligomer but also increases the concentration of free water. Although PEG is almost insoluble in pure alcohol, the solubility of PEG increases considerably even by the slight incorporation of water as listed in Table 5.8. Furthermore, the interaction of PEG to hydrolyzed titania oligomer possibly enhances the dissolution of PEG. These suppositions do not contradictory to the experimental results.

In the PEG2000 system, t_g increases with an increase in p_{PEG} because the complexation of PEG with the titania oligomer suppresses the polycondensation of titania oligomer. In general, complexation strength of polymeric compound increases by increasing the molecular weight and the number of monomer-monomer pairs [9,10]. While it is expected that the enhanced complexation between PEG and the titania oligomer suppresses the polycondensation, t_g decreases with an increase in molecular weight as shown in Fig. 5.11. Then it is suggested that the macroscopic phase separation resulting from the lower solubility of PEG reduces t_g typically in the PEG10000 system as also discussed in Section 2.2.

Similarly to the case of PEG, the hydrogen-bonding ability of PVP is expected to be high due to the polar amide-carbonyl group [10, 14, 15]. However, clear evidence of the titania-PVP complexation could not be found from the gelation test A because t_g does not increase with an increase in p_{PVP} even if the molecular weight is as small as 10,000. In addition, the results of TG-DTA listed in Table 5.6 suggest that PVP prefers to be dissolved in the fluid phase rather than exist in the gel phase. It is supposed that both water and alcohol are good solvents of PVP as listed in Table 5.3 in contrast to the case of the PEG10000 system, in which the lower solubility of PEG prominently increases the polymer concentration in the gel phase. Moreover, the fraction of fluid phase increases probably because the lower complexation strength of PVP enhances the polycondensation and the subsequent syneresis. Although the results of gelation test B may not directly be comparable to that of lower pH systems, it is supposed that the interaction between PVP and the titania oligomer is weaker than that of PEG because of the higher solubility and the bulky five-membered ring of PVP.

In contrast to PEG, the solubility of PVP decreases with an increase in r as listed

in Table 5.7. This result indicates that the dissolution behaviors of PEG and PVP are quite different in the present system. Furthermore, white precipitation is temporarily formed when the ethanol-water-PVP mixture is dropped to the ethanol solution of TIP, but the solution is always clear when the ethanol-PVP mixture is added to the TIP solution. It is supposed that the violent oligomerization around the drop exsolutes PVP on the assumption that the interaction between PVP and the titania oligomer is rather repulsive. According to the Flory-Huggins theory [16], free energy change on mixing (ΔG) for polymer solutions can be expressed as Eq. 1.2 of Chapter 1. The ΔG can be positive when the oligomerization degree of titania oligomer (P_1) is high and the the interaction between the titania oligomer and the polymer content is repulsive, that is, $\chi_{12}(T)$ is positive. This mechanism can explain the behavior of the PVP system.

Table 5.9 lists the morphology of the TiO_2 films prepared from the several PEG-free systems containing PVP anticipating the formation of macroporous morphology by decreasing the solubility of PVP. The $r = 1.25$ solution even became translucent after the dissolution of PVP. However, the resultant films were always smooth. Therefore, it is supposed that the complexation between the titania oligomer and polymer content may play some important roles for the macroscopic domain formation in the present systems.

Table 5.9: Macroscopic morphology of the TiO_2 films prepared from the solution containing PVP: -, smooth; C, macroscopic cracks.

	p_{PVP}	%RH	r	Withdrawal speed ($mm \cdot min^{-1}$)			
				7.5	15.0	22.5	30.0
PVP10000	5.0	30	1.00	-	-	-	-
PVP360000	1.0	70	1.00	-	-	C	C
PVP360000	1.0	30	1.25	-	C	C	C

5.4 Conclusions

The morphology and thickness variations were investigated for the TiO_2 films prepared from the solution containing PEG and PVP in relation to the dissolution behavior of polymer contents. The results obtained are summarized as follows:

(1) Macroporous TiO_2 films having interconnected pore structure are fabricated from the system containing not only PEG but also PVP. The thickness of the films is increased by incorporating PVP having higher molecular weight to increase the viscosity of the dipping solution. The average domain size is simply dominated by the PEG concentration. The excess incorporation of PVP suppresses the domain formation and enhances the formation of macroscopic cracks.

(2) The thickness and the preparation speed of the macroporous films are increased at higher dipping temperature. The macropores are not filled by the repetitive dippings and macroporous TiO_2 film having interconnected pore structure as thick as 1 μm has been successfully prepared by repeating the deposition five times. The dipping solution is free from the gelation and stable longer than a week under a sealed condition owing to the lower water to alkoxide ratio as 1.

(3) Although both PEG and PVP are hydrogen bonding polymers having proton accepting ability, the complexation with the titania oligomer seems to occur only for PEG. The dissolution behavior of PVP can be explained by using the thermodynamic theory of polymer mixing. The preparation of macroporous film was unsuccessful in the systems containing PVP as an only polymer content.

References

[1] H. Kozuka and M. Kajimura, Chem. Lett. **1999**, 1029 (1999).

[2] G. Philip and H. Schmidt, J. Non-Cryst. Solids **63**, 283 (1983).

[3] C. Sanchez and M. In, J. Non-Cryst. Solids **147&148**, 1 (1992).

[4] J. D. Mackenzie, J. Ceram. Soc. Jpn. **101**, 1 (1993).

[5] J. D. Mackenzie, J. Sol-Gel Sci. Technol. **2**, 81 (1994).

[6] M. In, C. Gérardin, J. Lambard, and C. Sanchez, J. Sol-Gel Sci. Technol. **5**, 101 (1995).

[7] C. Barglik-Chory and U. Schubert, J. Sol-Gel Sci. Technol. **5**, 135 (1995).

[8] J. Rubio and J. A. Kitchener, J. Colloid Interface Sci. **57**, 132 (1976).

[9] G. L. Howard, C. C. Ma, and C. W. Yip, Polym. Commun. **24**, 182 (1983).

[10] B. Siffert and J. F. Li, Colloid. Surf. **40**, 207 (1989).

[11] E. Kokufuta, A. Yokota, and I. Nakamura, Polymer **24**, 1031 (1983).

[12] Pradip, C. Maltesh, P. Somasundaran, R. A. Kulkarni, and S. Gundiah, Langmuir **7**, 2108 (1991).

[13] T. Ikawa, K. Abe, K. Honda, and E. Tsuchida, J. Polym. Sci. **13**, 1505 (1975).

[14] S. K. Chatterjee, A. Malhotra, and D. Yadav, J. Polym. Sci. Polym. Chem. **22**, 3697 (1984).

[15] T. Saegusa, J. Macromol. Sci.: Chem. A **28**, 817 (1991).

[16] P. J. Flory, *Principles of Polymer Chemistry* (Cornell University Press, Ithaca, New York, 1971).

Chapter 6

Photoelectrochemical property of dye-sensitized macroporous titania films prepared by sol-gel method

6.1 Introduction

Titania (TiO_2) has been extensively studied as an electrode material for photoelectrochemical cells of water decomposition [1] and light to electricity conversion [2, 3]. Typically, TiO_2 becomes respondent to visible light by photosensitizing the TiO_2 electrodes with dye molecules. Since the efficiency of the cell is largely dominated by the adsorption amount of dye molecules, morphology control of the electrode material is important to increase the surface area of the electrode. However, almost all the porous TiO_2 electrodes were fabricated so far by sintering colloidal titania paste, and the pore structure was usually modified by controlling the morphology of colloidal titania particle [4].

Sol-gel method is quite attracting for the preparation of porous materials because the pore structure can be tailored over wide ranges. The micro- and mesopores are formed mainly as cavities after the removal of solvent. On the other hand, macroporous structure is typically formed by inducing the macroscopic phase separation among the constituents during the gelation. Interconnected macroporous silica gels have been prepared from the reaction mixture containing polar solvents [5] or organic polymers [6–8], each of which decreases the stability of solution and induces the spinodal decomposition parallel to the gelation. These silica gels have been successfully applied as column materials for high performance liquid chromatography (HPLC) because the gels have not only the interconnected macropores for the material transport but also the mesoporous structure for the material separation [9].

Macroporous TiO_2 films can directly be prepared from the solution containing poly(ethylene glycol) (PEG) by a dip-coating method as described in Chapters 1–5. Although the relationship between the morphology and the preparation conditions is not simple, the variety of morphology as well as the simple one-step deposition from the homogeneous alkoxide-based solution are quite unique as a new route to fabricate porous TiO_2 films. Furthermore, the sol-gel method is essentially suitable for the preparation of thinner electrodes to decrease the internal resistance and homogeneous protection layers to reduce the leak current.

In this chapter, photoelectrochemical properties of the sol-gel derived TiO_2 films having interconnected macroporous morphology are examined. In particular, attention is payed to the effects of macroscopic morphology and organic dyes on electrochemical properties.

6.2 Experimental procedure

Smooth and macroporous TiO_2 films were deposited by dip-coating method from the solutions of which compositions are listed in Table 6.1. The gel film was deposited on both sides of the Corning #7059 glass substrate coated with ITO electrode ($10\,\Omega \cdot \square^{-1}$, Kinoene Kogaku Kogyo Ltd.) at $30.0\,\mathrm{mm \cdot min^{-1}}$ of withdrawal speed at 40°C, 30% RH following the procedure described in Section 5.2.2. The macroscopic morphology was modified by changing the PEG to ethanol ratio ($p \equiv$ PEG/EtOH). The $p = 0$ smooth film was always deposited just on the substrate before depositing the $p \neq 0$ macroporous films to prevent the direct contact between the ITO electrode and the electrolyte solution. Heat treatment at 500°C for 10 min was done after each dipping. The deposition and the heat treatment were repeated up to 10 times. The number of depositions is indicated by n.

Table 6.1: Compositions of the dipping solutions (unit: mol).

H_2O	EtOH	TIP	HNO_3	PEG (g)	PVP (g)
0.12	1.0	0.12	0.02	0, 3.0–6.0	0.5

Photoelectrochemical properties of the TiO_2 films were measured using a potentiostat/galvanostat (NPGS301, Nikko Keisoku Ltd.) and an electrochemical cell schematically illustrated in Fig. 6.1. Aqueous solution containing 0.3 M of Na_2SO_4, 0.2 M of $Na_2B_4O_7$, and 0.14 M of H_2SO_4 was used as a pH 7 buffered electrolyte solution [10]. The counter and the reference electrodes were a Pt wire and a 3.33 M KCl silver-silver chrolide (Ag/AgCl) electrode (Horiba Ltd.), respectively. The TiO_2 film was illuminated by a 300 W Xe lamp (Hamamatsu Electronics Ltd.) combined with a monochromator (Model 270M, Instruments S. A. Ltd.) both the forward (ITO side) and the backward directions as shown in Fig. 6.1. The cyclic voltammetry was done at 0.05 $V \cdot s^{-1}$ of scan rate under dark or the illumination of white light of which power was about 200 $mW \cdot cm^{-2}$ obtaind from the zero-order diffraction of the monochrometor at 20 nm of bandpass. The photocurrent spectrum was measured at 0.5 V vs Ag/AgCl under the illumination of monochromated light at 10 nm of bandpass. At the wavelengths longer than 420 and 620 nm, UV-35 and O-56 filters were respectively equipped to cut the higher order diffractions. The power spectrum of the monochromated light was measured using an optical power meter having a thermopile sensor head (Model 13PEM001, Melles Griot Ltd.). The measurements under dye sensitization were executed simply contacting the TiO_2 electrode with the electrolyte solution dissolved by 1×10^{-3} M of organic dye. The measurement was not done under the forward illumination because the incident light was severely attenuated by the dyed electrolyte solution. Fluorescein, eosin Y (Tokyo Kasei Ltd.), and 7-diethylaminocoumarin-3-carboxylic acid (coumarin; Fluka Ltd.) were employed as photosensitizers of which chemical structures are shown in Fig. 6.2.

6.3 Effect of film morphology on photoelectrochemical property

The titania gel film was transformed into anatase TiO_2 film after the heat treatment at 500°C. The TiO_2 films prepared at $p = 0$ was transparent and macroscopically smooth, whereas the appearance of the film changed from translucent to opaque with an increase in p. Figure 6.3 shows the SEM photographs of the macroporous TiO_2 films. The average pore diameter as well as the porosity increased with an increase in p. Table 6.2 lists

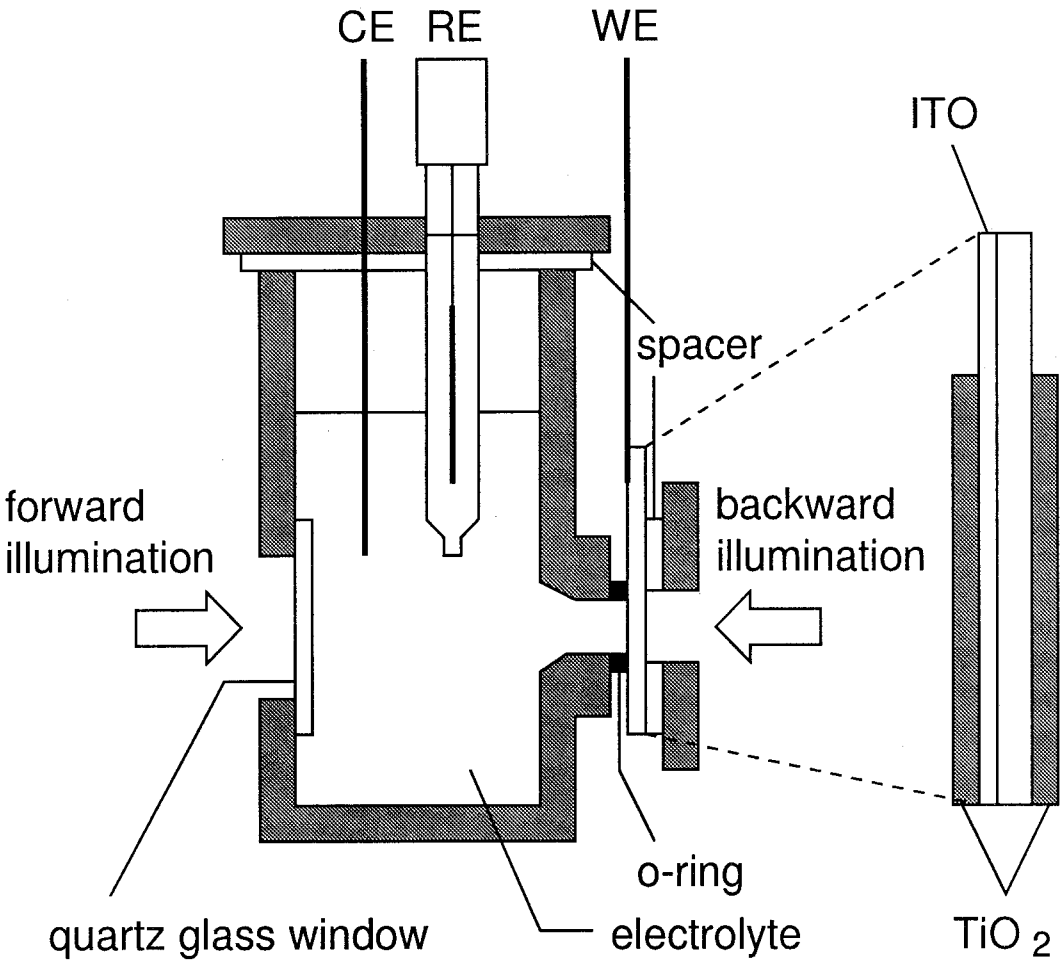

Fig. 6.1: Schematic illustration of the photoelectrochemical cell.

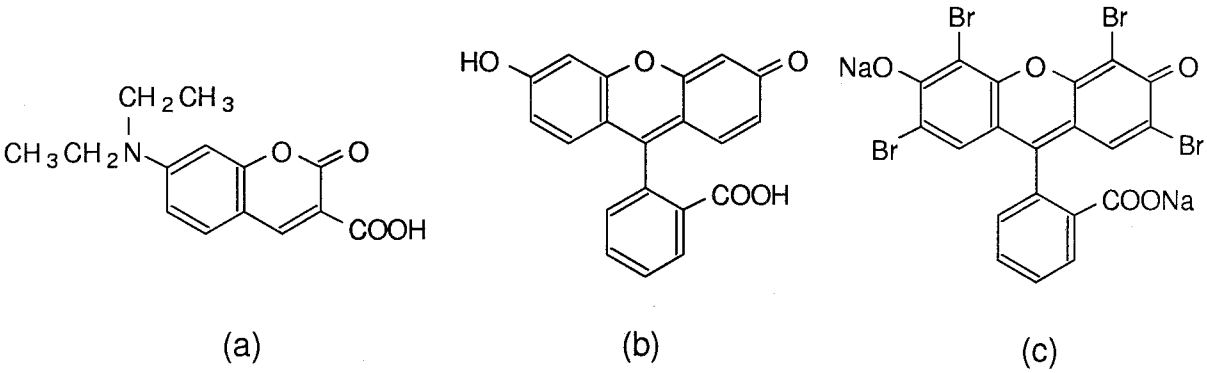

Fig. 6.2: Chemical structure of the organic dyes employed. (a) 7-diethylamino-coumarin-3-carboxylic acid (coumarin), (b) fluorescein, (c) eosin Y.

the thickness of the TiO_2 films evaluated from the SEM photographs. The incorporation of PEG increased the thickness slightly. Figures 6.4–6.6 show the optical absorption spectra of the TiO_2 films deposited on the ITO-coated substrate. The transparency of the film decreased with an increase in p especially at shorter wavelength because of the light scattering from the macroscopic domain. For the $n = 2$ films, absorption maximum appeared at about 400 nm when $p = 5.0$ and 6.0 as shown in Fig. 6.4 corresponding to the correlation length of the macroscopic domain. For the $p \neq 0$ films, the transparency decreased with increases in p and n but did not differ significantly between the $n = 5$ and 10 films as shown in Figs. 6.5 and 6.6.

Table 6.2: Thickness of the TiO_2 films (unit: μm).

Number of depositions, n	PEG concentration, p				
	0	3.0	4.0	5.0	6.0
5	0.4	0.6	0.5	0.5	0.6
10	1.2	1.3	1.0	1.4	1.4

Figures 6.7 and 6.8 show the dark and photo cyclic voltammograms of the $n = 5$ films at $p = 0$ and 5.0, respectively. The basic shapes of the cyclic voltammogram were similar irrespective of p and n as typically seen from Figs. 6.7 and 6.8. The photocurrent emerged when the TiO_2 electrode was biased at more anodic potential than -0.4 V vs Ag/AgCl in consistent well with the values reported previously [10,11]. The current density increased significantly at anodic bias more than 1.5 V vs Ag/AgCl due to the direct injection of electron from the water redox couple. The cathodic bias less than -1 V vs Ag/AgCl destroyed the TiO_2 electrode. The photocurrent density under the backward illumination was smaller than that under the forward illumination, but the sensitization by coumarin increased the photocurrent density. The values of photocurrent density taken from the cyclic voltammograms at 0.5 V vs Ag/AgCl are summarized in Tables 6.3 and 6.4.

Figures 6.9 and 6.10 show the collection efficiency and the photocurrent density spectra of the $n = 5$ films at $p = 0$ and 5.0, respectively. The collection efficiency indicates the number of electrons generated per illuminated photon, and is defined as follows:

$$\text{Collection efficiency} = \frac{P_{\text{out}}(\lambda)}{P_{\text{in}}(\lambda)} = \frac{hc}{e\lambda}\frac{J_{\text{out}}(\lambda)}{P_{\text{in}}(\lambda)}$$

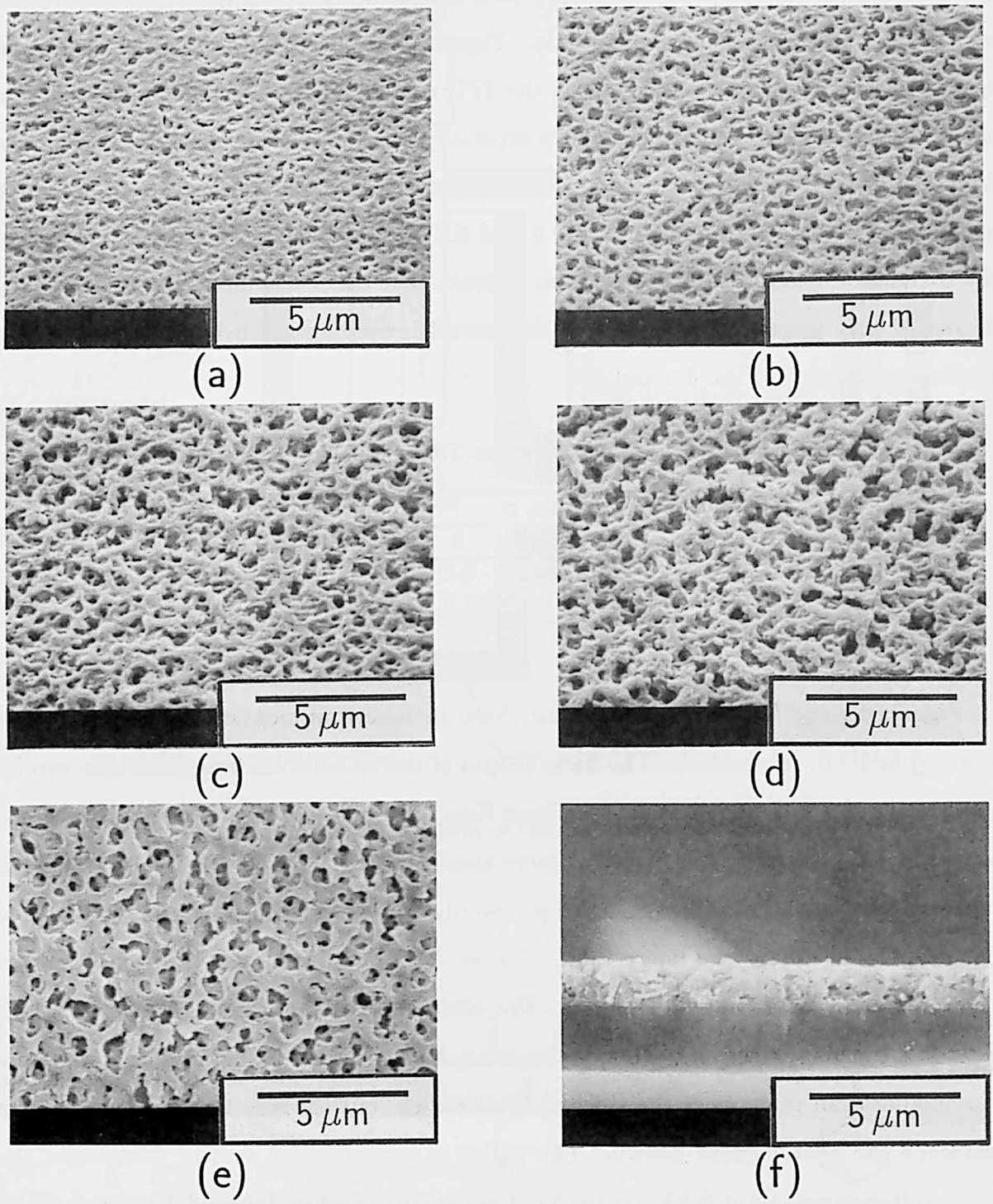

Fig. 6.3: SEM photographs of the macroporous TiO_2 films. p is (a) 3.0, (b) 4.0, (c) 5.0, (d) 6.0 for the $n = 5$ films at 45° of view angle. View angle is (e) 0°, (f) 90° for the $n = 10$, $p = 5.0$ film.

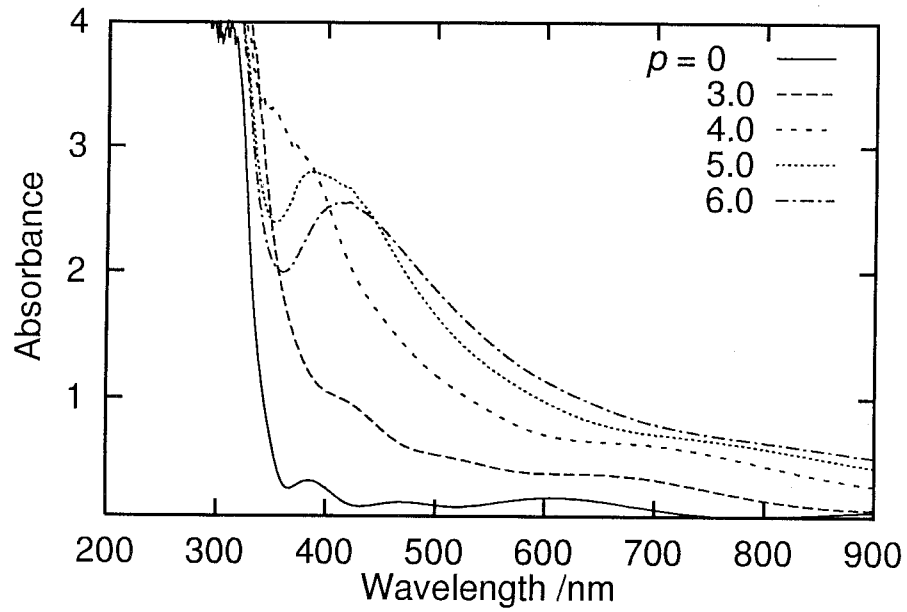

Fig. 6.4: Optical absorption spectra of the $n = 2$ films.

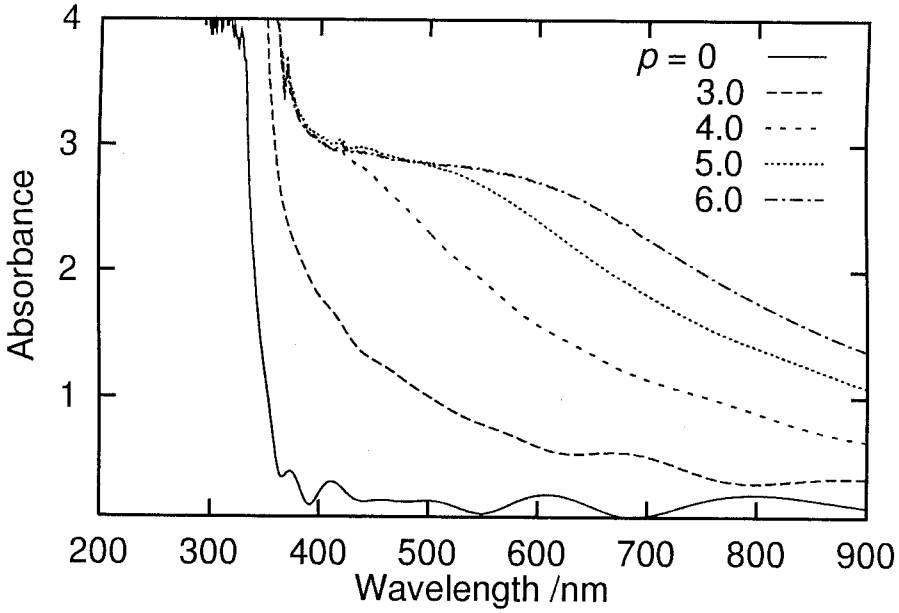

Fig. 6.5: Optical absorption spectra of the $n = 5$ films.

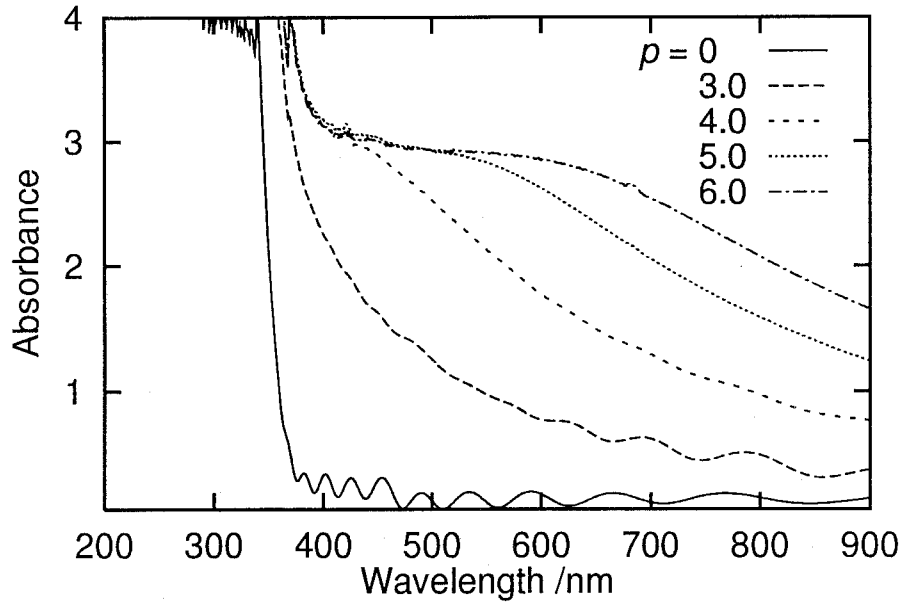

Fig. 6.6: Optical absorption spectra of the $n = 10$ films.

Table 6.3: Photocurrent density at 0.5 V vs Ag/AgCl under the forward illumination (unit: $mA \cdot cm^{-2}$).

Number of depositions, n	PEG concentration, p				
	0	3.0	4.0	5.0	6.0
2	0.164	0.136	0.110	0.144	0.131
5	0.192	0.179	0.158	0.174	0.179
10	0.167	0.206	0.188	0.211	0.214

Table 6.4: Photocurrent density at 0.5 V vs Ag/AgCl under the backward illumination (unit: $mA \cdot cm^{-2}$).

Number of depositions, n		PEG concentration, p				
		0	3.0	4.0	5.0	6.0
2	No sensitization	0.019	0.017	0.020	0.019	0.022
	Coumarin	0.033	0.035	0.036	0.041	0.041
5	No sensitization	0.021	0.016	0.015	0.018	0.015
	Coumarin	0.039	0.051	0.041	0.055	0.052
10	No sensitization	0.019	0.019	0.015	0.021	0.018
	Coumarin	0.041	0.060	0.066	0.066	0.075

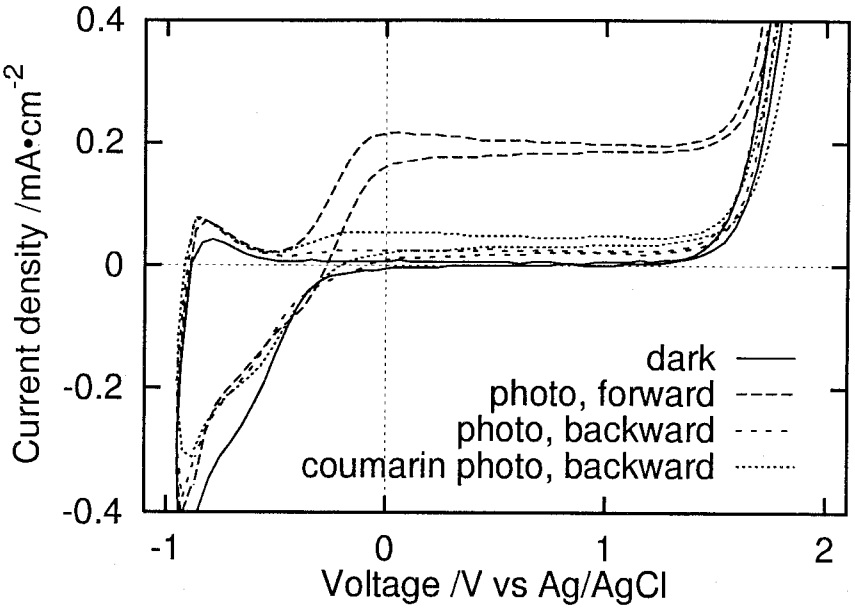

Fig. 6.7: Dark and photo cyclic voltammograms of the $p = 0$, $n = 5$ film. Scan rate is $0.05\,\mathrm{V{\cdot}s^{-1}}$.

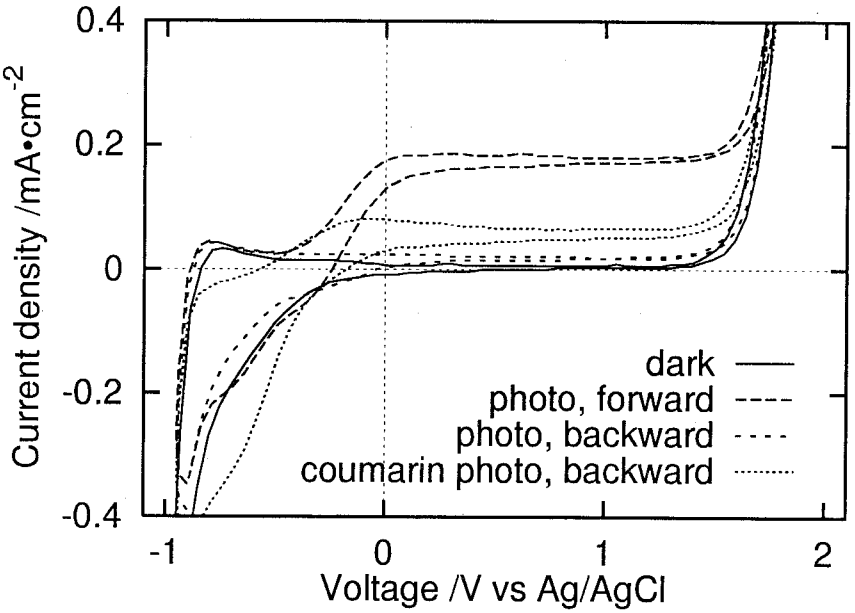

Fig. 6.8: Dark and photo cyclic voltammograms of the $p = 5.0$, $n = 5$ film. Scan rate is $0.05\,\mathrm{V{\cdot}s^{-1}}$.

$$= \frac{1.24 \times 10^3}{\lambda(\mathrm{nm})} \times \frac{J_{\mathrm{out}}(\lambda)(\mathrm{A \cdot cm^{-2}})}{P_{\mathrm{in}}(\lambda)(\mathrm{W \cdot cm^{-2}})}, \tag{6.1}$$

where $P_{\mathrm{in}}(\lambda)$ and $P_{\mathrm{out}}(\lambda)$ respectively denote the powers of the illuminated light and the electrical output, $J_{\mathrm{out}}(\lambda)$ the photocurrent density, λ the wavelength, h the Planck constant, c the speed of light, and e the elementary charge. The correction efficiency was as large as 0.5–0.6 over the wavelength shorter than 350 nm under the forward illumination whereas the light of shorter wavelength than 350 nm contributed little to the photocurrent generation under the backward illumination both the $p = 0$ and 5.0 films.

It is considered that the photoelectrochemical property of the TiO_2 electrode is largely dominated by the electronic structure of the space charge layer formed near the surface of the electrode. Since the thickness of the space charge layer formed on the sol-gel derived TiO_2 crystalline particle is reported to be about the order of 10^1 nm [11], it is expected that the charge separation mechanism is insensitive to the macroporous morphology of which scale is far larger than that of the space charge layer. Indeed, the basic shape of the cyclic voltammogram is influenced little by n and p as typically shown in Figs. 6.7 and 6.8 for the $p = 0$ and 5.0 films, respectively.

Under the forward illumination, the TiO_2 electrode absorbs most of the illuminated ultraviolet light to generate the photocarriers. The enlargement of surface area is expected to increase the photocurrent density in case that the rate of photocarrier generation is larger than the rate of water oxidation. Additionally, penetration of electrolyte solution into the film can also increase the photocurrent density supposing that the diminished distance to the electrode surface for the diffusion of photogenerated holes decreases the recombination rate of photocarriers. In the $p = 0$ smooth films, the photocurrent density is the largest of the $n = 2$ films whereas the photocurrent density does not increase considerably with an increase in n as listed in Table 6.3. The smaller photocurrent density at $n = 10$ would be due to the higher resistivity of the TiO_2 film. In the $p \neq 0$ macroporous films, in contrast, the photocurrent density increases monotonically with an increase in n because of the increased surface area as well as the enhanced penetration of the electrolyte solution into the film.

Under the backward illumination, only the light of which wavelength is little shorter than the absorption edge of TiO_2 can generate the photocarriers because the light of

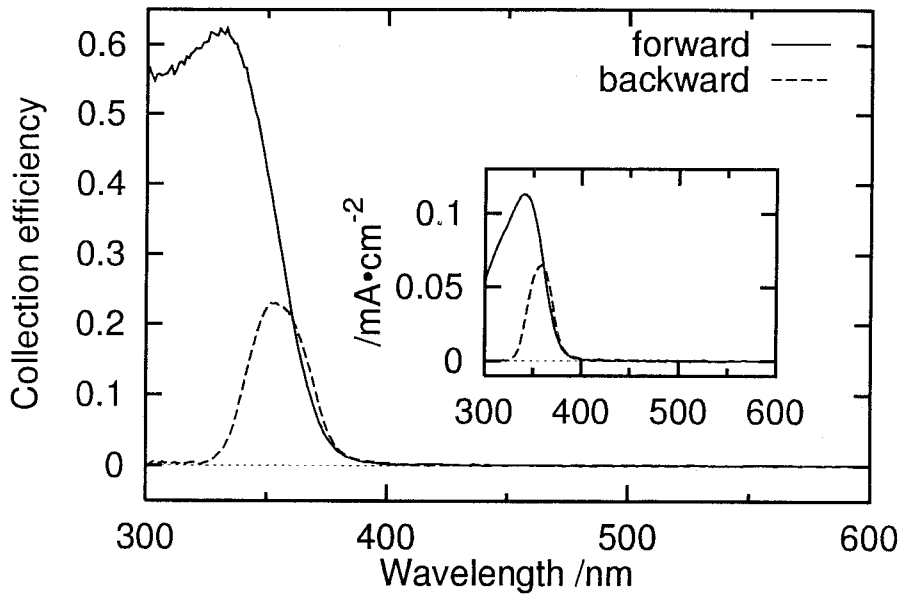

Fig. 6.9: Collection efficiency spectra of the $p = 0$, $n = 5$ film at 0.5 V vs Ag/AgCl. Photocurrent density spectra are also shown in the inset.

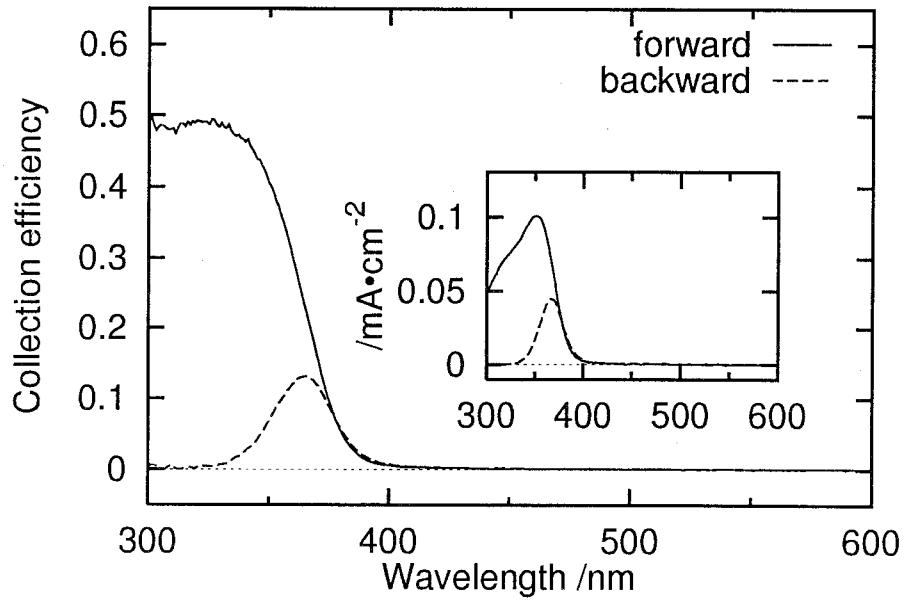

Fig. 6.10: Collection efficiency spectra of the $p = 5.0$, $n = 5$ film at 0.5 V vs Ag/AgCl. Photocurrent density spectra are also shown in the inset.

much shorter wavelength is largely absorbed by the TiO_2 film deposited on the opposite side. In addition, the light scattering from the macroscopic domain also impairs the transmittance in the $p \neq 0$ films as shown in Figs. 6.4–6.6. The suppressed transmittance seems to cancel the advantage of enhanced surface area as listed in Table 6.4. The photosensitization of the TiO_2 electrodes by coumarin clearly increases the photocurrent density. Under coumarin sensitization, the photocurrent density increases with an increase in n even at $p = 0$. It is supposed that the some dye molecules penetrate into the film because the sol-gel derived films are generally micro- and mesoporous even if the film is macroscopically smooth. In general, the photocurrent density of the $p \neq 0$ systems is larger than that of the $p = 0$ system especially at larger n in spite of their suppressed transparency. Hence it is suggested that the enhanced optical absorption as well as the considerable surface area of the thicker macroporous films are preferable to increase the photocurrent density. In contrast, the almost comparable photocurrent density at $n = 2$ indicates that the enhancement of surface area is not remarkable for the films deposited only one macroporous layer.

In order to improve the efficiency, the TiO_2 film should be more transparent for visible light and should be deposited only one side of the substrate. Efficient TiO_2 electrode can be prepared if the average pore diameter of the macropores could be decreased so as to increase the transparency with maintaining the porosity of the film so as not to lose the surface area and the penetrability of the electrolyte solution. Such condition is not fulfilled by decreasing p because both the pore diameter and the porosity decrease as shown in Fig. 6.3. Therefore other appropriate preparation condition should be explored. Recently reported "laminar flow coating method" [12] seems to be promising for the one-side deposition of the larger macroporous TiO_2 films.

6.4 Photosensitization by organic dyes in an aqueous system

Figure 6.11 shows the optical absorption spectra of the electrolyte solutions containing 4×10^{-5} M of coumarin, fluorescein, or eosin Y, and Fig. 6.12 shows the collection efficiency spectra of the dye-sensitized $p = 0$, $n = 3$ film. The photoresponse emerged in accordance with the wavelength of optical absorption of organic dye but the sensitization efficiencies of fluorescein and eosin Y were quite low. Therefore coumarin was employed as the sensitizer of the present experiment. Figure 6.13 shows the collection efficiency spectra of the bare and coumarin-sensitized $p = 5.0$, $n = 5$ film. The collection efficiency of the coumarin-sensitized TiO_2 film became as large as 0.1 between 400 and 450 nm due to the photosensitization by coumarin and the value seems to be notable for an aqueous system. Figures 6.14 and 6.15 show the variation of collection efficiency spectra with n. The collection efficiency at longer wavelength than 400 nm increased only little with an increase in n for the $p = 0$ system while increased considerably for the $p = 5.0$ system. Figures 6.16 and 6.17 show the variation of collection efficiency spectra with p. All the spectra were similar at $n = 2$. At $n = 10$, the collection efficiency between 400 and 500 nm increased with an increase in p whereas that at about 360 nm decreased.

Semiconductive oxides such as TiO_2, SnO_2, and ZnO can be efficient and stable photoelectrodes, but they are transparent for visible light. The photoelectrodes respondent to visible light are commonly fabricated by combining the semiconductive oxides with organic and metalorganic dyes [13]. Macrocyclic compounds such as porphyrin derivatives [14], ruthenium-based complexes [2,3], 9-phenyl xanthene dyes such as rhodamines, rose bengal [10] and eosin Y [15,16], and coumarins [17,18] are typically used as photosensitizers.

In order to attain continuous current flow, the dye molecule adsorbed on the electrode surface should be reduced quickly subsequent to the electron transfer to the TiO_2 electrode. In the present case, water is supposed to work as the reductant of the dye molecule as follows:

$$2H_2O \rightleftharpoons O_2 + 4H^+ + 4e^- \qquad 0.82\,\text{V vs NHE (pH = 7)}. \tag{6.2}$$

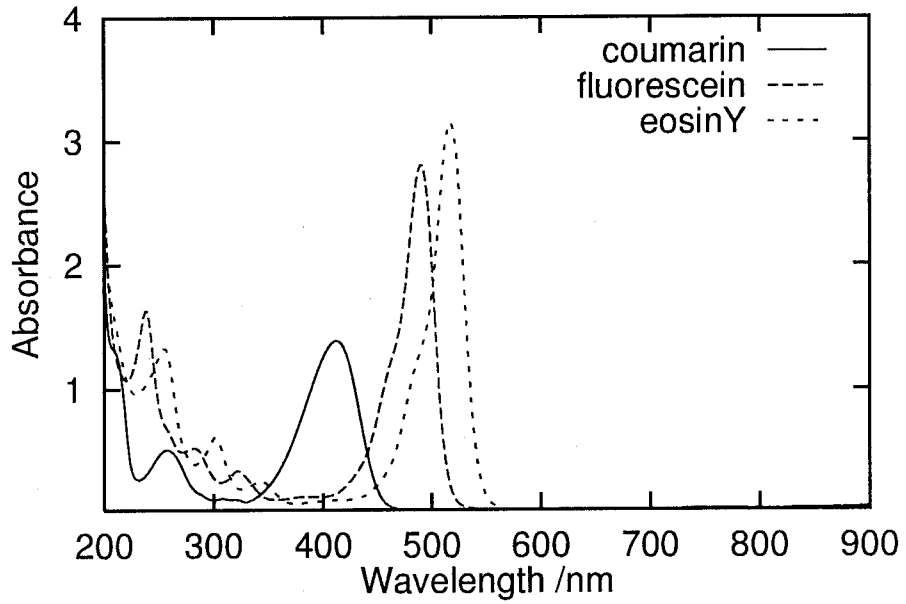

Fig. 6.11: Optical absorption spectra of the buffered electrolyte solutions containing 4×10^{-5} M of coumarin, fluorescein or eosin Y.

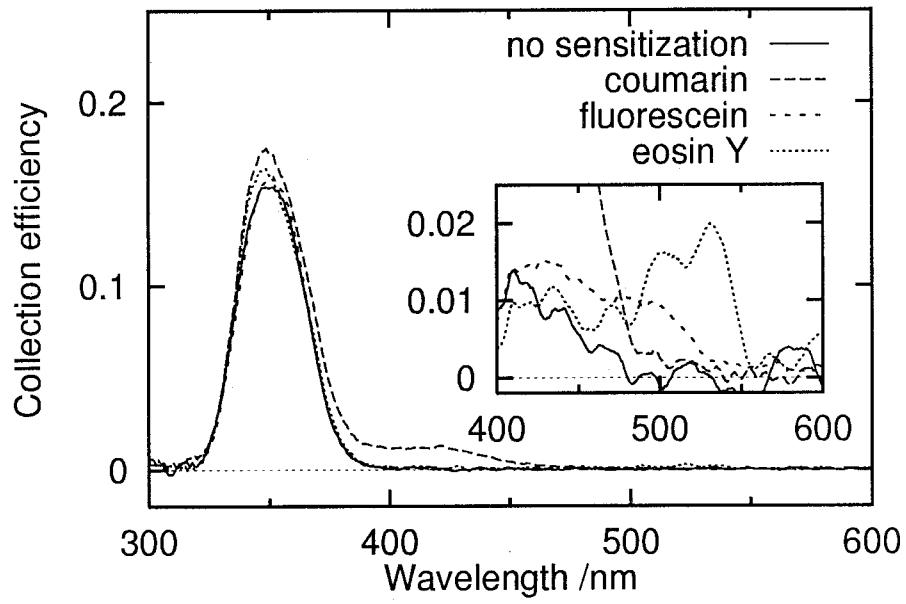

Fig. 6.12: Collection efficiency spectra of the $p = 0$, $n = 3$ film at 0.5 V vs Ag/AgCl. The inset shows the magnified spectra.

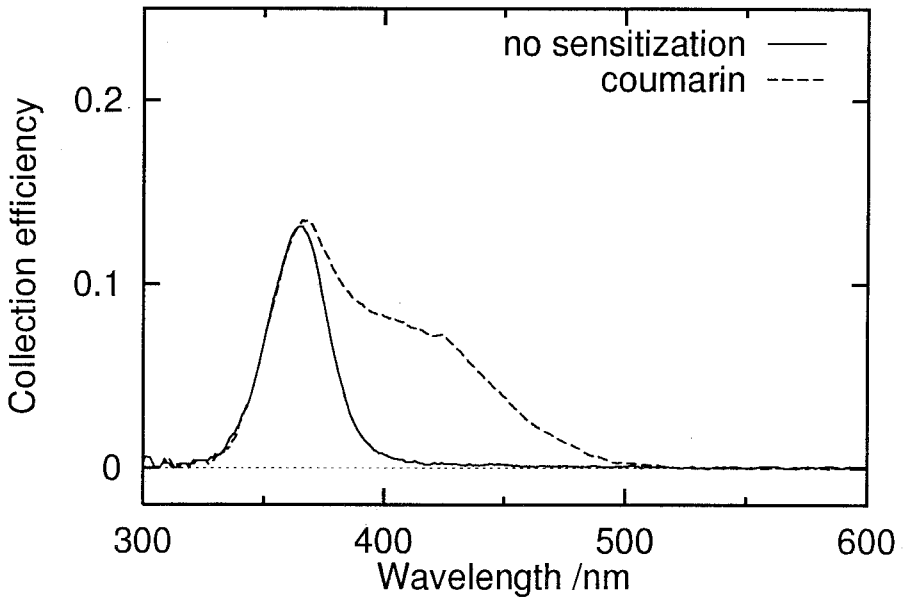

Fig. 6.13: Collection efficiency spectra of the $p = 5.0$, $n = 5$ film without and with coumarin sensitization at 0.5 V vs Ag/AgCl.

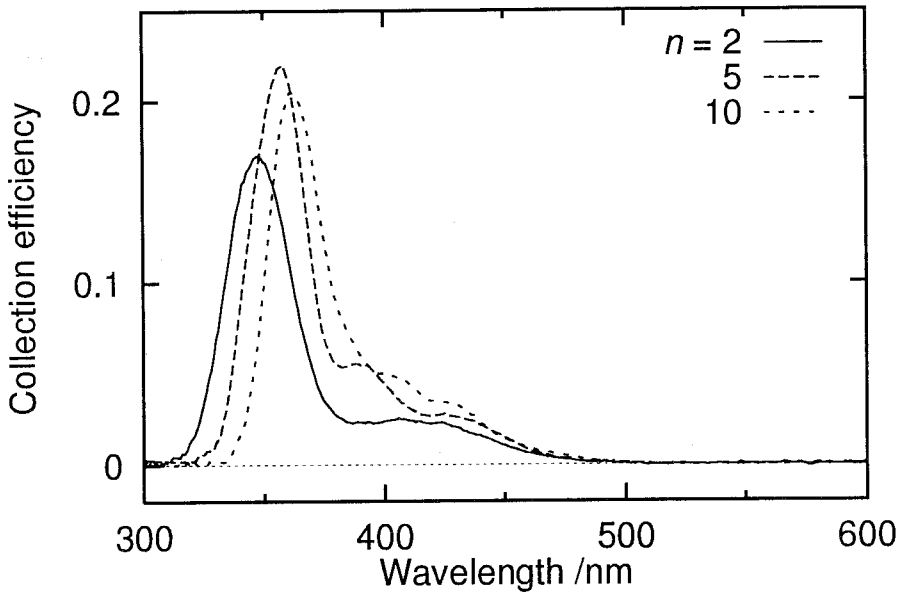

Fig. 6.14: Collection efficiency spectra of the coumarin-sensitized $p = 0$ films at 0.5 V vs Ag/AgCl.

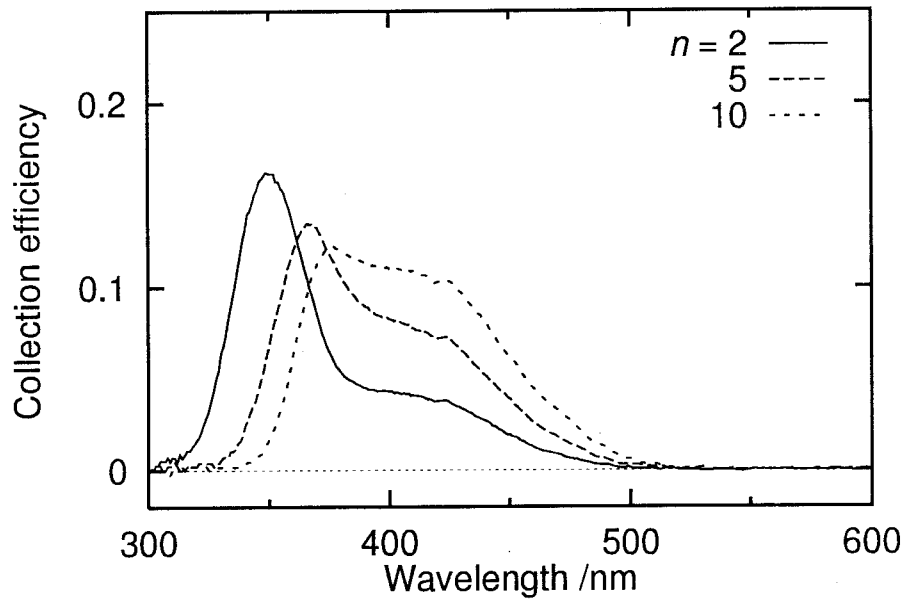

Fig. 6.15: Collection efficiency spectra of the coumarin-sensitized $p = 5.0$ films at 0.5 V vs Ag/AgCl.

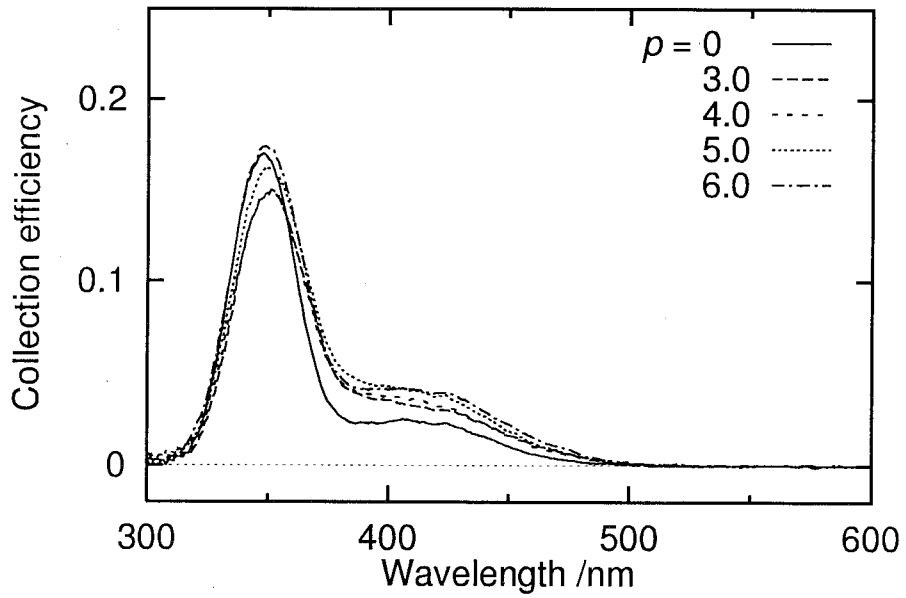

Fig. 6.16: Collection efficiency spectra of the coumarin-sensitized $n = 2$ films at 0.5 V vs Ag/AgCl.

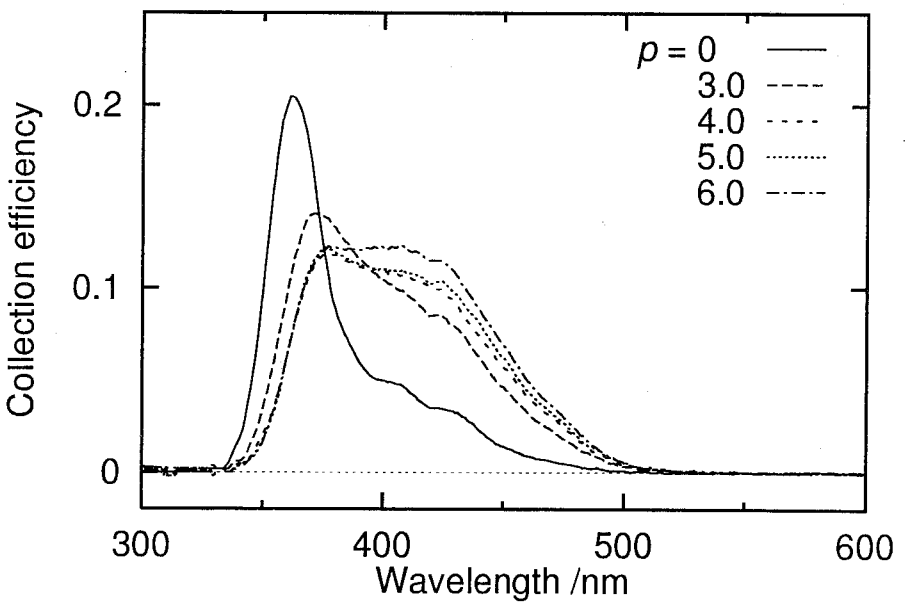

Fig. 6.17: Collection efficiency spectra of the coumarin-sensitized $n = 10$ films at 0.5 V vs Ag/AgCl.

The energy diagram of the electrode as well as the redox potentials of the dyes employed [18–20] are schematically illustrated in Fig. 6.18. The normal hydrogen electrode (NHE) and the conduction band edge of TiO_2 are assumed to reside at 4.5 eV [20] and 4.35 eV [21] below the vacuum level, respectively. The potentials of the Ag/AgCl electrode and the saturated caromel electrode (SCE) are assumed to be 0.21 V and 0.24 V vs NHE, respectively. All of the reduction potentials (E_{red}) of coumarin, fluorescein, and eosin Y are more negative than the conduction band edge of TiO_2. All of the oxidation potentials (E_{ox}) of those dyes are also more negative than E_{ox} of water. Hence the electron transfer from water to TiO_2 through the dye molecule is thermodynamically allowed. The sensitization efficiency is expected to increase in the order of eosin Y, fluorescein, and coumarin because the electron transfer is generally supposed to be improved by increasing the energy difference between the relevant levels. This supposition is consistent with the result that the efficiency of TiO_2 electrode sensitized by fluorescein is better than that sensitized by rose bengal [10], a xanthene dye of which E_{red} and E_{ox} are respectively estimated to be -0.84 V and 1.01 V vs NHE [19,20].

Another important condition for the efficient charge transfer is the degree of interaction between the dye molecule and the electrode. Usually, strong coupling of dye molecule with the electrode surface is necessary for the efficient sensitization. All of coumarin, fluorescein, and eosin Y have carboxy group as shown in Fig. 6.2 through which the dye molecule is specifically bound to the oxide surface such as TiO_2 and ZnO [3]. In the xanthene dyes, the rather bulky molecular framework outside the carboxy group does not seem to afford stronger interaction of the carboxy group with the TiO_2 electrode. On the other hand, it is reported that colloidal ZnO is efficiently sensitized by 3-carboxy coumarins. Such efficient charge transfer is attributed to the strong adsorption of 3-carboxy coumarins to the colloidal ZnO surface, because 3-carboxy coumarins is capable of coordinating to the surface metal atom in a salicylate geometry with the cooperative effect of 3-carboxy oxygen and 2-keto oxygen [18]. Indeed, the above phenomenon is no longer seen in system containing 4-acetic acid coumarin, in which such chelation of coumarin is not anticipated. Then it is suggested that the adsorption strength of coumarin to the TiO_2 surface is considerably larger than that of fluorescein and eosin Y. Accordingly, it

would be appropriate to consider that both the larger energy difference in charge transfer and the larger adsorption strength result in the efficient charge injection in the coumarin system.

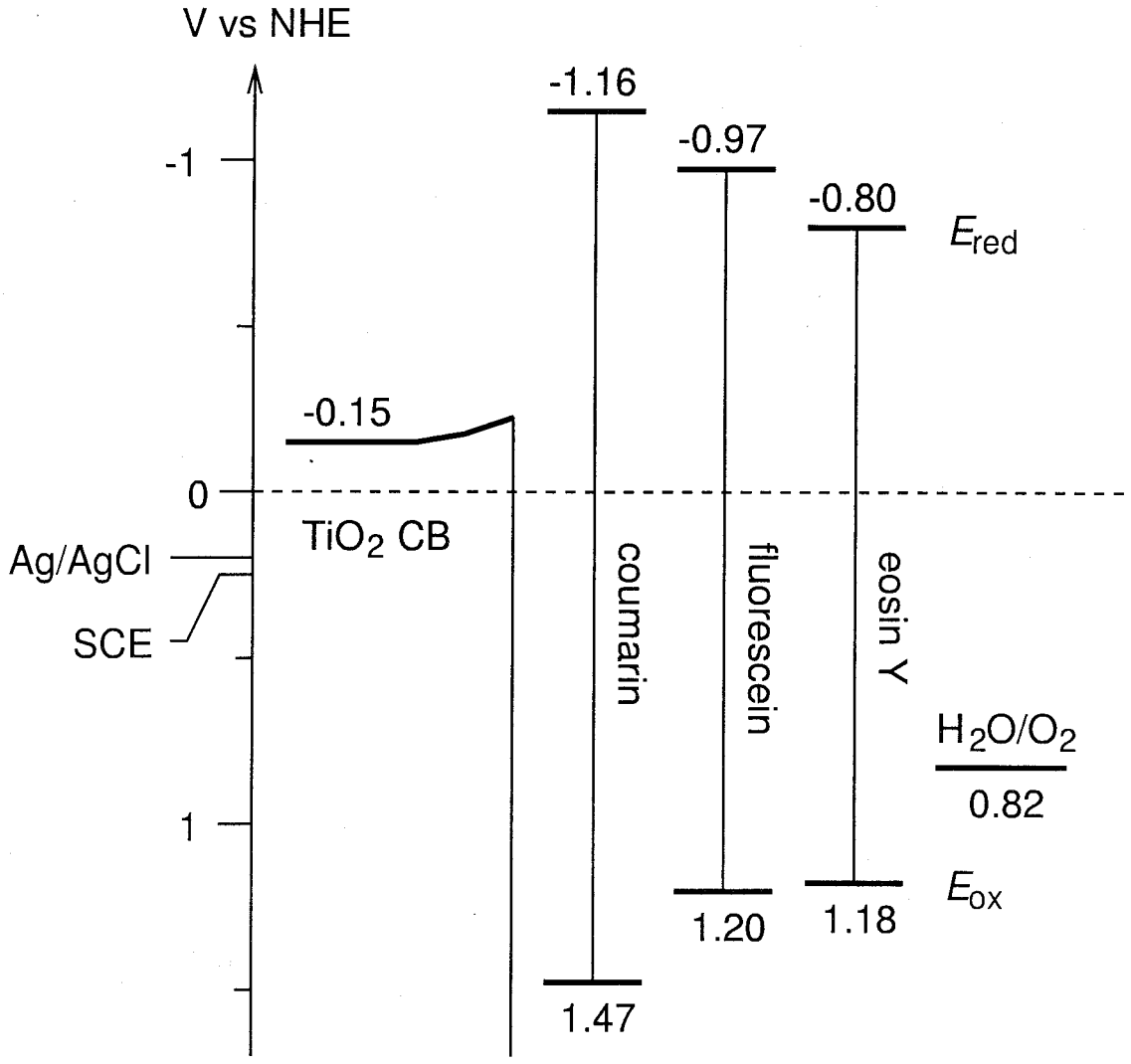

Fig. 6.18: Schematic energy diagram.

Eosin Y is one of the efficient organic sensitizers because about 0.1–0.5 of collection efficiency and about 1 % of energy conversion efficiency were reported for an eosin Y-sensitized TiO_2 photoelectrochemical cell [16]. In preparing dye-sensitized photoelectrochemical cells, refluxing method is often used so as to anchor the dye molecule to the TiO_2 electrode surface through ester-like Ti–O–C bond [3, 22]. The performance of the TiO_2 photoelectrochemical cells is often degraded by the water contamination into the

dye-sensitized TiO_2 cells. The hydrolysis of the ester-like bond and the preference adsorption of water molecule on the electrode surface might be the reasons of lower performance. On the other hand, the chelating compounds of β-diketone and salicylic acid derivatives with Ti atom are quite stable even under water-rich conditions [23, 24]. Therefore, the suppressed adsorption of dye molecules in an aqueous condition probably brings about the extremely lower collection efficiency in the fluorescein and eosin Y systems as shown in Fig. 6.12. Conversely, the introduction of efficient chelating groups into the dye molecule can improve both the efficiency of charge injection and the stability. Since the optical absorption of coumarin is not only limited within the narrower range of wavelength but also displaced to the solar spectrum, such chelating groups should be introduced to the dyes having wide and strong optical absorption.

The dye-sensitized photoelectrodes are typically characterized so far by fabricating actual cells, of which properties are sometimes quite sensitive to the fabricating conditions as well as the contaminations. The present coumarin-sensitized aqueous system can be a simple and reproducible technique to characterize porous semiconductive films as the electrode materials of photoelectrochemical cells.

6.5 Conclusions

Sol-gel derived TiO_2 films having interconnected macropores morphology were applied for electrode materials of the photoelectrochemical cell. The results obtained are summarized as follows:

(1) Photocurrent density of the macroporous TiO_2 films increases with an increase in thickness in spite of the impaired transparency of the macroporous films. It is considered that the surface area of the TiO_2 film is considerably increased by the formation of macropores. The property of the TiO_2 electrode would be improved by decreasing the pore diameter so as to increase the transparency and surface area with maintaining the higher porosity.

(2) Among the dyes tested, coumarin exhibits the notable sensitization efficiency although the energy diagram suggests that the sensitization is thermodynamically allowed for all of coumarin, fluorescein, and eosin Y. The strong complexation of coumarin with

the TiO_2 electrode owing to the 6-membered salycilate chelating geometry of coumarin is supposed to be the main reason of efficient sensitization in the coumarin system. The present aqueous coumarin system can be applicable for the convenient evaluation of the porous electrode materials for the photoelectrochemical cells.

References

[1] A. Fujishima and K. Honda, Nature **238**, 37 (1972).

[2] B. O'Regan and M. Grätzel, Nature **353**, 737 (1991).

[3] M. K. Nazeeruddin, A. Kay, I. Rodicio, R. Humphry-Baker, E. Müller, P. Liska, N. Vlachopoulos, and M. Grätzel, J. Am. Chem. Soc. **115**, 6382 (1993).

[4] C. J. Barbé, F. Arendse, P. Comte, M. Jirousek, F. Lenzmann, V. Shklover, and M. Grätzel, J. Am. Ceram. Soc. **80**, 3157 (1997).

[5] H. Kaji, K. Nakanishi, and N. Soga, J. Non-Cryst. Solids **181**, 16 (1995).

[6] K. Nakanishi and N. Soga, J. Am. Ceram. Soc. **74**, 2518 (1991).

[7] K. Nakanishi and N. Soga, J. Non-Cryst. Solids **139**, 1 (1992).

[8] K. Nakanishi, H. Komura, R. Takahashi, and N. Soga, Bull. Chem. Soc. Jpn. **67**, 1327 (1994).

[9] K. Nakanishi, J. Porous Mater. **4**, 67 (1997).

[10] G. Zhao, H. Kozuka, and T. Yoko, J. Ceram. Soc. Jpn. **104**, 164 (1996).

[11] T. Yoko, A. Yuasa, K. Kamiya, and S. Sakka, J. Electrochem. Soc. **138**, 2279 (1991).

[12] P. F. Belleville and H. G. Floch, J. Sol-Gel Sci. Technol. **3**, 23 (1994).

[13] P. V. Kamat, Chem. Rev. **93**, 267 (1993).

[14] A. Kay and M. Grätzel, J. Phys. Chem. **97**, 6272 (1993).

[15] J. Moser and M. Grätzel, J. Am. Chem. Soc. **106**, 6557 (1984).

[16] K. Sayama, M. Sugino, H. Sugihara, Y. Abe, and H. Akakawa, Chem. Lett. **1998**, 753 (1998).

[17] O. Enea, J. Moser, and M. Grätzel, J. Electroanal. Chem. **259**, 59 (1989).

[18] K. Murakoshi, S. Yanagida, M. Capel, and J. Edward W. Castner, ACS Symposium Series **679**, 221 (1997).

[19] T. Tani, S. I. Kikuchi, and K. I. Honda, Photogr. Sci. Eng. **12**, 80 (1968).

[20] R. O. Loutfy and J. H. Sharp, Photogr. Sci. Eng. **20**, 165 (1976).

[21] Y. Yonezawa, R. Hanawa, and H. Hada, J. Imaging Sci. **34**, 249 (1990).

[22] K. Murakoshi, G. Kano, Y. Wada, S. Yanagida, H. Miyazaki, M. Matsumoto, and S. Murasawa, J. Electroanal. Chem. **396**, 27 (1995).

[23] C. Sanchez and M. In, J. Non-Cryst. Solids **147&148**, 1 (1992).

[24] M. In, C. Gérardin, J. Lambard, and C. Sanchez, J. Sol-Gel Sci. Technol. **5**, 101 (1995).

Chapter 7

Oxygen detection in titania films doped with tantalum

7.1 Introduction

Semiconductive oxides such as TiO_2 [1–3], SnO_2 [4], and ZnO [5] have been used as gas sensors by utilizing the change in their electrical conductivity. The TiO_2-based sensors have attracted considerable attention especially as a practical candidate for stoichiometric air-fuel (A/F) ratio sensor of combustion systems because of their simple structure and small size compared to self-generating galvanic-type O_2 sensors as ZrO_2 [6–8]. Thin film sensors have been actively developed because quick response and proper operation are expected at lower temperature [8]. The TiO_2 is thought to be difficult to use in thin film form because TiO_2 has been believed to be highly resistive compared to other oxides such as Nb_2O_5 [9]. Recently, however, the electron mobility in anatase TiO_2 is proved to be much larger than that in rutile [10, 11]. Furthermore, the electrical conductivity of TiO_2 can also be increased by doping typically pentavalent cations such as Ta [12, 13].

Sol-gel method is considered to be suitable to prepare sensor materials, because the resultant gels are highly porous which is suitable for gas diffusion, and the purification and homogenization of constituents are generally easier than the powder sintering processes. Moreover, the gel morphology can be controlled from microscopic to macroscopic scales by choosing appropriate preparation conditions [14–16]. In spite of such advantages, few systematic studies have been performed on the TiO_2-based thin film gas sensors prepared by sol-gel method.

In this chapter, the influence of O_2 on electrical properties is investigated as a function of Ta concentration for the TiO_2 films prepared by sol-gel dip-coating method.

7.2 Experimental procedure

Titanium tetraisopropoxide (TIP), product of Wako Pure Chemical Industries Ltd., and tantalum pentachloride, product of Mitsuwa's Pure Chemicals Ltd. were used as received. Half of the prescribed amount of ethanol, water, and 60 wt% aqueous solution of nitric acid were mixed together, and added quickly to an ice-cooled solution of TIP and tantalum pentachloride dissolved in the remainder of ethanol under vigorous stirring for 10 min. The compositions of the dipping solutions are listed in Table 7.1. Subsequently, the solution container was sealed and moved to a 40°C chamber to remain stirring for 1 h. The temperature inside the chamber was then lowered to 25°C at which the dipping operations were performed. The humidity inside the chamber was set at 50% RH. A titania gel film was deposited on a Corning #7059 alkali-ion-free borosilicate glass plate covered with patterned ITO electrodes ($10\,\Omega \cdot \square^{-1}$, Kinoene Kogaku Kogyo Ltd.) at $30.0\,\mathrm{mm \cdot min^{-1}}$ of withdrawal speed, immediately followed by heat treatment at 700°C for 10 min. After three times repetition of the dipping and heat treatment, the film was finally heated at 700°C for 1 h.

Table 7.1: Compositions of the dipping solutions (unit: mol).

H_2O	EtOH	TIP	HNO_3	$TaCl_5$	mol% Ta/Ti
0.14	1.0	0.14	0.02	-	0
				0.0001	0.07
				0.0005	0.36
				0.0025	1.79

Figure 7.1 shows the schematic illustration of the device fabricated. The separation (l) and the width (w) of the ITO electrode were set at 1 and 10 mm, respectively. The electrical conductivity of the film (σ) is defined as follows:

$$\sigma = \frac{1}{\rho} = \frac{l}{wtR} = \frac{lI}{wtE}, \tag{7.1}$$

where t denotes the thickness of the TiO_2 film, ρ the resistivity, R the resistance, E the applied voltage, and I the measured current. Figure 7.2 shows the schematic illustration of the apparatus employed for the measurement of electrical properties. The sample was

heated up to 600°C in the furnace and blowed with the test gas. The separation between the sample and the nozzle was about 3 mm. The typical flow condition was 100 ml·min^{-1} of Ar as a carrier gas arbitrarily mixed with 10 ml·min^{-1} of O_2. An electrometer (TR8652, ADVANTEST Ltd.) was used to measure DC conductivity under the voltage bias at 10 V. The frequency dependence of complex impedance was measured using an impedance analyser (3531Z, Hioki E. E. Ltd.) from 5×10^6 through to 42 Hz.

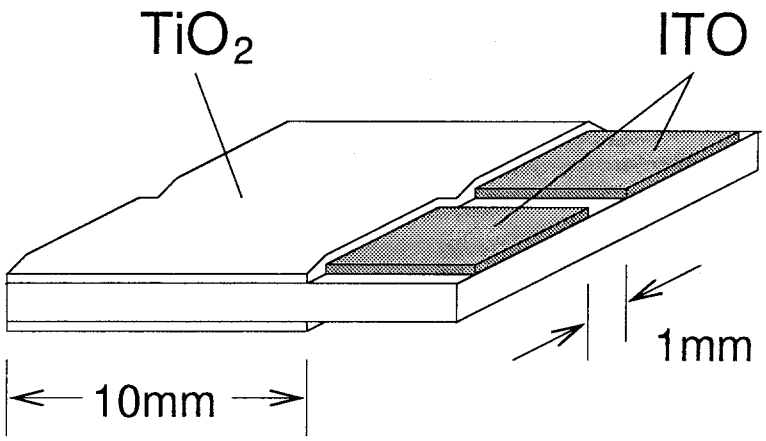

Fig. 7.1: Schematic illustration of the device.

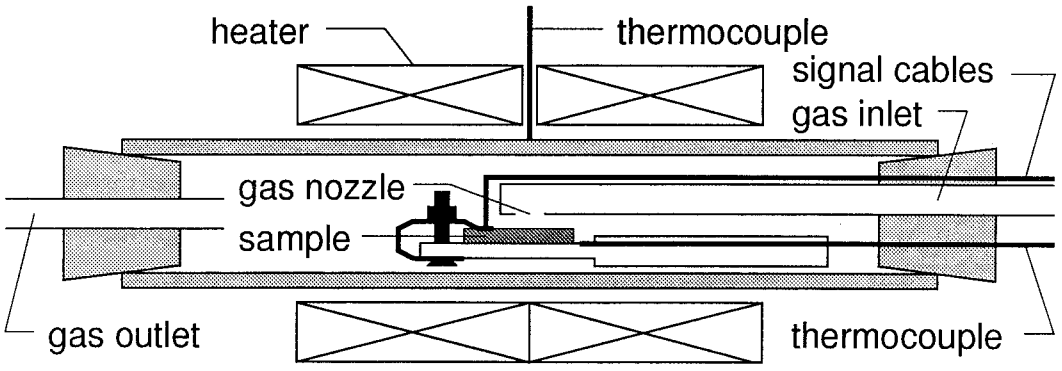

Fig. 7.2: Schematic illustration of the apparatus for the measurement of electrical properties.

7.3 DC conductivity measurement

The resultant TiO_2 film was colorless and transparent. The thickness and the refractive index of the film were respectively determined to be about 230±10 nm and 2.2±0.05 by ellipsometry. The value of refractive index is comparable to that of other sol-gel derived TiO_2 films fired at 700°C [17]. No crystalline phases other than anatase TiO_2 were detected by XRD analysis. Figure 7.3 shows the a and c axes lattice constants of the tetragonal anatase crystalline phase calculated from the position of the diffraction lines. The lattice constants increased with an increase in Ta concentration, but their increases saturated at higher Ta concentration. Figure 7.4 shows the variation of σ with temperature in air without gas flow. The σ decreased monotonically with a decrease in temperature but gradually saturated below 400°C. There was no clear correlation between the Ta concentration and σ, except for the slight increase in σ with an increase in Ta concentration above 500°C. Figure 7.5 shows the variation of σ with temperature under 100 ml·min^{-1} of Ar flow. The σ clearly increased with an increase in Ta concentration. The contribution from the ITO electrodes can be neglected because σ of ITO is usually as large as 10^1–10^2 S·cm^{-1} [18,19].

Figure 7.6 shows the variation of σ with gas composition at 500°C. The 10 ml·min^{-1} of O_2 was mixed with 100 ml·min^{-1} of Ar. The sensitivity of σ toward O_2 was enhanced with an increase in Ta concentration. The inset of Fig. 7.6 shows the magnification of σ curves of the TiO_2 film doped with 1.79 mol% Ta. The decrease in σ was completed within a few seconds when O_2 was turned on. However, more than a hundred seconds were required to stabilize σ when O_2 was turned off although the initial onset of σ was sharp. The 90% response time when O_2 was turned on and the 10% recovery time when O_2 was turned off were respectively estimated to be about 1–2 s and 95 s for the TiO_2 film doped with 1.79 mol% Ta. The spikes accompanied by the O_2 incorporation were attributed to small burst of gas flow, which can be eliminated by improving the gas supplying system. When O_2 was turned on, σ increased at first by the enhanced flow of Ar but then decreased excessively after O_2 reached the sample. Figure 7.7 shows the dependence of σ on Ar flow rate for the TiO_2 film doped with 1.79 mol% Ta. The σ increased considerably by

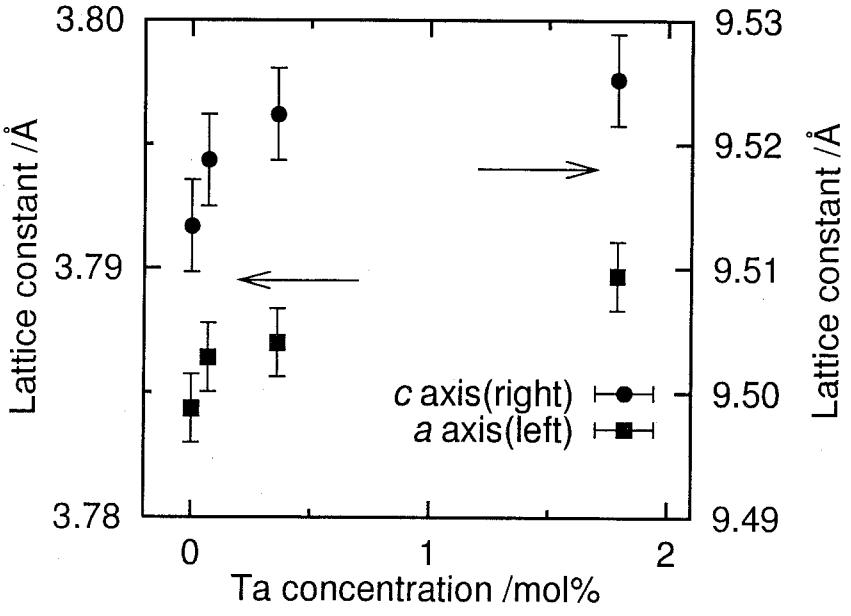

Fig. 7.3: Dependence of a and c axes lattice constants of tetragonal anatase TiO_2 crystalline phase on Ta concentration.

increasing the Ar flow rate.

The activation energy (E_a) of electrical conduction in semiconductive materials is about half the band gap energy (E_g) in the temperature range of intrinsic excitation. Considering that E_gs of anatase single crystal and sol-gel derived anatase film are respectively reported to be 3.2 [11] and 3.1 [20]–3.4 eV [21], E_a for intrinsic excitation should be about 1.5–1.7 eV. The E_a of present TiO_2 films is between 1.0 and 1.5 eV above 500°C as shown in Figs. 7.4 and 7.5. Nonetheless, such dependences of σ on temperature can be attributed to the intrinsic excitation of conduction carriers because the gradients of the σ curves can be 1.6 at much higher temperatures at which the σ–T relationship is determined only by the intrinsic excitation. The σ becomes almost temperature independent below 400°C. The surface conduction due to the higher bulk resistivity and the thin film geometry might be the probable reason, but the definite mechanism is currently unknown.

It has been reported that σ of sol-gel derived TiO_2 film increases more than two orders of magnitude at room temperature by doping 2.4 mol% Ta [13]. Such a σ increase is explained by the formation of a Ti^{3+} valence state, which works as the donor site of the conductive electron in accordance with the following mechanism:

$$(1-x)\mathrm{Ti}^{4+}\mathrm{O}_2^{2-} + \frac{x}{2}\mathrm{Ta}_2^{5+}\mathrm{O}_5^{2-} \rightleftarrows (\mathrm{Ti}^{4+})_{1-2x}(\mathrm{Ti}^{3+})_x(\mathrm{Ta}^{5+})_x\mathrm{O}_2^{2-} + \frac{x}{4}\mathrm{O}_2. \quad (7.2)$$

However, the valence state of the Ti ion can be determined by Eq. 7.2 only when Ta ions are completely dissolved in the TiO_2 crystalline lattice. In the present case, such Ta doping is not effective in increasing σ in air as shown in Fig. 7.4, although σ increases with an increase in Ta concentration under Ar flow as shown in Fig. 7.5. Therefore Ta ion is supposed to segregate to the TiO_2 surface. Indeed, the equilibrium solid solubility of Ta_2O_5 into TiO_2 has been reported as low as 1–2 mol% at lower temperature as 700°C [22]. Furthermore, the saturated increase in lattice constant at higher Ta concentration shown in Fig. 7.3 strongly suggests the segregation of Ta ion.

As shown in Fig. 7.6, the sensitivity of σ against O_2 depends strongly on Ta concentration. Hence it is supposed that the Ta ion segregated to the surface possibly plays a catalytic role for the surface reactions with O_2. It is also possible to consider that the Ti ion near the Ta ion could be the transient site between Ti^{3+} and Ti^{4+} which provides conductive electrons. When O_2 is turned on, σ decreases much faster than the σ increase

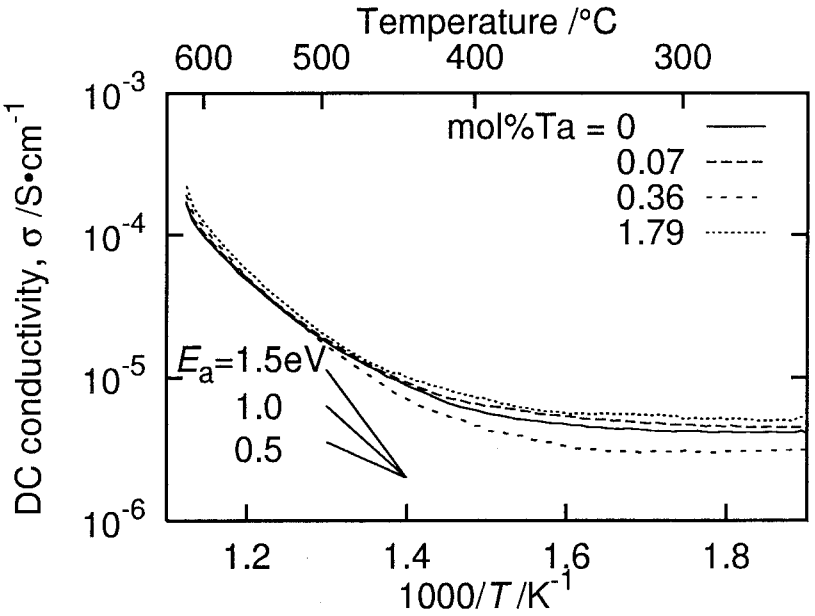

Fig. 7.4: Temperature dependence of DC conductivity σ of the TiO_2 films in air without gas flow.

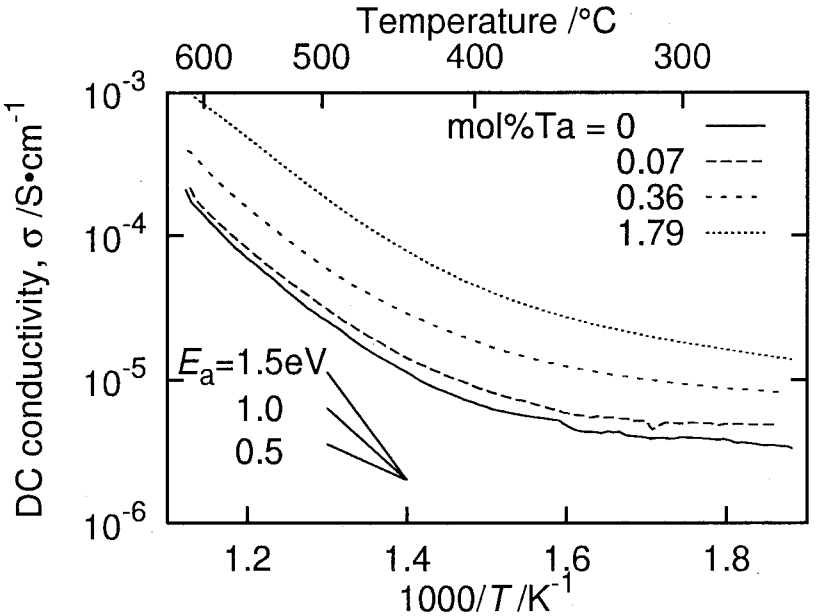

Fig. 7.5: Temperature dependence of DC conductivity σ of the TiO_2 films under 100 ml·min^{-1} of Ar flow.

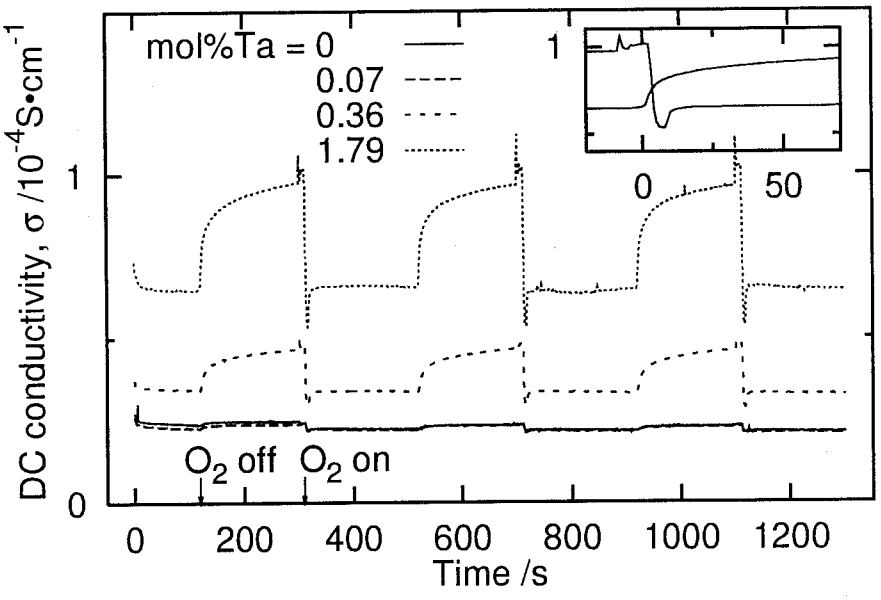

Fig. 7.6: Variation of DC conductivity σ of the TiO_2 films with gas composition at 500°C. The 10 ml·min^{-1} of O_2 was mixed with 100 ml·min^{-1} of Ar. The variation for the film doped with 1.79 mol% Ta is magnified in the inset.

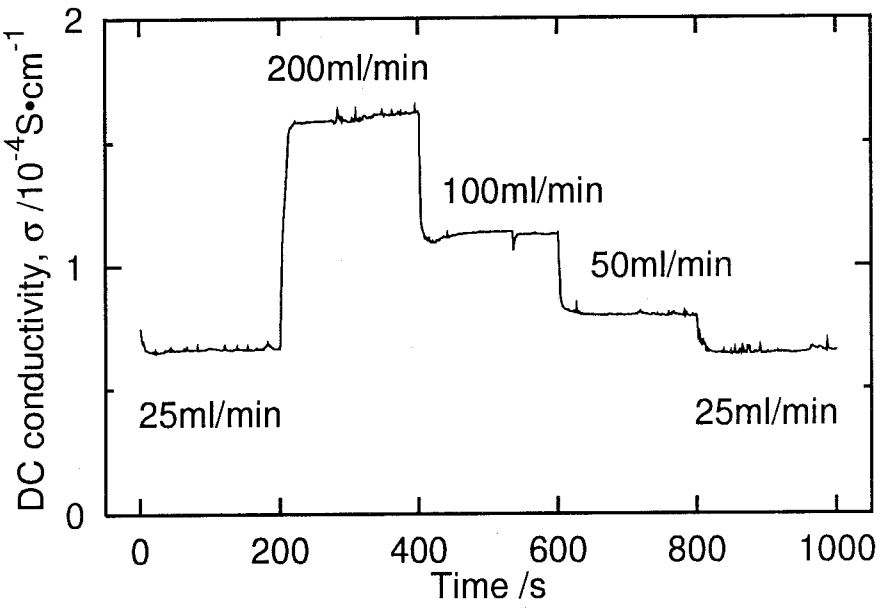

Fig. 7.7: Dependence of DC conductivity σ on Ar flow rate for the TiO_2 film doped with 1.79 mol% Ta.

when O_2 is turned off. This result suggests that the oxidized surface state is rather stable. The σ is less dependent on gas composition for the films of lower Ta concentration. Then it is supposed that Ti^{4+} ion is hardly reduced under an Ar flow at 500°C without the aid of Ta ion. As shown in Fig. 7.7, σ increases significantly with an increase in flow rate of Ar carrier gas. In the present tubular furnace, complete exchange of O_2 with Ar is difficult mainly due to the larger furnace volume and nozzle geometry. At higher flow rate, the decrease in local O_2 concentration around the nozzle and sample may enhance the O_2 desorption and then increase σ.

7.4 Complex impedance analysis

Typical results of complex impedance analysis are shown in Figs. 7.8 and 7.9. The insets show the magnifications around the origin. Since only one downward arc was observed on the complex plane in all the measurements, a parallel connection of resistance (R_p) and capacitance (C_p) shown in Fig. 7.10(a) was suggested to be an equivalent circuit for the present TiO_2 film. The total impedance (Z) is theoretically expressed as follows:

$$\begin{aligned} Z = Z_{re} + iZ_{im} &= \left(\frac{1}{Z_r} + \frac{1}{Z_c}\right)^{-1} = \left(\frac{1}{R_p} - \frac{1}{i/\omega C_p}\right)^{-1} \\ &= \frac{R_p}{1+(\omega R_p C_p)^2} - i\frac{\omega R_p^2 C_p}{1+(\omega R_p C_p)^2}, \end{aligned} \tag{7.3}$$

where Z_{re} and Z_{im} respectively denote the real and imaginary parts of total impedance, Z_r and Z_c the complex impedances of circuit components connected in parallel, ω the angular velocity, and i the imaginary unit. The calculated distribution of (Z_{re}, Z_{im}) is also shown in Figs. 7.8 and 7.9 as dashed lines. The radius of the semicircle was smaller for the film of higher Ta concentration. The radius was varied little by introducing O_2 in the pure TiO_2 film as shown in Fig. 7.8, while the semicircle was expanded considerably by O_2 introduction in the TiO_2 film doped with 1.79 mol% Ta as shown in Fig. 7.9.

Figure 7.11 shows the Ta concentration dependence of R_p and C_p estimated by Eq. 7.3. Both R_p and C_p generally decreased with an increase in Ta concentration but increased by introducing O_2. The R_p and C_p values obtained without O_2 introduction were respectively normalized by those measured under O_2 introduction as shown in Fig. 7.12. The C_p

ratio was almost independent of Ta concentration. In contrast, the R_p ratio decreased significantly at higher Ta concentration.

The complex impedance analysis brings further information about the electrical property. The obtained distributions of complex impedance agree well with the parallel RC model shown in Fig. 7.10(a). Since the center of the arc is on the Z_{re} axis, C_p is approximated to a Debye-type capacitance consisting of just a single relaxation process. On the other hand, the equivalent circuit of polycrystalline ceramics is assumed to be expressed as the series connection of bulk, grain-boundary and electrode impedances as shown in Fig. 7.10(b). Since their impedances are usually different, more than one arc can be observed [23, 24]. The arc of bulk impedance is normally nearer the origin of the complex plain than that of grain-boundary impedance, because the resonance frequency $(1/2\pi RC)$ of the former is larger than the latter due to the smaller R_b and C_b [23]. The contribution from the electrode impedance of which resonance frequency was too low to be measured in this experiment is assumed to be neglected. The resistivity evaluated from Fig. 7.11 using Eq. 7.1 is in the order of $10^4\,\Omega$·cm. Since the resistivity of anatase single crystal annealed at 600°C for 15 d in air is reported to be about $10^1\,\Omega$·cm at room temperature [10], the arcs shown in Figs. 7.8 and 7.9 can not be attributed to bulk impedance although the arcs begin almost from the origin. The porosity of the coating films can be estimated by following equation [25]:

$$\text{Porosity} = 1 - \frac{n^2 - 1}{n_d^2 - 1}, \tag{7.4}$$

where n and n_d respectively denote the refractive indices of the porous coating film and the pore-free anatase ($n_d = 2.52$ [26]). The porosity of the present TiO_2 films is calculated to be 24–32%. The crystalline size of such sol-gel derived TiO_2 film is estimated to be as small as the order of 100 nm by atomic force microscopy (AFM) [21]. Then it is suggested that the contribution from the grain boundary is significantly large in the sol-gel derived TiO_2 film. In consequence, R_p and C_p would represent the impedance of the grain-boundary component. Similar results are also reported from the impedance analyses of titania-based ceramics [27,28] and sol-gel derived TiO_2 films [29]. Since the bulk resistance is estimated to be about 10^3 times smaller than the grain-boundary resistance, the arc radius of bulk impedance should be 10^3 times smaller than that of the grain-boundary

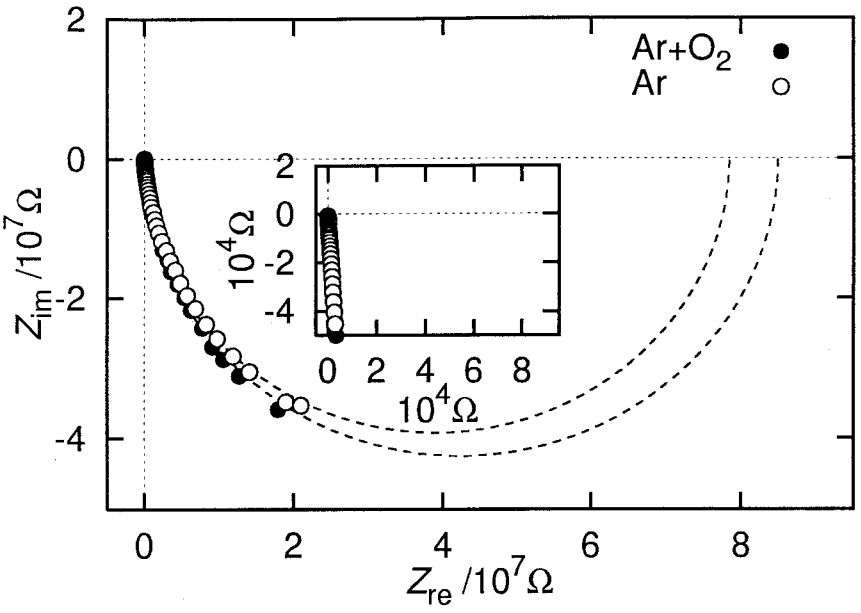

Fig. 7.8: Dependence of complex impedance on gas composition for the pure TiO_2 film at 500°C. The inset shows the magnification around the origin.

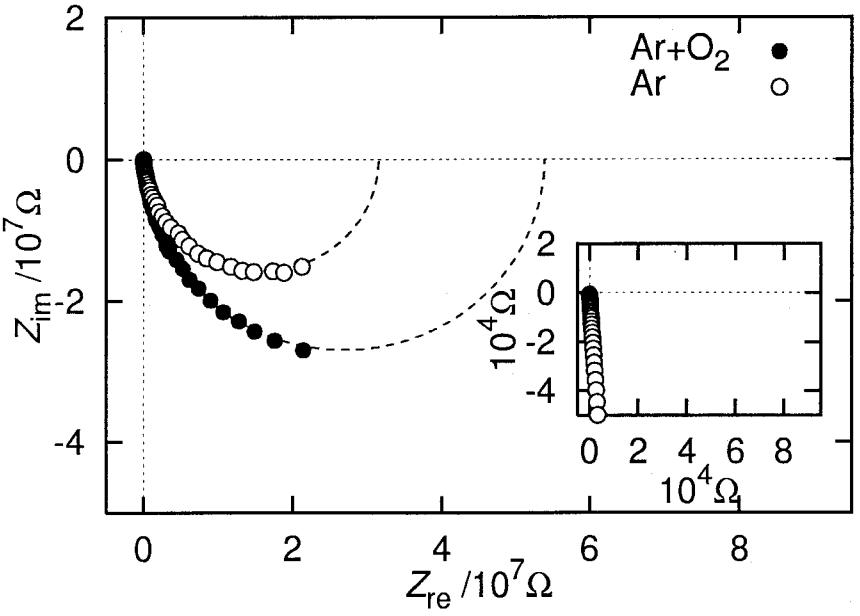

Fig. 7.9: Dependence of complex impedance on gas composition for the TiO_2 film doped with 1.79 mol% Ta at 500°C. The inset shows the magnification around the origin.

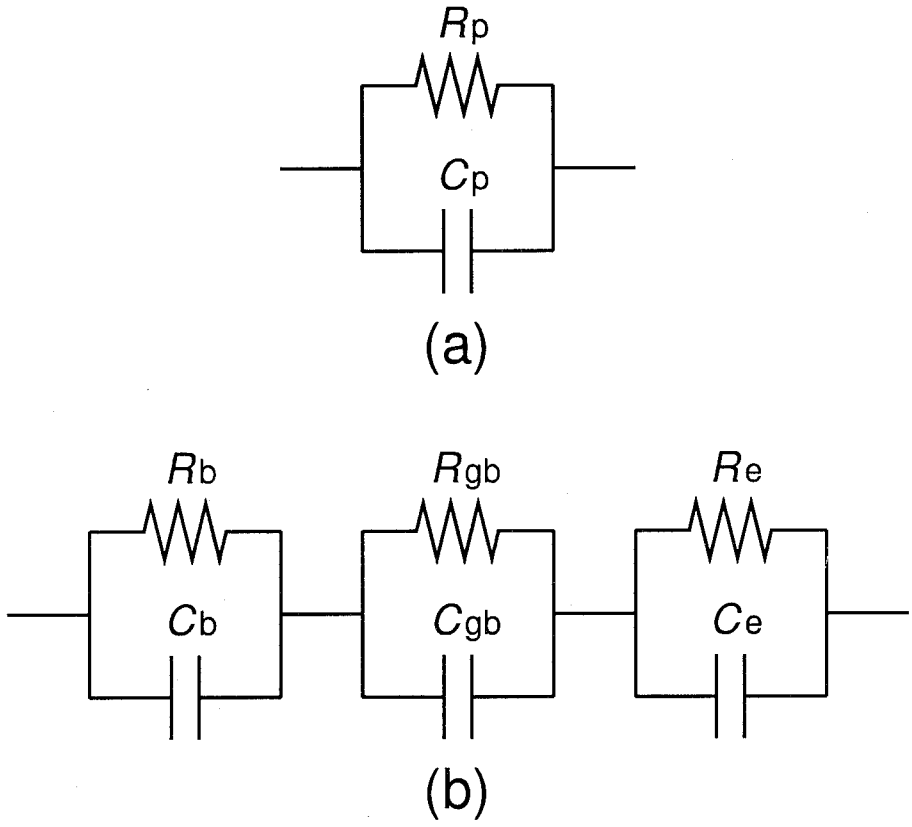

Fig. 7.10: Equivalent circuits for (a) present TiO_2 films, and for (b) common polycrystalline ceramics. The subscripts b, gb, and e respectively indicate the bulk, grain boundary, and electrode components.

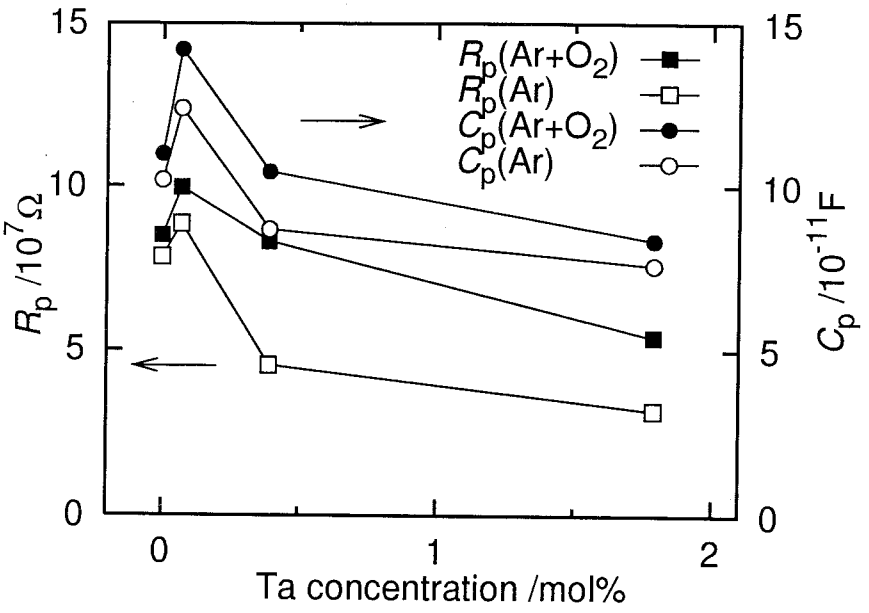

Fig. 7.11: Dependence of R_p and C_p on Ta concentration and gas composition at 500°C.

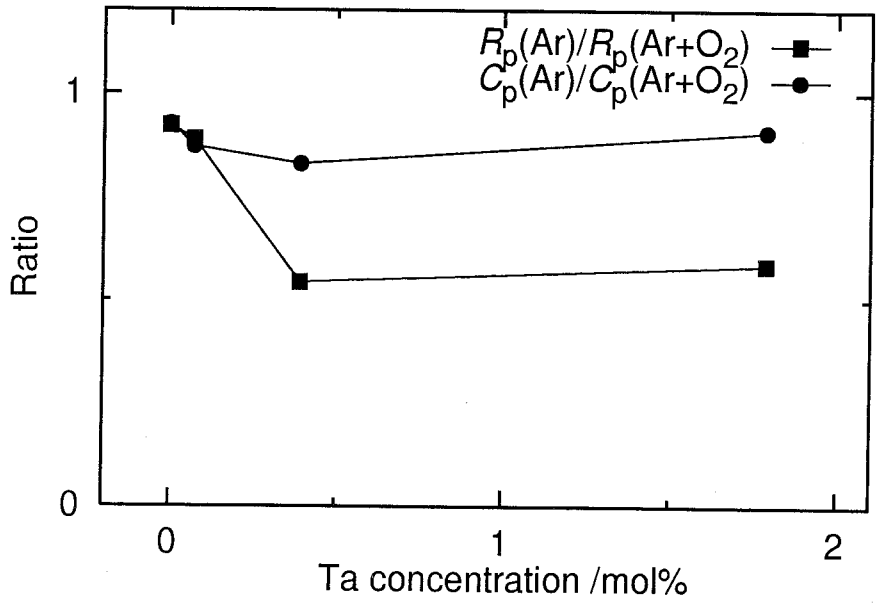

Fig. 7.12: Relationship between the gas composition sensitivities of R_p and C_p, and Ta concentration at 500°C. The R_p and C_p values measured under Ar flow are respectively normalized by those measured under Ar+O_2 flow.

impedance. Therefore the arc of the former could not be distinguished.

As shown in Fig. 7.12, the R_p ratio decreases at higher Ta concentrations whereas the C_p ratio remains almost constant, suggesting that σ is mainly dominated by the variation of R_{gb}. It is thought that the space charge layer is formed on the surface of the n-type semiconductive oxides in air, because atomic oxygen adsorbed on the surface extracts the conductive electrons. The resistivity increases due to the decrease in carrier concentration and the formation of surface barrier layer. In a reducing atmosphere, electrons are regenerated by the desorption of adsorbed oxygen and by the direct injection from the reducing gas molecules adsorbed. These mechanisms would be dominant at relatively low temperature because the adsorption of gas molecule is generally suppressed with an increase in temperature. On the other hand, thermodynamically induced Frenkel disorder of oxide ions is suggested to occur at elevated temperatures [30]. The removal and reinsertion of lattice oxide ions especially at the shallower region of the grain could enhance the sensor response. Both mechanisms would contribute to the σ change in the present TiO_2 film.

It has been reported that operation temperatures above 700°C are required for TiO_2-based O_2 sensors without the noble metal catalysts such as Pt and Pd to improve the response time [7, 24]. In the present study, however, σ of the TiO_2 film doped with Ta varies quickly especially when O_2 is turned on even at relatively lower temperature as 500°C although the change in σ would be still insufficient for the practical applications, in which the resistance commonly changes more than two orders of magnitude.

7.5 Conclusions

The influence of O_2 on electrical properties was investigated for the sol-gel derived TiO_2 films doped with Ta. The results obtained are summarized as follows:

(1) The electrical conductivity of the TiO_2 films is comparable under O_2 introduction irrespective of Ta concentration, while increases considerably when O_2 is cut off for the TiO_2 films doped with Ta. Then the sensitivity against O_2 is enhanced with an increase in Ta concentration. The initial onset of electrical conductivity is as quick as several seconds due to the thin film geometry.

(2) The electrical conductivity is mainly dominated by the grain-boundary resistance,

which is considered to be much larger than the bulk resistance of anatase TiO_2. It is supposed that the Ta ion segregated to TiO_2 surface at higher Ta concentration plays important roles in changing the electrical conductivity with respect to gas composition.

References

[1] T. Y. Tien, H. L. Stadler, E. F. Gibbons, and P. J. Zacmanidis, Am. Ceram. Soc. Bull. **54**, 280 (1975).

[2] L. D. Birkefeld, A. M. Azad, and S. A. Akbar, J. Am. Ceram. Soc. **75**, 2964 (1992).

[3] K. Satake, A. Katayama, H. Ohkoshi, T. Nakahara, and T. Takeuchi, Sens. Actuators B, Chem. **20**, 111 (1994).

[4] N. Yamazoe, J. Fuchigami, M. Kishikawa, and T. Seiyama, Surf. Sci. **86**, 335 (1979).

[5] T. Seiyama, A. Kato, K. Fujiishi, and M. Nagatani, Anal. Chem. **34**, 1502 (1962).

[6] A. L. Micheli, Am. Ceram. Soc. Bull. **63**, 694 (1984).

[7] A. Takami, Am. Ceram. Soc. Bull. **67**, 1956 (1988).

[8] T. Takeuchi, Sens. Actuators **14**, 109 (1988).

[9] V. Demarne, S. Balkanova, A. Grisel, D. Rosenfeld, and F. Lévy, Sens. Actuators B, Chem. **13-14**, 497 (1993).

[10] L. Forro, O. Chauvet, D. Emin, L. Zuppiroli, H. Berger, and F. Lévy, J. Appl. Phys. **75**, 633 (1994).

[11] H. Tang, K. Prasad, R. Sanjinès, P. E. Schmid, and F. Lévy, J. Appl. Phys. **75**, 2042 (1994).

[12] F. A. Grant, Rev. Modern Phys. **31**, 646 (1959).

[13] H. Lin, S. Kumon, H. Kozuka, and T. Yoko, Thin Solid Films **315**, 266 (1998).

[14] K. Nakanishi, J. Porous Mater. **4**, 67 (1997).

[15] K. Makita, Y. Akamatsu, S. Yamazaki, Y. Kai, and Y. Abe, J. Ceram. Soc. Jpn. **105**, 1012 (1997).

[16] K. Tadanaga, N. Katata, and T. Minami, J. Am. Ceram. Soc. **80**, 3213 (1997).

[17] L. Hu, T. Yoko, H. Kozuka, and S. Sakka, Thin Solid Films **219**, 18 (1992).

[18] Y. Shigesato and I. Yasui, Oyo-Buturi **64**, 1225 (1995).

[19] Y. Shigesato and I. Yasui, New Ceramics **1996**, 5 (1996).

[20] T. Yoko, A. Yuasa, K. Kamiya, and S. Sakka, J. Electrochem. Soc. **138**, 2279 (1991).

[21] K. Kajihara, K. Tanaka, K. Hirao, and N. Soga, Jpn. J. Appl. Phys. **35**, 6110 (1996).

[22] E. M. Levin, C. R. Robbins, and H. F. McMurdie, in *Phase Diagrams for Ceramists 1969 Supplement*, edited by M. K. Reser (The American Ceramic Society, Inc., Ohio, 1969), Fig. 2403.

[23] S. A. Akbar and L. B. Younkman, J. Electrochem. Soc. **144**, 1750 (1997).

[24] J. Sheng, N. Yoshida, J. Karasawa, and T. Fukami, Sens. Actuators B, Chem. **41**, 131 (1997).

[25] B. E. Yoldas and D. P. Partlow, Thin Solid Films **129**, 1 (1985).

[26] W. D. Kingery, H. K. Bowen, and D. R. Uhlmann, in *Introduction to Ceramics*, 2 ed. (John Wiley & Sons, New York, 1976), p. 669.

[27] Y.-C. Yeh, T.-Y. Tseng, and D.-A. Chang, J. Am. Ceram. Soc. **72**, 1472 (1989).

[28] Y.-C. Yeh, T.-Y. Tseng, and D.-A. Chang, J. Am. Ceram. Soc. **73**, 1992 (1990).

[29] G. Gusmano, G. Montesperelli, P. Nunziante, E. Traversa, A. Montenero, M. Braghini, G. Mattogno, and A. Bearzotti, J. Ceram. Soc. Jpn. **101**, 1095 (1993).

[30] A. M. Azad, S. G. Mhaisalkar, L. D. Birkefeld, S. A. Akbar, and K. S. Goto, J. Electrochem. Soc. **139**, 2913 (1992).

Summary

The present thesis has described the studies on the macroscopic morphology formation and the electrical property of the TiO_2 films prepared by sol-gel dip-coating method. The variation of macroscopic morphology induced by the addition of PEG was investigated intensively to develop the procedures preparing TiO_2 films having controlled pore structure. Besides, several attempts were made aiming at the application of sol-gel derived TiO_2 films for electrical devices. The results obtained are summarized as follows.

In General introduction, the general background and the purpose of the present study were outlined. The importance of oxides as electroconductive materials was pointed out and the features of sol-gel method in fabricating ceramics and glasses were described. In particular, several interesting features and unresolved problems concerning the morphology control and the electrical application of TiO_2 films were suggested.

In Chapter 1, the dependence of macroscopic morphology on relative humidity and withdrawal speed was investigated at several water and alkoxide concentrations under a precisely controlled dipping condition. It was found that the resultant morphology is determined by the competitive contributions among the three principal morphology determining parameters, namely, (a) decrease in fluidity owing to the evaporation of solvent, (b) network formation by polycondensation, and (c) macroscopic domain formation during the phase separation into gel and solvent phases. Since the effect of solvent evaporation was the most important at lower withdrawal speed whereas the morphology was dominated by the polycondensation at higher withdrawal speed, the macroporous morphology was observed at moderate withdrawal speed at which neither the polycondensation nor the fluidity reduction were remarkable. The macroscopic domain formation became less distinct with an increase in relative humidity due to the accelerated polycondensation at higher relative humidity. The withdrawal speed at which the domain formation was most apparent decreased with an increase in relative humidity, suggesting that both the

polycondensation and the phase separation are accelerated as a consequence of enhanced water adsorption. It was supposed that the enhanced hydrolysis of titania oligomer and subsequent complexation with PEG result in the accelerated phase separation as long as the water concentration in the sol film is moderate. The above result was consistent with the morphology change in system having higher initial water concentration, in which the macropores evidently formed at lower relative humidity was suppressed quickly by only a little increase in relative humidity. The domain formation was enhanced with an increase in TIP concentration at almost all the dipping conditions. It was considered that the macroporous morphology becomes evident mainly due to the slower polycondensation at higher TIP concentration.

In Chapter 2, the dependence of macroscopic morphology on molecular weight of PEG and dipping temperature was explored. The macroporous morphology was observed only in the limited range of molecular weight because the compatibility between PEG and the solvent mixture was quite sensitive to molecular weight. At higher molecular weight, formation of macroscopic cracks became evident because the polycondensation was suppressed by the stronger interaction between the titania oligomer and PEG. The withdrawal speed for macroscopic domain formation increased with an increase in dipping temperature. Then it was suggested that the fluidity reduction and the phase separation are more accelerated than the polycondensation due to the enhanced solvent evaporation.

In Chapter 3, the variation of morphology was studied under the addition of various types of organic solvents. The macroscopic domain formation was enhanced when the compatibility between the titania-PEG complex and the external solvent was poor. Even if the incorporation of the external solvent enhanced the compatibility among the titania oligomer, PEG, and the solvent mixture, the domain formation was apparent as long as the external solvent was volatile. The polycondensation rate of titania oligomer was greatly influenced by the addition of external solvent as well. It was thought that the polycondensation rate of titania oligomer should be moderate to enhance the domain formation. The effect of alcohols having larger alkyl groups than ethanol was discussed individually. The domain formation occurred even in the system containing PEG of which molecular weight was as small as 1,540 by decreasing the compatibility between

PEG and the solvent mixture. However the domain formation was inhibited when the polycondensation rate was greatly increased by the addition of the external alcohol. It was found that the clear formation of macroporous morphology is possible even at higher relative humidity by incorporating external alcohol such as 1-butanol so as to slow down the polycondensation and to increase the phase separation strength.

In Chapter 4, the variation of macroscopic morphology was investigated at various preparation conditions to elucidate the general mechanism of morphology formation during the dipping procedure. The variation of morphology was explained comprehensively by considering the volume fraction of solvent phase during the phase separation and the water to TIP ratio in the sol film. The volume fraction of solvent phase mainly determined the type and rate of phase separation. On the other hand, the water to TIP ratio not only determined the period during which the macroscopic domain formation can progress but also modified the phase separation rate. It was pointed out that laminar flow coating method can be an efficient process for the continuous one-side deposition of larger macroporous films. The densification and crystallization behaviors during the heat treatment were also examined. The thermal decomposition of PEG dominated the shrinkage of gel film and the concurrent increase in average pore diameter, while was responsible for little of the crystallization of titania gel film.

In Chapter 5, the variations of morphology and thickness were investigated for the system containing PVP together with PEG. The thickness of macroporous film increased with an increase in PVP concentration but the excess incorporation of PVP suppressed the macroscopic phase separation and enhanced the formation of macroscopic cracks. The porosity and the domain size were determined simply by PEG concentration. The thickness and the preparation speed of the macroporous films were increased by increasing the dipping temperature. Macroporous TiO_2 film as thick as 1 μm having interconnected pore structure has been successfully realized by repeating the deposition several times because the macropores were not filled by the repetitive dippings. It was quite advantageous for practical uses that the dipping solution is free from the gelation as well as stable for a long time under a sealed condition owing to the lower water to alkoxide ratio as 1. It was found that the dissolution properties of PEG and PVP, which are both hydrogen bonding

polymers having proton accepting ability, are quite different. Although the solubility of PVP was low at several solution compositions, the preparation of macroporous film was unsuccessful in systems containing PVP as an only polymer content.

In chapter 6, the sol-gel derived macroporous TiO_2 films were applied for the photoelectrode material of the aqueous photoelectrochemical cell. The macroporous morphology increased the photocurrent density although the transparency of the film was impaired due to the light scattering from the macroscopic domain. Photosensitization of the TiO_2 films by organic dyes was attempted as well to utilize the visible light. The macroporous films were sensitized better than the smooth films because of the larger surface area. Among the dyes tested, 7-diethylaminocoumarin-3-carboxylic acid (coumarin) exhibited notable sensitization efficiency. The efficient charge transfer from coumarin to TiO_2 was attributed not only to the larger energy differences among the relevant energy levels but also to the larger complexation strength of coumarin to surface Ti atom actualized by the salicylate-like coordination geometry. It was expected that the present aqueous system sensitized by coumarin can be applicable for convenient evaluation of the porous electrode materials for photoelectrochemical cells.

In Chapter 7, the influence of O_2 on electrical properties was investigated for the sol-gel derived TiO_2 films doped with Ta. Although the electrical conductivity of the TiO_2 films was comparable under O_2 introduction irrespective of Ta concentration, that of the films doped with Ta increased significantly when O_2 was cut off because the conductive electrons were released by the desorption of O_2 from TiO_2 surface. The rapid onset of electrical conductivity as quick as several seconds was accomplished by the thin film geometry. The complex impedance analysis revealed that the electrical conductivity is mainly governed by the grain-boundary resistance which is suggested to be much larger than the bulk resistance of anatase TiO_2. The XRD analyses indicated that surface segregation of Ta ion is appreciable at higher Ta concentration. Then it was considered that the change in electrical conductivity with respect to O_2 concentration is mainly ascribable to the surface segregation of Ta. The present thin film can be a candidate for O_2 sensing materials.

List of publications

Chapter 1

"Macroscopic morphology of the titania films prepared by a sol-gel dip-coating method from the system containing poly(ethylene glycol). I. Effect of humidity",
Koichi Kajihara and Takeshi Yao,
Journal of Sol-Gel Science and Technology, **12**(3), 185–192(1998).

"Macroscopic morphology of the titania films prepared by a sol-gel dip-coating method from the system containing poly(ethylene glycol). II. Effect of solution composition",
Koichi Kajihara and Takeshi Yao,
Journal of Sol-Gel Science and Technology, **12**(3), 193–201(1998).

Chapter 2

"Preparation of macroporous titania films by a sol-gel dip-coating method from the system containing poly(ethylene glycol)",
Koichi Kajihara, Kazuki Nakanishi, Katsuhisa Tanaka,
Kazuyuki Hirao, and Naohiro Soga,
Journal of the American Ceramic Society, **81**(10), 2670–2676(1998).

"Macroscopic morphology of the titania films prepared by a sol-gel dip-coating method from the system containing poly(ethylene glycol). Effect of molecular weight and dipping temperature",
Koichi Kajihara and Takeshi Yao,
Journal of Sol-Gel Science and Technology, accepted for publication

(Proceedings of 10 th International Workshop on Glasses, Ceramics, Hybrids and Nanocomposites from Gels, Yokohama, 1999)

Chapter 3

"Macroscopic morphology of the titania films prepared by a sol-gel dip-coating method from the system containing poly(ethylene glycol). III. Effect of chemical additives",
Koichi Kajihara and Takeshi Yao,
Journal of Sol-Gel Science and Technology, **16**(3), 257-266(1999).

"Sol-gel derived macroporous titania films prepared from the system containing poly(ethylene glycol) together with long-chain alcohols",
Koichi Kajihara and Takeshi Yao,
Journal of Sol-Gel Science and Technology, accepted for publication.

Chapter 4

"Macroscopic morphology of the titania films prepared by a sol-gel dip-coating method from the system containing poly(ethylene glycol). IV. General principle of morphology formation and effect of heat treatment",
Koichi Kajihara and Takeshi Yao,
Journal of Sol-Gel Science and Technology, accepted for publication.

Chapter 5

"Macroporous morphology formation on titania films prepared by sol-gel dip-coating method from system containing poly(ethylene glycol) and poly(vinylpyrrolidone)",
Koichi Kajihara,
Physical Chemistry, Chemical Physics, submitted.

"Sol-gel derived interconnected macroporous titania films prepared from system containing poly(ethylene glycol) and poly(vinylpyrrolidone)",

Koichi Kajihara,

Chemical Communications, submitted.

Chapter 6

"Photoelectrochemical property of dye-sensitized macroporous titania films prepared by sol-gel method",

Koichi Kajihara,

Physical Chemistry, Chemical Physics, submitted.

Chapter 7

"Oxygen detection in sol-gel derived titania thin films doped with tantalum",

Koichi Kajihara and Takeshi Yao,

Physical Chemistry, Chemical Physics, **1**(8), 1979–1983(1999).

Related publications

"Photovoltaic effect in titanium dioxide/zinc phthalocyanine cell",

Koichi Kajihara, Katsuhisa Tanaka, Kazuyuki Hirao, and Naohiro Soga,

Japanese Journal of Applied Physics **35**(12A), 6110–6116(1996)

"Photovoltaic effect in titanium dioxide/polythiophene cell",

Koichi Kajihara, Katsuhisa Tanaka, Kazuyuki Hirao, and Naohiro Soga,

Japanese Journal of Applied Physics **36**(9A), 5537–5542(1997)

Acknowledgements

Most of the present work has been carried out at Graduate School of Energy Science, Kyoto University under Professor Takeshi Yao.

The author wishes to express his gratitude to Professor Takeshi Yao for his continuous understanding and assistance in completion of the present thesis. Also, the author wishes to express his appreciation to Professor Naohiro Soga of University of Shiga Prefecture for his continuous encouragement and beneficial suggestions. The author is grateful to Professor Yasuhiko Ito and Professor Yukio Ogata for their guidance and useful advice in preparing the present thesis. The author is indebted to Professor Tadashi Kokubo, Professor Teiichi Hanada, Professor Toshinobu Yoko, and Professor Kazuyuki Hirao for their kind support in proceeding with the present study. The author wishes to thank Professor Kazuki Nakanishi and Professor Katsuhisa Tanaka for their instructive discussions and important suggestions throughout the present study. Valuable suggestions from Professor Yoshiharu Uchimoto and Dr. Setsuhisa Tanabe are gratefully acknowledged. Hearty thanks are made to Dr. Koji Fujita and all the laboratory members for their collaboration.

The author wishes to thank Professor Hiromitsu Kozuka of Kansai University for valuable instruction for sol-gel experiments and viscosity measurements.

The author would like to thank the colleagues of Kyoto University Cheering Party and the persons concerned for their heartful encouragement.

Finally, the author expresses his sincere gratitude to Mr. Yoshifumi Kajiwara and Mrs. Ryoko Kajiwara, his parents, for their understanding, support, and encouragement.

Kyoto, January 2000 Koichi Kajiwara